1989

Aqueous iron-thiolate chemistry: relevance to iron-sulfur proteins

Mark Thomas Werth
Iowa State University

Order Number 9003578

Aqueous iron-thiolate chemistry: Relevance to iron-sulfur proteins

Werth, Mark Thomas, Ph.D.

Iowa State University, 1989

U·M·I
300 N. Zeeb Rd.
Ann Arbor, MI 48106

Aqueous iron-thiolate chemistry: Relevance to iron-sulfur proteins

by

Mark Thomas Werth

A Dissertation Submitted to the

Graduate Faculty in Partial Fulfillment of the

Requirements for the Degree of

DOCTOR OF PHILOSOPHY

Department: Chemistry

Major: Inorganic Chemistry

Approved:

Signature was redacted for privacy.

In Charge of Major Work

Signature was redacted for privacy.

For the Major Department

Signature was redacted for privacy.

For the Graduate College

Iowa State University
Ames, Iowa

1989

TABLE OF CONTENTS

ABBREVIATIONS

C.p.	Clostridium pasteurianum
D.v.	Desulfovibrio vulgaris
D.g.	Desulfovibrio gigas
Rd	rubredoxin
Ds	desulforedoxin
Fd	ferredoxin
Triton X-100	poly(oxyethylene) p-tert-octyl phenyl ether
S_2-o-xyl	o-xylyl-α,α'-dithiolate
dts	dithiosquarate, $S_2C_4O_2^{2-}$
TDT	toluenedithiol
Me	methyl
Et	ethyl
Pr	propyl
Bu	butyl
Ph	phenyl
Me_2SO	dimethyl sulfoxide
DMSO	dimethyl sulfoxide
DMF	N,N-dimethylformamide
NMA	N-methylacetamide
Cys	cysteine
Pro	proline
Leu	leucine
Gly	glycine

Z	N-carbobenzoxyl
Tris	trishydroxymethylaminomethane
S.C.E.	saturated calomel electrode
N.H.E.	normal hydrogen electrode
NMR	nuclear magnetic resonance
N.O.E.	nuclear Overhauser effect
T_1	nuclear spin-lattice relaxation time
TMS	tetramethylsilane
DSS	2,2-dimethyl-2-sila-5-pentanesulfonate
EPR	electron paramagnetic resonance
MCD	magnetic circular dichroism

DEDICATION

TO MY MOTHER

I. INTRODUCTION

A broad definition of the iron-sulfur proteins might be stated as any protein which contains iron that is tetrahedrally coordinated by organic and inorganic sulfur. Such a definition would include the ferredoxins, nitrogenase, hydrogenase, and the many other proteins which contain iron-sulfur clusters composed of multiple iron atoms held together by bridging sulfide ligands. The simplest iron-sulfur protein that would meet the requirements of the above stated definition would need only to contain a single iron atom held in the protein by four cysteinyl alkylthiolate sulfur ligands. The protein rubredoxin from the bacterium Clostridium pasteurianum is an example of such a simple iron-sulfur protein. A detailed discussion of rubredoxins is included in a later section.

More commonly, the iron-sulfur proteins contain a cluster composed of iron and bridging sulfide ions. The simplest proteins of this type are the ferredoxins (1). The ferredoxins are relatively low molecular weight proteins, containing either [2Fe2S] or [4Fe4S] clusters, which function as biological electron carriers. The structures of the [2Fe2S] and [4Fe4S] clusters are shown schematically in Figure I-1. Ferredoxins with the [2Fe2S] cluster are typically found in the chloroplasts of higher plants, such as spinach and parsley. Bacteria are the most common sources of ferredoxins with the [4Fe4S] cluster.

Rubredoxin and the ferredoxins are examples of the simplest iron-sulfur proteins. Nature contains a rich variety of simple and more complex iron-sulfur proteins which are found in organisms ranging from bacteria to humans (2). Usually, these more complex iron-sulfur proteins are enzymes which catalyze reactions that play a fundamental role in biological processes. These enzymes range from small proteins with a single iron-sulfur cluster to large multi-component systems utilizing several iron-sulfur

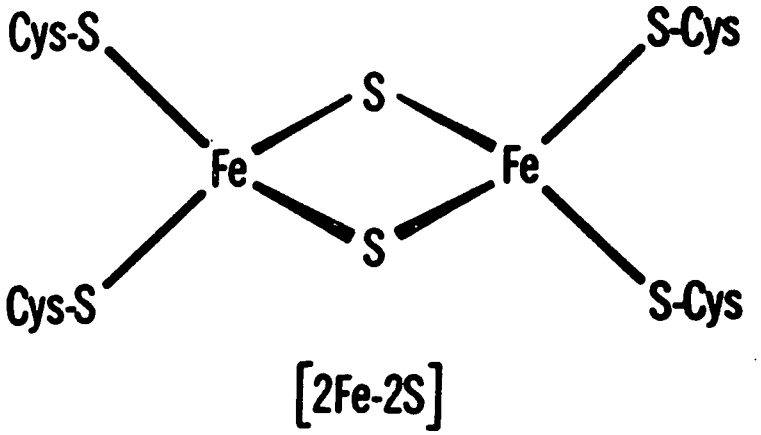

[2Fe-2S]

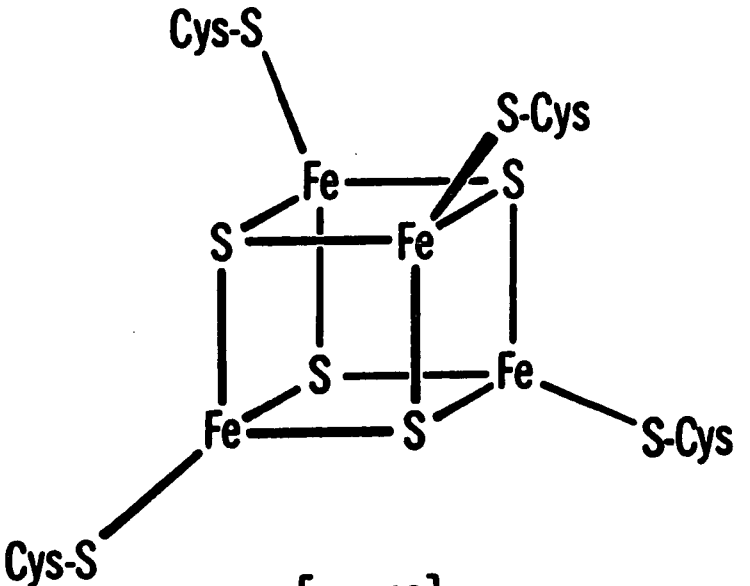

[4Fe-4S]

Figure I-1. Schematic diagrams of the [2Fe2S] and [4Fe4S] clusters found in iron-sulfur proteins

clusters in combination with other prosthetic groups, e.g., flavin or heme moieties. Here, again, the iron-sulfur clusters usually function as electron carriers.

Bacteria are the source of two of the most important iron-sulfur proteins, namely nitrogenase (3) and hydrogenase (4). The enzyme nitrogenase combines several iron-sulfur clusters with a molybdenum-iron-sulfur (or vanadium-iron-sulfur) cofactor to perform the catalytic reduction of dinitrogen to ammonia. This process is the key step in providing nitrogen to all living organisms. Hydrogenase catalyzes what is probably the simplest known chemical reaction, the cleavage of the hydrogen-hydrogen bond to produce two protons and two electrons. The exact chemical mechanisms by which these two enzymes function is currently the focus of intensive scientific research motivated by desires ranging from the answer to basic chemical questions to potential commercial applications.

Examples of iron-sulfur enzymes found in the human body include succinate dehydrogenase and aconitase. Physiologically, succinate dehydrogenase (5) removes two electrons from succinate and funnels them into the mitochondrial respiratory chain where they are ultimately used to reduce molecular oxygen. The enzyme contains a [2Fe2S], a [3Fe4S] and a [4Fe4S] iron-sulfur cluster, as well as a flavin cofactor. Aconitase catalyzes the interconversion of citrate and isocitrate and is the only enzyme currently established to function by direct interaction of the iron-sulfur cluster with a substrate molecule (6).

Chemically, the iron-sulfur proteins can be pictured as having an iron-based active site isolated in a highly specific environment provided by a huge multidentate chelating ligand, namely the protein. The iron site may be as simple as a single iron atom or as complex as an eight atom cluster, i.e., four iron atoms and four sulfur atoms. The iron atom cluster is normally held within the protein by four iron-alkylthiolate chemical

bonds. The alkylthiolate groups are provided by the protein in the form of the amino acid cysteine. Chemical bonds between the metal site and the protein are the primary means by which the protein influences the physical and chemical properties of the metal site.

There are also numerous secondary means by which the protein can influence the properties of the metal site. X-ray crystallography provides evidence for hydrogen bonding (7,8) between amide groups and terminal alkylthiolate sulfur atoms in iron-sulfur proteins. Adman et al. (9) have postulated that the NH···S hydrogen bonds modulate the reduction potential of the cluster by differential stabilization of oxidation levels. More recently, it has been proposed that hydrogen bonding occurs directly between the protein and the bridging sulfur atoms in the iron-sulfur clusters (10). The polarity of the surrounding amino acid residues and the degree of solvent exposure determine the local dielectric constant of the medium in which the iron site functions. Specific amino acid residues may be placed near the iron site to enhance the ability of the metal site to perform a specific function. For example, an aromatic amino acid residue may be placed in a position suitable for pi orbital overlap between the aromatic ring and p orbitals of the sulfur, thereby, facilitating electron transfer between the surface of the protein and the iron site.

The plant ferredoxins, which contain the [2Fe2S] cluster, have redox potentials spanning the range of -0.23 V to -0.46 V (vs. N.H.E.) for the $2^+/1^+$ couple depending on the source of the protein and the experimental conditions. In every case studied, so far, the protein restricts the cluster to only two of the available oxidation levels for the cluster. The bacterial ferredoxins use the $2^+/1^+$ pair of oxidation levels for the $[Fe_4S_4]$ core and, like the plant ferredoxins, they have a redox potential in the range of -0.28 V to -0.49 V. The high potential iron-sulfur proteins (HIPIP's) use the $3^+/2^+$

levels of the [4Fe4S] cluster, and have a much higher redox potential of +0.35 V. Both rubredoxin and desulforedoxin exhibit a redox potential of approximately -0.05 V for the Fe(III)/Fe(II) couple.

Iron-Thiolate Complexes

The iron-alkylthiolate bond linking the iron-sulfur cluster and the protein is a natural focus of interest for the bioinorganic chemist. The study of the chemistry of iron-alkylthiolate compounds is an important part of the overall exploration of the chemistry of the iron-sulfur proteins. By studying the simple $[Fe(SR)_4]^{n-}$ (R = alkyl, n = 1,2) cluster the behavior of iron in a coordination sphere comprised of a tetrahedral arrangement of thiolate sulfur has been described in terms of structural, electrochemical and spectroscopic properties (11-14). Chemically, simple iron-alkylthiolate compounds serve as precursors from which the iron-sulfur-thiolate clusters can be synthesized (15-19). Perhaps most importantly, $[Fe(SR)4]^{n-}$ serves as the synthetic model for the iron site in the proteins rubredoxin and desulforedoxin.

In 1970, preliminary results from an X-ray diffraction study of rubredoxin demonstrated that the iron atom was tetrahedrally coordinated by four cysteinyl thiolate sulfur atoms (20). Surprisingly, this result proved to be the first structural characterization of iron with a tetrahedral thiolate-sulfur coordination sphere. Although several attempts had been made at preparing a small mononuclear tetrahedral iron-thiolate analog, only poorly characterized species in solution and intractable polymeric solids had been reported in the literature.

In 1975, Anglin and Davison (21) reported the preparation of an iron-peptide complex with tetrahedral iron coordination. Using the peptide Boc-(Gly-l-Cys-Gly)$_4$-NH_2, which molecular models indicated was capable of providing tetrakis thiolate

coordination to a single iron atom, they prepared an iron(II)-peptide complex in dimethyl sulfoxide. The near-IR absorption spectrum of the complex in dimethyl sulfoxide contained a very broad band at 5100 cm^{-1}. The band was assigned to a $^5E \rightarrow {}^5T_2$ transition for high spin tetrahedral Fe(II) by comparison with Fe(II) doped into a ZnS lattice where the iron was known to have tetrahedral Fe(II)-S_4 coordination. Air oxidation of the Fe(II) complex produced a deep red-violet species with visible absorption maxima at 495 and 565 nm. These absorption bands bear some resemblance to those of oxidized rubredoxin. Unfortunately, Anglin and Davison were unable to obtain reversible electrochemical behavior for the Fe(III)/Fe(II) couple. While the early spectroscopic results were consistent with a monomeric, tetrahedral iron complex, the inability to grow crystals of the iron-peptide complex precluded confirmation of the structure by X-ray diffraction.

That same year, Lane and co-workers (22) reported the synthesis of crystalline tetraethylammonium salts of the $[Fe(S_2\text{-}o\text{-}xyl)_2]^{1-}$ and $[Fe_2(S_2\text{-}o\text{-}xyl)_3]^{2-}$ anions. The ligand, o-xylyl-α,α'-dithiolate, is a chelating dithiol. The mononuclear anion was the first rubredoxin analog to be characterized by X-ray crystallography. The electronic absorption, EPR and Mössbauer spectral properties of the mononuclear anion demonstrated a clear resemblance to the oxidized iron site in rubredoxins. The anion exhibited a reduction potential of -1.03 V (vs. S.C.E.) in DMF. Thus, in spite of the structural and spectral similarities between the synthetic model and rubredoxin, the measured reduction potential for the model compound was approximately 0.7 volts more negative than the measured reduction potential of rubredoxin (23).

Later in 1975, Holah and Coucouvanis (24) reported the preparation of crystalline tetraphenylphosphonium salts of several transition metals with tetrahedral thiolate sulfur coordination. Both of the iron complexes, $(Ph_4P)_2[Fe(SPh)_4]$ and $(Ph_4P)_2[Fe(SPh)_2(dts)]$

(dts = dithiosquarate, $[S_2C_4O_2]^{2-}$), possessed a near-IR band consistent with monomeric tetrahedral Fe(II). Magnetic susceptibility measurements showed that both complexes contained high spin Fe(II), as does reduced rubredoxin. The Mössbauer parameters for the model compounds (25) were comparable to those obtained for reduced rubredoxin.

Since these initial reports appeared in the mid-'70s, a general description of the properties of iron in a tetrahedral thiolate coordintion sphere has emerged. Several of the model complexes have been examined by X-ray crystallography (24-26). Lengths and angles for the iron-sulfur bonds are listed in Table I-1. All of the compounds exhibit ranges of S-Fe-S bond angles which produce a rhombic distortion of the $Fe-S_4$ unit from T_d symmetry to S_4 or lower symmetry. The distortion can be described as the result of a compression of the tetrahedron along one of the S_4 axes. There is no evidence in either the benzenethiolate or the xylenedithiolate mononuclear species for cation-anion interactions, solvate-anion interactions or chelate effects sufficient to induce the observed distortions (12). The d^6 electronic configuration of Fe(II) presents the possibility of distortion occurring via the Jahn-Teller effect. Coucouvanis and co-workers argued against the Jahn-Teller effect as a significant cause of the distortion on the basis of the results of X-ray structural studies of a variety of mononuclear transition metal thiolates (12). In each case, significant distortions from tetrahedral symmetry occurred even when Jahn-Teller distortion was forbidden due to the presence of a non-degenerate ground state. Consequently, the degree to which the Jahn-Teller effect contributes to the rhombic distortion of $[Fe(SR)_4]^{n-}$ is unknown.

As previously mentioned, the reduced forms, $[Fe(SR)_4]^{2-}$, exhibit a d-d band in the near-IR region from 5,000 to 6,000 cm^{-1} for the $^5E \rightarrow {}^5T_2$ transition in tetrahedral symmetry (11,12,21). In addition, an intense UV band is observed at 310-330 nm with a characteristic shoulder at 340-360 nm (11,19). The oxidized forms, $[Fe(SR)_4]^{1-}$ possess

Table I-1. Selected bond lengths and angles for iron-thiolate[a] synthetic analogs of the active site of rubredoxin

Distance (Å)	$[Fe(S_2\text{-o-xyl})_2]^{1-}$	$[Fe(SC_{10}H_{13})_4]^{1-}$	$[Fe(S_2\text{-o-xyl})_2]^{2-}$
Fe-S(1)	2.265 (2)	n.r.[b]	2.378 (5)
Fe-S(2)	2.258 (2)	n.r.	2.324 (5)
Fe-S(3)	2.268 (2)	n.r.	2.347 (5)
Fe-S(4)	2.279 (2)	n.r.	2.376 (5)
average	2.268	n.r.	2.356

Distance (Å)	$[Fe(SPh)_4]^{2-}$	$[Fe(S_2C_4O_2)_2]^{2-}$
Fe-S(1)	2.359 (2)	2.379 (3)
Fe-S(2)	2.360 (2)	2.394 (3)
Fe-S(3)	2.338 (2)	2.396 (3)
Fe-S(4)	2.355 (2)	2.387 (3)
average	2.353	2.389

Angle (deg)	$[Fe(S_2\text{-o-xyl})_2]^{1-}$	$[Fe(SC_{10}H_{13})_4]^{1-}$	$[Fe(S_2\text{-o-xyl})_2]^{2-}$
S(1)-Fe-S(2)	112.60 (8)	114.4 (1)	109.1 (2)
S(1)-Fe-S(3)	105.82 (7)	107.8 (5)	108.5 (2)
S(1)-Fe-S(4)	109.35 (7)	107.8 (5)	106.9 (2)
S(2)-Fe-S(3)	111.44 (7)	114.4 (1)	103.5 (2)
S(2)-Fe-S(4)	108.49 (7)	107.8 (5)	114.9 (2)
S(3)-Fe-S(4)	109.97 (1)	107.8 (5)	113.8 (2)

[a]Thiols are abbreviated as follows: S_2-o-xyl, xylene-α,α'-dithiol; SPh, benzenethiol; $SC_{10}H_{13}$, 2,3,5,6-tetramethylbenzenethiol; $S_2C_4O_2$, dithiosquarate.

[b]Not reported.

Table I-1. (Continued)

Angle (deg)	$[Fe(SPh)_4]^{2-}$	$[Fe(S_2C_4O_2)_2]^{2-}$
S(1)-Fe-S(2)	97.89 (9)	95.57 (11)
S(1)-Fe-S(3)	119.00 (10)	124.86 (13)
S(1)-Fe-S(4)	112.67 (10)	115.11 (13)
S(2)-Fe-S(3)	111.47 (11)	112.42 (12)
S(2)-Fe-S(4)	115.27 (9)	114.23 (12)
S(3)-Fe-S(4)	101.34 (10)	95.83 (12)

bands at approximately 370 and 490 nm (22,26) which gives them a red color similar to that of oxidized rubredoxin.

Mössbauer spectroscopy has proven to be an especially useful tool in delineating the properties of iron in a tetrahedral thiolate sulfur coordination sphere. Measurements of the isomer shift and quadrupole splitting, in the absence of a magnetic field, identifies the oxidation and spin states of the iron in the sample. As expected from the magnetic moments, Mössbauer spectroscopy showed that $[Fe(SR)_4]^{2-}$ contains high spin Fe(II) and that $[Fe(SR)_4]^{1-}$ contains high spin Fe(III) (11,12,22,24,25). Selected Mössbauer parameters for several of the model compounds are listed in Table I-2. The appearance of quadrupole doublets implies deviations from strict cubic symmetry, suggesting that the distortions observed in the crystal structures remain when the anions are in frozen solution. The almost negligible dependence of the quadrupole splitting on temperature in $[Fe(SR)_4]^{2-}$ reflects an energy separation of at least 900 cm^{-1} between the two lowest orbital levels. An exception to this behavior is the $[Fe(S_2C_4O_2)_2]^{2-}$ anion, where the temperature dependence of ΔE_q gives an orbital splitting of only 400 cm^{-1}. Measurement of the Mössbauer spectrum at high temperature and high magnetic field (e.g., 150-200K, 60-80kG) provides information which can be used to determine the ground state orbital (27). The $[Fe(SR)_4]^{2-}$ species consistently have $\Delta E_q < 0$ and $\eta > 0.5$, which suggests d_z2 as the ground state orbital.

The results of the near-IR and Mössbauer spectroscopies produce a picture of the electronic energy levels of $[Fe(SR)_4]^{2-}$. Figure I-2 shows that the energy level diagrams for the Fe(II) analogs are quite similar to that of reduced rubredoxin.

The EPR properties of two $[Fe(SR)_4]^{1-}$ complexes at 77 K have been reported. $[Fe(S_2\text{-o-xyl})_2]^{1-}$ exhibits a g=4.3 signal at 77 K (22), while, the $[Fe(SC_{10}H_{13})_4]^{1-}$ ($SC_{10}H_{13}$ = 2,3,5,6-tetramethylbenzenethiol) produced a more complicated spectrum with

Table I-2. Mössbauer results for synthetic analogs of the rubredoxin iron site

Complex	δ(mm/s)[a]	ΔE_q(mm/s)[b]	D(cm^{-1})	E/D	Δ(cm^{-1})[c]	V_{zz}[d]	Ref.
$[Fe(S_2\text{-}o\text{-}xyl)_2]^{1-}$	0.13	0.57	n.r.	n.r.	n.r.	n.r.	11
$[Fe(S_2\text{-}o\text{-}xyl)_2]^{2-}$	0.61	-3.34	n.r.	n.r.	n.r.	(-)	11
$[Fe(SC_6H_5)_4]^{2-}$	0.66	-3.24	6.1	0.24	1.01	(-)	12
$[Fe(S_2C_4O_2)_2]^{2-}$	0.668	-3.97	6.6	0.27	1.37	(-)	12

[a]Spectra were recorded at 4 K. By convention the isomer shift value is reported relative to metallic iron at room temperature.

[b]Value obtained at 4 K.

[c]Energy value for the splitting of $|\pm 2\rangle$ spin state doublet.

[d]Negative sign for the value of V_{zz} indicates that d_z2 is the ground state under tetrahedral symmetry.

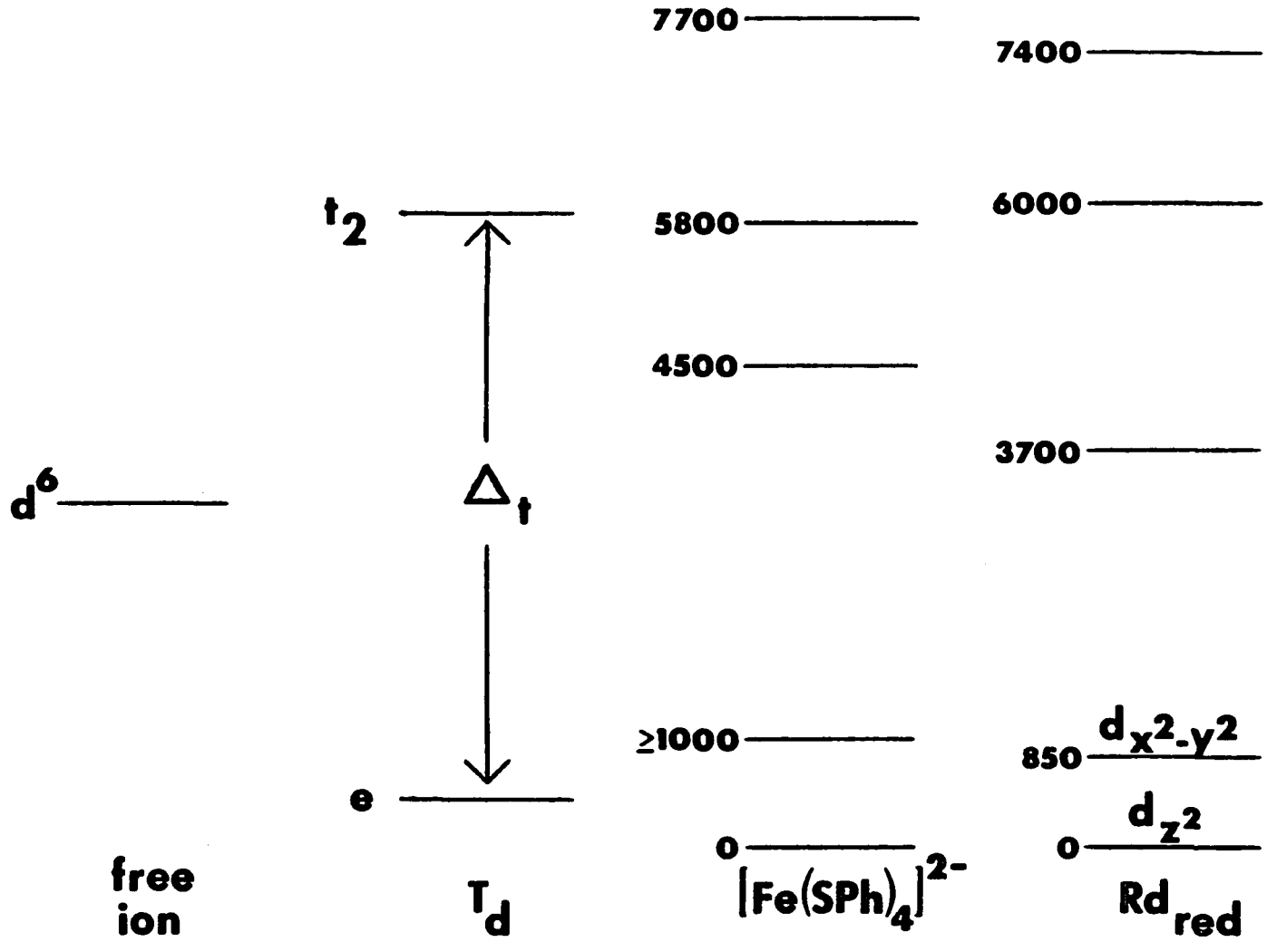

Figure I-2. Ground state electronic structures of the tetrahedral Fe(II)-S_4 units in $[Fe(SC_6H_5)_4]^{2-}$ and reduced rubredoxin (see references 12 and 28)

g values of 8.4, 5.3, and 4.3 (26).

The presence of unpaired electrons on the iron atom leads to substantial paramagnetic shifts of ligand resonances in the ^1H NMR spectra of the model complexes. The meta protons in the benzenethiolate ligand in $[Fe(SPh)_4]^{2-}$ resonate at 21-22 ppm downfield of DSS (17). For $[Fe(SEt)_4]^{2-}$ the methylene proton resonance is shifted to 196 ppm downfield with the methyl proton peak appearing 10 ppm downfield of TMS (19).

Since the iron-sulfur proteins operate as electron carriers in biology, a knowledge of the electrochemical properties of the $Fe-S_4$ unit is required to fully understand how these metalloproteins function. The redox potentials for $[Fe(SR)_4]^{1-/2-}$ with various thiolate ligands are listed in Table I-3. Bair and Goddard (29) have estimated a value of -0.52 V (vs. N.H.E.) for the reduction potential from an ab initio calculation of the ionization potential. The highly negative reduction potential values clearly describe the strong reducing power of the Fe(II) monomers. Not surprisingly, these reduced species are extremely air sensitive, especially in solution.

While small aryl- and alkylthiolates have been used successfully as the terminal ligand, a more physiologically relevant analog would have a cysteine containing peptide for the terminal ligand. Indeed, the first reported attempt to prepare a rubredoxin analog used a peptide ligand (30). Unfortunately, these iron-peptide complexes have resisted all attempts at crystallization. Consequently, there have been only a few additional reports of studies with peptide ligands.

Christou et al. (31), using dimethyl sulfoxide as the solvent, mixed ferric chloride with a 13 amino acid peptide, containing 4 cysteine residues, in dimethyl sulfoxide. When triethylamine was added, a species resembling oxidized rubredoxin was formed based on the visible absorption spectrum. Ueyama et al. (32) prepared oxidized

Table I-3. Reduction potentials for the Fe(III)/Fe(II) couple in synthetic analogs of the rubredoxin iron site

Complex	$E^{\circ\prime}$(V)[a]	Technique[b]	Reference
$[Fe(SC_2H_5)_4]^{1-/2-}$	-1.08	D.P.P	18
$[Fe(SC_{10}H_{13})_4]^{1-/2-}$	-0.85	n.r.[c]	26
$[Fe(S_2\text{-o-xyl})_2]^{1-/2-}$	-1.03	P., C.V.	11,22
$[Fe(SC_6H_5)]^{1-/2-}$	-0.53	C.V.	17
$[Fe(Z\text{-Cys-Pro-Leu-Cys-OMe})_2]^{1-/2-}$	-0.37	C.V.	33

[a]Reduction potential versus S.C.E..

[b]D.P.P., differential pulse polarography; P., polarography; C.V., cyclic voltammetry.

[c]Not reported.

rubredoxin models, using two different peptides, in an attempt to compare a monodentate peptide with a chelating bidentate peptide. Their spectroscopic results are difficult to interpret in the absence of any structural data for the complexes.

Nakata and co-workers (33) prepared Fe(II)-peptide complexes as models of the reduced rubredoxin iron site. Using the peptide Z-Cys-Pro-Leu-Cys-OMe (Z = N-carbobenzoxyl), they prepared a mononuclear complex which appeared to exhibit a reduction potential of -0.37 V (vs. S.C.E.) in 10% aqueous Triton X-100. This value is much closer to the measured redox potential in rubredoxin than had been previously obtained with other synthetic analogs in organic solvents. The positive shift of the redox potential was attributed to the higher dielectric constant of the aqueous Triton medium. The differences in redox potentials between monomeric iron-thiolate clusters in organic solvents and an aqueous medium suggests that the presence of water may be an important factor in the iron-thiolate chemistry that occurs in a living cell. Further examination of these species in aqueous media is needed to delineate any unique effects of water on the chemistry of iron-thiolate complexes.

Iron-thiolate chemistry extends beyond the mononuclear species to iron-thiolate clusters of higher nuclearity. The $[Fe_2(SR)_6]^{2-}$ and $[Fe_4(SR)_{10}]^{2-}$ anions are relevant to results presented in this thesis, and their structures are shown schematically in Figure I-3. For a more complete summary of transition metal-thiolate chemistry, the reader is directed to a recent review by Blower and Dilworth (14). $[Fe(SR)_4]^{2-}$ has been shown to equilibrate with $[Fe_4(SR)_{10}]^{2-}$ in an aqueous detergent medium (34). This latter anion is referred to as the "adamantyl" because of its structural similarity to admantane (see Figure I-3). The binuclear iron-thiolate species, $[Fe_2(SR)_6]^{2-}$, has been synthesized by Hagen and Holm (13). In CH_3OH, $[Fe_2(SR)_6]^{2-}$ is reported to equilibrate with the mononuclear and the adamantyl species according to the following reaction:

$[Fe(SR)_4]^{2-}$

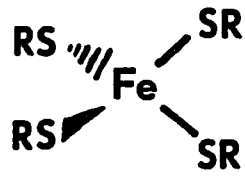

$[Fe_2(SR)_6]^{2-}$

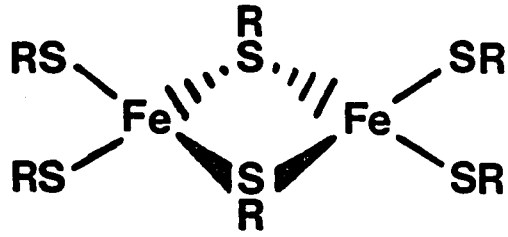

$[Fe_4(SR)_{10}]^{2-}$

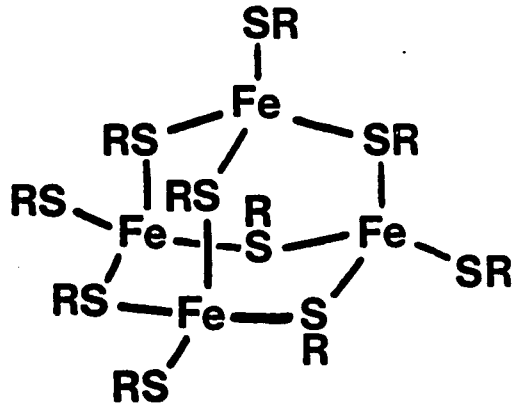

Figure I-3. Schematic diagrams of iron-alkylthiolate anions

$$3[Fe_2(SR)_6]^{2-} = 2[Fe(SR)_4]^{2-} + [Fe_4(SR)_{10}]^{2-} \quad (1)$$

Iron-Thiolate Proteins

Rubredoxin is one of the smallest known proteins (M_r=6,000), and contains one iron atom tetrahedrally coordinated by four thiolate sulfur atoms from protein cysteinyl residues (28). The active site of rubredoxin is depicted schematically in Figure I-4. The protein from Clostridium pasteurianum was first characterized by Buchanan and co-workers (35) in 1963. Rubredoxins have so far been found only in bacteria where they are believed to function as electron carriers, but in most cases their exact biological role remains unclear. A unique rubredoxin, which has two separate, identical iron sites, has been obtained from Pseudomonas oleovorans (36). This latter protein is the only rubredoxin with a well-established biological function, namely, as an electron carrier in the steroid hydroxylation pathway (36). While identification of the biological roles of rubredoxins have proceeded slowly, studies of the physical and chemical properties of this class of proteins have been very fruitful.

Oxidized rubredoxin can be readily crystallized. Its X-ray crystal structure has been refined to a resolution of 1.2 angstroms for the protein from Clostridium pasteurianum (37). The crystal structures of rubredoxins from Desulfovibrio vulgaris and Desulfovibrio gigas have both been refined to at least 2 Å resolution (38,39). All three rubredoxins have a distorted tetrahedral iron site. The iron-sulfur bond lengths are equal within experimental uncertainty but the S-Fe-S bond angles deviate significantly from equality (see Table I-4). When amino acids in the immediate vicinity of the iron are taken into account, there is a local region of pseudo C_2 symmetry.

The X-ray crystal structure also provides evidence for hydrogen bonding to the cysteine sulfur atoms. There are six probable hydrogen bonds between amide groups

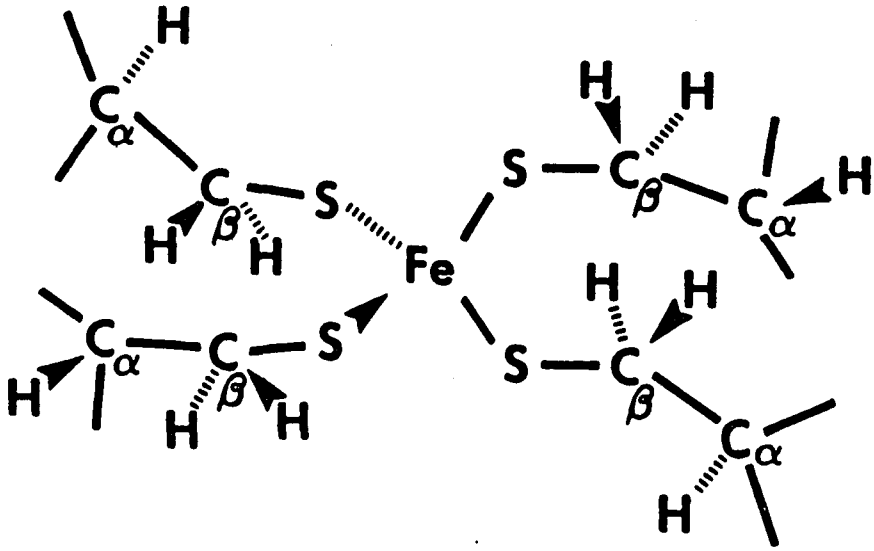

Figure I-4. Schematic diagram of the active site of the rubredoxin. The cysteinyl carbons are labeled using the standard biochemical convention

Table I-4. Bond lengths and angles for the Fe-S sites in rubredoxins

Length (A)	C.p.[a]	D.v.[b]	D.g.[c]
Fe-S6	2.33	2.24	2.31
Fe-S9	2.29	2.30	2.30
Fe-S3	2.30	2.24	2.27
Fe-S4	2.24	2.28	2.27
average	2.29	2.27	2.29
Angle (deg.)	**C.p.**	**D.v.**	**D.g.**
S6-Fe-S9	113.8	113.3	115
S6-Fe-S39	109.0	112.4	111
S6-Fe-S42	103.8	107.3	106
S9-Fe-S39	103.7	102.4	103
S9-Fe-S42	114.3	108.2	110
S39-Fe-S42	112.4	113.3	112
average	109.5	109.5	109.5

[a]Clostridium pasteurianum, 1.2 A resolution, ref. 37.

[b]Desulfovibrio vulgaris, 2 A resolution, ref. 38.

[c]Desulfovibrio gigas, 1.4 A resolution, ref. 39.

from the peptide backbone and electron lone pairs on the thiolate sulfur atoms. The proposed hydrogen bonding pattern is depicted in Figure I-5. Adman and co-workers have implicated hydrogen bonds as an important factor modulating the reduction potential of an iron-sulfur cluster (9). The presence of these hydrogen bonds may account for some of the observed discrepancy between the reduction potentials of the synthetic analogs and rubredoxin.

The iron site of the protein has been well characterized by a variety of physical techniques. Mössbauer spectroscopy and magnetic susceptibility have been utilized to determine the oxidation and spin states of the iron atom (40-42). Reduced rubredoxin contains high spin Fe(II), while the oxidized protein has high spin Fe(III). The sign of ΔE_q is negative, which indicates that d_z2 is the ground state orbital (27,43). The magnetic susceptibility exhibits Curie behavior over the temperature range 5 °C to 60 °C (40).

Oxidized rubredoxin is deep red in color due to a $^6A_1 \rightarrow {}^6T_2$ transition at 490 nm (28,44), whereas, the reduced form is colorless (see Figure I-6). Detailed study of the electronic transitions of the oxidized protein by near-IR, CD, and MCD spectroscopies led to an energy level diagram (Figure I-2) which is most consistent with a tetragonally distorted iron site with pseudo-D_{2d} symmetry (28).

Further support for the distorted tetrahedral symmetry is provided by Mössbauer and EPR spectroscopies. The Mössbauer spectra exhibit large quadrupole splitting values for both oxidation states, which are indicative of distortion from tetrahedral symmetry (40-42). The results of Mössbauer studies of rubredoxin and desulforedoxin for both oxidation states are listed in Table I-5. The zero-field splitting parameter ratio, E/D, obtained from EPR spectroscopy, has a value of 0.28 for oxidized rubredoxin (28). This relatively high E/D ratio is consistent with a significant rhombic distortion from T_d

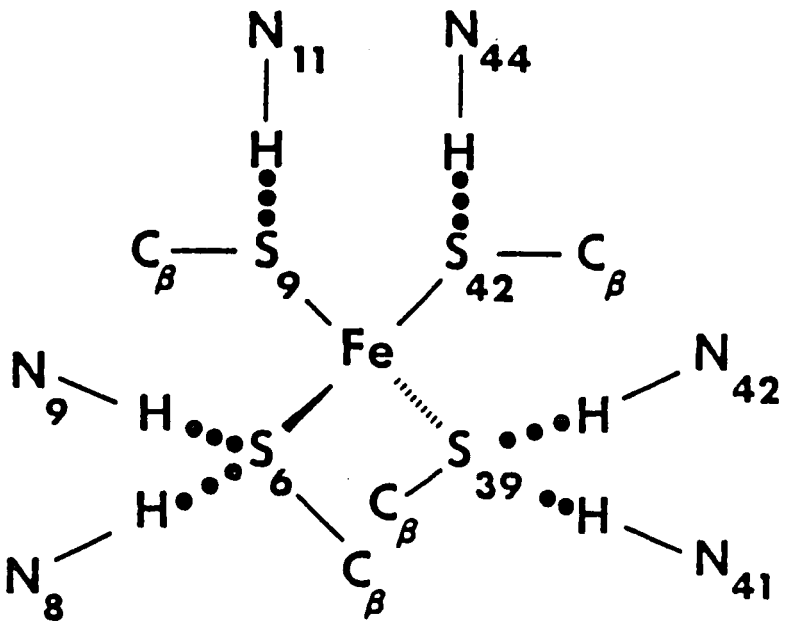

Figure I-5. Schematic diagram depicting the N-H··S hydrogen bonding pattern based on the 1.2 Å X-ray crystal structure of C. pasteurianum rubredoxin

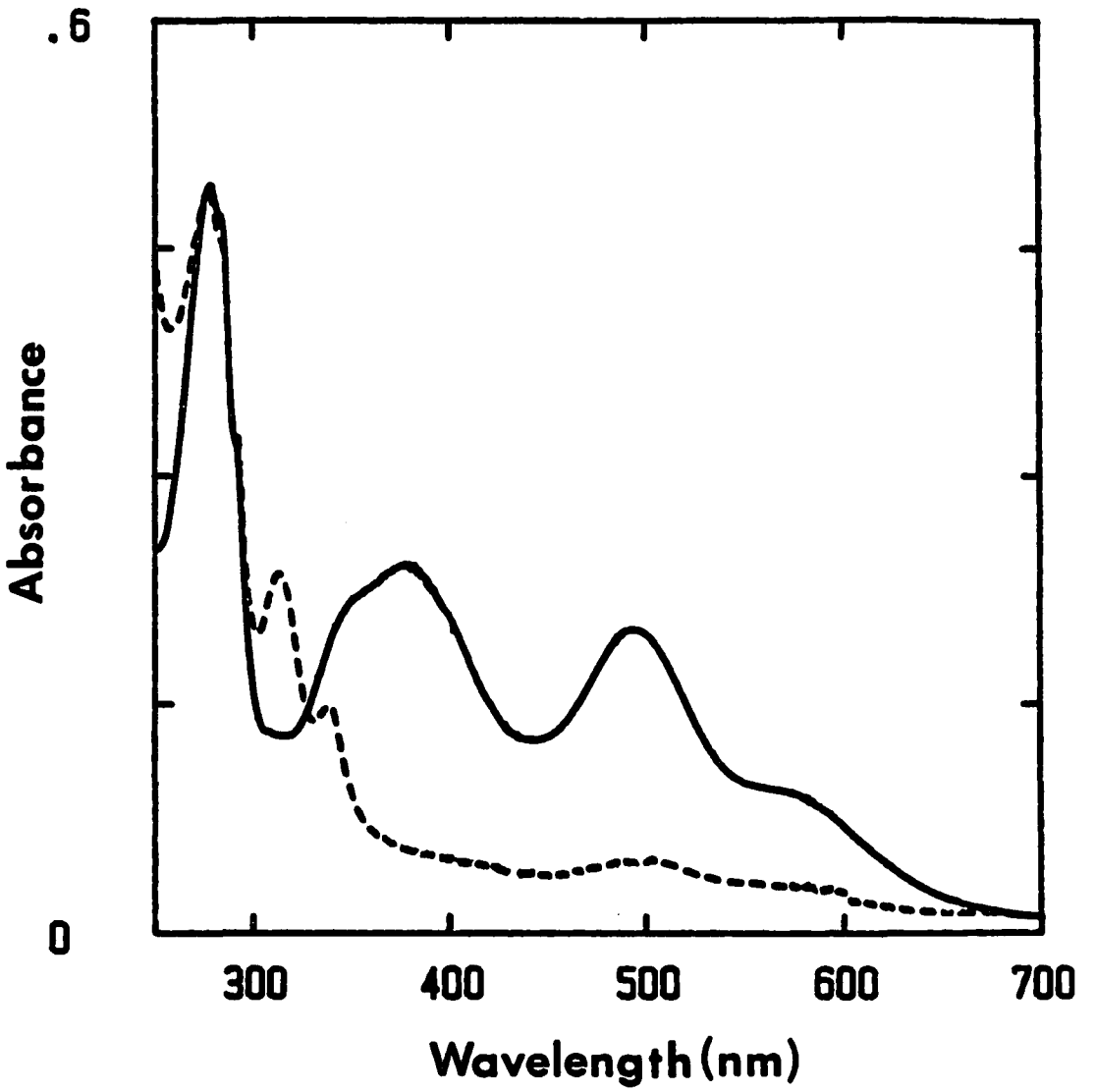

Figure I-6. UV-visible spectra of D. gigas rubredoxin. Solid line represents the oxidized form. Dashed line represents ~80% reduction

Table I-5. Mössbauer parameters for the proteins rubredoxin and desulforedoxin[a]

	Rubredoxin		Desulforedoxin	
parameter	oxidized	reduced	oxidized	reduced
δ (mm/s)	0.32	0.70	0.25	0.70
ΔE_q (mm/s)	-0.50	-3.25	-0.75	3.55
D (cm^{-1})	1.9	7.63	2.2	-6
E/D	0.23	0.28	0.080	0.19
Δ (cm^{-1})[b]	n.a.[c]	1.70	n.a.	0.63
V_{zz}[d]	n.r.[e]	(-)	n.r.	(+)
asymmetry	0.2	0.65	0.6	0.35
A_{xx}	-165	-201	-154	-200
A_{yy}	-159	-83	-154	-200
A_{zz}	-169	-301	-154	-67

[a]Refs. 43 and 49.

[b]Energy splitting of the $|\pm 2\rangle$ spin state doublet.

[c]Not applicable.

[d]The sign of V_{zz} under T_d symmetry determines the ground state orbital. Negative sign indicates d_z2 is the ground state orbital; positive sign indicates d_{x2-y2} is the ground state orbital. See reference 27.

[e]Not reported.

symmetry (46).

The initial report of the resonance Raman spectrum of oxidized rubredoxin (47) described the iron site as being tetrahedral by analogy with the resonance Raman spectrum of the tetrachloroferrate anion $[FeCl_4]^{1-}$. Recently, the resonance Raman spectrum of oxidized rubredoxin was reexamined (48,49) using a higher resolution spectrometer. Some of the single vibrational bands in the original spectrum were resolved into pairs of overlapping bands. Detailed analysis of the higher resolution spectrum indicated a substantial contribution from the S-C-C bending mode to the Fe-S frequencies. The best correlation between the observed and calculated spectra occurred when two pairs of Fe-S-C-C dihedral angles, having values of 90 and 180 degrees, were used in the calculations. The X-ray crystal structure of the iron site in the protein contains pairs of Fe-S-C-C dihedral angles at 90 and 180 degrees arranged around a pseudo C_2 axis (37). Thus, the resonance Raman spectral data are also consistent with an approximate D_{2d} distortion of the tetrahedral iron site.

The ^1H NMR spectrum of rubredoxin was first reported in 1970 by Phillips and co-workers (40). A 6 mM solution of reduced rubredoxin isolated from C. pasteurianum produced a rich spectrum from -1 to 10 ppm containing all the protein diamagnetic resonances. Using a wider sweep width, they searched from -27.5 to +40 ppm for possible paramagnetically shifted resonances arising from interactions with the iron atom. They detected three peaks located from -2 to -6 ppm upfield from DSS, which they attributed to effects of the unpaired electrons on the iron atom. The chemical shifts of the three upfield resonances displayed a reciprocal dependence on temperature from 5 to 65 °C, proportional to the Curie behavior of the magnetic susceptibility over the same temperature range. These authors stated only that these resonances arose from hydrogen atoms located close to the iron atom. The ^1H NMR spectrum of the

oxidized rubredoxin was less clearly resolved and lacked any sign of paramagnetically shifted resonances appearing in the ±30 ppm sweep width used in their experiments. The β-CH_2 protons of the cysteinyl amino acid residues are closest to the iron (not including hydrogen bonded protons). However, Phillips and co-workers argued that the signals for these hydrogens may have been broadened into the baseline due to their proximity to the iron. They also pointed out that the assignment of upfield paramagnetic shifts for the cysteinate ligands was inconsistent with the previous observation of downfield paramagnetic shifts for hydrogens on cysteinate ligands to the iron-sulfur clusters in ferredoxins. This study remained for over 15 years the only report in the literature describing the ^1H NMR spectrum of rubredoxin.

In 1986, Krishnamoorthi and co-workers (50) reexamined the ^1H NMR spectrum of C. pasteurianum rubredoxin using a 470 MHz FT-NMR spectrometer. Three new downfield resonances were found in the spectra of both reduced and oxidized rubredoxin. The new peaks appeared between 8 and 11 ppm. No other new peaks were observed from -120 to 130 ppm. Krishnamoorthi and co-workers assigned resonances to the β-CH_2 and α-CH hydrogens of the cysteinate ligands based on the following arguments. They assumed that no peaks remained undetected for the reduced rubredoxin sample. Obviously, the cysteinate ligand hydrogens would be the most paramagnetically shifted, implying to these authors that the previously reported upfield resonances (-2 to -5 ppm) and the newly discovered downfield resonances (8 to 10 ppm) belonged to the α-CH and β-CH_2 hydrogens of the cysteinate ligands. The upfield resonances were broader than the downfield resonances and the relative area of the upfield set was twice that of the downfield set. Based on these criteria, they assigned the upfield set to the β-CH_2 hydrogens and the downfield set to the α-CH hydrogens. The authors commented on the relatively small magnitude of the paramagnetic contact shifts found

for rubredoxin (upper limit 7 ppm) compared to the larger contact shifts observed for the ferredoxins (upper limit 130 ppm).

The assignments by Krishnamoorthi et al. for the β-CH_2 cysteinyl hydrogens in rubredoxin are inconsistent with the large downfield chemical shift observed for similar hydrogens in synthetic model complexes. For this reason, the ^1H NMR spectra of rubredoxin deserve reexamination.

Desulforedoxin provides another example of a protein containing iron which is apparently tetrahedrally coordinated by thiolate sulfur. Found in the sulfate reducing bacterium Desulfovibrio gigas, desulforedoxin is a small non-heme iron protein (M_r=7900) composed of two identical subunits (51). Each subunit contains one iron atom and four cysteine residues. The primary amino acid sequence of desulforedoxin (52) differs from that of rubredoxin in one significant respect. In the rubredoxins, there is a recurring pattern of pairs of cysteine residues which are usually separated by two intervening residues (2,53). In desulforedoxin the first pair of Cys residues are separated by two intervening residues, but the second pair of Cys residues are adjacent to each other in the polypeptide chain. Unfortunately, the crystal structure of desulforedoxin has not been solved. Therefore, it is not yet known whether or not the adjacent placement of Cys residues produces any large structural deviations from that of the rubredoxin iron site.

The iron sites in ferric desulforedoxin have been characterized by UV-visible and EPR spectroscopies (43,54). The UV-visible spectrum of desulforedoxin is similar, but not identical, to the UV-visible spectrum of rubredoxin. By simulation of the EPR spectrum for oxidized desulforedoxin a value of 0.08 is obtained for the zero-field rhombicity parameter, E/D. This value is consistent with an iron site of close to axial magnetic symmetry, which is in contrast to the distinctly rhombic magnetic symmetry

exhibited by the oxidized rubredoxin iron site.

Results of the Mössbauer study of desulforedoxin are listed in Table I-5. The sign of the zero-field splitting parameter D is opposite to that found for rubredoxin. The sign of ΔE_q is positive, indicating that $d_{x^2-y^2}$ rather than d_{z^2} is the ground state orbital (27) in desulforedoxin. Based on EPR and Mössbauer spectroscopic evidence, the two iron atoms in desulforedoxin are found in identical, non-interacting mononuclear sites (43).

By most measures rubredoxin and desulforedoxin are well characterized metalloproteins. The similarities between the properties of the metal sites in these two proteins and their synthetic analogs are striking. However, there are still inconsistencies remaining to be resolved. These include the differences in the redox potentials and in the ^1H NMR spectra of the cysteinyl hydrogens.

Reactions of Iron-Thiolate Complexes with sulfur

Sugiura and co-workers (55) studied the reaction of various iron-dithiolate species formed in solution with sodium sulfide. Alkanedithiols complexed with Fe(III), when reacted with sulfide, produced electronic absorption spectra similar to that of the [2Fe2S] ferredoxins. However, if a hydroxylated alkyldithiol, e.g., dithiothreitol, was used, the resulting spectrum more closely resembled that of a [4Fe4S] ferredoxin. This result implied that the nature of the thiolate ligand played a role in determining which cluster is produced. However, the true nature of the clusters produced by Sugiura and co-workers remains in doubt, since no compounds were isolated.

The first unambiguous analogs of the iron-sulfur clusters in the ferredoxins came out of the laboratory of Professor R. H. Holm in the early seventies (56-58). The synthesis of the [4Fe4S] ferredoxin analog was performed in two stages (57). In the

first stage, the reaction of ferric chloride with 3 equivalents of a sodium thiolate in methanol produced an insoluble dark green solid. The green solid was assumed to be a polymeric iron-thiolate, when analysis revealed a 3:1 thiol to iron stoichiometry. Upon addition of a solution of NaHS and NaOMe in methanol a dark brown color formed as the solid reacted. The $[Fe_4S_4(SR)_4]^{2-}$ cluster was readily isolated from these solutions as a crystalline solid by addition of a tetraalkylammonium salt.

The initial synthesis of the [2Fe2S] ferredoxin analog, used o-xylene-α,α'-dithiol (S_2-o-xyl) instead of a monothiol (58). Once again, the first stage of the synthesis involved the mixing of 2 equivalents of sodium methoxide and dithiol with 1 equivalent of iron(III) chloride in methanol. The iron-sulfur cluster formed when a methanolic solution of sodium methoxide/sodium hydrosulfide was added.

It was not until 1977, when Cambray and co-workers reported the reaction of the rubredoxin analog, $[Fe(S_2\text{-o-xyl})_2]^{2-}$, with sulfur to produce $[Fe_2S_2(S_2\text{-o-xyl})_2]^{2-}$ that the synthesis of an iron-sulfur cluster from a discrete iron-thiolate complex was clearly demonstrated (15). Two years later, Coucouvanis and co-workers (16) reacted $[Fe(SPh)_4]^{2-}$ with various trisulfides to produce $[Fe_2S_2(SR)_4]^{2-}$.

The biological relevance of iron-thiolate intermediates to the <u>in vivo</u> assembly of iron-sulfur clusters in proteins was first suggested by the formation in solution of a metastable complex between Fe(III) and apoadrenodoxin, a [2Fe2S] iron-sulfur protein (59). Experimental evidence indicated that the intermediate could be formulated as a Fe(III)-Cys_4 unit. Reaction of the metastable iron/apoadrenodoxin species with sulfide produced a 50% yield of native adrenodoxin. Cristou and co-workers (31) were able to react a rubredoxin-like iron-peptide complex with sodium sulfide to produce a [4Fe4S] cluster. Remarking on the similarity between the synthetic reaction of the $[Fe(SR)_4]^{2-}$ to give $[Fe_2S_2(SR)_4]^{2-}$ and the proposed reconstitution pathway for adrenodoxin,

Cambray and co-workers (15) suggested that further study of the reactions of iron-thiolates with inorganic sulfur could provide insights into the pathway by which iron-sulfur clusters are assembled in proteins.

In the early eighties, Hagen and co-workers (17-19) described the assembly pathways to several iron-sulfur clusters starting from $[Fe(SR)_4]^{2-}$ or $[Fe_4(SR)_{10}]^{2-}$. In the initial reactions, a simple iron salt was converted to an iron-thiolate complex. This complex was then reacted with elemental sulfur to produce a variety of iron-sulfur clusters depending on the reaction conditions. The reaction of $[Fe(SR)_4]^{2-}$ with sulfur to give $[Fe_2S_2(SR)_4]^{2-}$ was shown to be a general reaction for a range of terminal thiolate ligands (Figure I-7). $[Fe_4S_4(SR)_4]^{2-}$ was readily obtained by three different routes: (i) reaction of $[Fe_4(SR)_{10}]^{2-}$ with sulfur, (ii) dimerization of two $[Fe_2S_2(SR)_4]^{2-}$ clusters, (iii) the addition of Fe(II) to the "linear" $[Fe_3S_4(SR)_4]^{3-}$ cluster. The results of these studies are summarized in Figures I-7 and I-8. This work clearly demonstrated the chemical relationships between the iron-thiolate and iron-sulfur clusters. As the authors pointed out, these observations were based on reaction systems at equilibrium, i.e., the pathways shown in Figure I-7 include only those species which could be independently synthesized.

More recently, Stevens and Kurtz (34) and Kurtz and Stevens (60) have examined the $FeCl_3$/PhSH/S system in aqueous media in an effort to determine how these species behave in an environment that may more closely approximate that of a living cell. In order to achieve a homogenous reaction mixture, the non-ionic detergent Triton X-100 was included. They found that the iron-thiolate complexes, $[Fe(SPh)_4]^{2-}$ and $[Fe_4(SPh)_{10}]^{2-}$, could be formed in aqueous media. They were further able to show that a facile equilibrium existed between the two anions in water.

$$4[Fe(SR)_4]^{2-} \rightleftharpoons [Fe_4(SR)_{10}]^{2-} + 6RS^- \qquad (2)$$

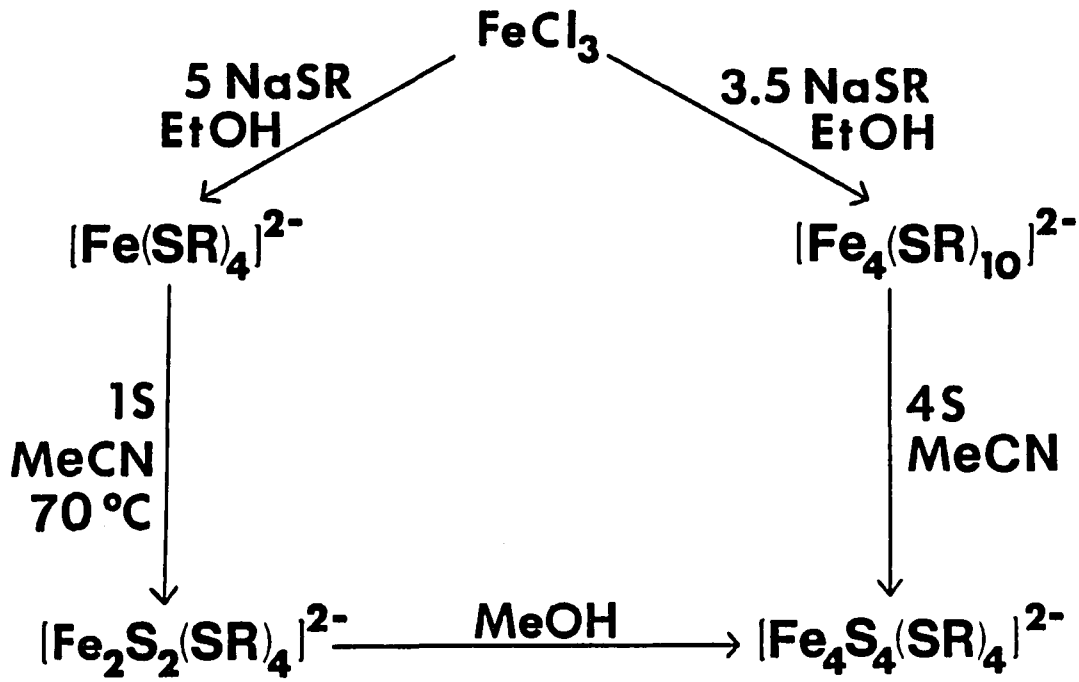

Figure I-7. Reaction scheme presented by Hagen and co-workers (17) describing two pathways for the production of $[Fe_4S_4(SR)_4]^{2-}$ (R = C_6H_5) from $FeCl_3$ in organic solvents

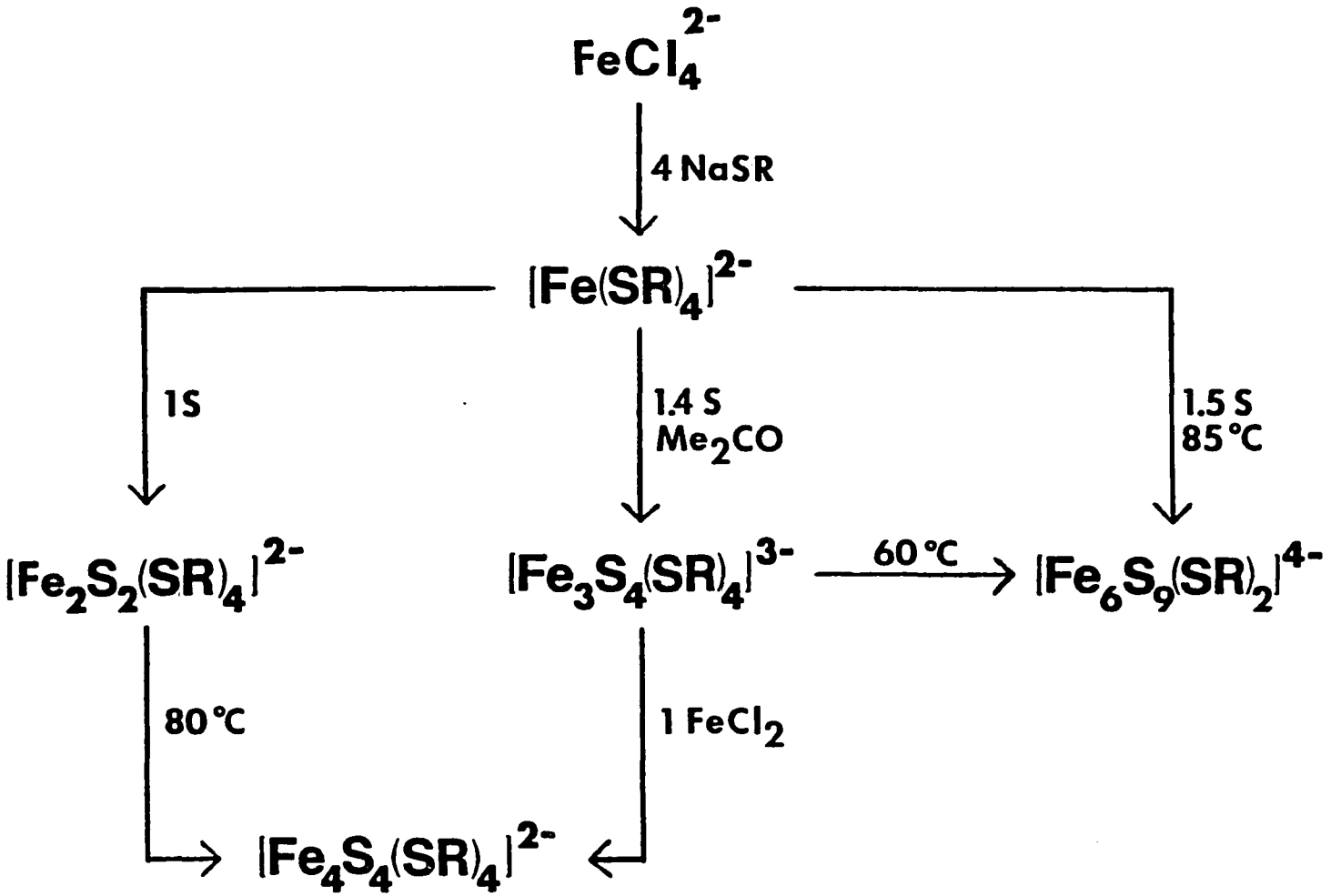

Figure I-8. Reaction scheme presented by Hagen and co-workers (19) describing the synthesis of several iron-sulfur clusters from the reaction of $[Fe(SR)_4]^{2-}$ ($R = C_2H_5$) with sulfur under various conditions. The solvent was MeCN, except where noted

The position of this equilibrium was found to be dependent on pH, thiol/Fe ratio and, when present, the nature of the tetraalkylammonium cation. No evidence was found for a presumed intermediate, namely, $[Fe_2(SR)_6]^{2-}$ in the above equilibrium. Addition of elemental sulfur to the aqueous iron-thiolate solutions led to the formation of the $[Fe_nS_n(SPh)_4]^{2-}$ (n=2,4) clusters. By appropriate adjustment of conditions, either the n=2 or n=4 cluster could be obtained in essentially quantitative yield from the same $4PhS^-/FeCl_3/S$ reagent system. This work demonstrated for the first time that these hydrolytically unstable clusters could indeed be assembled in an aqueous medium. Figure I-9 summarizes their results. As can be seen, the reaction sequences observed by Stevens and Kurtz in an aqueous detergent medium are fully consistent with those observed in Professor Holm's laboratory (17,19).

In addition, Stevens and Kurtz were able to characterize the effects of pH, detergent micelles and tetraalkylammonium cations on various steps in the assembly process. In aqueous media the optimum pH for cluster assembly is 7-8 (34). Near pH 8 in the presence of Triton the production of $[Fe_4S_4(SR)_4]^{2-}$ occurs almost exclusively via the $[Fe(SR)_4]^{2-} \rightarrow [Fe_2S_2(SR)_4]^{2-}$ pathway. Significant cluster assembly occurs even when the pH is below the pK_a of the thiol. The $[Fe(SR)_4]^{2-}/[Fe_4(SR)_{10}]^{2-}$ equilibrium shifts towards the formation of $[Fe_4S_4(SR)_4]^{2-}$ as the pH is lowered. On addition of sulfur at lower pH, the production of $[Fe_4S_4(SR)_4]^{2-}$ is favored due to the higher initial concentration of $[Fe_4(SR)_{10}]^{2-}$.

Cambray and co-workers demonstrated that $[Fe_2S_2(SR)_4]^{2-}$ spontaneously converts to $[Fe_4S_4(SR)_4]^{2-}$ in protic solvents (15). However, by combining the effects of detergent micelles with large tetraalkylammonium cations, Stevens and Kurtz (34) were able to effectively trap $[Fe_2S_2(SR)_4]^{2-}$ from water. If the cation was not included at the start of the reaction, the final product contained only $[Fe_4S_4(SR)_4]^{2-}$. In the

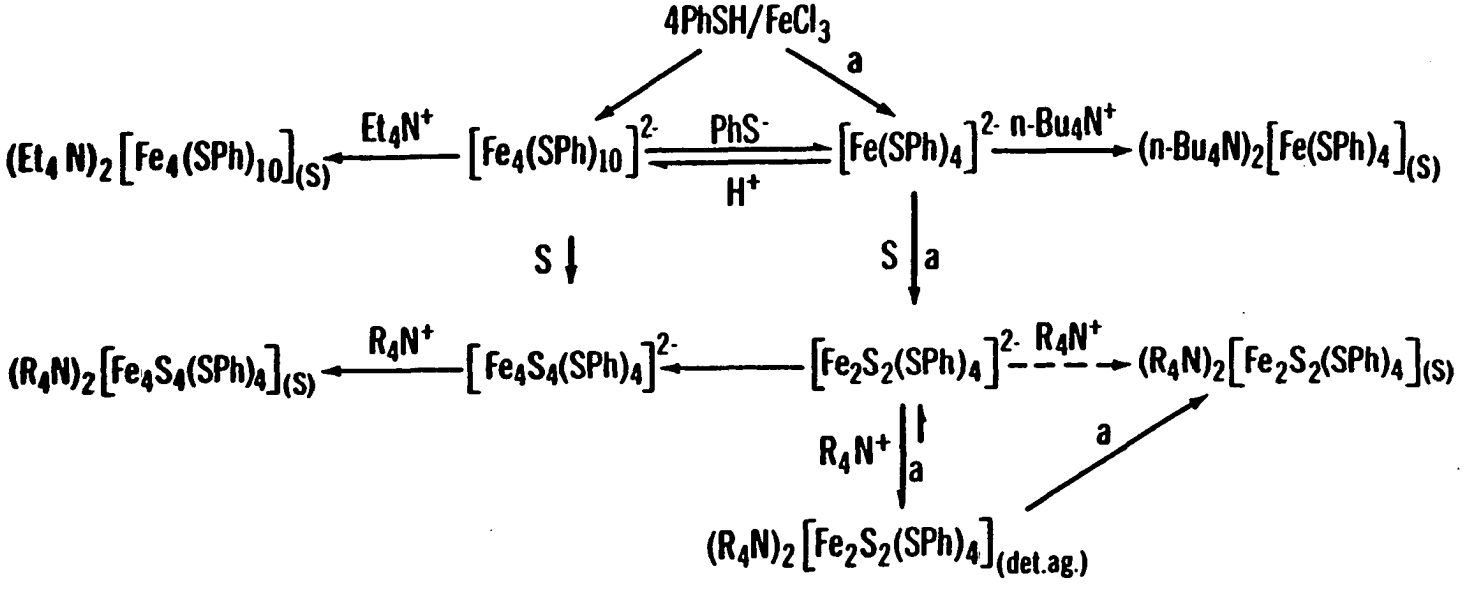

Figure I-9. Schematic diagram of cluster assembly pathways and effects thereon for 4/1/1 PhSH/$FeCl_3$/S in aqueous media (see ref. 34). Relative lengths of arrows upon reaction with S are meant to show qualitatively that pathways containing $[Fe(SPh)_4]^{2-}$ to $[Fe_2S_2(SPh)_4]^{2-}$ are favored. The dashed arrow refers to a pathway followed mainly in nondetergent media. det. ag. = detergent aggregate. The pathway marked "a" appears to be followed exclusively in 90/5/5 buffer/Triton/CH_3CN when R_4N+ = n-Pe_4N+

absence of Triton X-100, the effectiveness of the large tetraalkylammonium cations in trapping $[Fe_2S_2(SR)_4]^{2-}$ was greatly diminished.

The spontaneous self-assembly of the iron-sulfur clusters indicates that enzymes are not absolutely required for the assembly of these clusters in proteins (17). The biologically preferred pathway for cluster assembly appears to be $[Fe(SR)_4]^{2-} \rightarrow [Fe_2S_2(SR)_4]^{2-} \rightarrow [Fe_4S_4(SR)_4]^{2-}$. Pathways involving other iron-thiolate complexes are less biologically plausible, because the iron-sulfur proteins commonly contain only the 4 Cys residues required for the active site. Presumably, once the cluster assembly process is initiated, the chemistry proceeds in the direction of $[Fe_4S_4(SR)_4]^{2-}$, which is the most thermodynamically stable species in aqueous media (34). The apoprotein then selects the appropriate cluster from the pathway by some unknown mechanism (17).

The work of Stevens and Kurtz demonstrated the feasibility of studying iron-sulfur-thiolate chemistry in aqueous media. Further exploration of this chemistry in water may provide insights into how the iron-sulfur clusters are assembled in proteins.

Statement of the Problem

Our current knowledge of the bioinorganic chemistry of iron-sulfur proteins is the product of two different fields of research. The first field is biochemical studies performed directly on the proteins. The second field is the study of synthetic chemical analogs under what are often non-physiological conditions. The approach that will be taken in this work is to perform well-defined chemical and physical studies under what should be more physiologically relevant conditions. Therefore, the experiments reported here have been performed almost exclusively in 100% aqueous media.

The simplest iron-sulfur cluster is the $Fe\text{-}(SR)_4$ site found in rubredoxin and desulforedoxin. The synthesis of mononuclear iron(II) complexes with a wide variety of

water-soluble alkylthiolate ligands will be attempted. The basic chemical and physical properties of these complexes in aqueous media will be determined. It is hoped that studies of well-characterized mononuclear analogs in aqueous media will provide a basis for determining the complex effects of the protein on the metal site properties.

For example, the ^1H NMR spectra of mono- and dithiol Fe(II) complexes will be compared with the ^1H NMR of the proteins, rubredoxin and desulforedoxin. These experiments should resolve the contradiction in the literature concerning the assignment of the α-CH and β-CH_2 cysteinyl hydrogen resonances. Hopefully, more detailed analysis and comparison of these spectra will lead to a better understanding of the ^1H NMR spectra of the iron-sulfur proteins.

The preparation of water-soluble iron-alkylthiolate complexes presents a unique opportunity to examine the chemistry involved in the assembly of the [4Fe4S] cluster under physiological conditions. The eventual goal of such studies would be to make direct comparisons between the assembly of the synthetic analog and the assembly of the same cluster in the protein. These comparisons may provide a means for elucidating the specific effects of the apoprotein on the assembly process.

II. EXPERIMENTAL

General Procedures

All of the synthetic inorganic chemistry was performed under an atmosphere of argon at room temperature. The vacuum/argon apparatus has been previously described (61). Argon was passed through a column of reduced BASF catalyst R3-11 to further lower the concentration of residual oxygen present in the system. Anaerobic manipulations were accomplished by the use of standard inert-atmosphere techniques (62). Solvents and solutions were typically degassed by four or five cycles of vacuum and argon. Highly volatile solvents were freed of oxygen by bubbling with argon for 20 minutes. Solvents and solutions were transferred anaerobically using stainless steel 18 gauge cannulas. Synthetic reactions were performed in standard-taper round-bottom flasks equipped with stopcock sidearms, and products were isolated using additional pieces of Schlenk-type glassware. Often, the solids were briefly exposed to air without ill-effects during weighing or transferring. In some cases, however, it was essential that these manipulations be carried out in an argon-filled glove bag. These latter cases are specifically noted. Solids were stored under argon in standard-taper capped tubes with stopcock sidearms or in flame-sealed ampules. Elemental analyses were performed by Schwarzkopf Microanalytical Labs, Inc.

Solution samples for physical measurements were prepared under an argon atmosphere in septum-capped vials. Solutions were transferred to septum-capped argon-filled sample holders using gas-tight syringes.

The following general procedure was used to prepare solutions of the Fe(II)/alkylthiolate mononuclear complexes. The thiol was dissolved in the desired solvent under argon with sufficient base to achieve the desired ratio of deprotonated

thiolate groups to Fe(II). The calculation of the amount of base required included the amount of extra base required to deprotonate ligand carboxylate groups in the cases of glutathione and dihydrolipoate. LiOH was the base of choice for these experiments because solid LiOH is not hygroscopic and can, therefore, be weighed accurately in small amounts. Iron was then added as the solid ferrous salt. This basic procedure was modified to accommodate the particular experimental requirements. For example, the protocol for the aqueous ^1H NMR experiments was: solvent, D_2O; sufficient LiOH to deprotonate the thiolate group; thiol/Fe(II) ratio, 4/1; iron salt, $FeCl_2$; iron concentration, 20 mM. Specific details concerning the sample preparation for a given experiment are presented in the figure legends.

Preparation of Compounds

$Ba[Fe(SCH_2CH_2OH)_4]$. To 50 mL of water were added in order 6.42 g (20.4 mmol) $Ba(OH)_2 \cdot 8H_2O$, 7.1 mL (100 mmol) 2-mercaptoethanol, and 2.79 g (10.0 mmol) $Fe(SO_4) \cdot 7H_2O$. The heterogenous reaction mixture was stirred for 75 min. When the stirring was stopped a white solid (presumably $BaSO_4$) settled from the yellow supernatant. This dark yellow solution contained $[Fe(SCH_2CH_2OH)_4]^{2-}$, which is extremely air-sensitive. In order to preclude the slight exposure of the solution to air which sometimes occurs when Schlenk-type filter frits are used, the solution was not filtered. Instead, the top 20-30 mL of supernatant was transferred via cannula to another flask. The transferred solution was then concentrated by removal of the solvent in vacuo until it started to thicken into an oil. Slow addition of roughly 8 volumes of acetone with stirring eventually produced the sudden precipitation of off-white crystals and some small pieces of a red solid. The red solid disappeared as the solvent was removed, leaving light tan crystals. The crystals were washed with

methanol and thoroughly dried. The solid was collected from the flask and transferred to ampules in an argon filled glove bag. Anal. Calcd. for $C_8H_{20}O_4BaFeS_4$: C, 19.15; H, 4.02; Ba, 27.38; Fe, 11.13; S, 25.56. Found: C, 19.28; H, 4.12; Ba, 27.60; Fe, 11.11; S, 25.94.

$(n\text{-}Pr_4N)_2[Fe_4S_4(SCH_2CH_2OH)_4]$. Two equally successful methods were found for preparation of $(Pr_4N)_2[Fe_4S_4(SCH_2CH_2OH)_4]$ in water from iron salts, 2-mercaptoethanol and sulfur.

Method a. To 0.61 g (3.8 mmol) of $FeCl_3$ in 10 mL of CH_3CN was added 1.6 mL (22.7 mmol) of 2-mercaptoethanol. After 30 min. of stirring the transparent green solution was transferred to a stirred mixture of 150 mL of aqueous 0.2 M Tris-sulfate (pH 9.1) and 0.12 g (3.9 mmol) of sulfur. After 6-8 h of stirring, the dark green-brown solution was filtered through a Celite pad and 1.0 g (3.8 mmol) $n\text{-}Pr_4Br$ was added. Overnight storage at 4 °C resulted in black needlelike crystals in a pale red-brown solution. The pH at this point was 7.9. The crystals were collected by filtration, washed with isopropyl alcohol and ether, and dried in vacuo. The yield was 0.65-0.70 g (65-70%). Anal. Calcd. for $C_{32}H_{76}N_2O_4Fe_4S_4$: C, 37.21; H, 7.36; N, 2.72. Found: C, 37.26; H, 7.30; N, 2.77.

Method b. To 160 mL of 0.20 M Tris-sulfate (pH 9.1) were added in order 0.13 g (4.0 mmol) sulfur, 1.8 mL (25 mmol) 2-mercaptoethanol, and 0.49 g (3.9 mmol) of $FeCl_2$. After 4-6 h of stirring the reaction mixture was filtered through a Celite pad and 1.1 g (4.0 mmol) of $n\text{-}Pr_4NBr$ was added. Subsequent work-up was the same as used in method a. Yields of 65-70% of pure material were obtained. Anal. Found: C, 37.19; H, 7.26; N, 2.59. Comparable yields were obtained when 0.1 M LiOH was substituted for buffer. The ^1H NMR spectrum in $Me_2SO\text{-}d_6$ provided a good criterion of analytical purity. The ratios of integrated areas of the resonances at δ 12.4 ($FeSC\underline{H}_2CH_2OH$), 1.6

($NCH_2C\underline{H}_2CH_3$), and 0.9 ($NCH_2CH_2C\underline{H}_3$) ppm were found to be 1 : 2.0(±0.1) : 3.0(±0.1) for analytically pure material.

Solvents

Distilled water was passed through with a Millipore water purification system to remove ions and reduce organic contamination. Organic solvents were used without further purification. Deuterated H_2O and organic solvents were commonly obtained from Aldrich. Deuterated organic solvents were stored over 3 A molecular sieves to reduce the intensity of the residual HDO resonance.

Reagents

Solid NaHS was provided by Ms. Gudrun Lukat. Dihydrolipoic acid (Aldrich) was prepared by reducing the oxidized compound, usually at ~1 M, dissolved in H_2O and adjusted to pH 10 with NaOH, with a 20 fold molar excess of sodium borohydride. After 20 min at room temperature, excess reductant was destroyed by careful acidification with 6 M sulfuric acid under a stream of Ar. Finally, the solution was brought to pH 9.1 with solid Tris base. The concentrations of dihydrolipoate and of solutions of sodium sulfide (from reagent grade $Na_2S{\cdot}9H_2O$ or NaHS (63)) were determined with dithiobis(nitrobenzoate) (64). For some of the experiments Clostridium pasteurianum ferredoxin and bovine liver rhodanese (type II) were purchased from Sigma Chemical Company.

Isolation and Purification of Proteins

The purity of an iron-sulfur protein sample was determined by measuring the absorbance ratio between the protein band at 275-280 nm and a visible metal chromophore band (Table II-1). Protein concentrations were routinely obtained by measurement of the absorbance of the iron-site chromophore in the visible region and the use of published extinction coefficients (Table II-1). These methods were considered to be sufficiently accurate because these proteins have been well characterized.

Rubredoxins from Desulfovibrio gigas and Desulfovibrio vulgaris and desulforedoxin from D. gigas were isolated as previously described (51,65). These proteins were purified by Dr. Isabel Moura and co-workers in the laboratory of Professor Jean LeGall, University of Georgia. Drs. Larry Stults and T. Vance Morgan provided crude protein solutions which contained both Clostridium pasteurianum rubredoxin and ferredoxin. These proteins were further purified by ion-exchange chromatography. Spinach ferredoxin was isolated using the method of Petering and Palmer (66), using the RNA-ase treatment suggested by Meyer and co-workers (67). Rhodanese, isolated from bovine liver according to a published procedure (68), was provided by Professor Franco Bonomi of the University of Milan, Italy.

Samples of proteins recovered from NMR and EPR tubes were repurified by absorption on a DEAE (or Pharmacia Mono Q) anion-exchange column in 50 mM Tris-chloride pH 7.5 and elution with a 100-500 mM NaCl gradient. In the case of samples which showed significant deterioration, an excess of 2-mercaptoethanol and ferrous sulfate were added in an attempt to reconstitute any apoprotein that was present.

Apoferredoxins were prepared by the treatment of ferredoxin solutions (2-4 mg/mL) with concentrated HCl under argon which resulted in the precipitation of the

Table II-1. Extinction coefficients ($M^{-1}cm^{-1}$) for selected iron-sulfur proteins

Protein	Iron band[a]	Protein band[b]	Purity Index[c]	Reference
C.p. rubredoxin	ϵ_{490} = 8,850	ϵ_{280} = 21,300	2.41	23
D.g. rubredoxin	ϵ_{493} = 6,966	ϵ_{278} = 17,210	2.4	51
D.g. desulforedoxin	ϵ_{507} = 7,029	ϵ_{278} = 9,934	1.41	51
Spinach ferredoxin	ϵ_{422} = 9,680	n.r.[d]	0.47	69
C.p. ferredoxin	ϵ_{390} = 30,000	n.r.	0.81	70

[a]UV absorption band due to aromatic amino acid side chains.

[b]Visible absorption band due to ligand to metal charge transfer.

[c]Ratio of protein and iron absorption bands is used as a measure of protein purity. In the case of the rubredoxins and desulforedoxin the protein absorbance is divided by the iron absorbance, for the ferredoxins the ratio is reversed.

[d]Not reported.

apoprotein as described by Meyer and co-workers (67). The method was originally reported for the [2Fe2S] spinach ferredoxin and it has been successfully applied to the [4Fe4S] clusters in C. pastuerianum ferredoxin in this work. Stock solutions of the apoferredoxin were prepared centrifuging to collect the apoprotein precipitate and then dissolving the precipitate in a small volume of 50 mM Tris-Cl pH 8.5.

Physical Measurements

Electronic absorption spectra were obtained using either a Perkin-Elmer Model 554 dual-beam spectrophotometer or a Perkin-Elmer Model 8460 diode array spectrophotometer interfaced to a Perkin-Elmer 7300 series Professional computer. Cylindrical quartz cells with a pathlength of 0.05 or 0.01 cm were used for absorbance measurements on iron-thiolate and iron-sulfur complexes. These cuvettes were fitted with rubber septum caps to maintain an inert atmosphere and were filled using a gas-tight syringe. Standard 1 cm pathlength quartz microcuvettes were used for absorbance measurements on protein solutions.

^{1}H NMR spectra were recorded using a Nicolet NT-300 and Bruker WM-300 spectrometers at Iowa State University or Bruker AM-250 and Bruker AM-500 spectrometers at the University of Georgia. These spectrometers were equipped with either a 5 mm dedicated ^{1}H or a 5 mm dual $^{1}H/^{13}C$ probe. Samples were placed in 5 mm quartz NMR tubes obtained from Wilmad Glass Co. (527 PP) or Aldrich Chemical Company (Gold Label). Inert atmosphere was achieved by fitting the tubes with rubber septum caps and cycling between vacuum and argon several times prior to loading the sample. Chemical shifts were referenced to TMS using the solvent resonance as an internal reference. Downfield and upfield shifts are reported as positive and negative, respectively. For aqueous samples, a 50 ms presaturation pulse (~1 watt) was used to

reduce the intensity of the residual HDO solvent resonance. ^1H NMR spectra collected over wide sweep widths often contained severe baseline distortions. These distortions were removed by using a spline baseline correction program. Exponential apodization of spectra collected over wide sweep widths was performed prior to Fourier transformation using line broadening factors of 10-40 Hz.

Samples of solids isolated from synthetic reactions were dissolved in a minimum volume of deuterated organic solvent, typically Me_2SO-d_6, in a small vial under argon. The solution was then transferred to an argon-filled NMR tube using a syringe. Because of their heterogenous nature, reactions to be monitored by ^1H NMR were run on a small scale (typically 10 mL total volume) in D_2O. Aliquots were removed from the reaction and transferred to an argon-filled NMR tube. Acquisition of the ^1H NMR spectrum was completed within 10 minutes after the aliquot was withdrawn.

Some of the protein samples for NMR were exchanged into high quality D_2O (99.996 %D, Aldrich Chemical Co.), which eliminated the need for a solvent presaturation pulse. Samples of rubredoxins in phosphate buffer pH 7.5 (uncorrected) were lyophilized and redissolved in D_2O several times. After the final lyophilization the protein was redissolved in ~0.3 mL of degasssed D_2O under argon. The final phosphate buffer concentration ranged from 50 to 300 mM depending on the original concentration and the change in sample volume. Reduced rubredoxin was obtained by placing a small quantity of solid sodium dithionite in the NMR tube prior to adding the sample. Desulforedoxin was exchanged into D_2O by repeated concentration and dilution in an Amicon ultrafiltration cell using a YM-5 or a YM-2 membrane. Final protein concentrations ranged from 1-3 mM for rubredoxins and 0.5 mM for desulforedoxin.

Variable temperature ^1H NMR studies were done on the Bruker instruments using the variable temperature accessory to control the heater coil in the probe. The Bruker

WM-300 was equipped with a refrigerated air chiller capable of temperatures below -60 °C. All spectra were referenced to the chemical shift of D_2O at 25 °C using the spectral reference parameter in the Bruker software.

Measurements of the spin-lattice relaxation time, T_1, were performed using the conventional 180-τ-90 method (71). The 180° pulse was replaced by a composite $90_x°$-$240_y°$-$90_x°$ pulse which compensates for instrumental imperfections (72). Normally, ten to fifteen values of τ were used in order to ensure the availability of sufficient data for estimations of T_1. All spectra, for a given experiment, were scaled and phased to match the first data file. The spectra were plotted, baselines were drawn by hand and the intensities were measured with a ruler. Intensity data were fitted to equation (1)

$$M_Z = M_0[1-k*\exp(\tau/T_1)] \qquad (1)$$

where M_Z is the intensity of the resonance at delay time τ; M_0 is the intensity at infinite time; k is the nucleus flip angle from the first pulse in units of $\pi/2$ (k=2 for a perfect 180° pulse); τ is the delay time between the 180° and 90° pulses; and T_1 is the spin-lattice relaxation time with the same time unit as τ. Non-linear least-squares fits were obtained using the BASIC program EXPSUM provided to the Kurtz group by Prof. James Espenson. The program provided estimates of T_1, M_0 and k.

Nuclear Overhauser effect (N.O.E.) experiments were performed on synthetic analog and protein samples. Steady state N.O.E. experiments were done using a procedure similar to that described by LaMar and co-workers (73). The steady-state N.O.E. was generated using gated homonuclear irradiation from the decoupler, typically, for 50-200 msec at ~0.2-0.8 watts. Immediately after the decoupler is turned off the 90° observation pulse was applied and the free induction decay was recorded. The N.O.E. experiment requires the accumulation of two ^1H NMR spectra. In the first spectrum the decoupler is used to selectively irradiate a specific resonance in the ^1H

NMR spectrum until it is saturated (i.e., the intensity is reduced to zero). The second spectrum is a reference spectrum where the decoupler irradiation is directed to an empty region of the spectrum. The N.O.E. result is the difference spectrum obtained by subtracting the first spectrum (decoupler on-resonance) from the second spectrum (decoupler off-resonance). The difference spectrum should contain a negative signal at the chemical shift of the irradiated resonance equal to the original area of that resonance. Additional signals, usually of low, negative intensity, will appear for the resonances of hydrogens close to the hydrogens being irradiated. The N.O.E. is the consequence of energy being transferred through space (i.e. via a dipolar mechanism) to nearby nuclei when the irradiated nuclei relax from the excitation of the decoupler pulse. Because the N.O.E. operates by a dipolar mechanism, it shows an r^{-6} distance dependence (74).

An IBM model ER-220D EPR spectrometer with an Oxford Instruments model ESR-9 cryostat was used to obtain EPR spectra near liquid He temperature, typically 4.2 K. Essentially identical spectrometers were available at Iowa State University and the University of Georgia. The basic instrumental parameters used for a typical spectrum were: microwave frequency, 9.41 GHz; modulation, 16G at 100 MHz; time constant, 160 msec; and a phase of either 93.5° or 176° depending on the instrument being used. Samples were placed in 4 mm O.D. (3 mm I.D.) quartz tubes under argon and frozen in liquid nitrogen. Long term anaerobic storage was achieved by carefully flame sealing the tubes under dynamic vacuum such that no Ar (or other gases) condensed on top of the samples and storing them in a liquid nitrogen storage dewar.

Electrochemical experiments were performed using a Bioanalytical Systems model 100 Electrochemical Analyzer with an Auto Cell Stand. Cyclic voltammetry and Osteryoung square wave measurements were made using a glassy carbon working

electrode and a Ag/AgCl reference electrode with a platinum wire auxiliary electrode. The performance of the system was checked periodically by measuring the cyclic voltammagram of the ferrocenium/ferrocene couple in CH_3CN with tetramethylammonium bromide as the supporting electrolyte.

Samples of $[Fe(SCH_2CH_2OH)_4]^{2-}$ for electrochemical experiments were prepared as follows. To 50 mL of the desired solvent were added 1.08 g (5.0 mmol) of tetraethylammonium tetrafluoroborate (Aldrich) and 0.038 g (1.6 mmol) of LiOH. The solution was degassed by several cycles of vacuum and argon. This was followed by the addition of 0.45 mL (6.4 mmol) of neat 2-mercaptoethanol and 0.056 g (2.0 mmol) $Fe(SO_4)\cdot 7H_2O$. The final concentrations were 100 mM Et_4NBF_4, 31 mM LiOH, 128 mM 2-mercaptoethanol and 4 mM $Fe(SO_4)$. Aliquots were transferred to the electrochemical cell which had the capability to purge the solution with argon or maintain a continuous flow of argon over the solution. For experiments where the reduction potential was studied as a function of solvent composition, stock solutions of the $[Fe(SCH_2CH_2OH)_4]^{2-}$ in each solvent were prepared and then mixed in the electrochemical cell.

Mössbauer spectra were recorded for frozen solutions of $[Fe(SCH_2CH_2OH)_4]^{2-}$. The solution was prepared according to the general procedure. The final reagent concentrations were 480 mM LiOH, 600 mM 2-mercaptoethanol and 60 mM $Fe(SO_4)$. This highly concentrated solution made it possible to collect spectra in a reasonable amount of time without enriching with ^{57}Fe. The nylon cylindrical Mössbauer sample cup was placed in a plastic conical centrifuge tube. The centrifuge tube was capped with a rubber septum and degassed by several cycles of vacuum/Ar. The tube was then suspended in liquid nitrogen. A syringe was used to inject ~0.3 mL of solution into the chilled sample cup where it froze immediately. Once frozen, the Mössbauer sample could be exposed to air. The samples were kept frozen until after the spectra were

recorded.

The Mössbauer spectroscopy was performed by Prof. B.H. Vincent Huynh and Dr. Miguel Teixeira of the Dept. of Physics at Emory University. At 4.2 K, spectra were collected in magnetic fields of 0, 5, 10, 20, 40 and 70 kG applied parallel to the gamma-ray irradiation. In a fixed magnetic field of 70 kG, additional spectra were collected at 50, 90, 130 and ~170 K. The Mössbauer spectra at various temperatures and fields were computer-simulated using a Mössbauer spin Hamiltonian (75). Computer simulation of the spectra provides the sign of ΔE_q, values of the zero-field splitting parameters, D and E, and the electron-nuclear hyperfine coupling constants, A_n (n=x,y,z). The computer analyses of the Mössbauer spectra were performed under the supervision of Prof. Huynh.

III. RESULTS

Iron-Thiolate Complexes

The anion, $[Fe(SCH_2CH_2OH)_4]^{2-}$, is readily formed in aqueous solution by mixing 2-mercaptoethanol and an iron salt in the presence of enough base to deprotonate the thiol. The proper choice of base and iron salt made it possible to isolate the anion from aqueous solution. The combination of $Ba(OH)_2$ and $Fe(SO_4)$ in the synthesis led to the precipitation of $BaSO_4$ from the aqueous solution. The removal of these undesired spectator ions by precipitation proved to be the essential step in obtaining a pure solid product. $Ba[Fe(SCH_2CH_2OH)_4]$ was isolated in 54% yield as an analytically pure, microcrystalline solid. Larger crystals of $Ba[Fe(SCH_2CH_2OH)_4]$ were easily prepared from aqueous solution, as described in Appendix C. The properties of $[Fe(SCH_2CH_2OH)_4]^{2-}$ are summarized in Table III-1.

A single crystal X-ray analysis (Appendix C) of $Ba[Fe(SCH_2CH_2OH)_4]$ indicates that the iron site has S_4 point group symmetry. The Fe-S bond lengths are all 2.30(2) A. The four S-Fe-S bond angles of 108.3(6)° and two S-Fe-S bond angles of 111.9(6)° are the result of a tetragonal compression along the S4 axis. Thus, the tetrahedral coordination geometry is distorted towards a square planar geometry. "While the diffraction data were of sufficient quality to establish the positions of the Ba, Fe and S atoms, disorder of the hydroxyethyl groups is clearly evident in the bond distances derived for these atoms, from the positions of final refinement, and in the magnitudes of the anisotropic thermal parameters for these atoms" (76). The UV-visible spectrum of $Ba[Fe(SCH_2CH_2OH)_4]$ in Me_2SO (Figure III-1) contains a peak at 316 nm and a shoulder at ~340 nm. Figure III-2 shows the ^1H NMR spectrum of the solid dissolved in Me_2SO-d_6. The resonances at 211 and 6.2 ppm are assigned to the $Fe(SC\underline{H}_2CH_2OH)$ and

Table III-1. Physical properties of $[Fe(SCH_2CH_2OH)_4]^{2-}$ in solution[a]

UV-visible absorbance			316 nm (ϵ = 4,810 $M^{-1}cm^{-1}$)
			340 nm, sh (ϵ = 3,250 $M^{-1}cm^{-1}$)
^1H NMR	$FeSC\underline{H}_2CH_2OH$		211 ppm
	$FeSCH_2C\underline{H}_2OH$		6.2 ppm
	$FeSCH_2CH_2O\underline{H}$		12 ppm
Mössbauer[b]	δ_{Fe}		0.73 mm/s
	ΔE_q		-3.48 mm/s
Electrochemistry[c]	$E_{\frac{1}{2}}$ (vs. Ag/AgCl)		-797 mV
	ΔE_p		75 mV

[a]Experiments were performed at room temperature using solutions of analytically pure $Ba[Fe(SCH_2CH_2OH)_4]$ dissolved in Me_2SO except where noted.

[b]Experiment was performed on a frozen aqueous solution of $[Fe(SCH_2CH_2OH)_4]^{2-}$ at 4.2 K as described in Figure III-11 and the experimental section.

[c]Cyclic voltammametry was performed using a glassy carbon working electrode and a Ag/AgCl reference electrode. Scan rate was 50 mV/s.

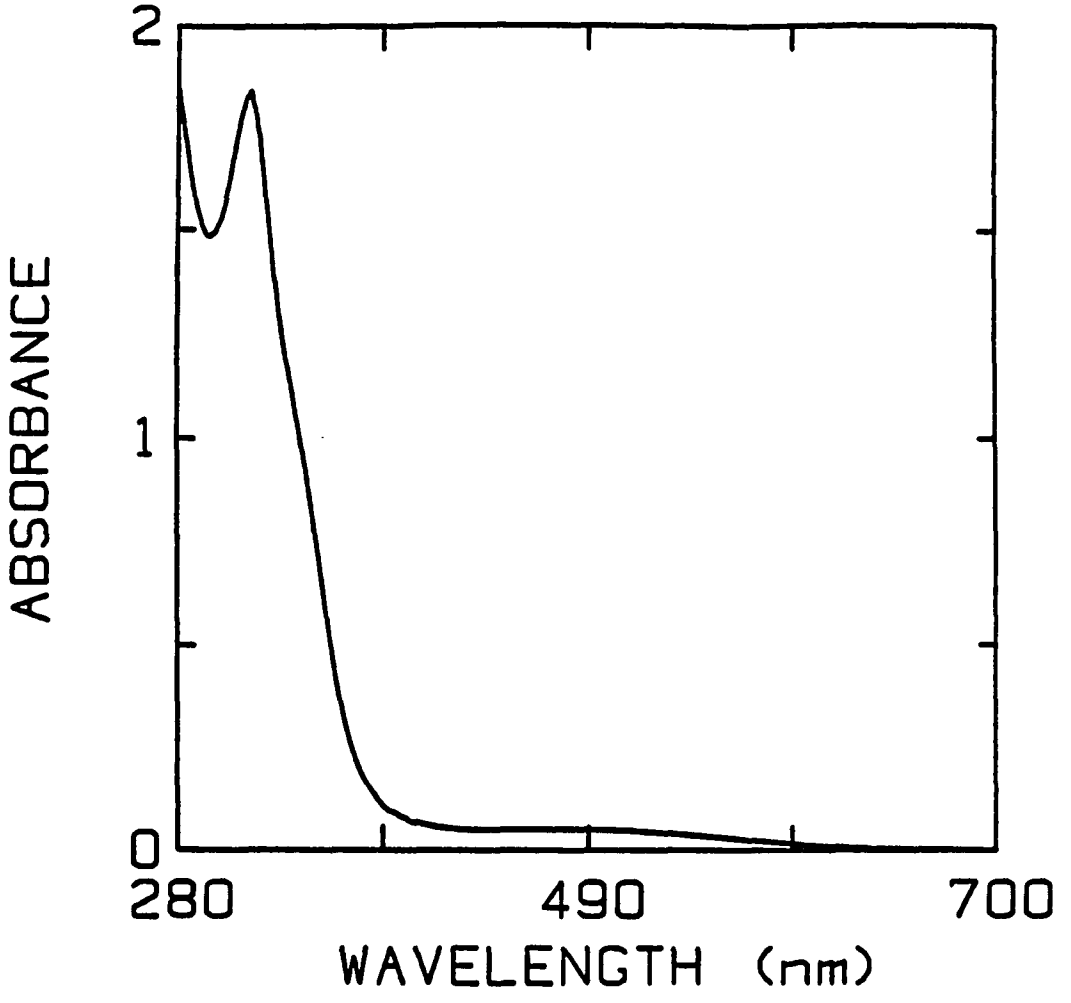

Figure III-1. UV-visible absorption spectrum of $Ba[Fe(SCH_2CH_2OH)_4]$ dissolved in Me_2SO. Concentration = 37 mM. Cell pathlength = 0.01 cm

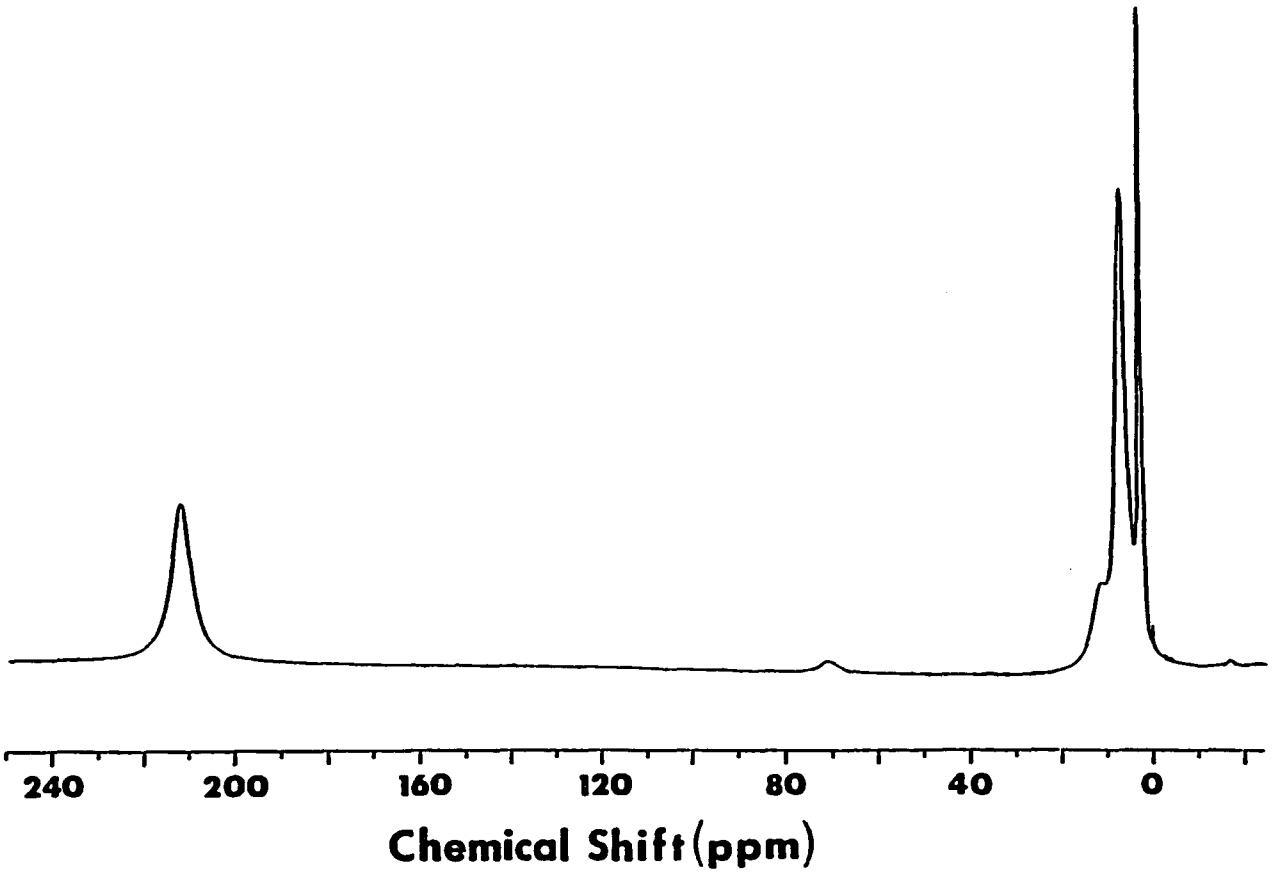

Figure III-2. 250 MHz ^{1}H NMR spectrum of $Ba[Fe(SCH_2CH_2OH)_4]$ dissolved in Me_2SO-d_6. The spectrum was recorded at 27 °C

Fe($SCH_2C\underline{H}_2OH$) hydrogens, respectively. The hydroxyl hydrogen on the ligand is assigned to the resonance at 12 ppm. The bases are given for these assignments in the Discussion. These spectral properties are very similar to those reported for $[Fe(SCH_2CH_3)_4]^{2-}$ in CH_3CN-d_3 (18,19). The weak resonance at 71 ppm is assigned to the $[Fe_2(SC\underline{H}_2CH_2OH)_6]^{2-}$ hydrogens (average of bridging and terminal thiolates). The formation of small amounts of the binuclear iron-thiolate species in solutions of $[Fe(SCH_2CH_3)_4]^{2-}$ has been reported (13).

Solutions of $[Fe(SR)_4]^{2-}$ can also be prepared with dithiothreitol (DTT), glutathione (GSH) and reduced 6,8-thioctic acid (dihydrolipoic acid) ligands. So far, none of these complexes has been isolated as a pure crystalline solid. The UV-visible spectra of these complexes in water are shown in Figure III-3. The 2-mercaptoethanol and glutathione complexes have spectra with a peak at 310 nm and a shoulder at 340 nm, almost identical to the spectrum reported for $[Fe(SCH_2CH_3)_4]^{2-}$ in CH_3CN (18,19). The spectra of the dithiothreitol and dihydrolipoate complexes are not as well resolved, showing only a broad shoulder at 310 nm. Reduced rubredoxin has two resolved UV bands, which appear at 311 and 333 nm (23), see Figure I-6 in the introduction.

The downfield ^1H NMR spectra of these complexes in D_2O solution at 25 °C are shown in Figure III-4. For the complexes in Figure III-4 resonances appear at 203 (2-mercaptoethanol); 219 and 199 (dithiothreitol); 213 (glutathione); 271, 264, 250 and 185 ppm (dihydrolipoate). The methylene protons in $[Fe(SCH_2CH_3)_4]^{2-}$ resonate at 196 ppm downfield in CH_3CN-d_3 (13,19). The multiple peaks observed in the cases of dithiothreitol and dihydrolipoate are presumably due to the S,S'-bidentate chelates formed with these dithiols. S,S'-Chelated dihydrolipoate has two methylenes β to the coordinated sulfurs, and the group of resonances between 13 and 16 ppm in Figure III-4 are assigned to these methylene hydrogens. For the other complexes the β methylene

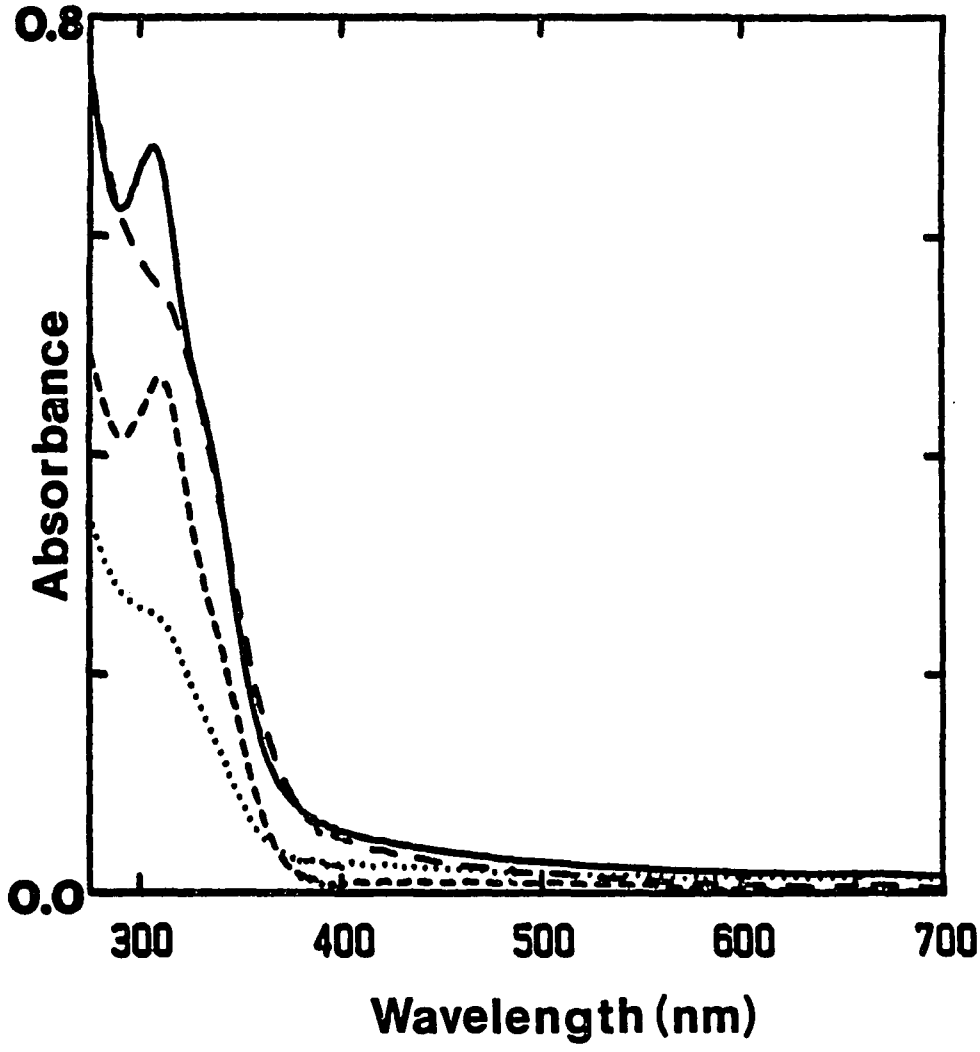

Figure III-3. UV-visible spectra of aliquots of the solutions of tetrakis-alkylthiolate-Fe(II) complexes. Solutions of these complexes were prepared under Ar by first dissolving thiols in D_2O with LiOH to deprotonate the thiol groups. The resulting solutions, 80 mM in thiol (40 mM in dithiol), were added to solid $FeCl_2$ to give solutions 20 mM in Fe(II). The dihydrolipoate spectrum is of a 2-fold dilution. From top to bottom at 300 nm, spectra are of solutions containing 2-mercaptoethanol, dithiothreitol, glutathione, and dihydrolipoate. Cell path length = 0.01 cm

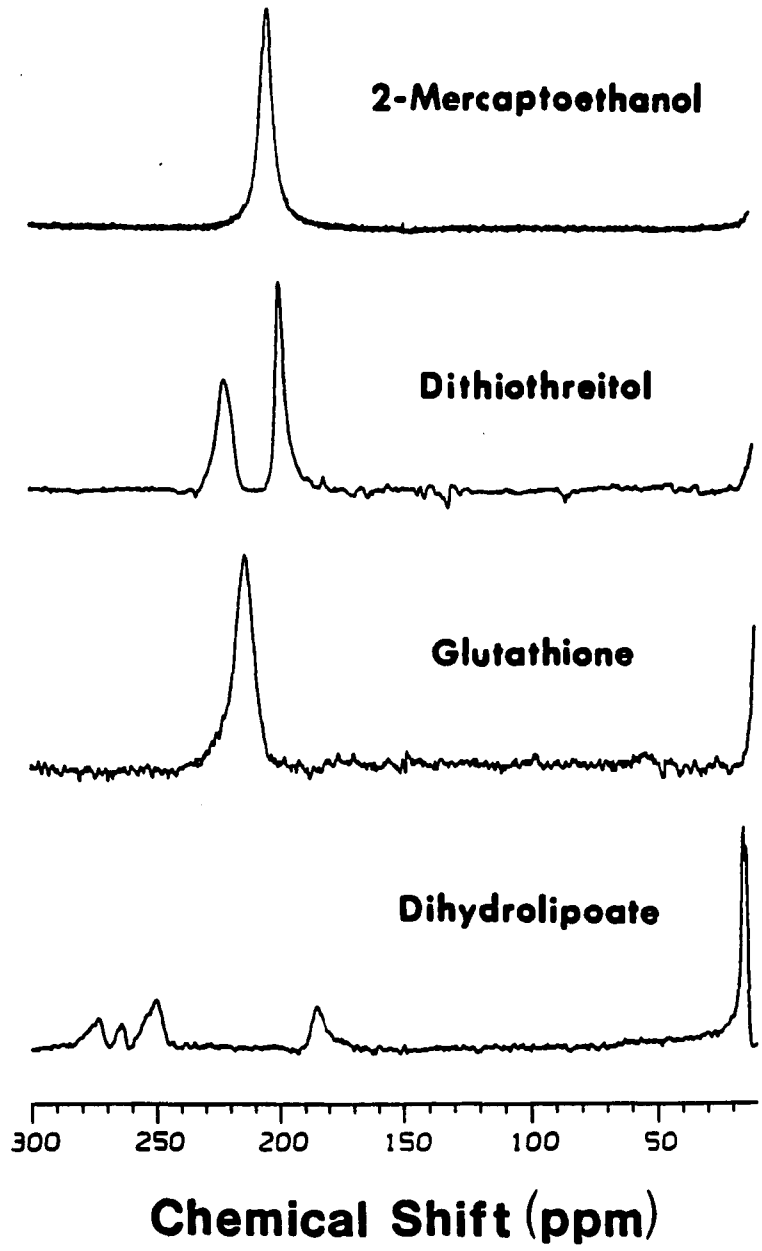

Figure III-4. 300 MHz ^{1}H NMR spectra of tetrakis-alkylthiolate-Fe(II) complexes in the region of 300 to 10 ppm. Spectra are of aliquots of the solutions described in Figure III-3. All spectra were obtained at 25 °C

proton resonances appear upfield of 10 ppm and are not shown in Figure III-4. In $[Fe(SCH_2CH_3)_4]^{2-}$ the methyl protons appear at 10 ppm downfield of TMS in CH_3CN-d_3. Thus, ^1H NMR studies of the synthetic analogs predict that the β-CH_2 cysteinyl protons of a rubredoxin-like site should resonate 180-280 ppm downfield. Previous studies of the ^1H NMR spectra of rubredoxin (40,50) have not examined the region downfield of 125 ppm.

Each of the resonances mentioned above shifts upfield with increasing temperature and exhibits a linear dependence of the chemical shift on T^{-1} in the range of 5-55 °C. Figure III-5 illustrates the chemical shift and line width changes that occur with increasing temperature for the 2-mercaptoethanol and glutathione complexes. Figure III-6 shows the temperature dependence of the chemical shift as a function of T^{-1} for the downfield resonances in the dithiothreitol complex. Similar plots were observed for the analogous resonances in each of the other mononuclear species. Chemical shift values as a function of temperature, for each of the mononuclear complexes, are listed in Table III-2.

The results of a nuclear Overhauser effect experiment on the 200 ppm downfield resonances of $[Fe(SCH_2(CHOH)_2CH_2S)_2]^{2-}$ are shown in Figure III-7. The goal was to perform a steady-state N.O.E. experiment in which the irradiated resonance is saturated (i.e., reduced to zero intensity). It was not possible to obtain a combination of pulse length and power capable of saturating these resonances, even though powers of up to ~ 1 mW were used. Powers greater than ~ 1 mW are routinely used for heteronuclear N.O.E. experiments, but may lead to probe damage in a homonuclear experiment. The experimental result shown in Figure III-7 is best described as a transient N.O.E. experiment (T.O.E.). In a T.O.E. experiment a short (~10-50 ms) irradiation pulse from the decoupler produces only a fraction of the maximum possible N.O.E. intensity, while

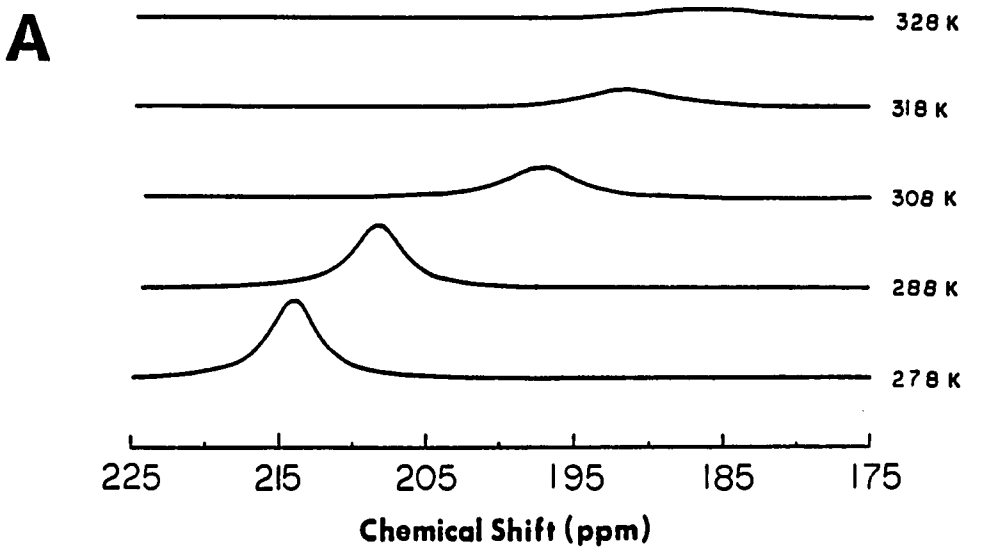

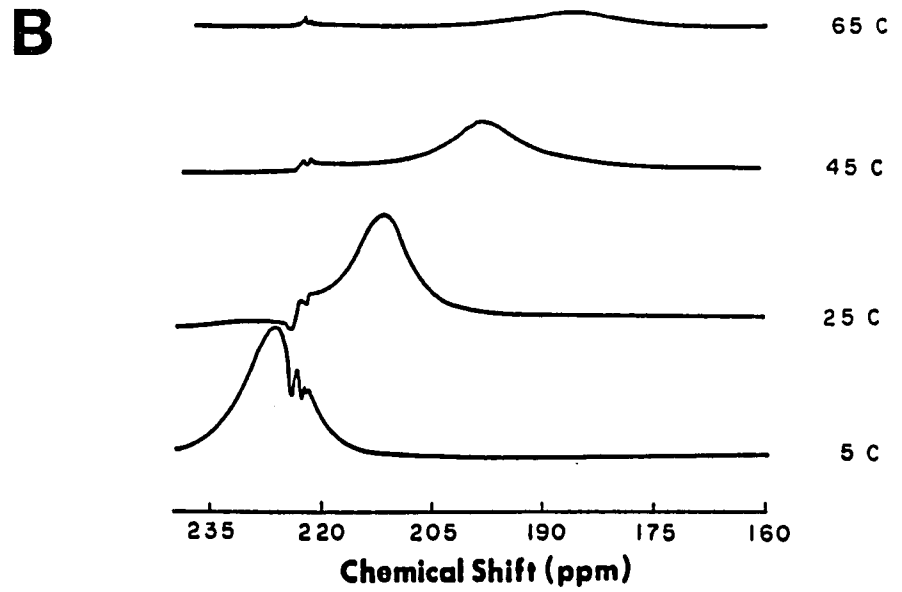

Figure III-5. The downfield region of 300 MHz ^{1}H NMR spectra of the 2-mercaptoethanol (A) and glutathione (B) Fe(II) complexes from Figure III-4 as a function of temperature

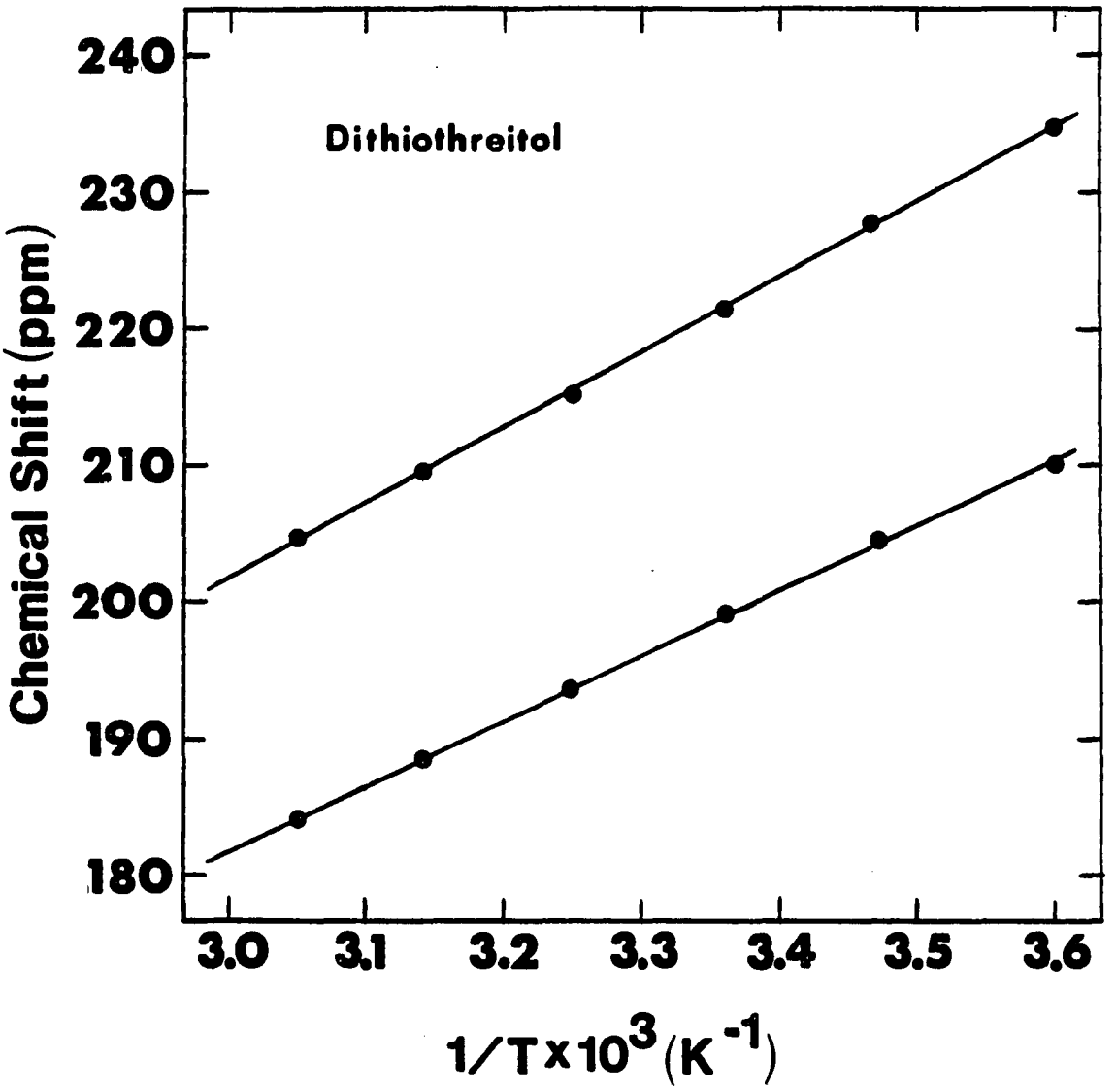

Figure III-6. Plot of chemical shift vs. reciprocal of absolute temperature for the ^1H NMR resonances of $[Fe(SCH_2(CHOH)_2CH_2S)_2]^{2-}$ shown in Figure III-4

Table III-2. Chemical shifts of the mononuclear iron(II)-alkylthiolate complexes as a function of temperature

Temperature (K)	2-mercaptoethanol	Dithiothreitol	Glutathione
278	214	235, 210	226
288	208	228, 204	219
298	203	221, 199	212
308	197	215, 194	205
318	192	210, 189	198
328	186	205, 184	192

Temperature (K)	Dihydrolipoate
283	296, 281, 271, 195
293	282, 272, 256, 184
303	269, 261, 247, 185
313	261, 253, 242, 181
323	253, 246, 236, 178

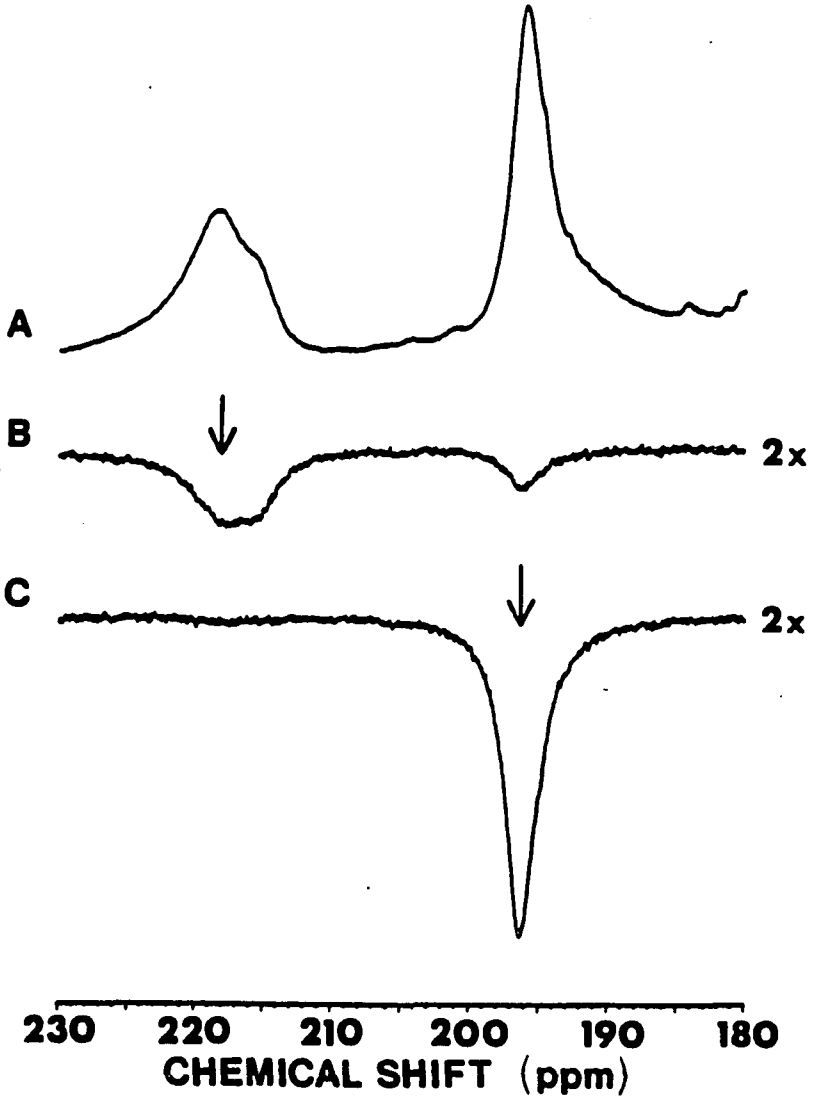

Figure III-7. Results of a transient N.O.E. experiment on $[Fe(SCH_2(CHOH)_2CH_2S]^{2-}$. Spectrum A is the 230-180 ppm downfield region of the 250 MHz ^1H NMR spectrum of the complex. Spectra B and C are two-fold expansions of the difference spectra obtained by subtracting the reference spectrum (A) from the spectrum where one of the resonances was irradiated (indicated by arrows). For spectrum B the 218 ppm resonance was irradiated. For spectrum C the 196 ppm resonance was irradiated. The spectra were recorded at 300 K.

the steady-state N.O.E. experiment is intended to produce the maximum N.O.E. intensity. Irradiation of the 221 ppm resonance produced an N.O.E. to the 196 ppm resonance. The reverse experiment, where the 196 ppm resonance was irradiated, did not produce a noticeable N.O.E. to the 221 ppm resonance. The fact that an N.O.E. is observed, in the case of irradiation at 221 ppm, means that the hydrogens which give rise to the two separate resonances must be close to each other. The inability to observe an N.O.E. from the 196 ppm resonance to the 221 ppm resonance suggests that, even though these hydrogens are close to each other in the molecule, they experience significantly different magnetic environments.

Figure III-8 shows the resonances in the 19-9 ppm region of 300 MHz ^1H NMR spectrum of the dihydrolipoate complex. These resonances are tentatively assigned to hydrogens β to the coordinated sulfur atoms of the bidentate dihydrolipoate ligand.

The EPR spectra of frozen aqueous solutions of these complexes are shown in Figure III-9. The $[Fe(SCH_2CH_2OH)_4]^{2-}$ complex has a broad EPR signal at low magnetic field. The dithiothreitol and glutathione complexes exhibit a similar broad, low field EPR resonance. The lipoate complex does not appear to be EPR active. EPR spectra of crystalline $Ba[Fe(SCH_2CH_2OH)_4]$ showed no features that could be unequivocally attributed to a S=2 EPR signal. These spectra are similar to those reported by Hagen (77) for S=2 iron in biological systems. A low field EPR resonance is also observed for high spin Fe(II) in $FeSiF_6 \cdot 6H_2O$ (69).

The temperature dependencies of the S=2 EPR signals for the 2-mercaptoethanol and dithiothreitol complexes are shown in Figure III-10. For both complexes the intensity of the signal decreases rapidly as the temperature is raised from 4 to 20 K. This result is similar to the temperature dependence of the S=2 EPR signal in cytochrome c oxidase reported by Hagen (77).

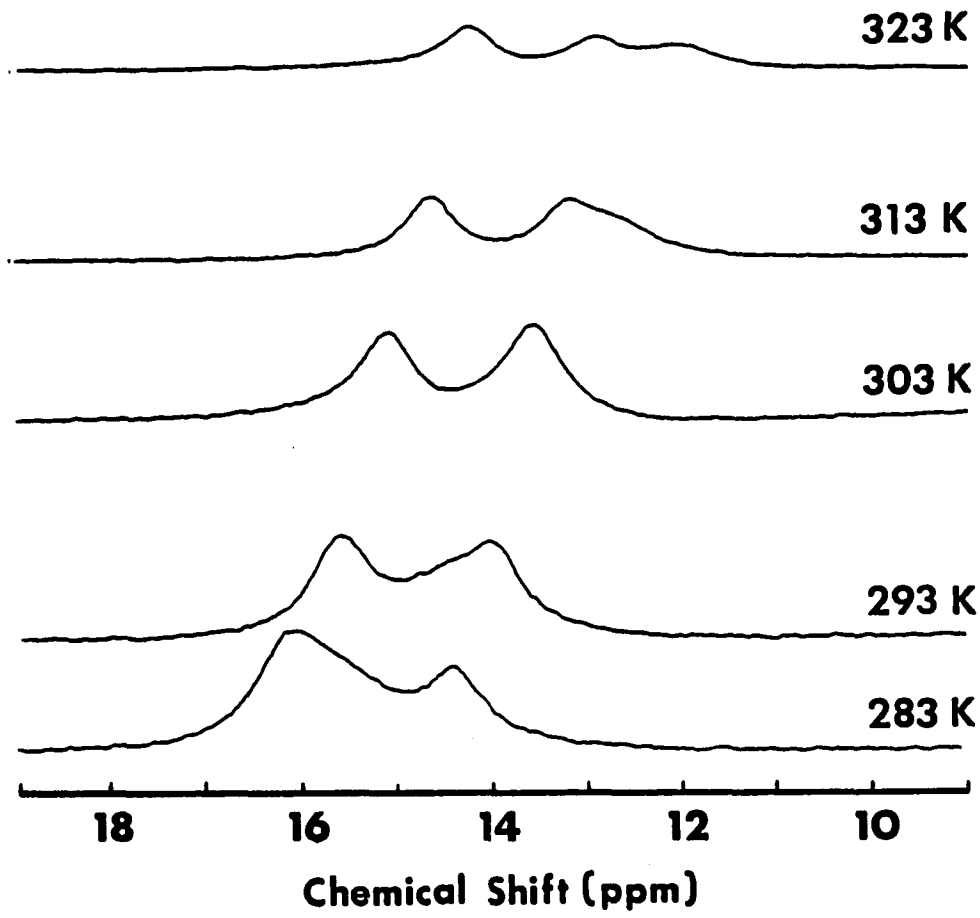

Figure III-8. The 19-9 ppm region of the 300 MHz ^{1}H NMR spectrum of the dihydrolipoate Fe(II) complex from Figure III-4. Note the resolution of three peaks at high temperature

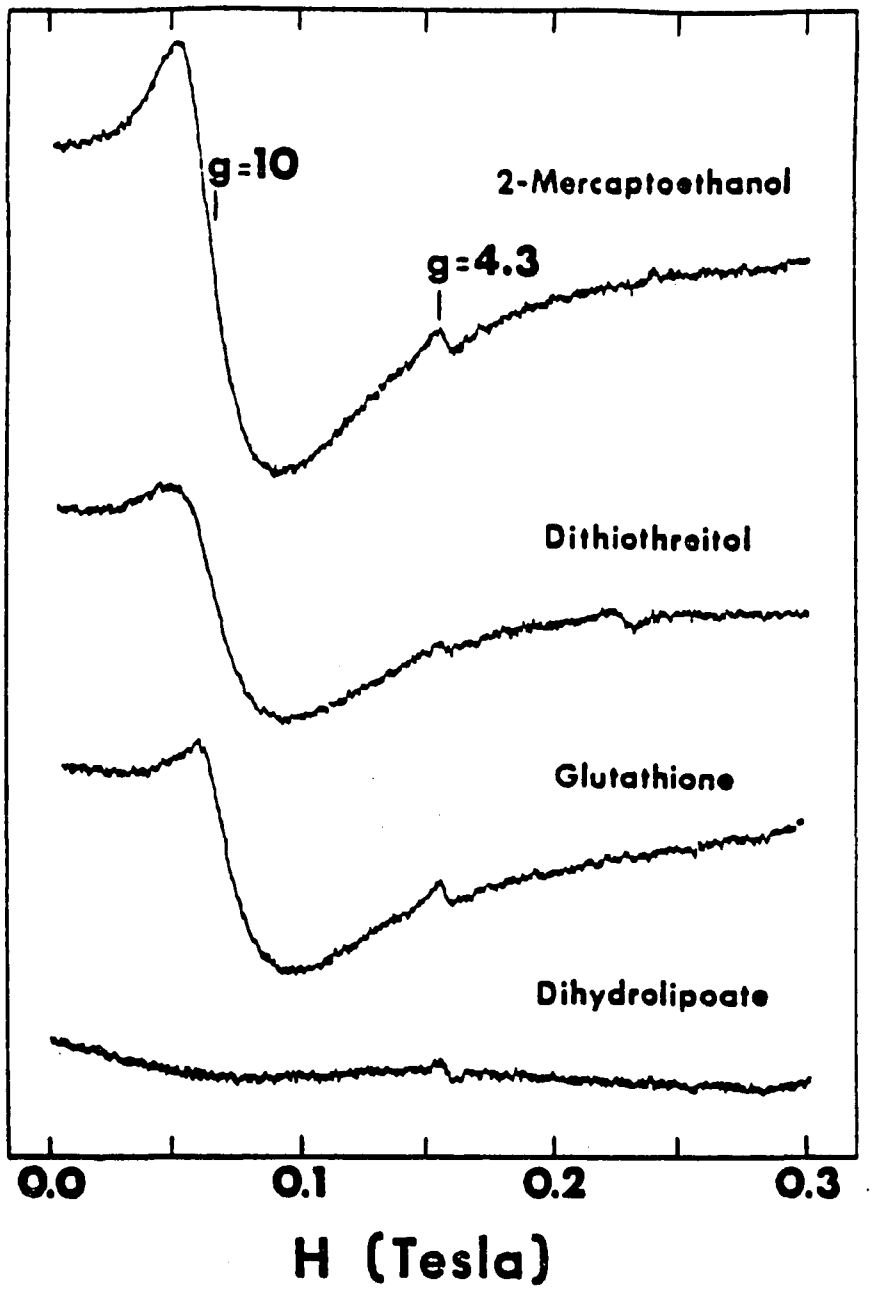

Figure III-9. X-band (9.41 GHz) EPR spectra of tetrakis-alkylthiolate-Fe(II) complexes at liquid He temperature (5-7 K). Solutions were prepared in water as described in Figure III-3. The solutions were 40 mM in thiol (20 mM in dithiol) and 10 mM in Fe(II). The solution of the dihydrolipoate complex was diluted 2-fold. Instrument parameters are given in the experimental section

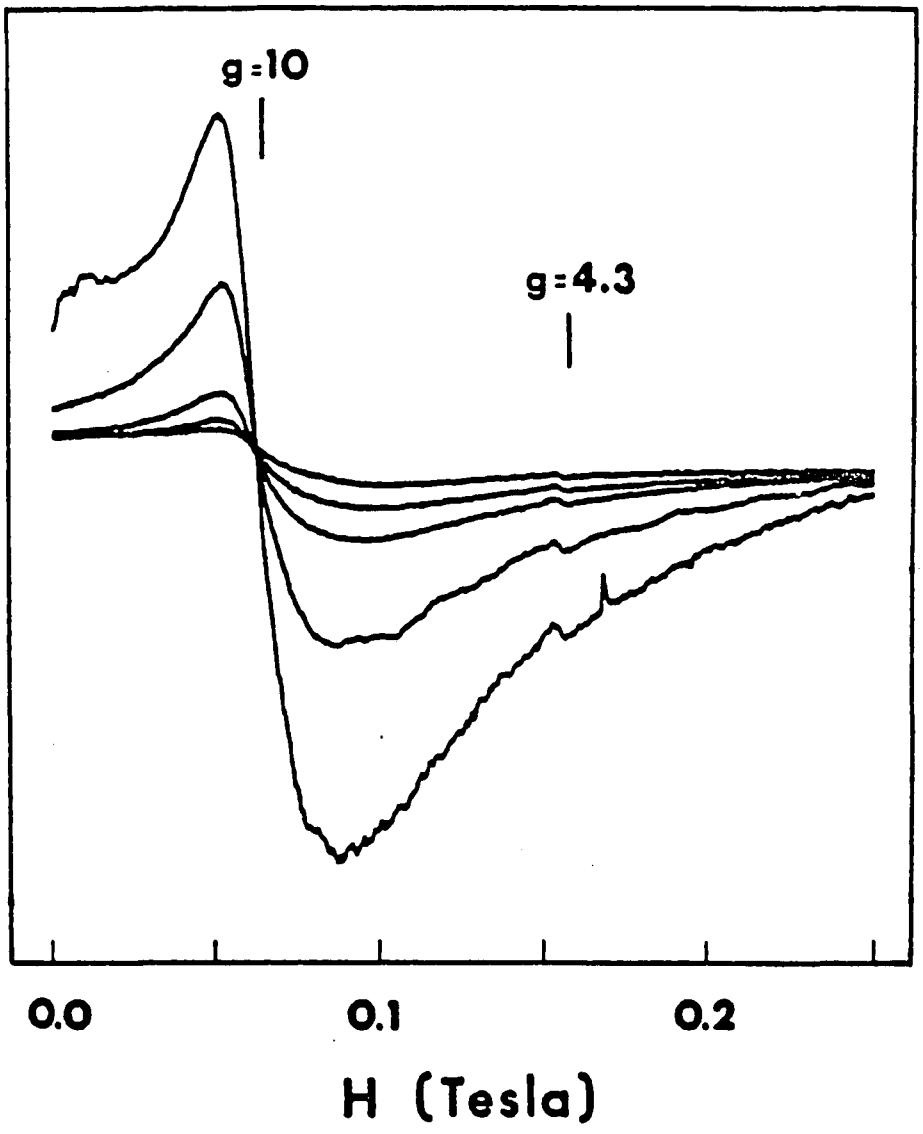

Figure III-10a. Temperature dependence of the low field S=2 EPR signal from $[Fe(SCH_2CH_2OH)_4]^{2-}$. The solution was prepared in water as described in Figure III-3. Final reagent concentrations were 470 mM LiOH, 600 mM 2-mercaptoethanol, and 60 $Fe(SO_4)\cdot 7H_2O$. Sample temperatures, in order of decreasing signal intensity, were 4, 8, 13, 18, and 28 K

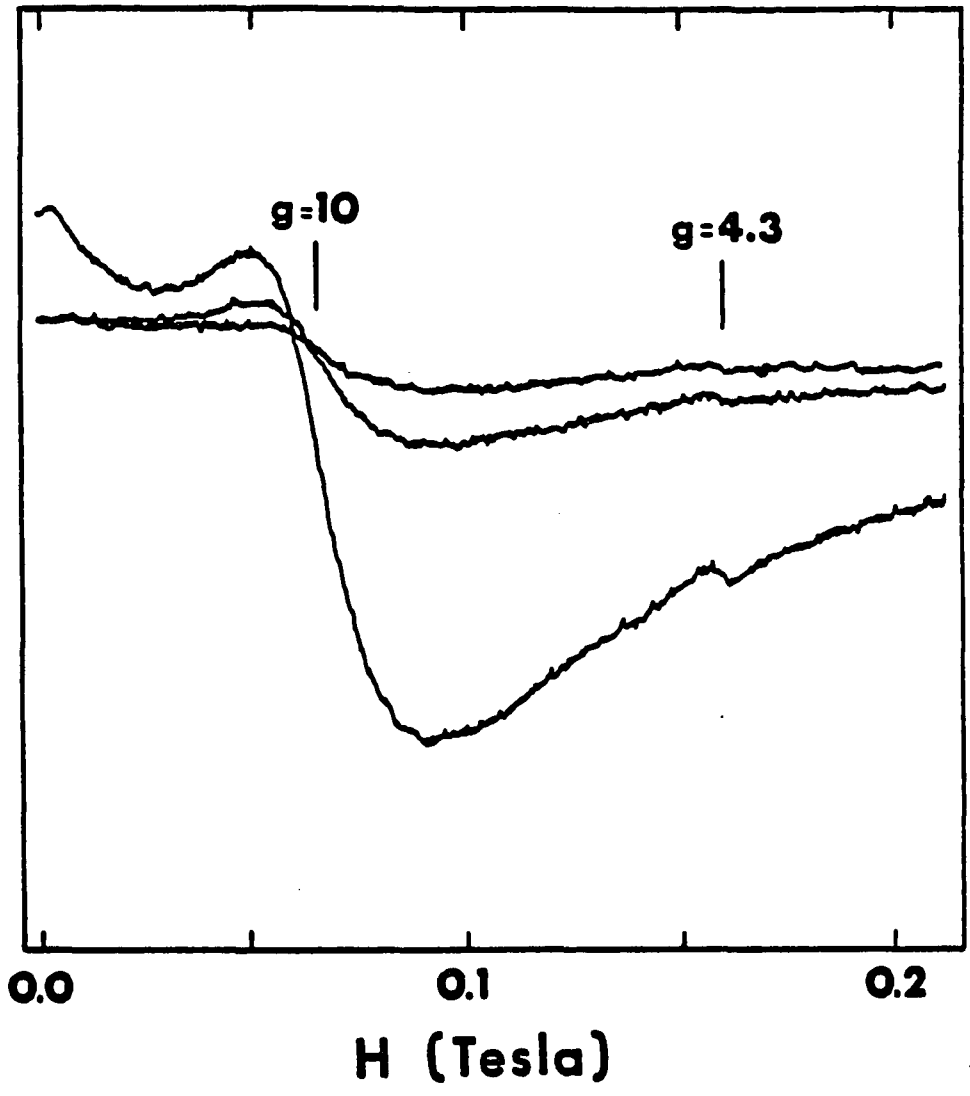

Figure III-10b. Temperature dependence of the low field S=2 EPR signal from $[Fe(SCH_2(CHOH)_2CH_2S)_2]^{2-}$. The solution was prepared in water as described in Figure III-4. Final reagent concentrations were 34 mM LiOH, 20 mM dithiothreitol, and 10 mM $FeCl_2$. Sample temperatures, in order of decreasing signal intensity, were 4, 10, and 21 K

The $[Fe(SCH_2CH_2OH)_4]^{2-}$ complex has also been characterized by Mössbauer spectroscopy. A solution of the anion with lithium as the cation was used instead of $Ba[Fe(SCH_2CH_2OH)_4]$. High atomic number elements, such as barium, scatter the gamma ray irradiation causing a significant loss of signal intensity.

Figure III-11 shows the Mössbauer spectrum, at 4.2 K in the absence of an applied magnetic field, of a frozen aqueous solution of $[Fe(SCH_2CH_2OH)_4]^{2-}$ with excess thiol. At 4.2 K, a single quadrupole doublet is observed with an isomer shift, δ_{Fe} = 0.73 mm/s, and quadrupole splitting, ΔE_q = -3.48 mm/s. These values are consistent with high spin Fe(II) tetrahedrally coordinated by alkylthiolate sulfur atoms (78). Table I-2 lists the Mössbauer parameters of similar complexes. The extremely weak absorption at ~ 0.35 mm/s is due to the presence of a small amount (less than 5%) of fast relaxing, high spin Fe(III). The isomer shift and quadrupole splitting values for $[Fe(SCH_2CH_2OH)_4]^{2-}$ are very similar to those of reduced rubredoxin and reduced desulforedoxin (see Table I-5).

Mössbauer spectra of $[Fe(SCH_2CH_2OH)_4]^{2-}$ have been obtained over a range of magnetic field strengths and temperatures. More detailed information pertaining to the magnetic Mössbauer experiments and the analyses of the data is presented in Appendix B. Preliminary analyses of these spectra indicate the presence of two distinctly different magnetic species. The preliminary analyses have not yet provided sufficient information to determine which species gives rise to the S=2 EPR signal.

The electrochemical properties of $[Fe(SCH_2CH_2OH)_4]^{2-}$ were examined by cyclic voltammetry and Osteryoung square wave voltammetry. In addition to the determination of the reduction potential, the cyclic voltammetry experiment allows evaluation of the electrochemical reversibility of the process being studied. The process may be categorized as reversible or quasi-reversible using the following criteria. For a

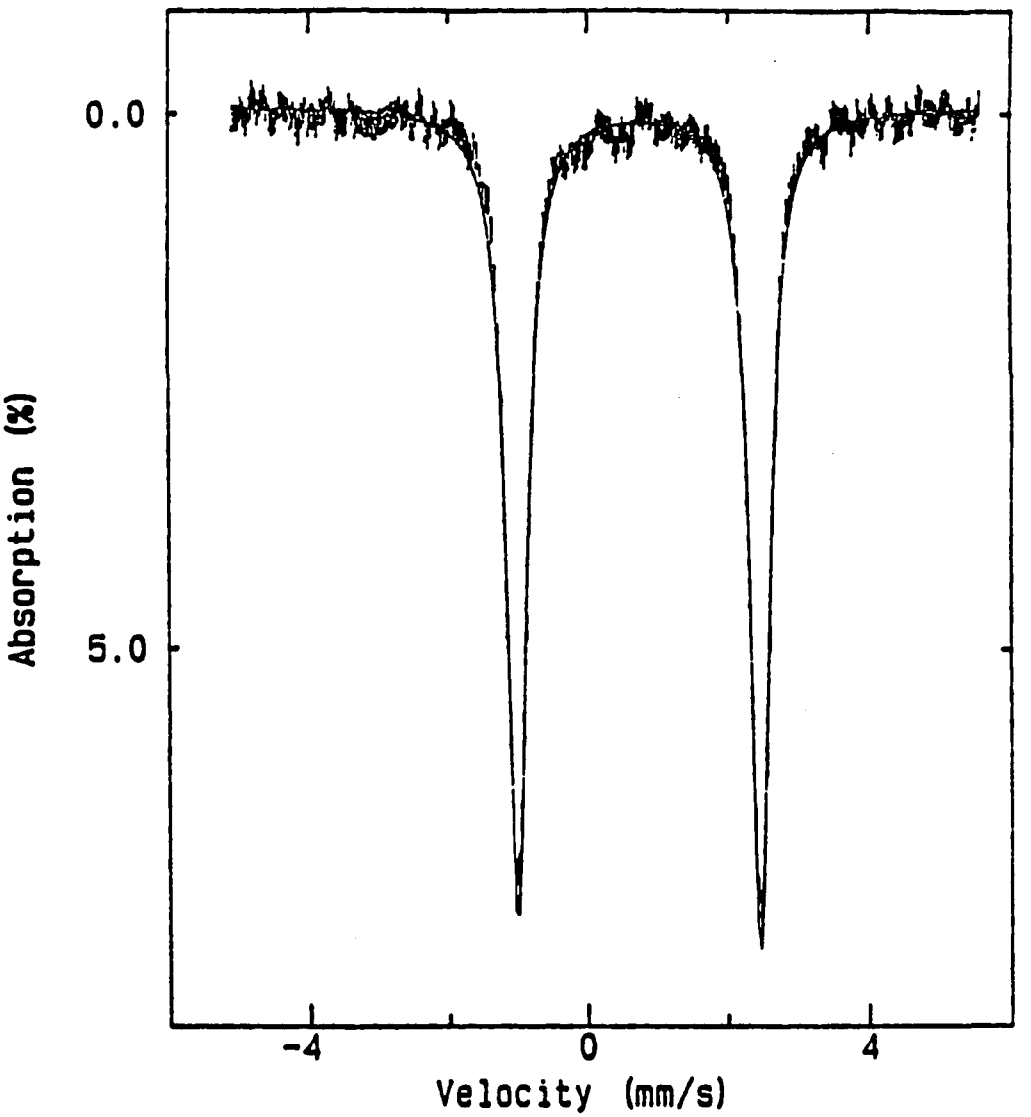

Figure III-11. Mössbauer spectrum of a frozen solution of $[Fe(SCH_2CH_2OH)_4]^{2-}$ in water. The spectrum was recorded at 4 K. The sample contained 467 mM LiOH, 595 mM 2-mercaptoethanol and 60 mM $FeSO_4$. The solid line represents the non-linear least-squares fit from which the values of the isomer shift and quadrupole splitting were obtained

reversible process, the peak potential separation (ΔE_p) between the anodic and cathodic waves should be 56.5 mV for a one-electron process and 28.4 mV for a two-electron process (79). During a reversible process, the current passage during the anodic sweep should be identical to the current passage during the cathodic sweep. This condition is usually expressed as the current ratio, i_a/i_c, which will have a value of unity for a reversible system. Many systems approach but do not meet the exact definition of a reversible process. For practical purposes, these "quasi-reversible" processes are somewhat arbitrarily defined by ΔE_p values of 60 to 100 mV for a one-electron process. In the presence of excess thiol, the $[Fe(SCH_2CH_2OH)_4]^{1-/2-}$ system displays quasi-reversible electrochemical behavior. Even with excess thiol present, it was not possible to obtain quasi-reversible electrochemistry for the dithiothreitol or glutathione mononuclear complexes.

Figures III-12 and III-13 show cyclic voltammagrams (vs. Ag/AgCl) in water and Me_2SO, respectively, for $[Fe(SCH_2CH_2OH)_4]^{2-}$ in the presence of excess thiol. In water the reduction potential is -338 mV (vs. Ag/AgCl) or -106 mV when corrected to the N.H.E. reference. This value is somewhat more negative than the -57 mV and -35 mV (vs. N.H.E.) reported for the reduction potentials of rubredoxin (23) and desulforedoxin (54), respectively, in aqueous solution. On the other hand, this value is much more positive than the values of ~ -700 mV (vs. N.H.E.) obtained for the reduction potentials of other synthetic analogs in organic solvents (see Table I-3). The iron-cysteinyl complex of Nakata and co-workers (33) is reported to have a potential of -140 mV (vs. N.H.E.) in an aqueous medium containing 10 vol% Triton X-100.

The reduction potentials (vs. Ag/AgCl) obtained for the $[Fe(SCH_2CH_2OH)_4]^{1-/2-}$ couple in four solvents, spanning a wide range of dielectric constant, are listed in Table III-3. The reduction potential spans a range from -785 mV in Me_2SO to -336 mV in

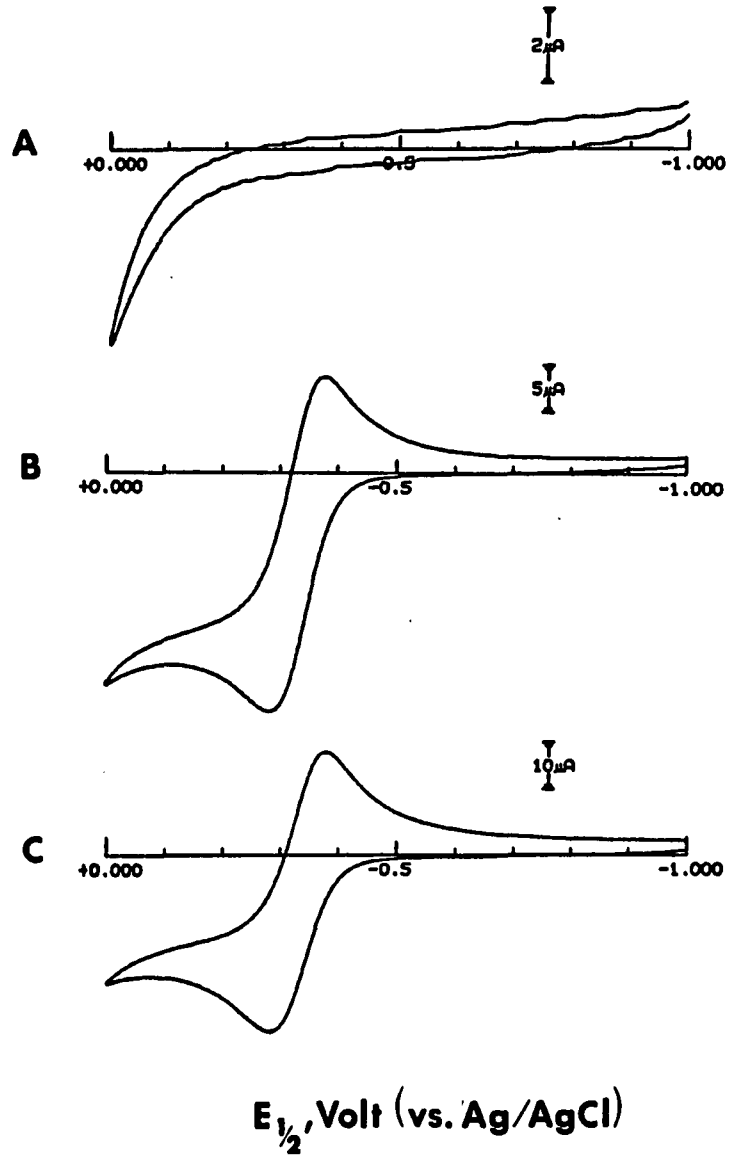

Figure III-12. Cyclic voltammagrams of $[Fe(SCH_2CH_2OH)_4]^{2-}$ in water. Reagent concentrations, in order of addition, were 510 mM sodium nitrate, 31 mM lithium hydroxide, 100 mM 2-mercaptoethanol and 4 mM iron (II) chloride. (A) prior to addition of iron, scan rate 10 mV/s; (B) after addition of iron, scan rate 10 mV/s; (C) after addition of iron, scan rate 50 mV/s. Note the different current (y-axis) scales

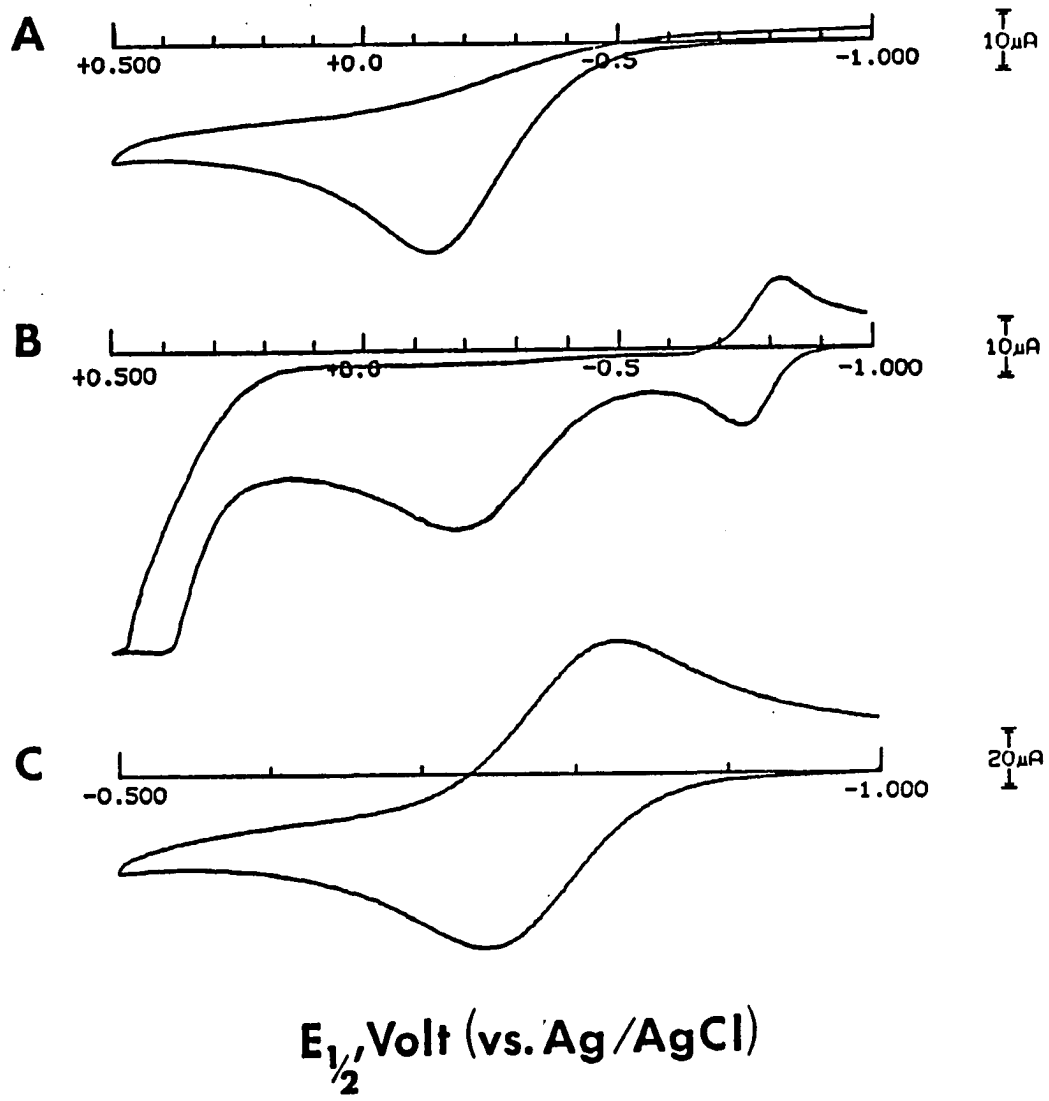

Figure III-13. Cyclic voltammagrams of $[Fe(SCH_2CH_2OH)_4]^{2-}$ in Me_2SO. Reagent concentrations, in order of addition, were 280 mM tetrapropylammonium bromide, 33 mM lithium hydroxide, 100 mM 2-mercaptoethanol and 4 mM iron (II) sulfate. (A) prior to addition of iron, scan rate 100 mV/s; (B) after addition of iron, scan rate 100 mV/s; (C) scan rate 250 mV/s. Note the different current (y-axis) scales

Table III-3. Reduction potential of the $[Fe(SCH_2CH_2OH)_4]^{1/2-}$ couple in various solvents[a]

Solvent	Dielectric constant	E° (mV)[b]
dimethyl sulfoxide	49	-784
water	78	-336
formamide	110	-502
N-methylacetamide	181	-582

[a]Samples were prepared as described in the experimental section.

[b]Potentials measured against a Ag/AgCl reference electrode using a glassy carbon working electrode. The Ag/AgCl electrode has a potential of 232 mV versus N.H.E.

water. The reduction potential has been examined using a mixed Me_2SO/H_2O solvent system. The value of the reduction potential increases as the percentage of water in the solvent is increased (see Figures III-14 and III-15 and Table III-4). Similar behavior is observed for the $[Fe(SCH_2CH_2OH)_4]^{1-/2-}$ couple in water mixed with a solvent having a dielectric constant much greater than that of water, e.g., formamide or N-methylacetamide (see Table III-3). The results of experiments with mixed water/formamide and water/N-methylacetamide solvent systems are listed in Tables III-5 and III-6, respectively. The results of these experiments show that there is no clear correlation between the reduction potential and the solvent dielectric constant (see Table III-3). Based on these results, it appears that water has a unique capacity to raise the reduction potential of the $Fe-S_4$ core.

The UV-visible spectrum (Figure III-16) of an air oxidized solution of $[Fe(SCH_2CH_2OH)_4]^{2-}$ in Me_2SO containing excess thiol shows increased absorbance around 470 nm, but retention of the features at 310 and 340 nm associated with the reduced mononuclear species. The ^1H NMR spectrum (Figure III-17) shows a new resonance at 37 ppm, but the relatively intense signal at 210 ppm indicates that $[Fe(SCH_2CH_2OH)_4]^{2-}$ is the dominant component. Figure III-18 shows the ^1H NMR spectrum obtained when the sample is prepared with a stoichiometric amount of thiol. In addition to the reduced monomer resonance at 219 ppm and the new resonance at 38 ppm (found in the sample with excess thiol), there are several resonances in the 160 to 100 ppm region. These resonances may be attributed to the formation of $[Fe_4(SCH_2CH_2OH)_{10}]^{2-}$ and similar substituted species. The ^1H NMR spectrum of a Me_2SO-d_6 solution of a sample prepared under argon starting from a 1/4 ratio of $FeCl_3$ and 4 $HOCH_2CH_2S^-$ contained resonances at 113 and 143 ppm. A pair of resonances at 113 and 143 ppm is characteristic of $[Fe_4(SR)_{10}]^{2-}$ (vide infra) (13). The methyl

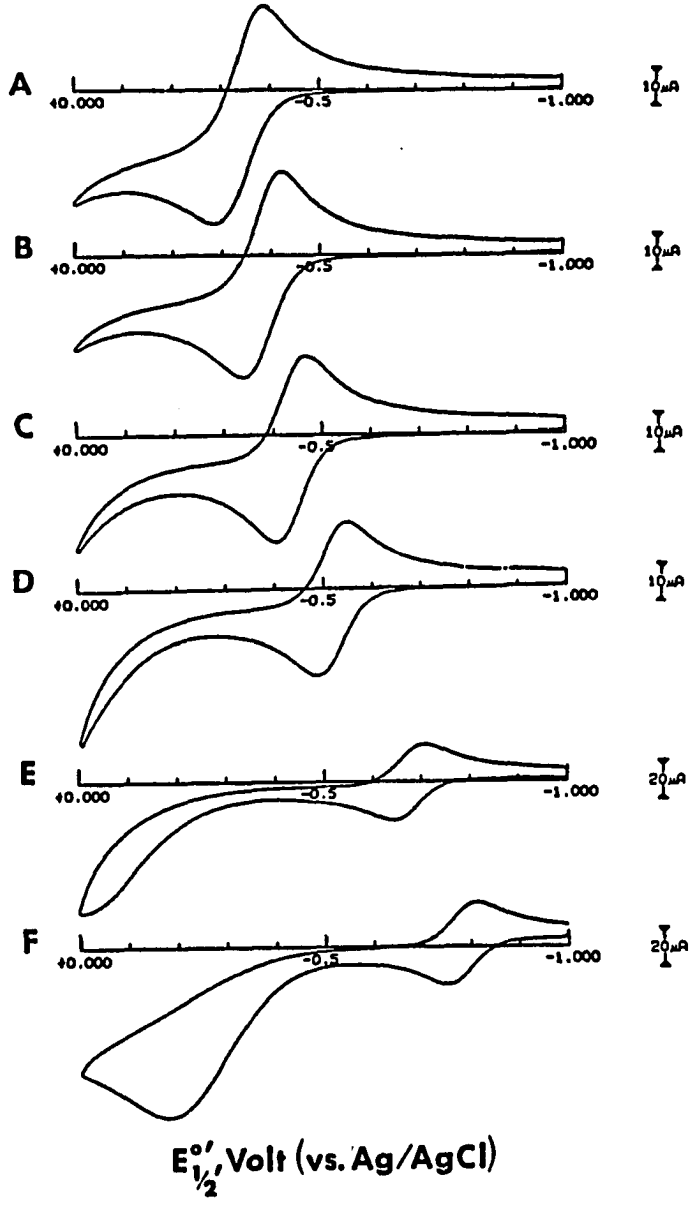

Figure III-14. Reduction potential of $[Fe(SCH_2CH_2OH)_4]^{2-}$ as a function of solvent composition. Stock solutions of the complex were prepared in H_2O and Me_2SO. Reagent concentrations for each solution were 100 mM tetraethylammonium tetrafluoroborate, 32 mM lithium hydroxide, 128 mM 2-mercaptoethanol and 4 mM iron (II) sulfate. Solvent compositions, by volume percentage H_2O, were: (A) 100; (B) 80; (C) 60; (D) 40; (E) 20; (F) 0. Note the change in the current (y-axis) scale for voltammagrams E and F

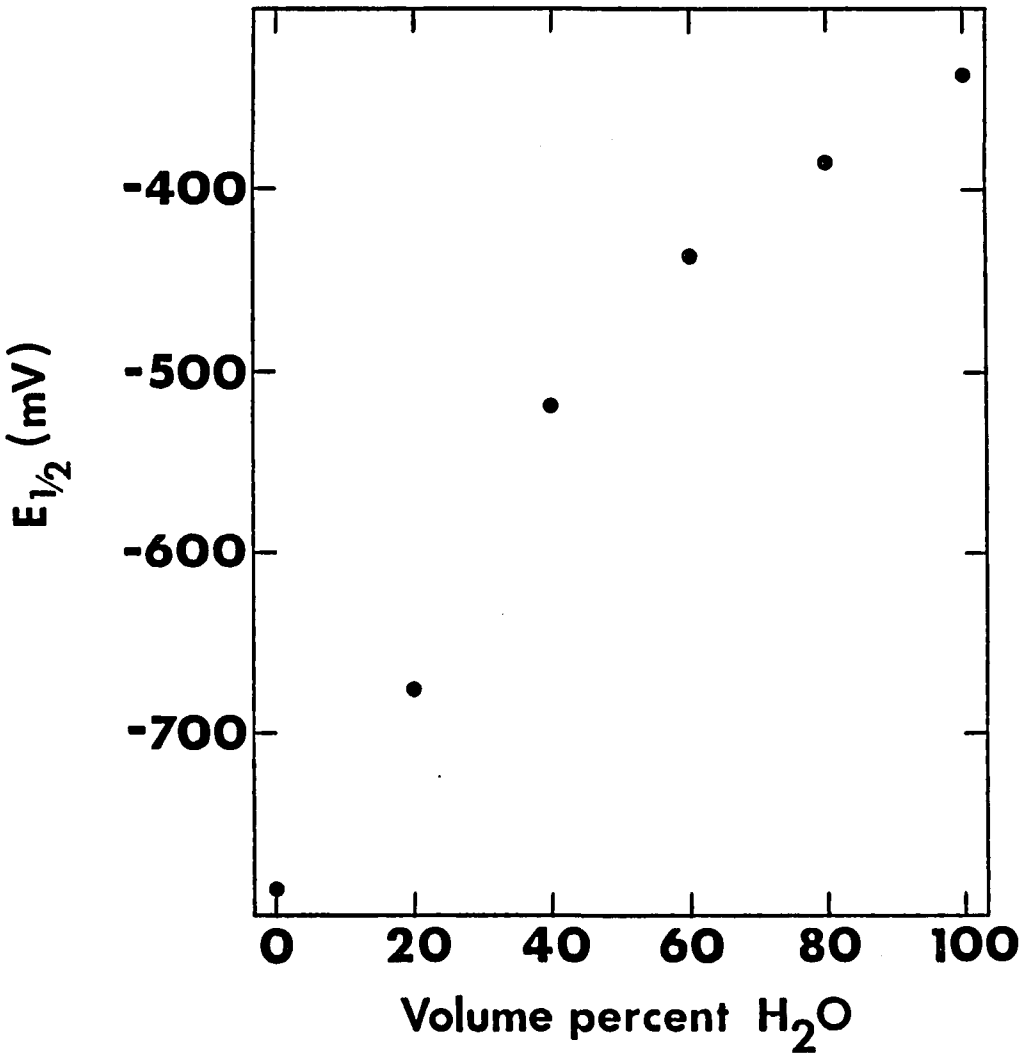

Figure III-15. Plot of $E_{\frac{1}{2}}$ (vs. Ag/AgCl) for the $[Fe(SCH_2CH_2OH)_4]^{1-/2-}$ couple versus solvent composition (% H_2O) in mixed water/dimethyl sulfoxide solutions

Table III-4. Reduction potential of the $[Fe(SCH_2CH_2OH)_4]^{1/2-}$ couple as a function of solvent composition in water/dimethyl sulfoxide solutions[a]

%H_2O	$E_{\frac{1}{2}}$ (mV)[b]	ΔE_p (mV)[c]	i_a/i_c[d]
0	-784	62	1.04
20	-676	69	1.05
40	-519	64	1.09
60	-438	63	1.07
80	-384	79	1.04
100	-336	103	1.04

[a]Stock solutions of the complex were prepared in water and dimethyl sulfoxide. Reagent concentrations for each solution were 100 mM tetramethylammonium tetrafluoroborate, 32 mM lithium hydroxide, 128 mM 2-mercaptoethanol and 4 mM iron (II) sulfate. Samples were prepared by mixing the appropriate volumes of each stock solution in the electrochemical cell.

[b]Potentials measured against a Ag/AgCl reference electrode using a glassy carbon working electrode.

[c]Potential separation between the anodic and cathodic peaks.

[d]Ratio of anodic peak current to cathodic peak current.

Table III-5. Reduction potential of the $[Fe(SCH_2CH_2OH)_4]^{1-/2-}$ couple as a function of solvent composition in water/formamide solutions[a]

%H_2O	$E_{\frac{1}{2}}$ (mV)[b]	ΔE_p (mV)[c]	i_a/i_c[d]
0	-502	62	1.02
20	-453	69	1.04
40	-414	114	1.04
60	-383	62	1.06
80	-361	93	1.13
100	-328	141	1.06

[a]Stock solutions of the complex were prepared in water and formamide. Reagent concentrations for each solution were 100 mM tetramethylammonium tetrafluoroborate, 32 mM lithium hydroxide, 128 mM 2-mercaptoethanol and 4 mM iron (II) sulfate. Samples were prepared by mixing the appropriate volumes of each stock solution in the electrochemical cell.

[b]Potentials measured against a Ag/AgCl reference electrode using a glassy carbon working electrode.

[c]Potential separation between the anodic and cathodic peaks.

[d]Ratio of anodic peak current to cathodic peak current.

Table III-6. Reduction potential of the $[Fe(SCH_2CH_2OH)_4]^{1-/2-}$ couple as a function of solvent composition in water/N-methylacetamide solutions[a]

%H_2O	$E_{\frac{1}{2}}$ (mV)[b]	ΔE_p (mV)[c]	i_a/i_c[d]
0	-582	72	0.99
20	-517	105	0.99
40	-450	77	1.01
60	-402	74	1.06
80	-363	76	1.00
100	-330	96	0.98

[a]Stock solutions of the complex were prepared in water and N-methylacetamide. Reagent concentrations for each solution were 100 mM tetramethylammonium tetrafluoroborate, 32 mM lithium hydroxide, 128 mM 2-mercaptoethanol and 4 mM iron(II) sulfate. Samples were prepared by mixing the appropriate volumes of the stock solutions in the electrochemical cell.

[b]Potentials measured against a Ag/AgCl reference electrode using a glassy carbon working electrode.

[c]Potential separation between the anodic and cathodic peaks.

[d]Ratio of anodic peak current to cathodic peak current.

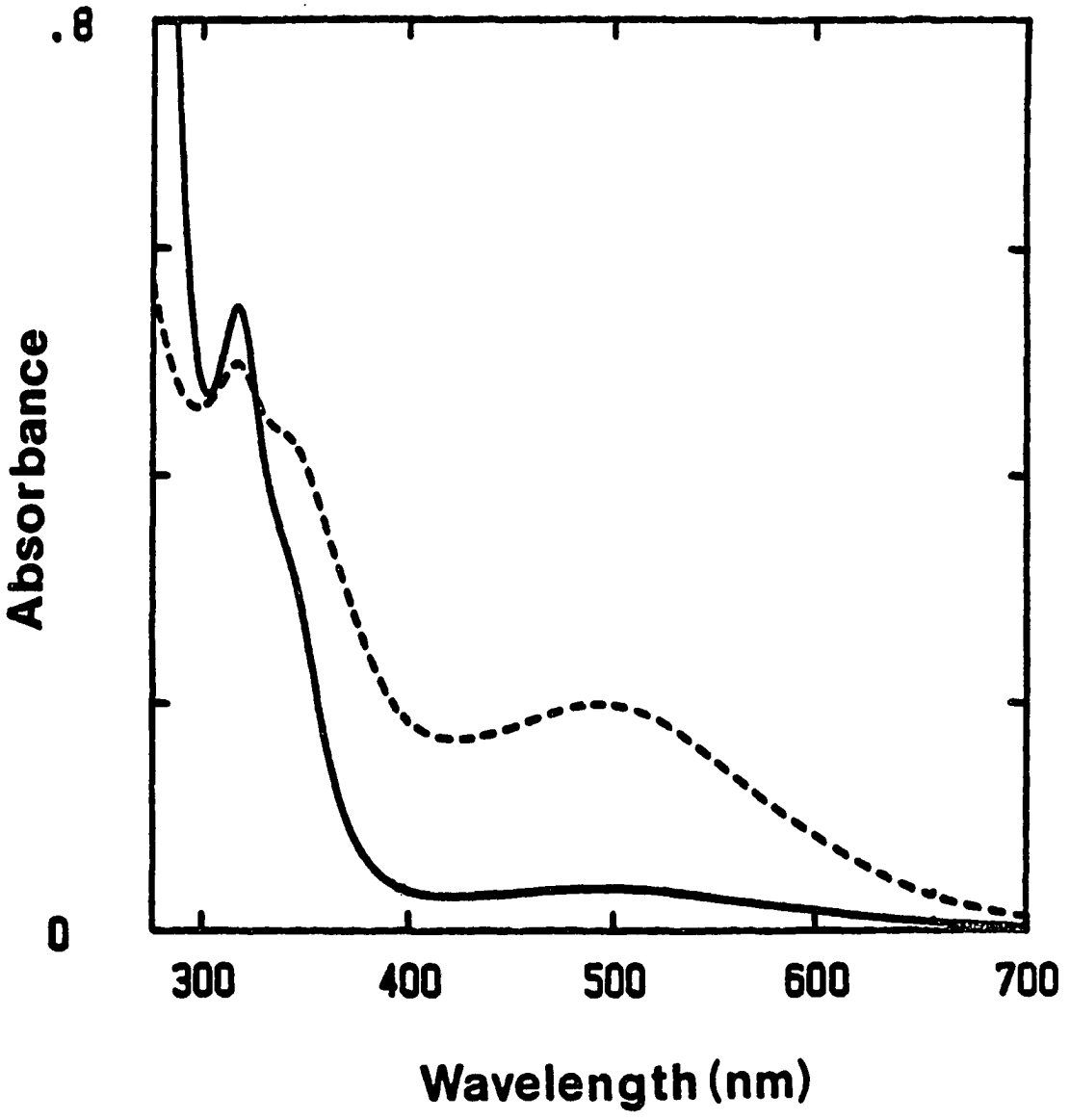

Figure III-16. UV-visible absorption spectrum of a Me_2SO solution of $[Fe(SCH_2CH_2OH)_4]^{2-}$. Solid line indicates solution under an argon atmosphere, dashed line indicates the same solution exposed to air. Final reagent concentrations were 50 mM lithium hydroxide, 50 mM 2-mercaptoethanol and 10 mM ferrous chloride. Cell pathlength = 0.01 cm

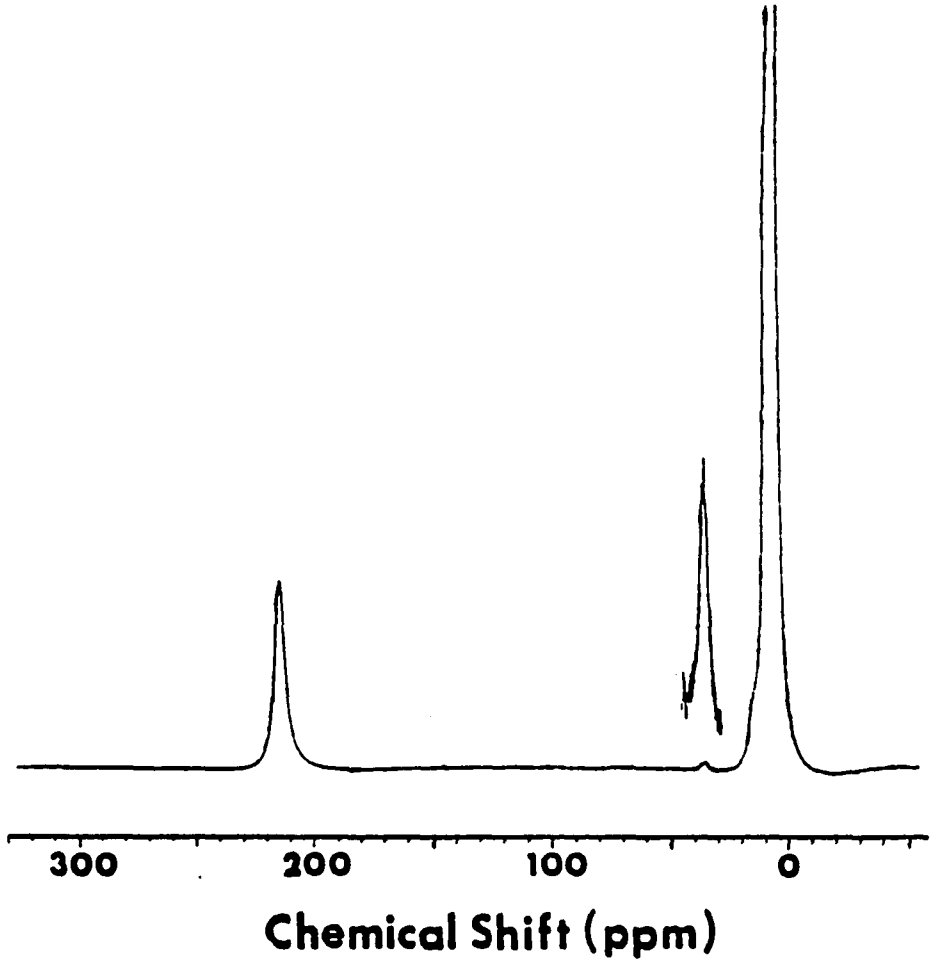

Figure III-17. 250 MHz ^{1}H NMR spectrum of a partially air-oxidized Me_2SO-d_6 solution of 140 mM LiOH, 200 mM $HOCH_2CH_2SH$ and 39 mM $FeCl_2$. The spectrum was recorded at 27 °C

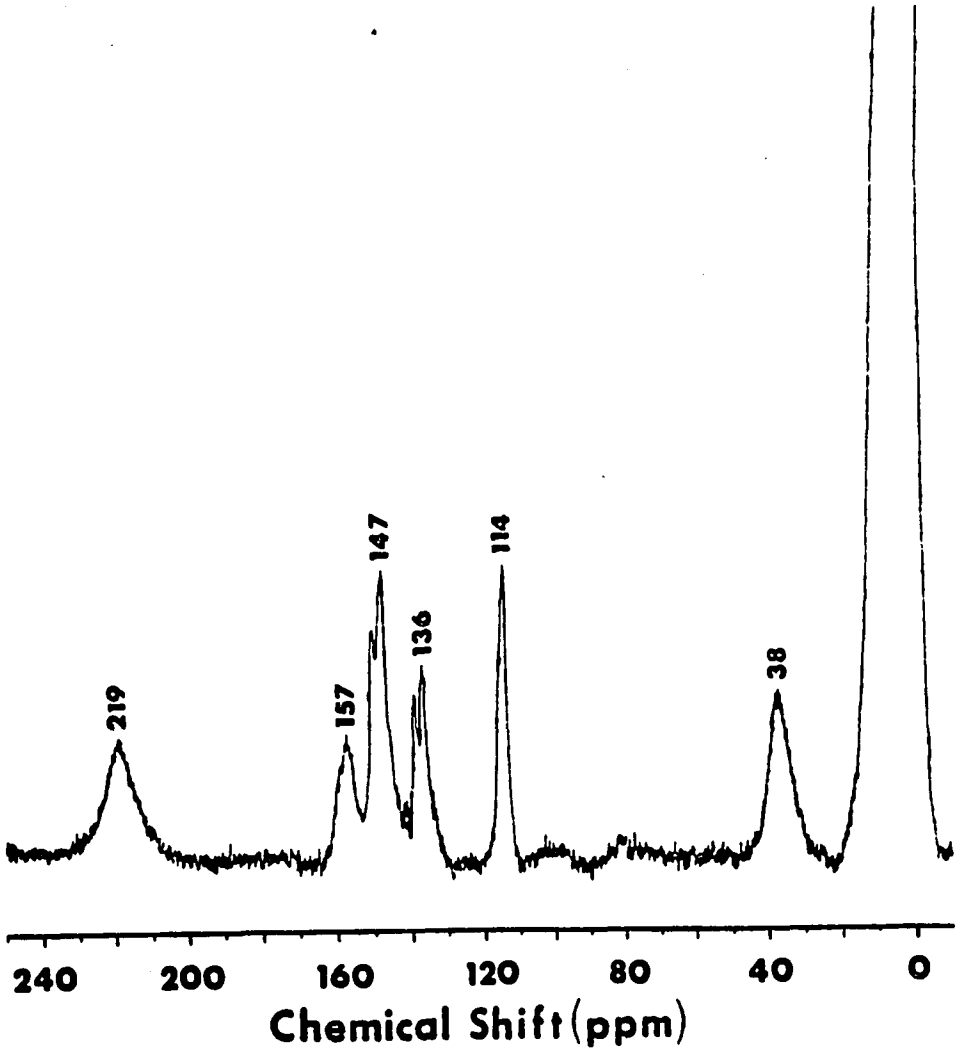

Figure III-18. 250 MHz ^1H NMR spectrum of a partially air-oxidized Me_2SO-d_6 solution of 520 mM LiOH, 1.1 M $HOCH_2CH_2SH$ and 63 mM $FeCl_3$. The spectrum was recorded at 27 °C

hydrogens of $[Fe(SCH_2CH_3)_4]^{1-}$ are reported to resonate at ~40 ppm downfield (80). On this basis, the new resonance at ~37 ppm is tentatively assigned to the $[Fe(SCH_2C\underline{H}_2OH)_4]^{1-}$ hydrogens.

The ^1H NMR spectrum of an air-oxidized sample of the mononuclear dithiothreitol complex contained at least a dozen resonances spread from 80 to 320 ppm downfield. The chemical shifts of the resonances in the dithiothreitol sample did not corresponded to any known iron-thiolate species. All attempts to isolate a $[Fe(SR)_4]^{1-}$ species using 2-mercaptoethanol, dithiothreitol or glutathione, were unsuccessful.

The ^1H NMR spectrum of a species generated by mixing a 2.5/5/1 mole ratio of LiOH/2-mercaptoethanol/$FeCl_2$ in D_2O is shown in Figure III-19. At 5 °C the spectrum has resonances at 105 and 142 ppm. By analogy to $[Fe_4(SCH_2CH_3)_{10}]^{2-}$ (13) the resonance at 142 ppm is assigned to the bridging thiolate groups and the resonance at 105 ppm is assigned to the terminal thiolate groups of $[Fe_4(SCH_2CH_2OH)_{10}]^{2-}$. As the temperature is increased these resonances begin to broaden. By 30 °C the resonance for the terminal thiolates has broadened into the baseline. Presumably, this differential broadening is due to the chemical exchange between free and bound thiolate occurring more readily at the terminal positions than at the bridging positions. The resonance at ~10 ppm is tentatively assigned to $[Fe_4(SCH_2C\underline{H}_2OH)_{10}]^{2-}$ hydrogens. Unfortunately, the resonance position(s) for the analogous hydrogens in $[Fe_4(SCH_2CH_3)_{10}]^{2-}$ were not reported. All attempts to isolate $[Fe_4(SCH_2CH_2OH)_{10}]^{2-}$ have been unsuccessful.

The synthesis of $[Fe(SR)_4]^{2-}$ in aqueous solution requires sufficient LiOH to deprotonate at least four moles of thiol per mole of Fe(II). When the ratio of thiolate to iron is between 2.5 and 4.0, ^1H NMR spectra of the solutions show a mixture of $[Fe(SR)_4]^{2-}$ and $[Fe_4(SR)_{10}]^{2-}$ (Figure III-20). This same pattern is observed even when the total thiol to Fe(II) ratio is increased. Thus, the equilibrium is dependent on the

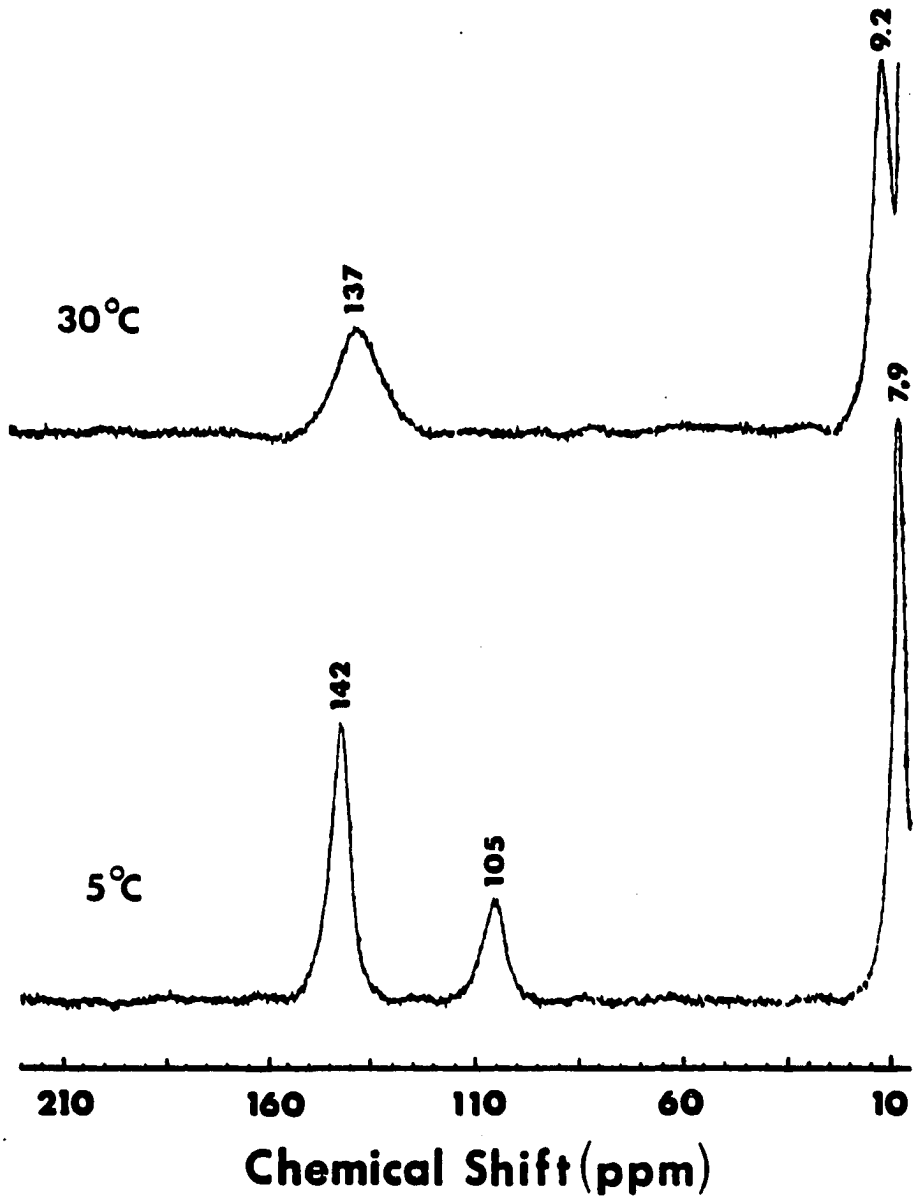

Figure III-19. 300 MHz ^1H NMR spectra of $[Fe_4(SCH_2CH_2OH)_{10}]^{2-}$ in D_2O solution at 5 and 30 °C. The sample was prepared by the general procedure using 50 mM LiOH, 130 mM 2-mercaptoethanol and 25 mM $FeCl_2$

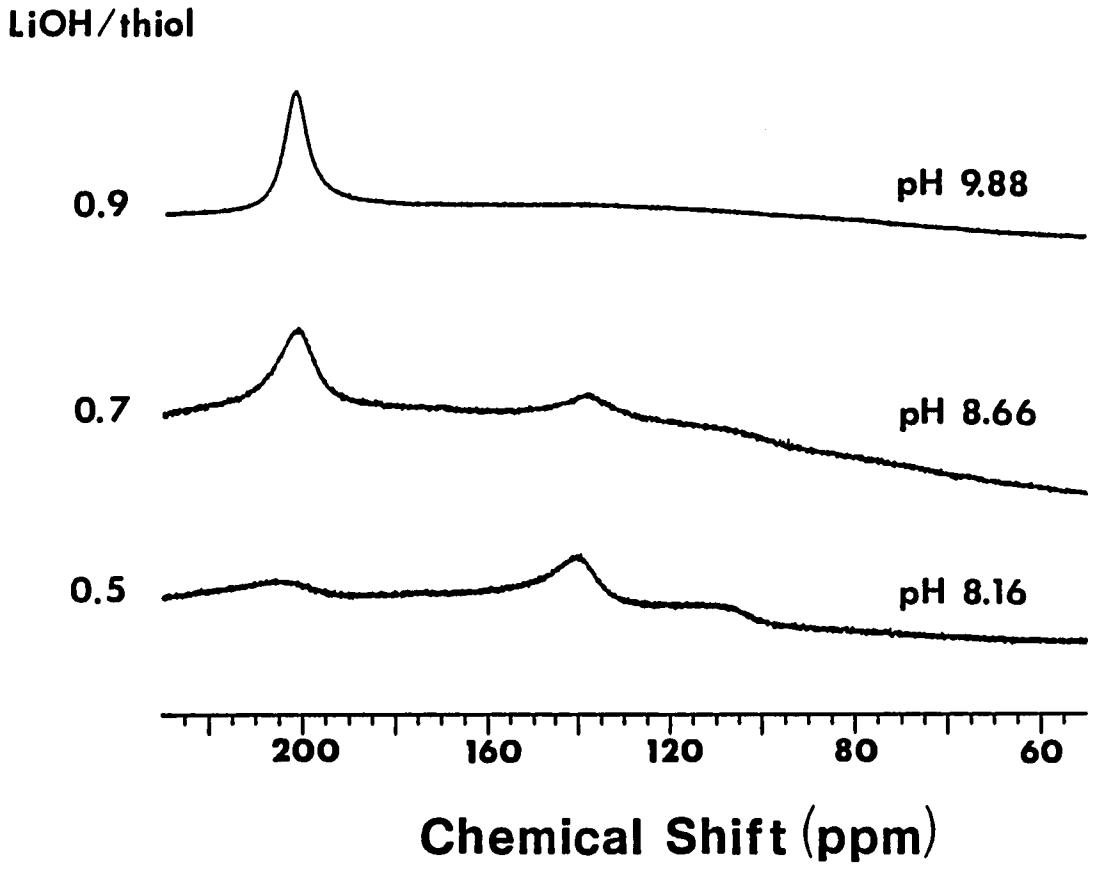

Figure III-20. 300 MHz ^{1}H NMR spectra of D_2O solutions of 5/1 2-mercaptoethanol/$FeCl_2$ where the LiOH/2-mercaptoethanol ratios are 2.5/5, 3.5/5, and 4.5/5. The spectra were recorded at 25 °C. pH values are uncorrected for the deuterium isotope effect and were measured with argon flowing over the solution

thiolate concentration, not the total concentration of thiol. Controlling the concentration of thiolate by pH buffering is impractical because the relatively high reagent concentrations used in these experiments overwhelm the capacity of the buffer system. Addition of solid LiOH, which could be readily weighed in the desired amount, proved to be a much simpler way of obtaining a desired thiolate concentration.

Attempts to prepare a discrete species by addition of iron to apoferredoxins from spinach and C. pasteurianum produced only one ill-defined complex. Figure III-21 shows the ^1H NMR spectrum of a complex formed at pH ~9 by the addition of 2.5-fold molar excess of Fe(II) to spinach apoferredoxin under argon. Two resonances were found downfield at 35 and 75 ppm, no other resonances were found out to 240 ppm. A similar complex could be formed with C.p. apoferredoxin. The UV-visible spectrum of this complex was essentially featureless, showing only additional absorbance on the tail of the 280 nm band of the protein.

Iron-Thiolate Proteins

The discrepancy between the ^1H NMR assignment of the methylene hydrogen resonances α to the coordinated sulfur in the $[Fe(SR)_4]^{2-}$ complexes (Figure III-4) and the corresponding β-CH_2 cysteinyl resonances in reduced rubredoxin (50) prompted the reexamination of the ^1H NMR spectra of rubredoxins. The initial goal was to search the 200 ppm downfield region for resonances similar to the 200-230 ppm resonances of the synthetic analogs.

Figure III-22 shows the region from 260 to 100 ppm downfield in the spectrum of D. gigas rubredoxin. Spectra A and B are of the reduced rubredoxin at 40 and 55 °C, respectively. Four resonances are found in the downfield region of the reduced protein. These resonances are all roughly equal in area. Spectrum C shows that these

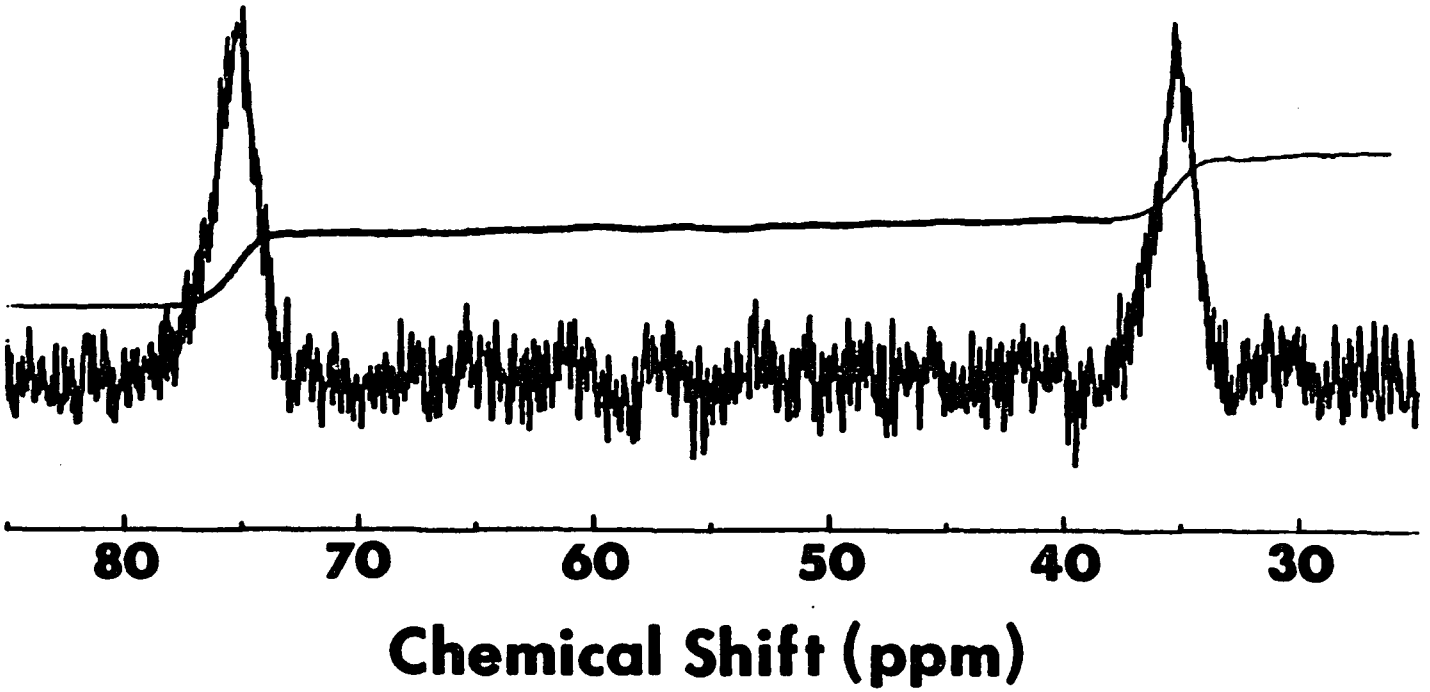

Figure III-21. 300 MHz ^{1}H NMR spectrum of a ~1 mM solution of spinach apoferredoxin after addition of 2.5 mM ferrous ammonium sulfate. The spectrum was recorded at 25 °C. The sample was prepared under an argon atomosphere in D_2O buffered to pH (uncorrected) 9 with 50 mM sodium borate

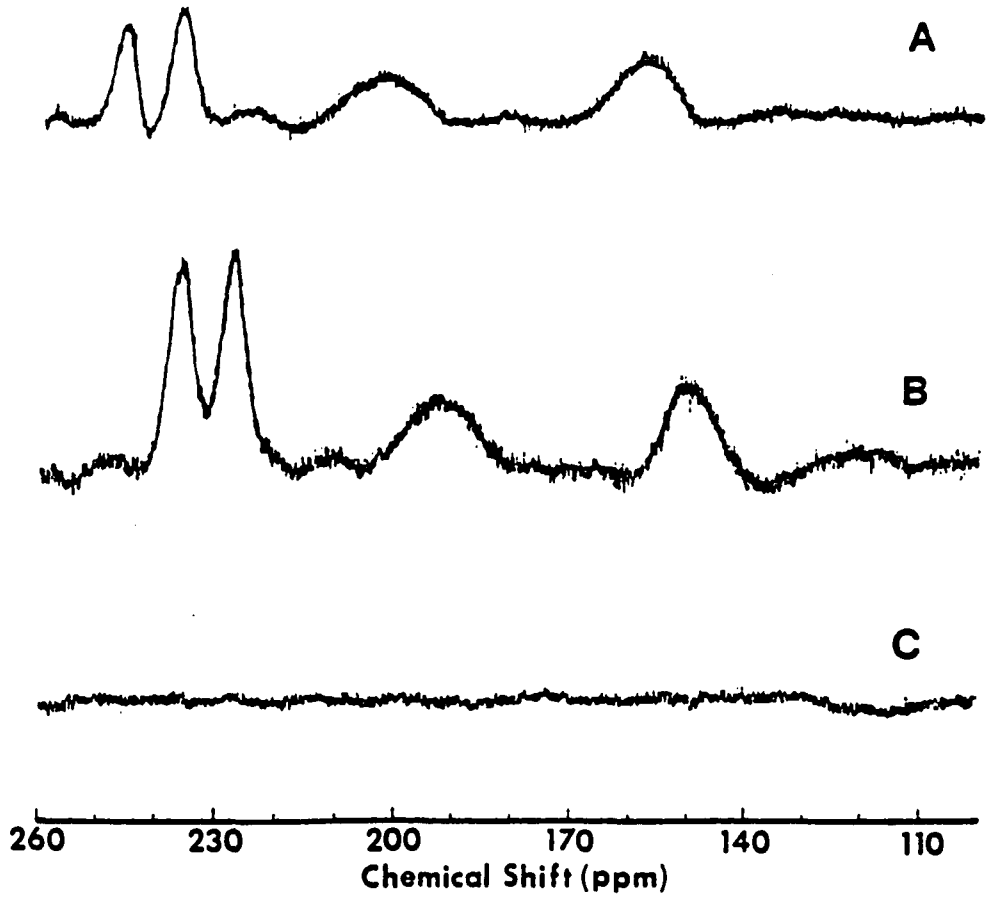

Figure III-22. 300 MHz ^{1}H NMR spectra of D. gigas Rd in the 260-100 ppm region. (A) reduced, 40 °C; (B) reduced, 55 °C; (C) oxidized, 55 °C

resonances disappear when the protein is oxidized. No new resonances were found in the spectrum of oxidized D. gigas rubredoxin from 428 to -128 ppm. Further comparison of spectra A and B shows that the resonances shift upfield and become sharper as the temperature is increased. A plot of the isotropic shifts of these four resonances as a function of T^{-1} is shown in Figure III-23. The chemical shift values of paramagnetically shifted resonances in rubredoxin as a function of temperature are listed in Table III-7. The spectra of reduced rubredoxins isolated from D. vulgaris and C. pasteurianum in the same region from 260 to 100 ppm downfield are shown in Figure III-24. Each of the three rubredoxins displays the same general pattern of resonances. There is a pair of relatively sharp partially overlapping resonances to the far downfield side of the spectrum. In the case of D. vulgaris these resonances are barely resolved even at 55 °C. The remaining two resonances are well resolved but are also very broad. Because of baseline and phasing problems, it is difficult to obtain precise integrations of the areas of these resonances. In the case of D. gigas rubredoxin, however, these areas appear to be roughly 1:1:1:1. These resonances can be assigned to the β-CH_2 cysteinyl hydrogens in rubredoxins by analogy to similar ^1H NMR resonances in the synthetic analogues (Figure III-4).

Figure III-25 shows the 20 to -10 ppm region of the ^1H NMR spectra of D. gigas rubredoxin both in the oxidized and reduced states. Vertical expansion of the 20 to 10 ppm region reveals four previously undiscovered resonances in the reduced form. These resonances display the same temperature dependence as the β-CH_2 resonances, shifting upfield with increasing temperature as a linear function of T^{-1}. The new resonances disappear when the protein is oxidized, leaving only a broad feature at ~13 ppm. By analogy to the group of resonances from 13 to 16 ppm in the Fe(II)/dihydrolipoate complex (Figures III-4 and III-8), these resonances can be assigned to the α-CH

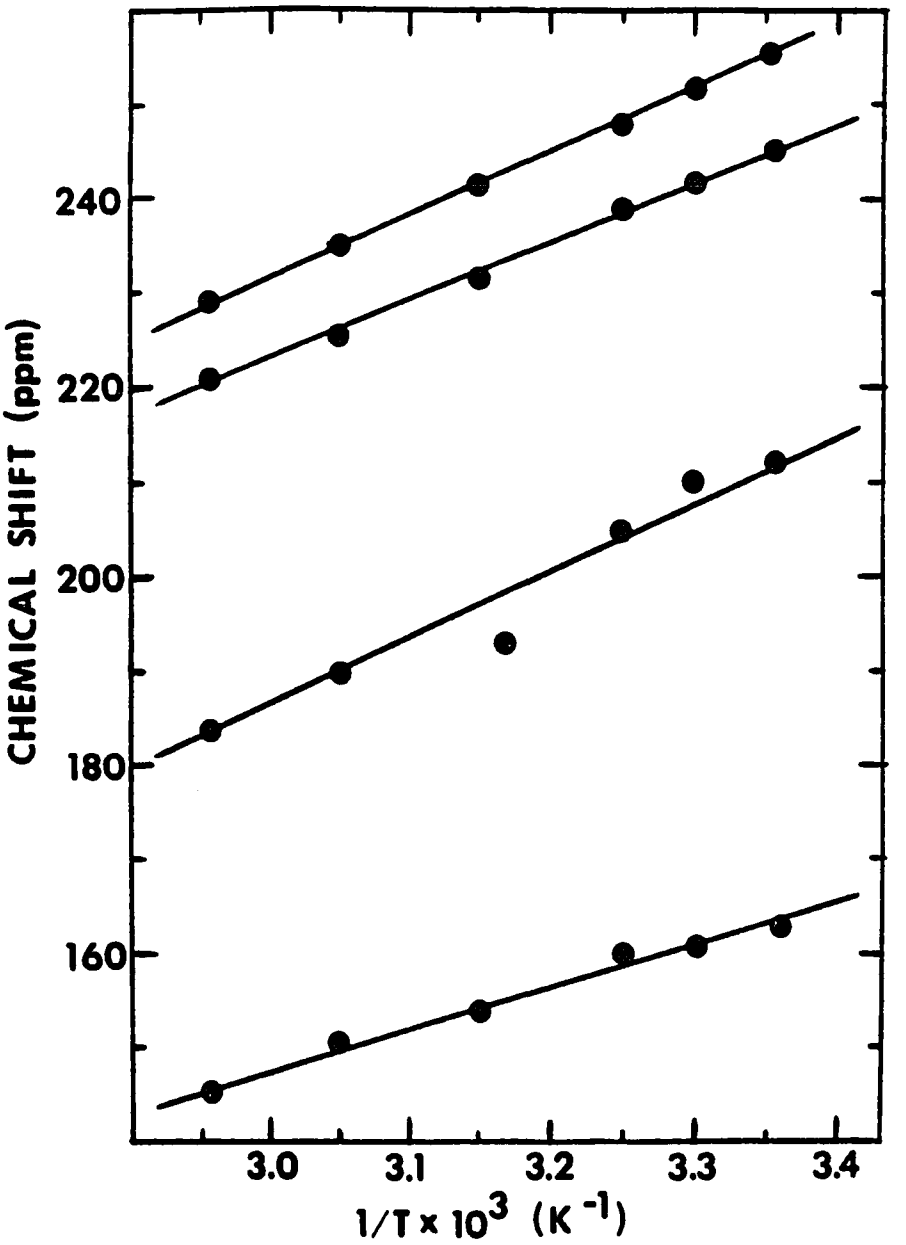

Figure III-23. Plot of chemical shift vs. reciprocal of absolute temperature for the 1H NMR resonances of reduced D. gigas rubredoxin shown in Figure III-22

Table III-7. Chemical shift values as a function of temperature for selected resonances in reduced D. gigas rubredoxin

Temperature (K)	β-CH_2 resonances	α-CH resonances
298	255, 245, 212, 163	17.1, 15.6, 12.6, 11.5
303	252, 242, 210, 161	16.9, 15.4, 12.6, 11.5
308	248, 239, 205, 160	16.7, 15.2, 12.5, 11.5
318	241, 232, 193, 154	16.6, 15.1, 12.5, 11.4
328	234, 226, 190, 151	16.4, 14.8, 12.5, 11.4
338	229, 221, 184, 146	16.2, 14.6, 12.4, 11.3

Temperature (K)	upfield resonances
298	-0.1, n.r.[a], -1.5, -4.5
303	-0.1, n.r., -1.5, -4.3
308	-0.1, -1.2, -1.4, -4.2
318	0.1, -1.0, -1.3, -3.9
328	0.2, -0.8, -1.2, -3.6
338	0.3, -0.6, -1.1, -3.4

[a]Resonance is not resolved at this temperature.

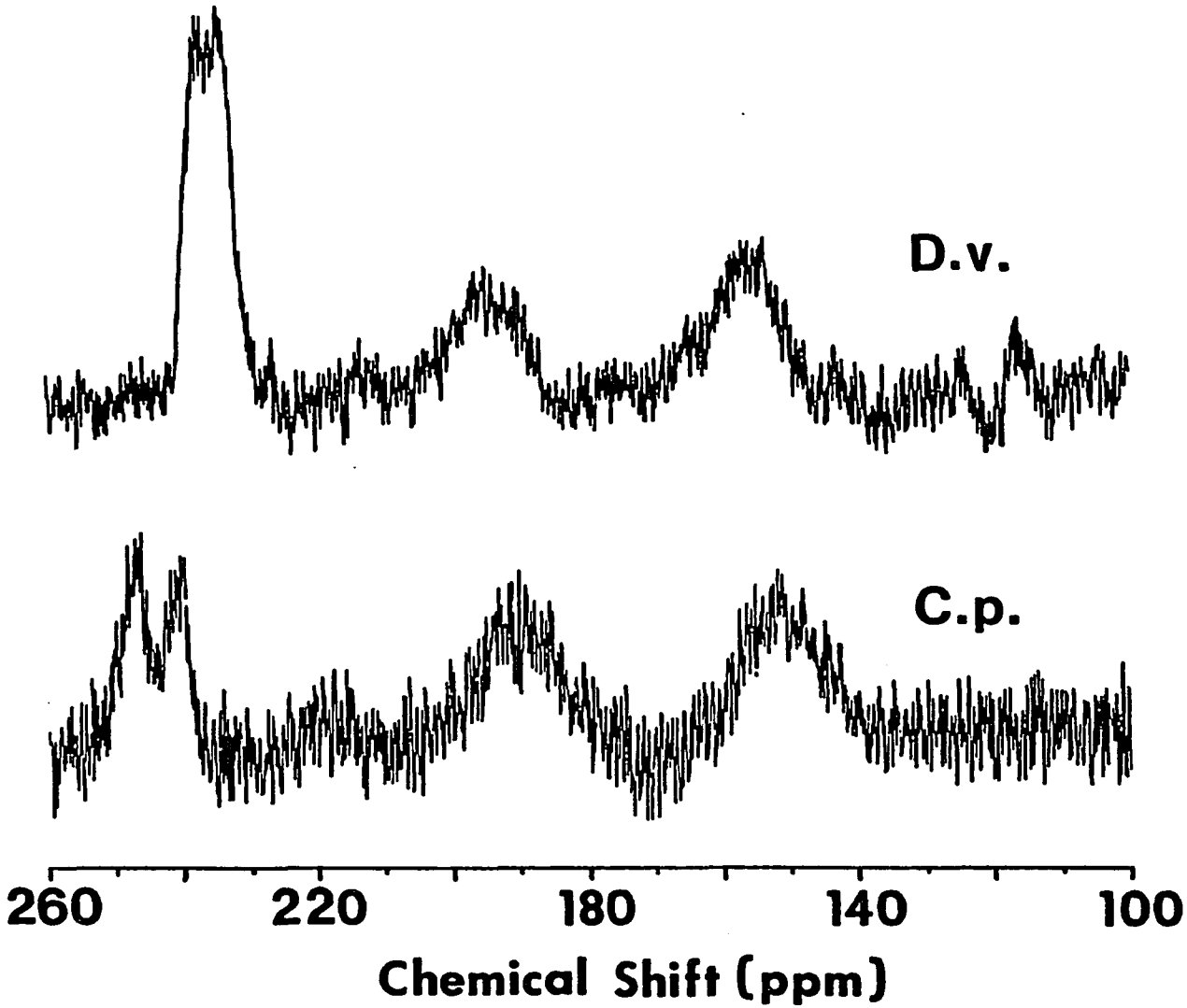

Figure III-24. ^{1}H NMR spectra in the 260-100 ppm downfield region of the reduced rubredoxins from D. vulgaris and C. pasteurianum

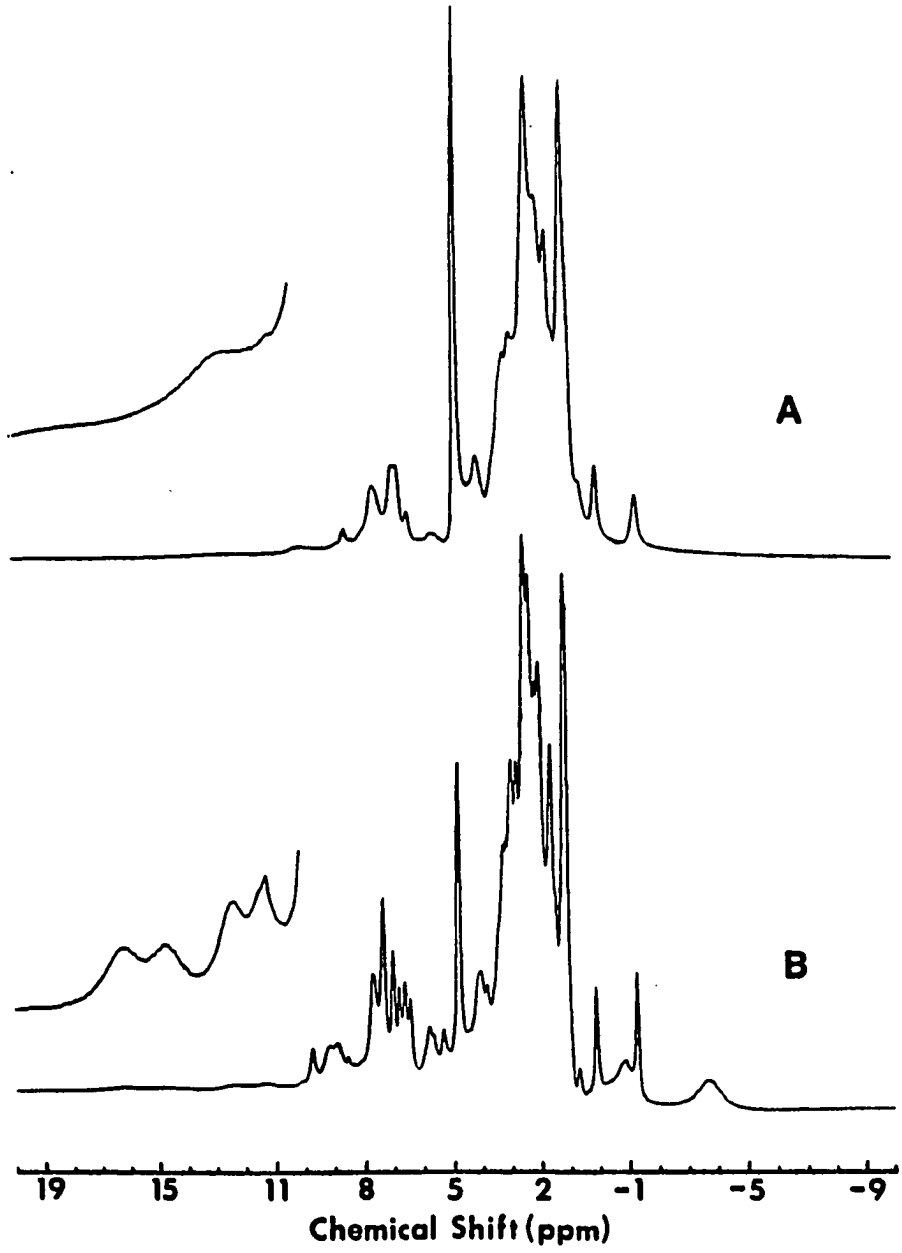

Figure III-25. 300 MHz ^1H NMR spectra of D. gigas Rd in the 20 to -10 ppm region. Spectra were obtained at 55°C: (A) air oxidized protein; (B) reduced protein prepared by addition of a small amount of solid $Na_2S_2O_4$. Insets show 16-fold vertical expansions of paramagnetically broadened resonances

cysteinyl hydrogens. Figure III-26 shows the same region of the spectra of reduced D. vulgaris and C. pasteurianum rubredoxins. Vertical expansions of the 20 to 10 ppm regions again reveal previously undiscovered resonances. Like those for D. gigas rubredoxin, these resonances disappear when the protein is oxidized.

For proteins the range of "diamagnetic" chemical shifts covers the region from 11 to -4 ppm (81). From a cursory examination of the spectra of oxidized and reduced rubredoxin both upfield and downfield of this region, it is obvious that several hydrogens in rubredoxin also experience effects of the paramagnetic iron site. A general broadening of all the peaks in the oxidized spectrum relative to the reduced spectrum is also observed. A good example of this broadening is found in the aromatic region (6 to 8 ppm) of the D. gigas spectrum (Figure III-25) where six sharp, well-resolved resonances for the reduced form collapse into three broad resonances for the oxidized form. In addition to the aforementioned cysteinyl hydrogen resonances, some resonances between 8 to 11 ppm and upfield of 0 ppm also disappear on oxidation.

The upfield region (0 to -15 ppm) of the ^1H NMR spectra of D. gigas is shown in Figure III-27. A new resonance at -10 ppm, with an area of 1-2 hydrogens, is seen in the spectrum of reduced D. gigas rubredoxin. This resonance was obscured by a probe artifact in the older instrument used in earlier experiments and, therefore, was not included in the previously published report of the rubredoxin ^1H NMR spectra (82). The reduced D. gigas rubredoxin spectrum contains a pattern of alternating sharp and broad resonances in the 0 to -5 ppm region (Figure III-27). The same pattern is observed for D. vulgaris rubredoxin, whereas, a significantly different pattern is observed for reduced C. pasteurianum rubredoxin (Figure III-26). These differences will be discussed in terms of amino acid substitutions.

The spin-lattice relaxation time, T_1, has been measured for several resonances in

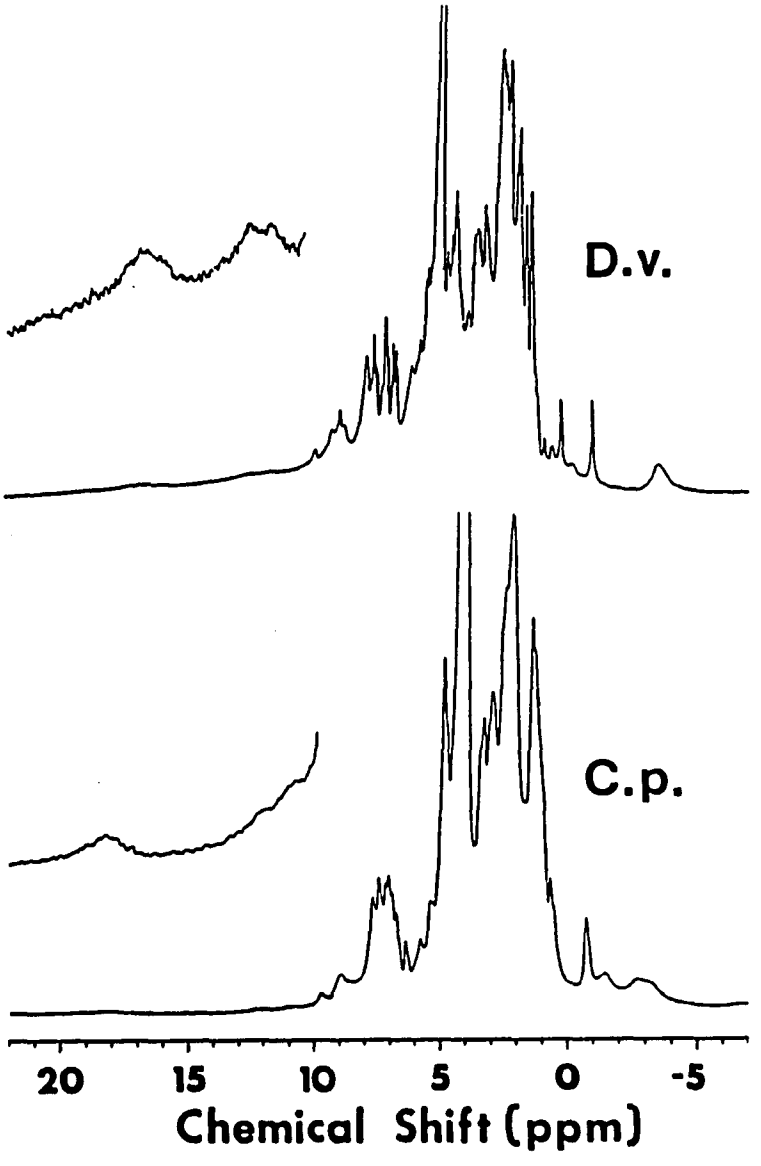

Figure III-26. ^{1}H NMR spectra from 20 to -10 ppm of dithionite reduced rubredoxins from (A) D. vulgaris (300 MHz) and (B) C. pasteurianum (250 MHz). Insets show 16-fold vertical expansions of paramagnetically broadened resonances

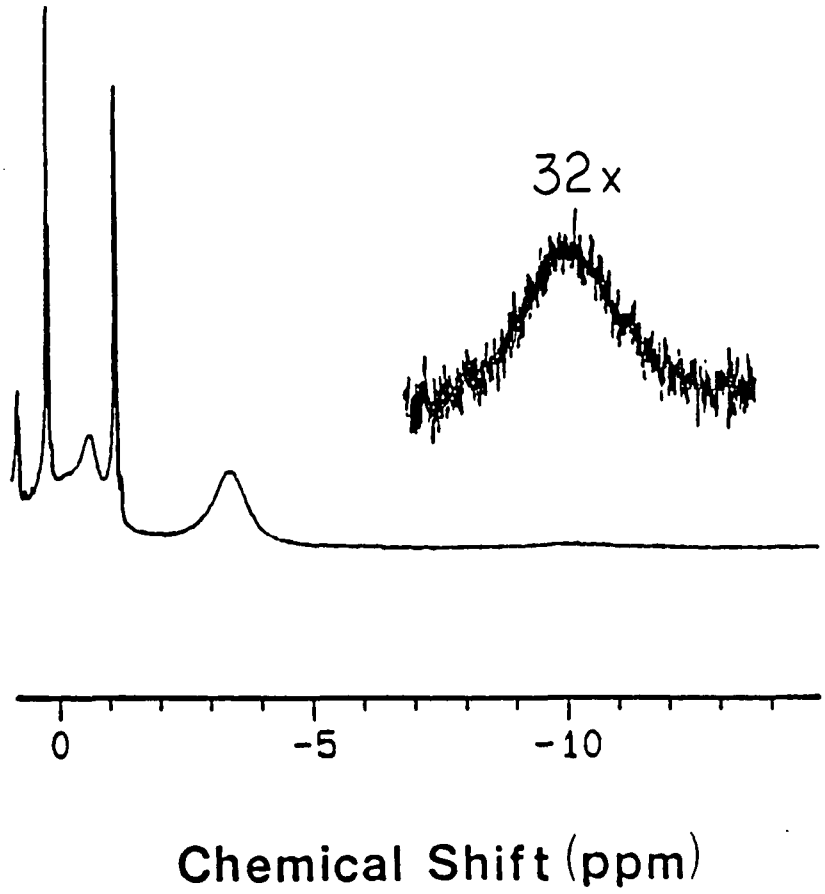

Figure III-27. Upfield region (0 to -15 ppm) of the 500 MHz ^{1}H NMR spectrum of reduced D. gigas rubredoxin showing the previously unobserved resonance at -10 ppm

the ^1H NMR spectrum of reduced D. gigas rubredoxin. ^1H NMR spectra illustrating the spin-lattice relaxation behavior of the α-CH cysteinyl hydrogen resonances in reduced rubredoxin are shown in Figure III-28. The resonance intensities as a function of the delay time, tau, were fitted to a single exponential (Figure III-29) to obtain the T_1 value. The T_1 values reported in Table III-8 are 2-3 orders of magnitude faster than for hydrogens in simple organic molecules. The primary relaxation mechanism for these hydrogens is through a dipolar interaction between the magnetic moment of the unpaired electrons on the metal and the nuclear magnetic moment. Direct measurement of the T_1 values for the β-CH_2 resonances in the 150-250 ppm region is technically difficult. The problems include loss of radiofrequency power when irradiating over large spectral bandwidths, inaccurate measurements of the intensities of broad, weak resonances and fold-over of intense resonances from outside the spectral window. Likewise, the T_1 value for the broad, weak resonance at -10 ppm could not be measured accurately due its very fast relaxation.

Several attempts were made to observe a steady-state nuclear Overhauser effect (N.O.E.) between the β-CH_2 and α-CH cysteinyl hydrogens. The steady-state N.O.E. experiment requires a pulse of sufficient duration and power to saturate the desired resonance (i.e., reduce the resonance intensity to zero). It was not possible to find a combination of pulse length and power (powers up to ~1 milliwatt were used) capable of completely saturating either the α-CH or β-CH_2 resonances in reduced rubredoxin. Nuclear Overhauser effects were not observed for any of the cysteinyl hydrogen resonances of reduced rubredoxin. However, the irradiation of the α-CH resonances (~1 mW for 400 msec) was sufficient to produce nuclear Overhauser effects to resonances in the diamagnetic region, particularly for the aromatic region around 6-8 ppm (Figure III-30). Unfortunately, resonances in that region have not yet been assigned.

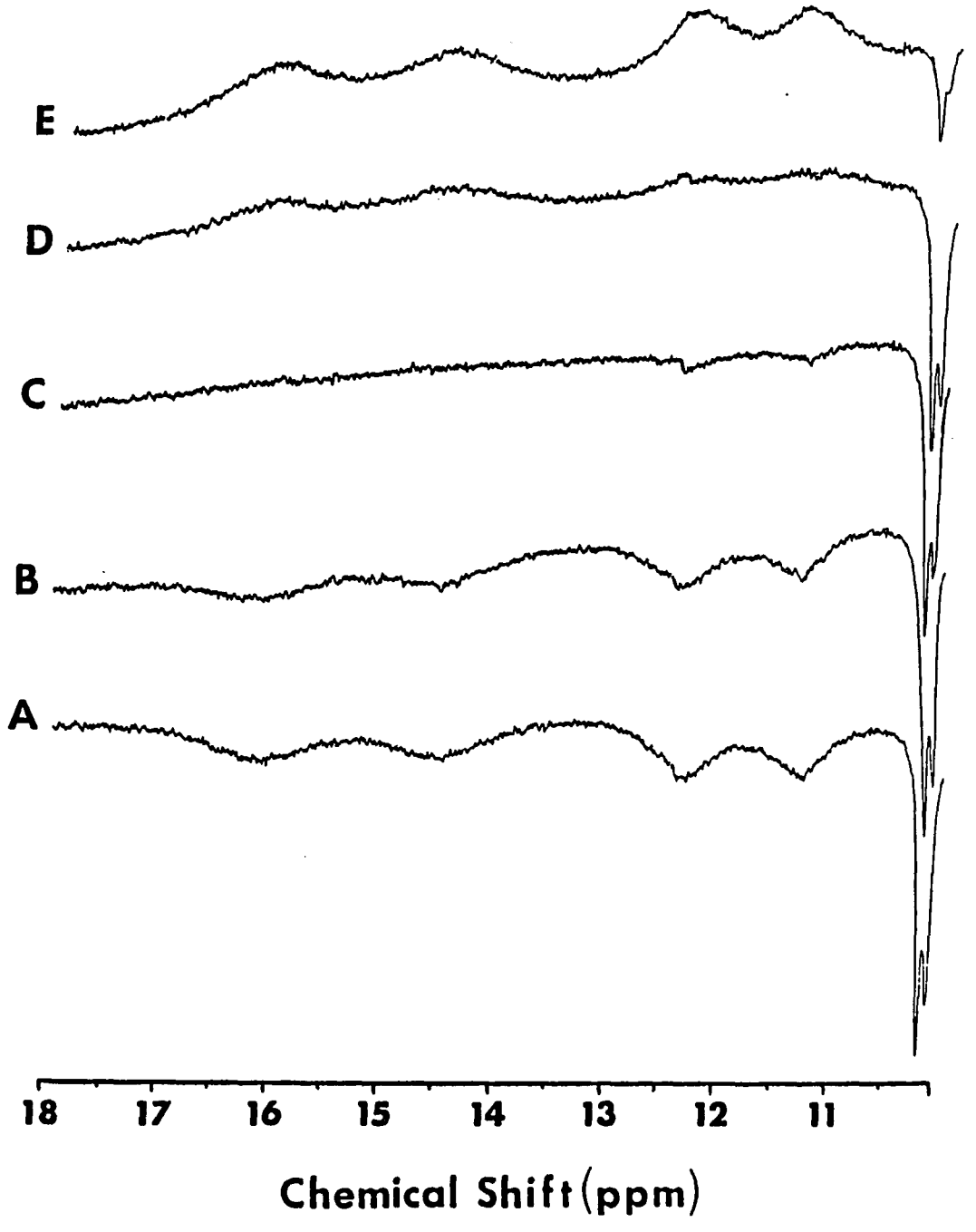

Figure III-28. 500 MHz ^{1}H NMR spectra illustrating the longitudinal relaxation of the α-CH cysteinyl hydrogens in D. gigas Rd at 55°C. The tau delay values (ms) were: (A) 0.001; (B) 0.10; (C) 0.50; (D) 1.0; (E) 10.0. Further details are given in the experimental section

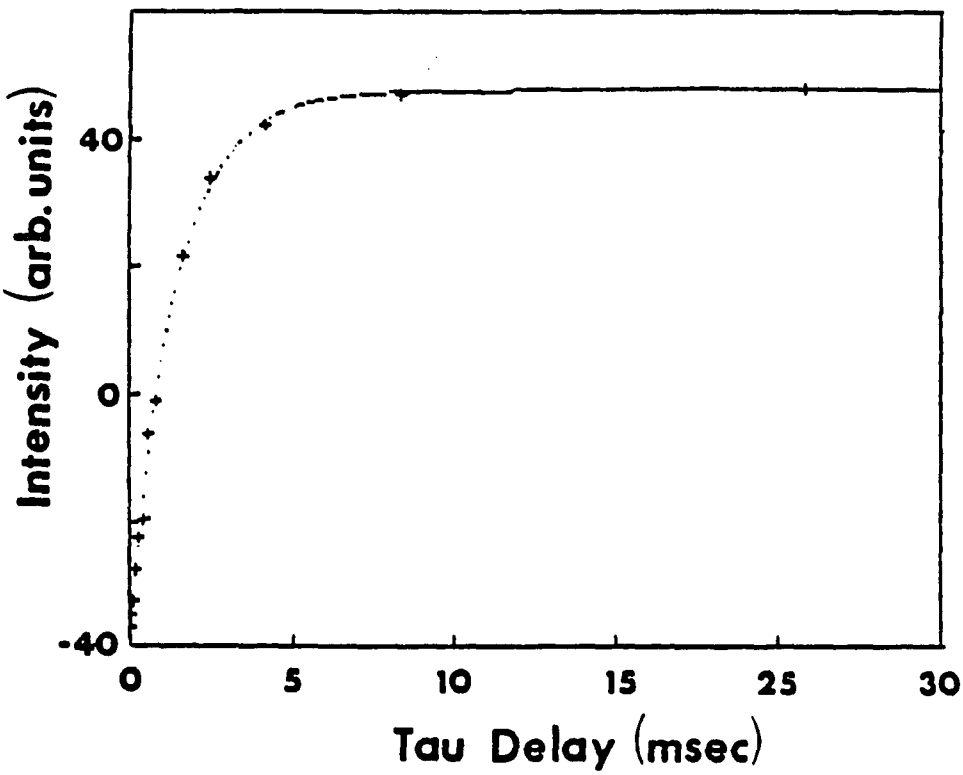

Figure III-29. Plot of peak intensity vs. tau delay for the -3.5 ppm resonance in reduced Rd at 55 °C. The data were fitted to a single exponential using the basic program EXPSUM. See the experimental section for further details

Table III-8. Longitudinal relaxation times (T_1) for selected ^1H NMR resonances in reduced D. gigas rubredoxin[a]

Chemical shift (ppm)	T_1 (msec)[b]
-3.4	1.7
11.3	1.0
12.4	1.0
14.5	0.64
16.1	0.70

[a]Experiment was performed at 328 K (55 °C).

[b]T_1's were measured using a 180° - τ - 90° pulse sequence. See the experimental section for further details.

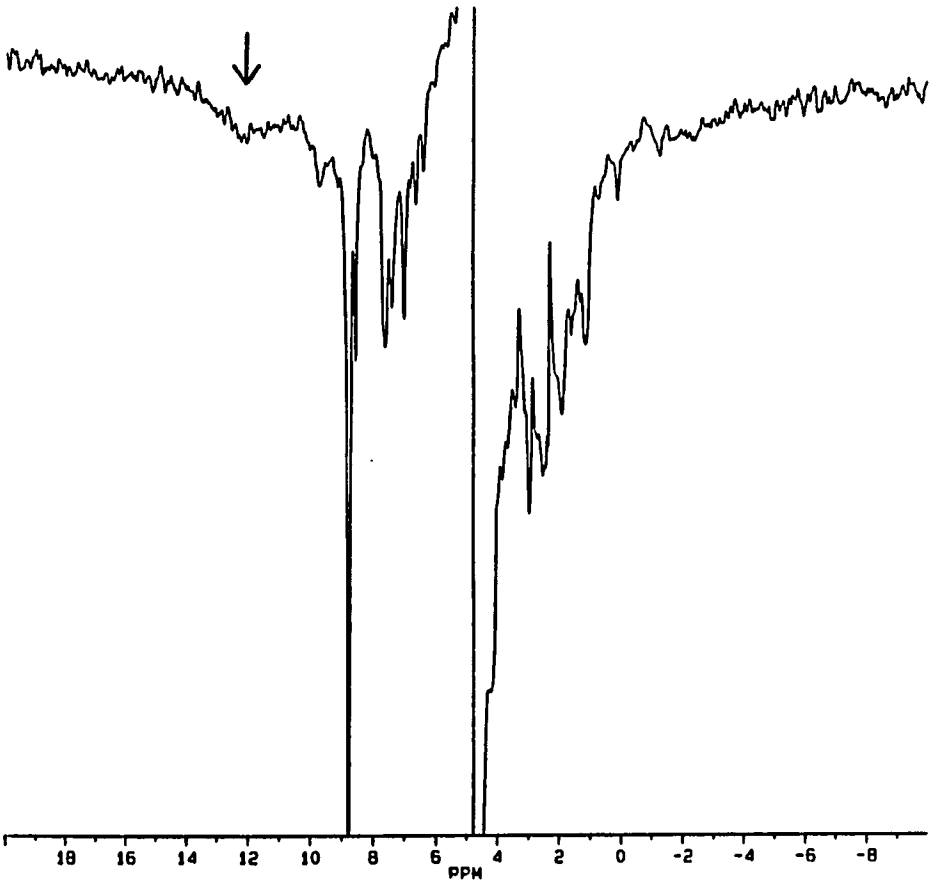

Figure III-30. 250 MHz N.O.E. difference spectrum of reduced D. gigas rubredoxin. The arrow denotes irradiation at 12.3 ppm

The protein desulforedoxin is found only in minute quantities in the bacterium Desulfovibrio gigas. Preliminary spectra have been obtained using a dilute sample (see Figures III-31a and III-31b). The reduced protein exhibited resonances in the 250-200 and 20-10 ppm downfield regions. For oxidized desulforedoxin no resonances were found outside the 0-11 ppm portion of the 290 to -35 ppm spectrum. These preliminary spectra demonstrate that the ^1H NMR spectra of desulforedoxin resemble the spectra of rubredoxins. Better quality spectra of desulforedoxin will be required before detailed comparisons can be made with the spectra of the rubredoxins.

Low field EPR spectra have been recorded for samples of reduced rubredoxin and reduced desulforedoxin. The EPR spectrum in the case of reduced D. gigas rubredoxin is shown in Figure III-32. There is no sign of a S=2 type EPR signal in the 700-1000 G region as seen for the synthetic analogues (Figure III-9). There is a g=4.3 signal characteristic of oxidized rubredoxin. Comparison of its intensity to a fully oxidized sample indicates that ~5 % of the protein was in the oxidized state.

Reactions of Iron-Thiolate Complexes with Sulfur

Starting with 6/1/1 mole ratio of $HOCH_2CH_2SH/FeCl_2/S$ the tetranuclear cluster, $[Fe_4S_4(SCH_2CH_2OH)_4]^{2-}$, can be synthesized in Tris-sulfate buffer (final pH ~8) with no organic solvent or detergent. The stoichiometry is most likely that of reaction (3).

$$4FeCl_2 + 4S + 10RS^- \rightarrow [Fe_4S_4(SR)_4]^{2-} + 8Cl^- + 3RSSR \qquad (3)$$

The 6/1 RSH/Fe mole ratio used in the reaction represents a 14-fold molar excess of RSH over $[Fe_4S_4(SR)_4]^{2-}$, even for a 100% yield. The excess 2-mercaptoethanol suppresses the hydrolysis of $[Fe_4S_4(SCH_2CH_2OH)_4]^{2-}$ (83). Figure III-33 shows the time course of absorbance changes for such a reaction. Use of ϵ_{374}= 15,400 $M^{-1}cm^{-1}$ gives a 92% spectrophotometric yield after 6 h, at which point the absorbance ratio of

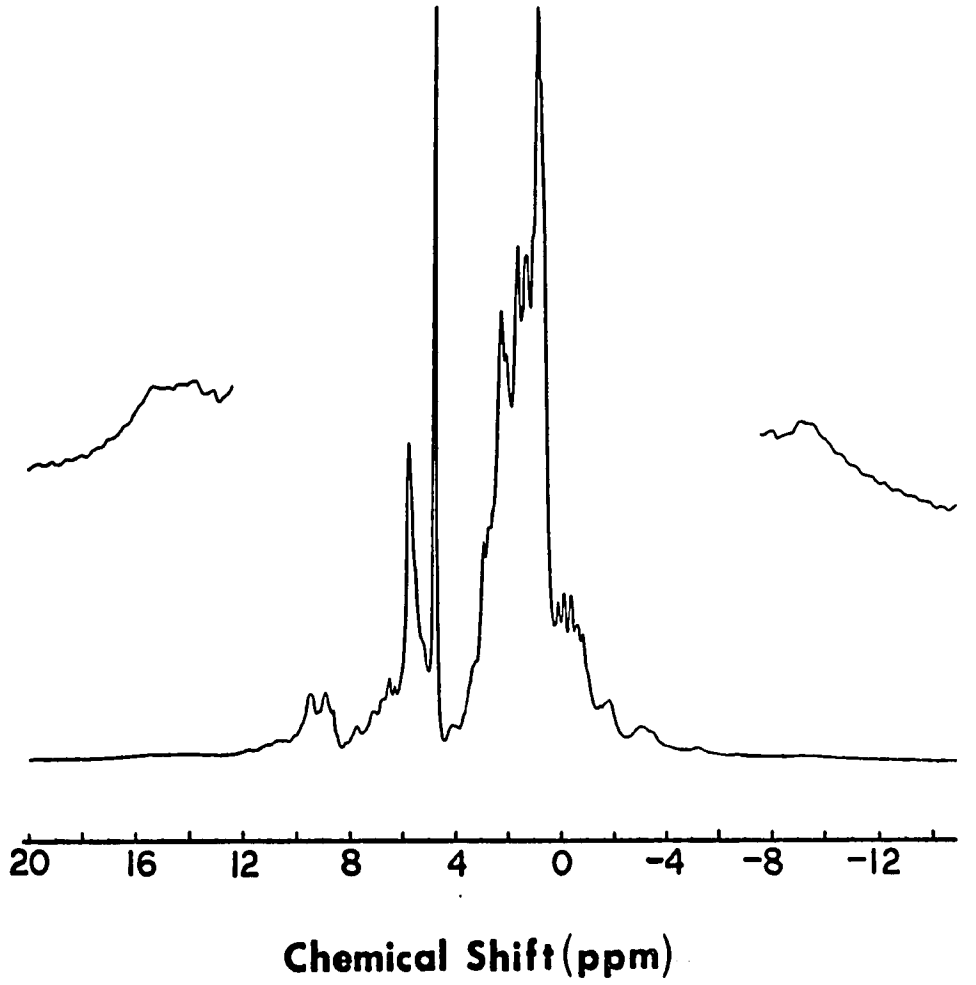

Figure III-31a. 500 MHz ^{1}H NMR spectrum of reduced D. gigas desulforedoxin from 20 to -15 ppm. The spectrum was recorded at 25 °C. Protein concentration was 0.5 mM. Insets show 16-fold expansions of selected regions

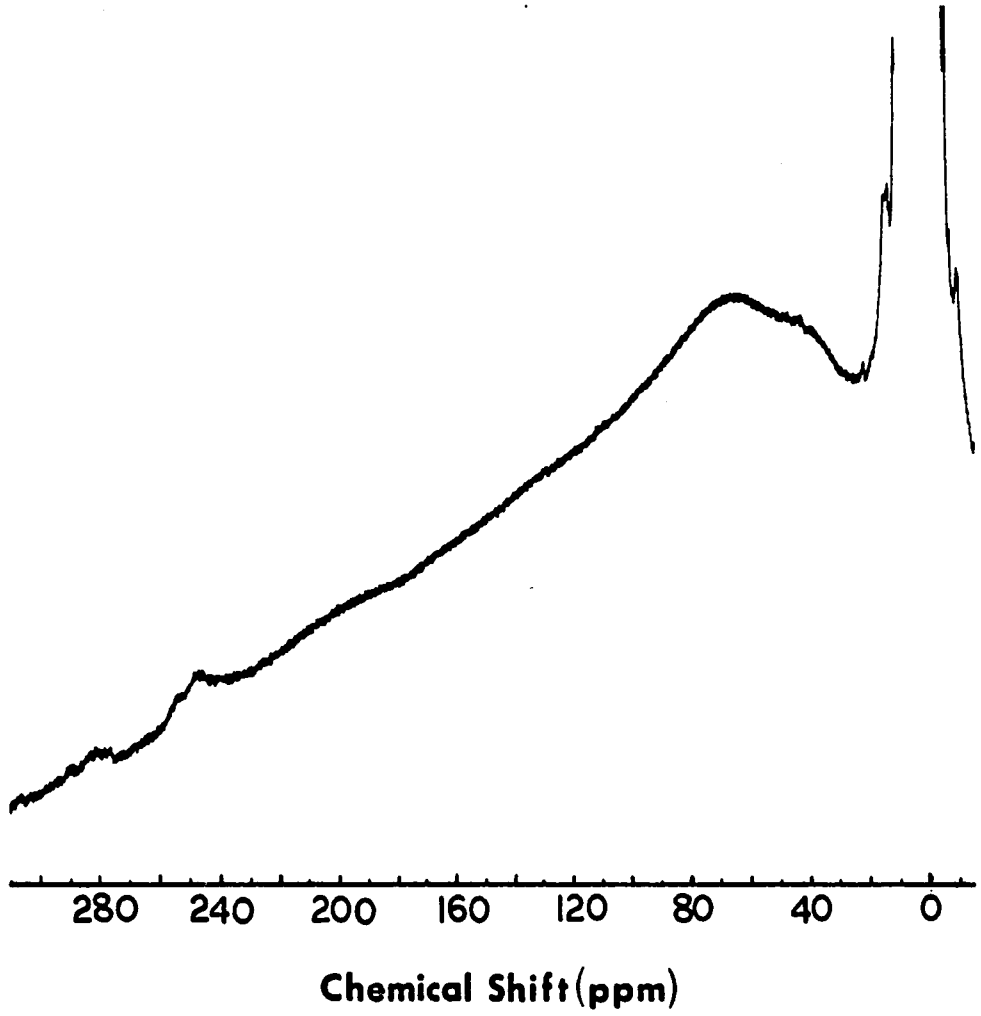

Figure III-31b. 500 MHz ^{1}H NMR spectrum of reduced D. gigas desulforedoxin from Figure III-31a plotted from 310 to -15 ppm. Vertical scale has been expanded 64-fold. A pair of peaks are observed in the 260-240 ppm region. The features between 300-270 ppm are fold-over from the intense diamagnetic protein resonances. The broad feature at ~ 75 ppm is a baseline distortion

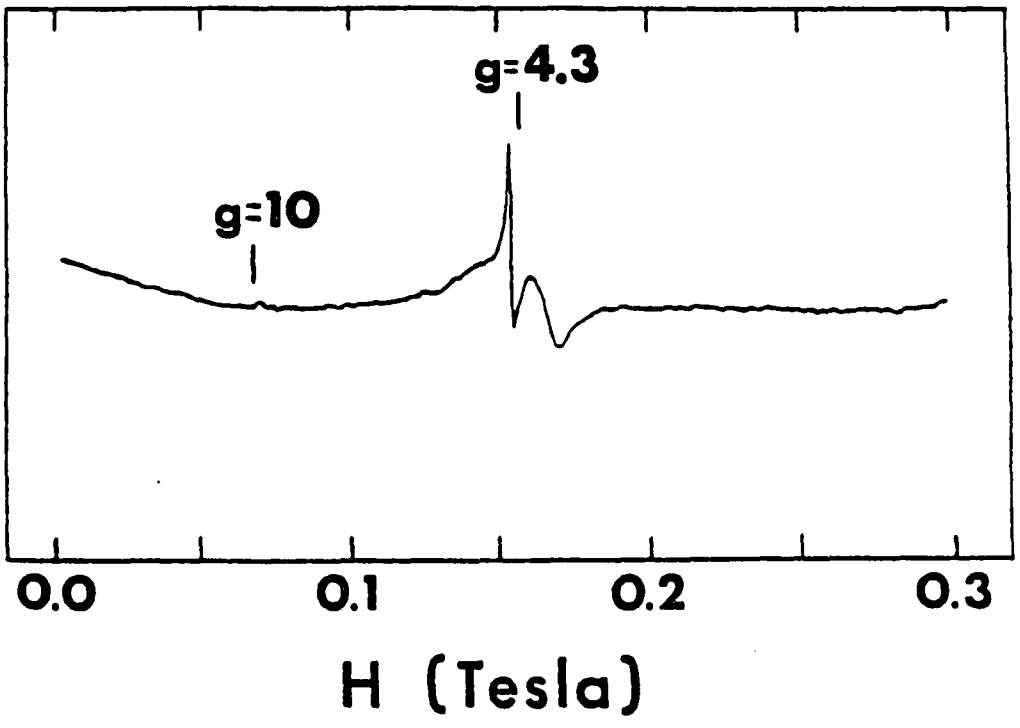

Figure III-32. X-band (9.41 GHz) EPR spectrum of reduced Rd at 5 K. Rubredoxin concentration was ~1 mM

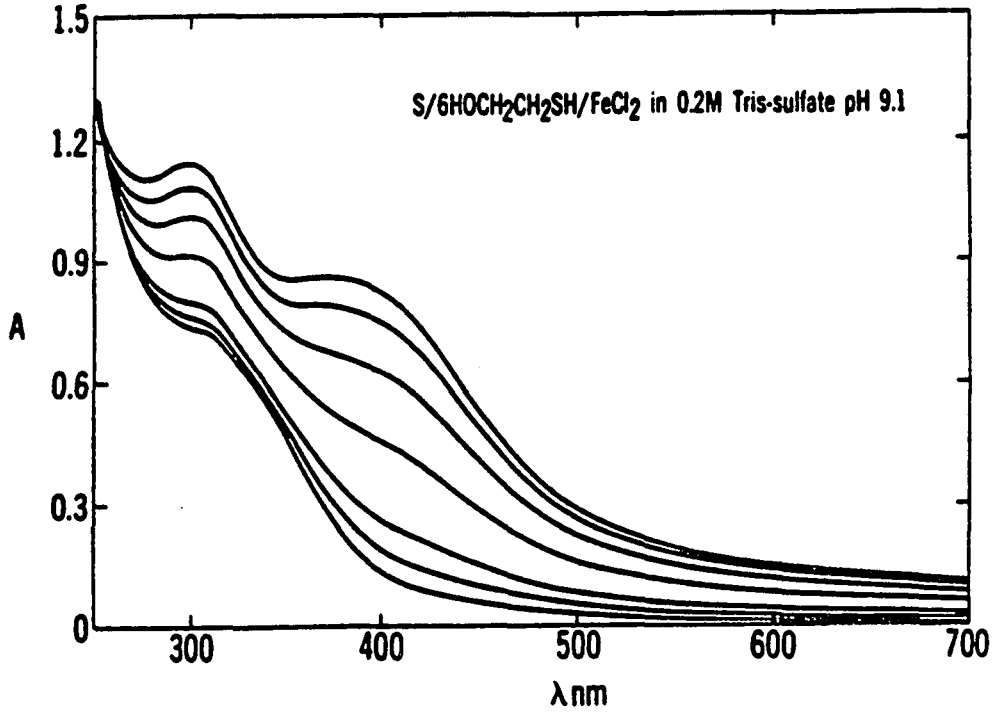

Figure III-33. UV-visible absorption time course for formation of $[Fe_4S_4(SCH_2CH_2OH)_4]^{2-}$ from a mixture of $S/6HOCH_2CH_2SH/FeCl_2$ in 0.2 M Tris-sulfate pH 9.1. Reagents are listed in order of addition, [Fe] = 24 mM. Cell pathlength = 0.01 cm. Spectra of aliquots of the reaction mixture were recorded with time in order of increasing absorbance. Bottom three spectra were recorded 2, 30 and 60 min after mixing of reagents. Subsequent spectra were recorded at 60 min intervals

A_{296}/A_{374} was 1.34. The published value of the absorbance ratio for pure $[Fe_4S_4(SCH_2CH_2OH)_4]^{2-}$ in aqueous solution is 1.35 (83).

Work-up of the reaction mixture as described in the Experimental Section (method b) led to a 70% yield of crystalline $(n\text{-}Pr_4N)_2[Fe_4S_4(SCH_2CH_2OH)_4]$. The UV-visible spectrum of the solid dissolved in Me_2SO (Figure III-34) has peaks at 296 and 414 nm. This spectrum is identical to the previously published spectrum of the Me_4N^+ salt in Me_2SO (83) The ^1H NMR spectrum in $Me_2SO\text{-}d_6$ is shown in Figure III-35. The terminal thiolate ligand resonances have been previously assigned (84) as follows: 12.4 $Fe(SC\underline{H}_2CH_2OH)$, 3.7 $Fe(SCH_2C\underline{H}_2OH)$, 4.7 $Fe(SCH_2CH_2O\underline{H})$. The remaining resonances are assigned to cation, solvent and residual HDO. These spectral properties are consistent with the formulation of the anion as a tetranuclear cluster.

The first successful demonstration of the synthesis of the [2Fe2S] cluster in aqueous media was performed by Stevens and Kurtz (34) and Kurtz and Stevens (60). Holm and co-workers had previously shown that in protic solvents $[Fe_2S_2(SPh)_4]^{2-}$ spontaneously dimerizes to $[Fe_4S_4(SPh)_4]^{2-}$ (17,83). Stevens and Kurtz were able to trap $[Fe_2S_2(SPh)_4]^{2-}$ by including a large alkylammonium cation, e.g., $n\text{-}Pe_4N^+$, at the start of the reaction (34,60). Higher yields of the binuclear cluster were obtained when the reaction medium contained 5% Triton X-100 (34). By analogy, it was hoped that addition of $n\text{-}Pe_4NBr$ and 5% Triton X-100 to the 6/1/1 $HOCH_2CH_2SH/FeCl_2/S$ system would produce a solid that contained a mixture of the binuclear and tetranuclear clusters. However, the solid product isolated from this reaction mixture contained only the salt of $[Fe_4S_4(SCH_2CH_2OH)_4]^{2-}$. Cambray and co-workers (15) found that the $[Fe_2S_2(SPh)_4]^{2-}$ could be stabilized in partially aqueous media by the addition of excess thiol. A reaction using 20/1/1 $HOCH_2CH_2SH$/Fe(III)/S in water produced a tarry black solid. The ^1H NMR spectrum of this solid in Me_2SO-d6 did not contain any resonances

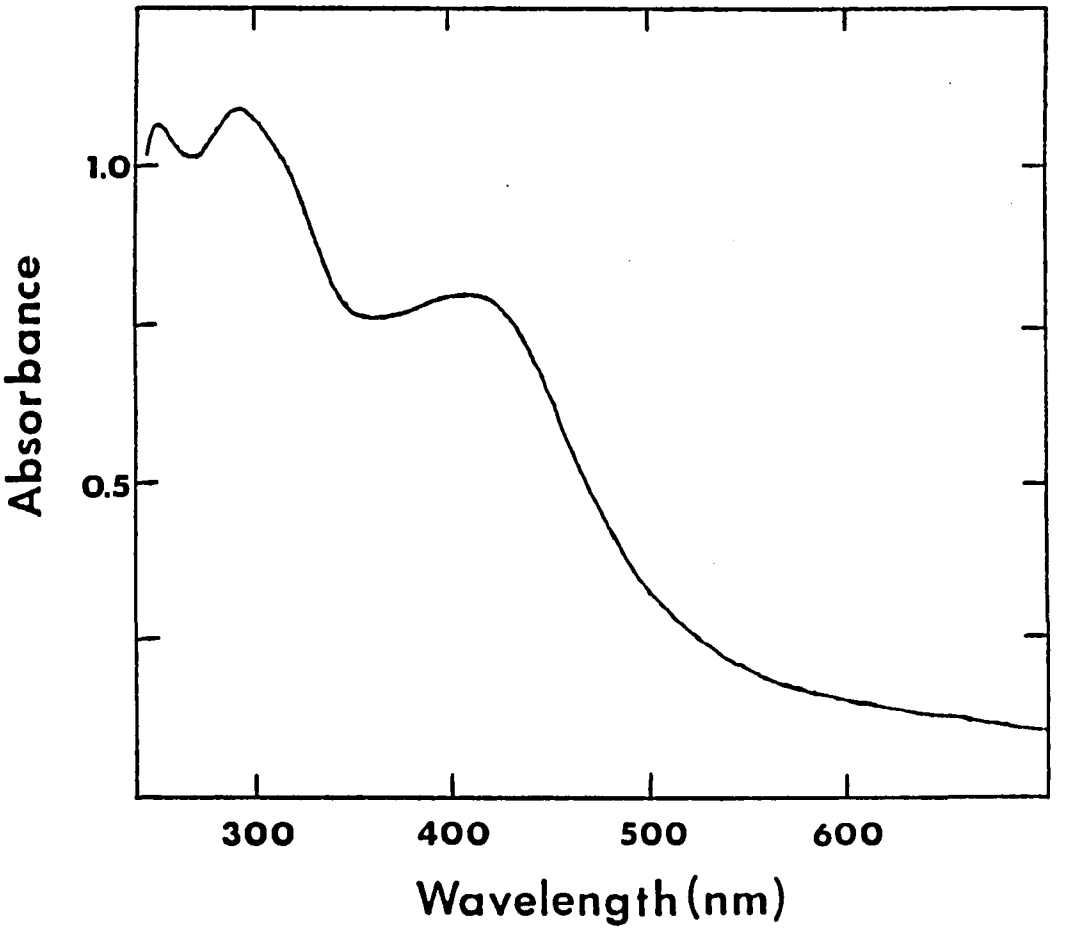

Figure III-34. UV-visible absorption spectrum of a Me_2SO solution of $(Pr_4N)_2[Fe_4S_4(SCH_2CH_2OH)_4]$. Concentration = 4.9 mM. Cell pathlength = 0.01 cm

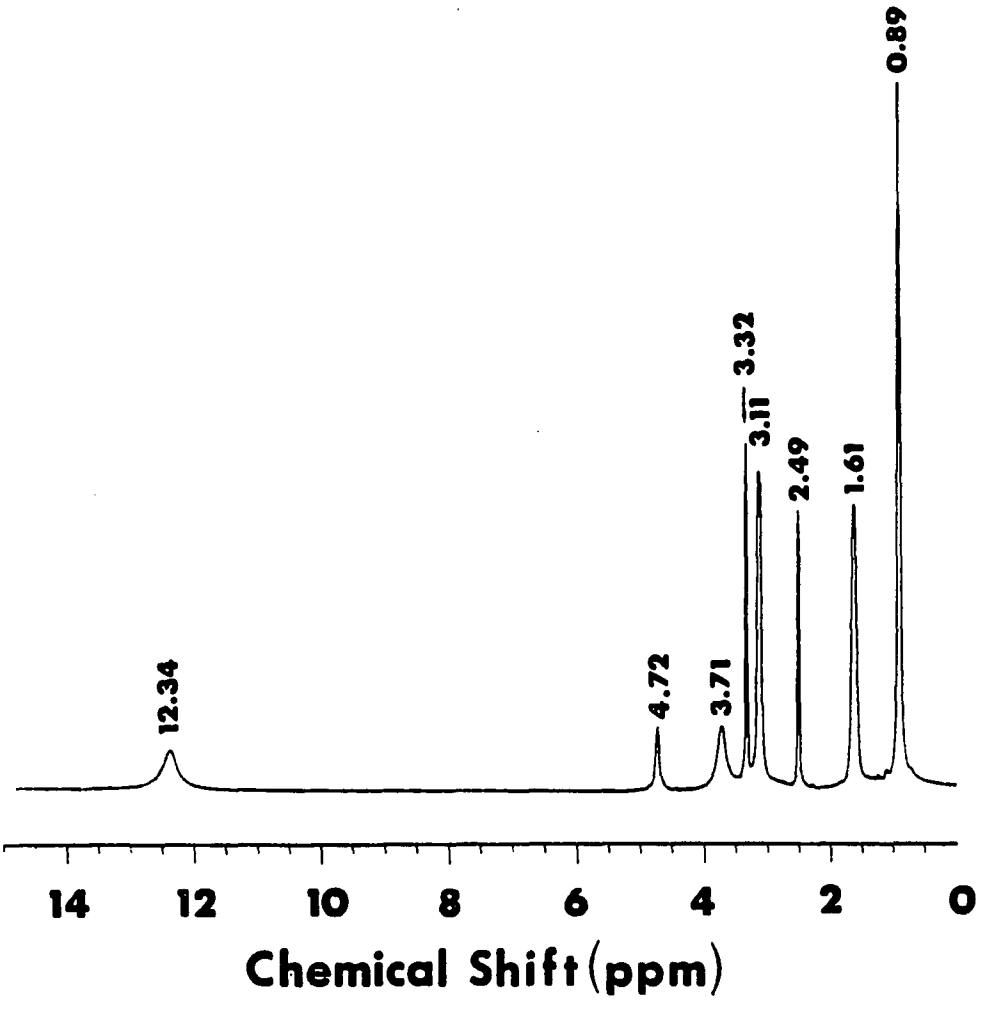

Figure III-35. 300 MHz ^1H NMR spectrum of a Me_2SO-d_6 solution of $(Pr_4N)_2[Fe_4S_4(SCH_2CH_2OH)_4]$. The spectrum was recorded at 25 °C

characteristic of the iron-sulfur clusters. All other attempts to isolate $[Fe_2S_2(SCH_2CH_2OH)_4]^{2-}$ from aqueous media produced either the tetranuclear cluster or intractable solids.

Figures I-7 and I-8 show that there are three pathways from a simple iron salt to the $[Fe_4S_4(SR)_4]^{2-}$ cluster. Previous studies (17,19,34) have successfully utilized ^1H NMR to monitor the formation and reaction of FeS clusters. Some variability is observed, among repeated reactions under the same conditions, due to the use of solid sulfur as a reagent and the occasional formation of a green precipitate from the iron-thiolate solutions. The observations reported below include only those features that were common to the series of reactions performed under the conditions specified.

When performed in borate-buffered D_2O pH 9, the synthesis of $[Fe_4S_4(SCH_2CH_2OH)_4]^{2-}$ can be followed by ^1H NMR (see Figure III-36). The ^1H NMR spectrum of the iron-thiolate mixture, prior to the addition of sulfur, reveals that both $[Fe(SR)_4]^{2-}$ and $[Fe_4(SR)_{10}]^{2-}$ are present. After the addition of sulfur the iron-thiolate resonances decrease in intensity. These resonances are replaced by features at 29 ppm and 11.8 ppm. The resonance at 29 ppm is tentatively assigned to $[Fe_3S_4(SCH_2C\underline{H}_2OH)_4]^{3-}$ (vide infra). The 11.8 ppm resonance represents the $[Fe_4S_4(SCH_2CH_2OH)_4]^{2-}$ cluster in D_2O (see Figure III-37). The UV-visible spectrum (Figure III-38) of the reaction mixture after 4 h shows $[Fe_4S_4(SCH_2CH_2OH)_4]^{2-}$ (A_{296}/A_{374}= 1.37) in 90% spectrophotometric yield.

By using LiOH instead of buffer it is possible to readily control the distribution of the iron-thiolate precursors. Using 3/5/1 mole ratio of LiOH/RSH/Fe(II) produces a solution of $[Fe(SR)_4]^{2-}$ and $[Fe_4(SR)_{10}]^{2-}$ similar to that obtained using borate buffer. Figure III-39 shows that addition of sulfur to such a mixture leads to the formation of the tetranuclear cluster (labeled t^{2-}) again with the appearance of the 29 ppm species.

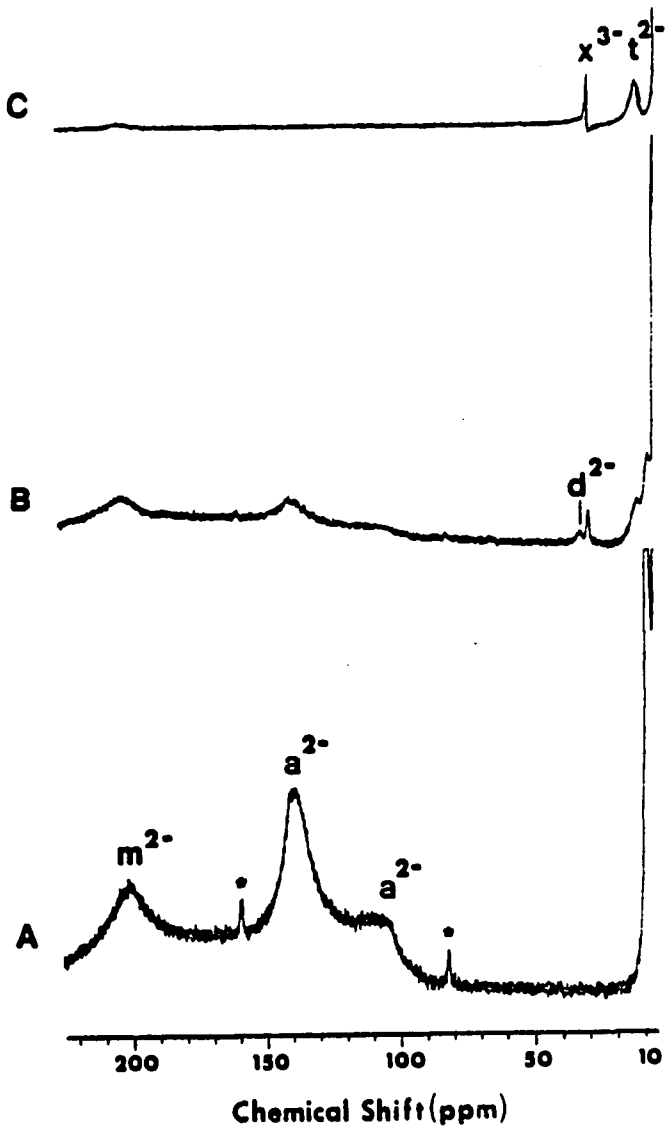

Figure III-36. 300 MHz ^1H NMR time course for formation of $[Fe_4S_4(SCH_2CH_2OH)_4]^{2-}$ in D_2O with 50 mM borate pH 9. Reagent concentrations, in order of addition, were 50 mM sodium borate, 125 mM 2-mercaptoethanol, 25 mM iron (II) chloride and 24 mM sulfur. Spectra were recorded for aliquots withdrawn from the heterogeneous reaction mixture: (A) prior to addition of sulfur and (B) 60 and (C) 240 min after addition of sulfur. Asterisk denotes artifact due to the presence of borate. The final pH (uncorrected) of the reaction was ~8.5

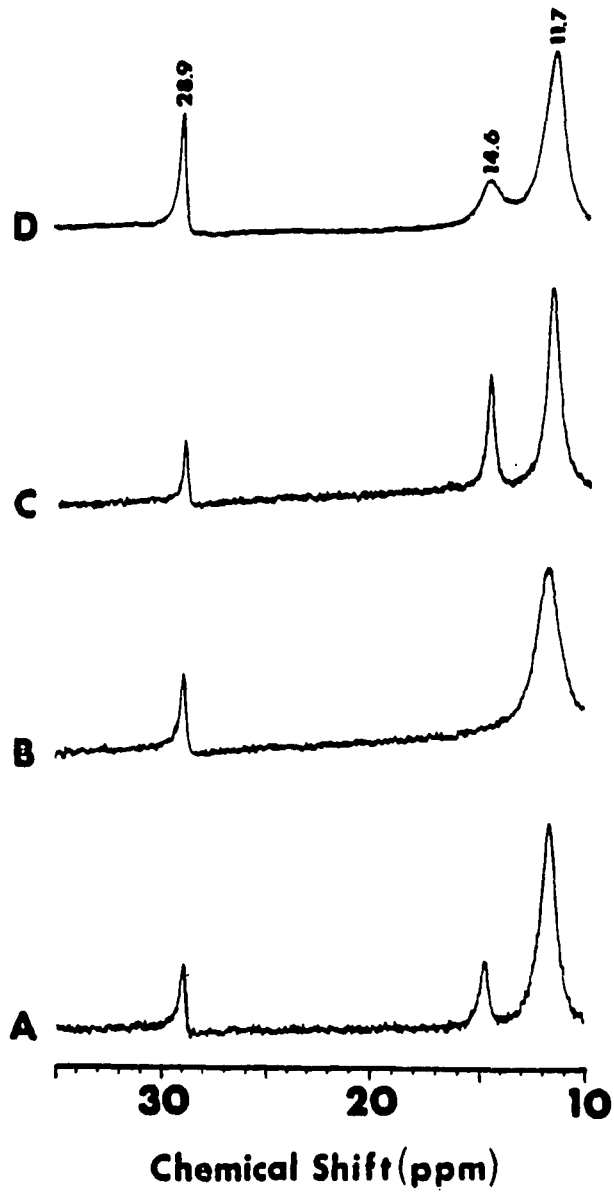

Figure III-37. 300 MHz ^1H NMR spectra of D_2O solutions of $(Me_4N)_2[Fe_4S_4(SCH_2CH_2OH)_4]$. (A) stock solution; (B) stock solution plus 25 mM excess thiol; (C) stock solution plus 170 mM NaCl; (D) solid dissolved in a D_2O solution buffered with 10 mM Tris-sulfate pD 9.5

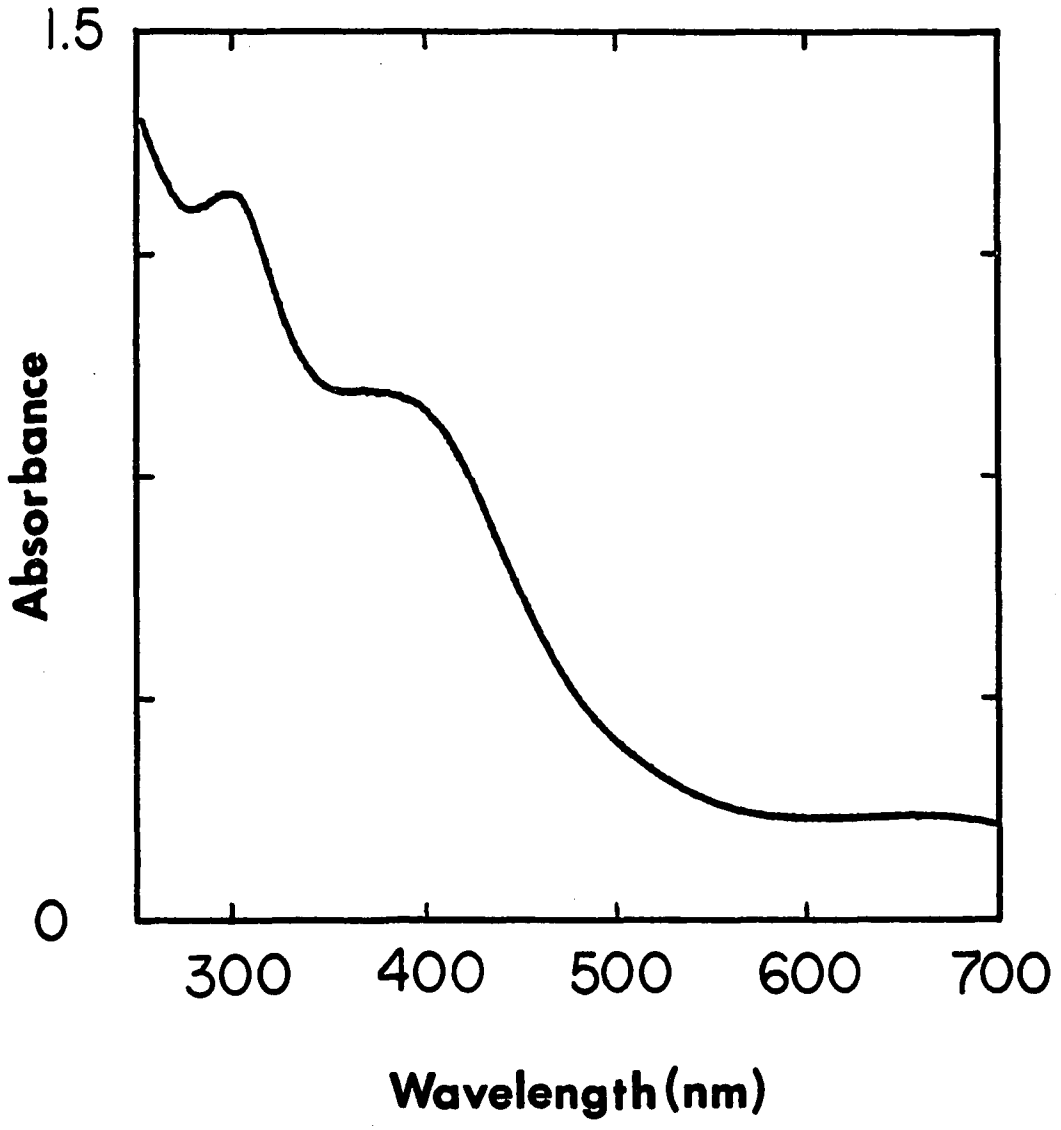

Figure III-38. UV-visible absorption spectrum taken 240 min. after the addition of sulfur to the reaction described in Figure III-36. Cell pathlength = 0.01 cm. No dilution

Figure III-39. 300 MHz ^1H NMR time course for the reaction of an alkaline D_2O solution containing both $[Fe(SCH_2CH_2OH)_4]^{2-}$ and $[Fe_4(SCH_2CH_2OH)_{10}]^{2-}$ with solid sulfur. Reagent concentrations, in order of addition, were 71 mM LiOH, 125 mM 2-mercaptoethanol, 25mM $FeCl_2$ and 23 mM sulfur. Spectra were recorded for aliquots withdrawn from the heterogeneous reaction mixture: (A) prior to addition of sulfur and (B) 60, (C) 120 and (D) 240 minutes after addition of solid sulfur. The final pH (uncorrected) of the reaction was ~9.0. The temperature of the NMR probe was set to 5 °C to improve the quality of the spectra. The baselines of the spectra were corrected using a spline routine

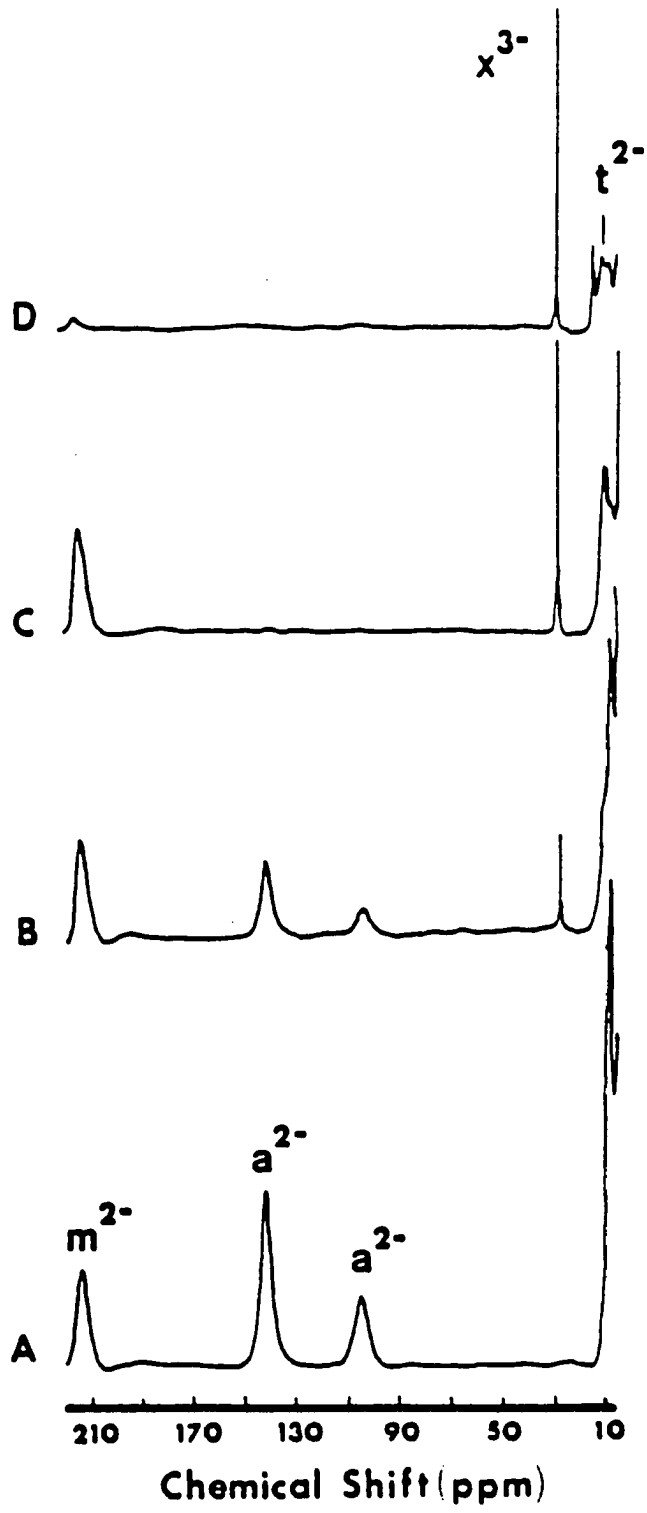
x3-
t2-
D
C
B
a2-
m2-
a2-
A
210
170
130
90
50
10
Chemical Shift (ppm)

The 11.8 ppm tetramer resonance is found in the center of a cluster of three resonances. The resonance to higher field is some residual intensity from the starting $[Fe_4(SCH_2C\underline{H}_2OH)_{10}]^{2-}$ resonance. The lower field resonance is assigned to a species which arises from the decomposition of the tetramer (see spectra a and b in Figure III-37). The $[Fe_4(SR)_{10}]^{2-}$ resonances appeared to react faster than the $[Fe(SCH_2CH_2OH)_4]^{2-}$ resonances. The UV-visible spectra for this reaction are shown in Figure III-40.

A 4/5/1 LiOH/RSH/Fe(II) ratio shifts the iron-thiolate equilibrium completely to $[Fe(SR)_4]^{2-}$. ^1H NMR spectra taken during the course of the reaction of $[Fe(SCH_2CH_2OH)_4]^{2-}$ with sulfur are shown in Figure III-41. Reaction of the mononuclear cluster with sulfur produces after 30 minutes a ^1H NMR spectrum with new resonances at ~32 and 29 ppm. By analogy with the ethanethiol ligated FeS clusters, the broad peak at ~32 ppm most likely represents $[Fe_2S_2(SR)_4]^{2-}$. As stated previously, efforts to isolate this cluster were not successful. This 32 ppm resonance disappears after 1 h, but, the sharp 29 ppm resonance is still visible 2-3 h later. There is no growth in intensity at 11.8 ppm, instead a new resonance at ~16.5 ppm appears late in the reaction. The methylene protons of $[Fe_6S_9(SR)_2]^{4-}$ resonate at 16.2 ppm downfield of TMS in CH_3CN-d_3 (19). Thus, ^1H NMR spectra indicate that the mononuclear cluster reacts with sulfur to give $[Fe_6S_9(SR)_2]^{4-}$ at high pH. The pH (uncorrected) at the end of these reactions ranged from 9.4 to 11. Further support for the assignment of the 16.5 ppm resonance to $[Fe_6S_9(SCH_2CH_2OH)_2]^{4-}$ comes from a reaction using 2/1 S/Fe which should favor the favor the formation of the [6Fe9S] cluster. In this case the reaction is complete in only one hour and the dominant resonance is at 16.5 ppm (see Figure III-42). Since the [6Fe9S] core is (apparently) not biologically relevant and the $[Fe_6S_9(SCH_2CH_3)_2]^{4-}$ cluster has been structurally characterized (19), no further

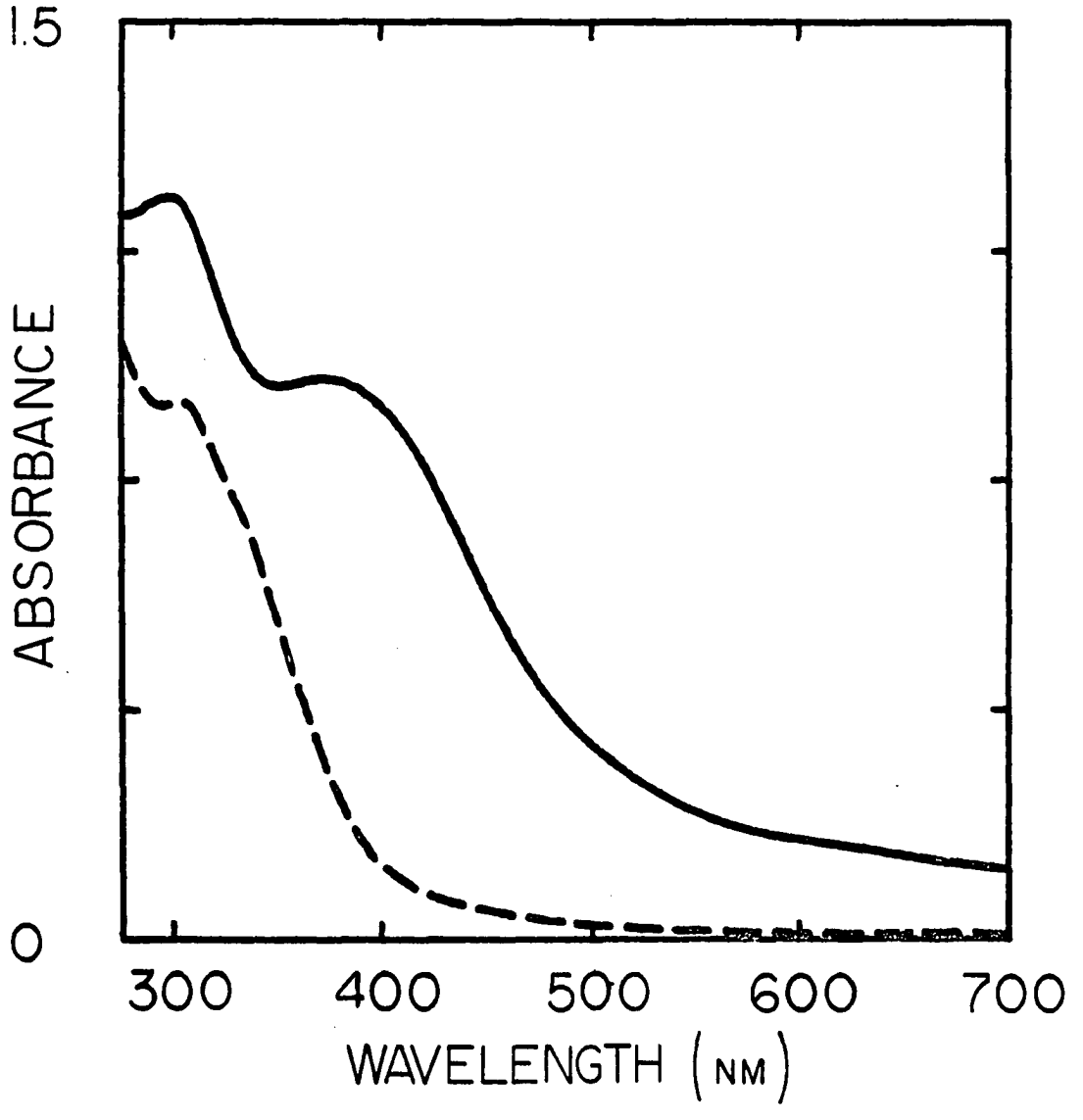

Figure III-40. UV-visible absorption spectra for the reaction described in Figure III-39. Spectra were recorded for aliquots of the reaction mixture prior to (dashed line) and 240 minutes after addition of sulfur (solid line). Cell pathlength = 0.01 cm. No dilution

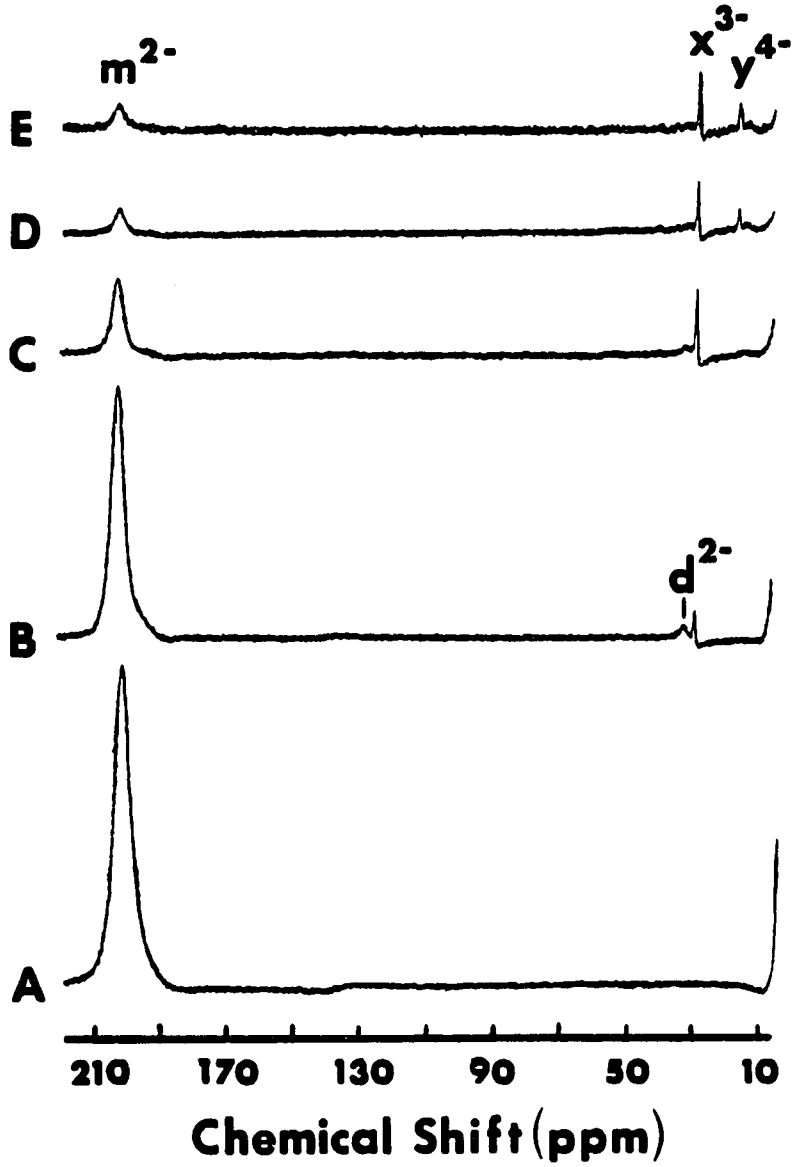

Figure III-41. 300 MHz ^1H NMR time course for reaction of $[Fe(SCH_2CH_2OH)_4]^{2-}$ with solid sulfur in alkaline D_2O solution. Reagent concentrations, in order of addition, were 110 mM LiOH, 125 mM 2-mercaptoethanol, 25 mM $FeCl_2$ and 23 mM sulfur. Spectra were recorded at 25 °C for aliquots withdrawn from the heterogeneous reaction mixture: (A) prior to and (B) 30, (C) 60, (D) 120 and (E) 180 minutes after the addition of sulfur. The final pH (uncorrected) of the reaction was ~10.3

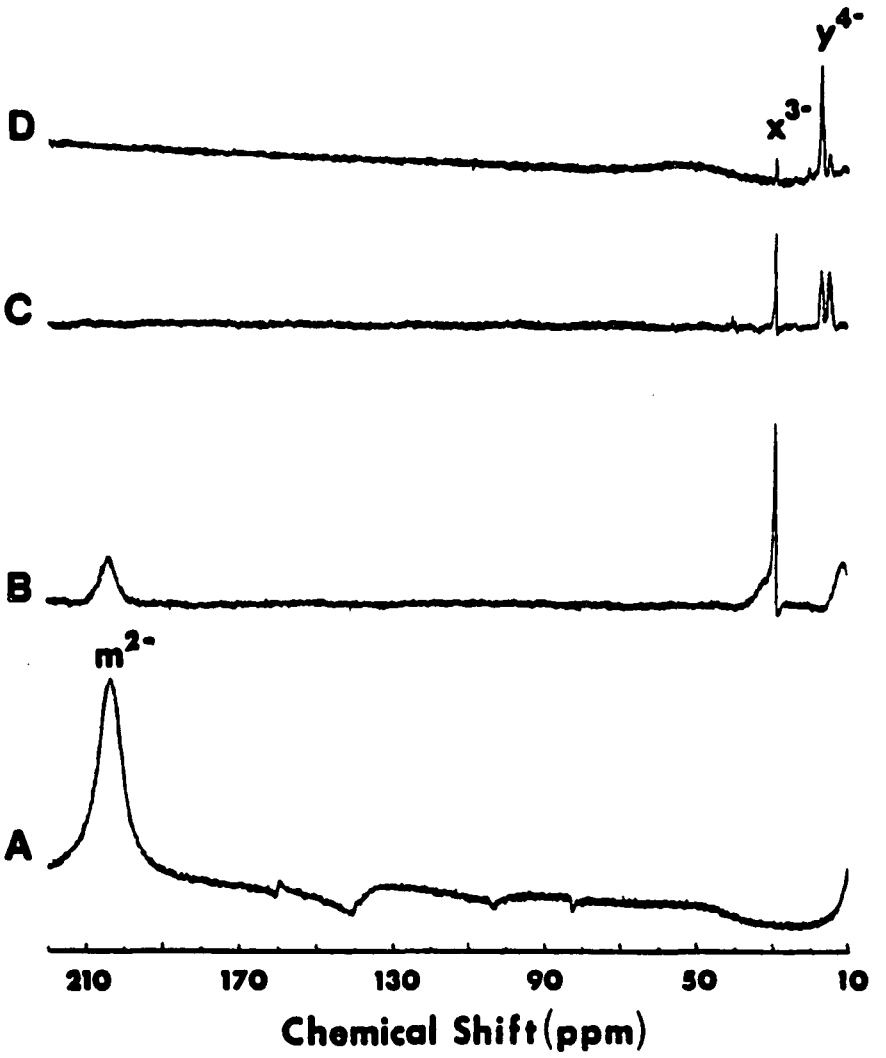

Figure III-42. 300 MHz ^1H NMR time course for the reaction of $[Fe(SCH_2CH_2OH)_4]^{2-}$ with a two-fold excess solid sulfur. Reagent concentrations, in order of addition, were 100 mM sodium borate, 124 mM 2-mercaptoethanol, 25 mM iron (II) chloride and 48 mM sulfur. Spectra were recorded at 25 °C for aliquots withdrawn from the heterogeneous reaction mixture (A) prior to and (B) 23, (C) 45 and (D) 65 minutes after the addition of solid sulfur. The final pH(uncorrected) of the reaction was ~10.3

characterization of the product was attempted.

As expected the lower LiOH/RSH ratio of 2/5 favored the formation the $[Fe_4(SR)_{10}]^{2-}$ cluster. These solutions often contained a green precipitate which is presumably polymeric $Fe(SR)_3$. Figures III-43 and III-44 depict the ^1H NMR and UV-visible changes during the course of the reaction with sulfur. Conversion of $[Fe_4(SR)_{10}]^{2-}$ to $[Fe_4S_4(SR)_4]^{2-}$, along with a small amount of the 29 ppm species, is observed in the ^1H NMR time course. The UV-visible spectrum is also consistent with $[Fe_4S_4(SR)_4]^{2-}$ as the reaction product. The absorbance at 374 nm indicates a lower yield of only ~50%. This result is not unexpected in light of the green precipitate formed in the iron-thiolate solution. The final pH (uncorrected) of these reactions was usually about 7.2.

A sharp resonance appears at 29 ppm in all of the ^1H NMR time courses of the reactions of iron-thiolates with sulfur. It appears in reactions that produce both the $[Fe_4S_4(SR)_4]^{2-}$ cluster and the $[Fe_6S_9(SR)_2]^{4-}$ cluster. The resonance also appears when the $[Fe_4S_4(SCH_2CH_2OH)_4]^{2-}$ cluster is dissolved in D_2O (see Figure III-37). The relative concentration of the 29 ppm species is increased when the solution is buffered to pH 9.5 (uncorrected) with Tris-sulfate. The relative intensity of this resonance is not affected by the addition of 25 mM excess thiol to the D_2O solution. The chemical shift of the resonance is within 5 ppm of known resonances for the $[Fe_2S_2(SCH_2CH_3)_4]^{2-}$ and $[Fe_3S_4(SR)_4]^{3-}$ clusters (19). The relatively narrow linewidth of the resonance is consistent with assignment to the [3Fe4S] cluster (19). Another argument in favor of assigning the 29 ppm resonance to the [3Fe4S] cluster is that this cluster has been shown to react to produce both the [4Fe4S] and [6Fe9S] clusters (see Figure I-8 and reference 19). In addition, $[Fe_2S_2(SCH_2CH_2OH)_4]^{2-}$ is not expected to be stable under these conditions.

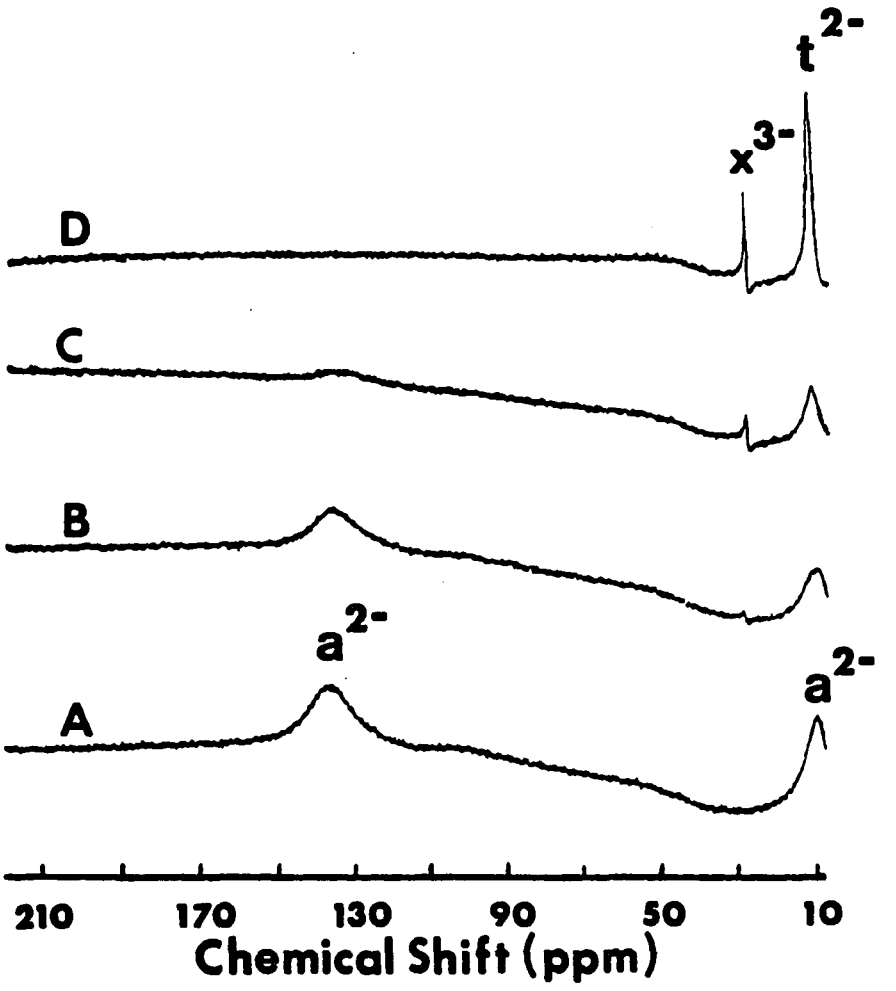

Figure III-43. 300 MHz ^1H NMR time course for reaction of $[Fe_4(SCH_2CH_2OH)_{10}]^{2-}$ with solid sulfur in alkaline D_2O solution. Reagent concentrations, in order of addition, were 49 mM LiOH, 125 mM 2-mercaptoethanol, 25 mM $Fe(NH_4)_2(SO_4)_2 \cdot 6H_2O$ and 26 mM sulfur. Spectra were recorded at 25 °C for aliquots withdrawn from the heterogeneous reaction mixture (A) prior to addition of sulfur and (B) 60, (C) 180 and (D) 300 minutes after addition of solid sulfur. The final pH (uncorrected) of the reaction was ~7.3

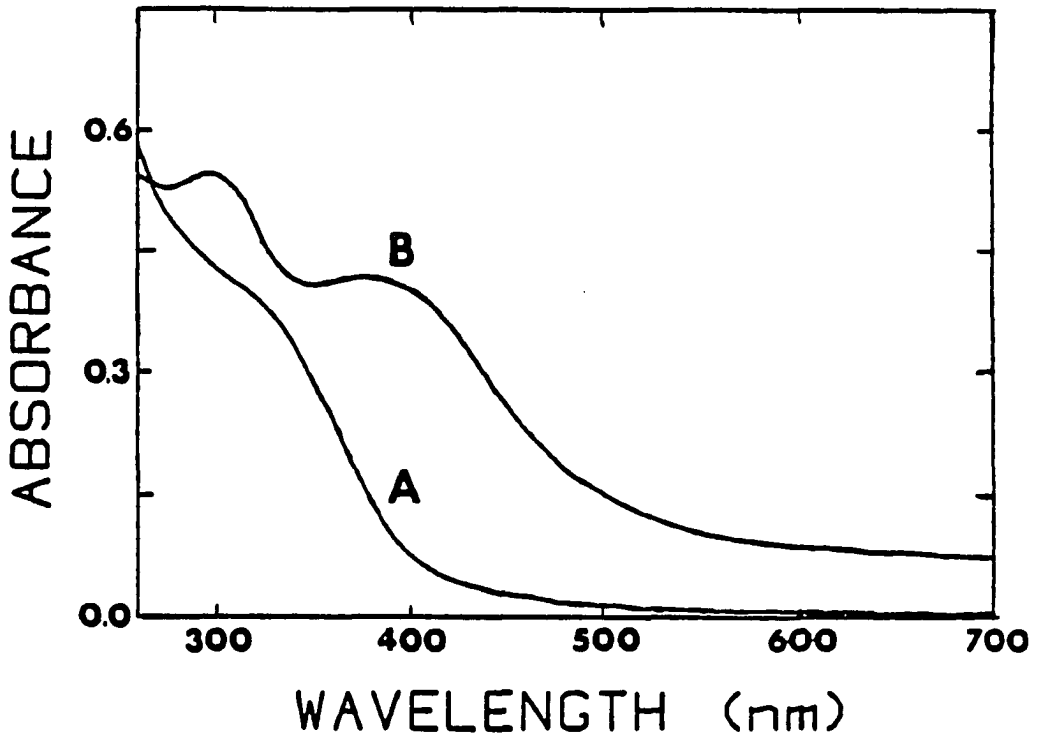

Figure III-44. UV-visible absorption spectra for reaction of $[Fe_4(SCH_2CH_2OH)_{10}]^{2-}$ with solid sulfur described in Figure III-43. Spectra were recorded for aliquots taken prior to the addition of solid sulfur (A) and 338 min after addition of solid sulfur (B). Cell pathlength = 0.01 cm. No dilution

The mononuclear $[Fe(SCH_2CHOHCHOHCH_2S)_2]^{2-}$ complex is the only soluble, stable iron-dithiothreitol species accessible in basic solution. The reaction of this species with sulfur was expected to produce $[Fe_2S_2(SCH_2CHOHCHOHCH_2S)_2]^{2-}$ in a reaction analogous to the reaction of $[Fe(S_2\text{-}o\text{-}xyl)_2]^{2-}$ with sulfur (15,58). The ^1H NMR time course for this reaction is shown in Figure III-45. The reaction proceeds to an equilibrium where presumably three species are present. The pair of resonances at 222 and 210 ppm are due to unreacted mononuclear iron-thiolate. The cluster of resonances around 12 ppm implies that the [4Fe4S], and possibly [6Fe9S], cores have formed. The poorly phased group of resonances that grow in at ~60 ppm are most likely due to $[Fe_2(SCH_2CHOHCHOHCH_2S)_3]^{2-}$. For the $[Fe_2(SCH_2CH_3)_3]^{2-}$ anion in $CH_3CN\text{-}d_3$ the methylene hydrogens from the bridging and terminal thiolates resonate at 70 ppm downfield (13). No distinct resonance is observed near 32 ppm, the position expected for $[Fe_2S_2(SCH_2(CHOH)_2CH_2S)_2]^{2-}$

Several reactions were carried out between the glutathione mononuclear iron complex and elemental sulfur. The mononuclear complex formed, based on UV-visible and ^1H NMR spectra, when there was 2 equivalents of LiOH per glutathione or in the presence of 1 M Tris-sulfate pH 9.0. The glutathione mononuclear complex did not react with sulfur as quickly as the 2-mercaptoethanol complex. These reactions were not complete after 7-8 hours, while the 2-mercaptoethanol reactions were complete in about 4 hours. UV-visible spectra recorded late in the reaction did not permit the determination of whether $[Fe_4S_4(SR)_4]^{2-}$ or $[Fe_6S_9(SR)_2]^{4-}$ was the major product. The ^1H NMR time courses did not contain any clearly discernible resonances that could be attributed to either the $[Fe_4S_4(SR)_4]^{2-}$ or $[Fe_6S_9(SR)_2]^{4-}$ clusters. Even after more than 8 hours, the ^1H NMR spectra indicated that there was still a noticeable amount of unreacted mononuclear complex.

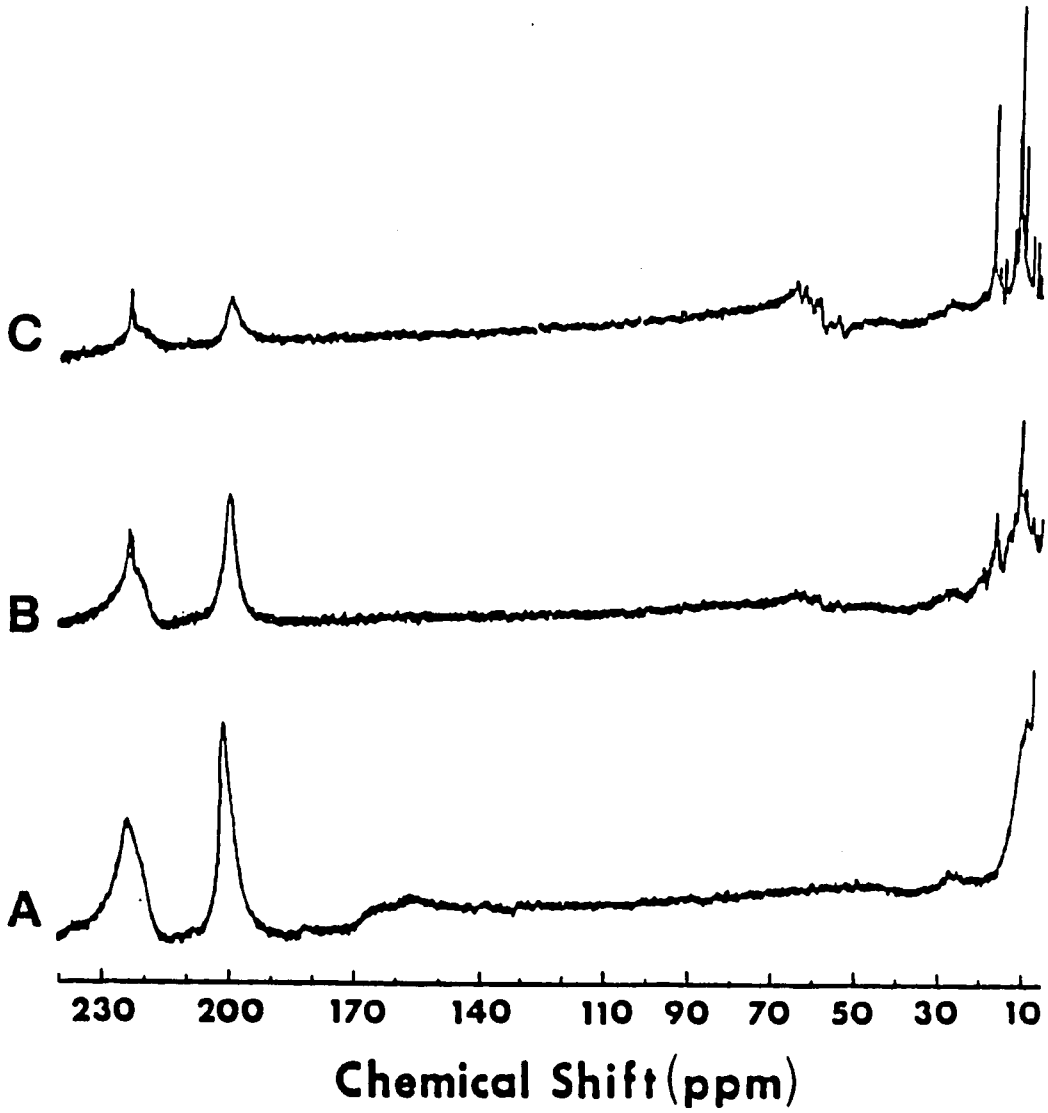

Figure III-45. 300 MHz ^{1}H NMR time course for the reaction of $[Fe(SCH2(CHOH)_2CH_2S)_2]^{2-}$ with solid sulfur. Reagent concentrations, in order of addition, were 77 mM lithium hydroxide, 65 mM dithiothreitol, 21 mM iron (II) chloride, and 19 mM sulfur. Spectra were recorded for aliquots withdrawn from the reaction: (A) prior to addition of sulfur and (B) 60 and (C) 240 minutes after the addition of sulfur

Elemental sulfur is probably not a physiologically relevant source of sulfide for FeS cluster assembly in vivo. Coucouvanis et al. (16) have demonstrated that trisulfides, which formally contain S^0, can be used to synthesize the [2Fe2S] core. Perhaps a more likely possibility is that sulfide is generated by some enzymatic process. Cellular regulation of the enzyme activity would maintain the delicate balance between too little sulfide for FeS cluster assembly and an excess of sulfide which is toxic to the cell. An example of an enzyme which produces sulfide is rhodanese. Rhodanese catalyzes the cleavage of the terminal sulfane sulfur atom from thiosulfate according to reaction 5.

$$^{*}SSO_3^{2-} + 2RSH \rightarrow H^{*}S^{-} + HSO_3^{-} + RSSR \qquad (5)$$

There is currently no well-documented evidence supporting a physiological role for any enzyme in iron-sulfur cluster assembly in vivo. However, rhodanese has been demonstrated to be capable of successfully generating sulfide for the reconstitution of FeS cores of proteins in vitro (85-89). For this reason rhodanese was chosen for use in these synthetic cluster assembly studies as an example of how the cell may generate sulfide for use in cluster synthesis.

The ability of both enzymatically-generated sulfide and stock solutions of sulfide to replace elemental sulfur were examined. The formation of water-insoluble iron sulfides has prevented the synthesis of $[Fe_4S_4(SCH_2CH_2OH)_4]^{2-}$ from aqueous mixtures of 6-10/1 $HOCH_2CH_2SH$/Fe and sulfide. Even the gradual addition of NaSH to buffered aqueous solutions 20-25 mM in ferric ammonium citrate and 150-270 mM in 2-mercaptoethanol led to intractable black precipitates. The dithiol dihydrolipoate combines with Fe(III) to form a green complex (absorbance maxima at 380 and 630 nm). This iron-thiolate complex is sufficiently stable in the presence of sulfide that the rapid formation of iron sulfides is prevented. Addition of sodium sulfide to solutions of ferric ammonium citrate, dihydrolipoate and 2-mercaptoethanol results in the progressive disappearance of

the spectrum of the green Fe(III)/dihydrolipoate complex with the concomitant appearance of the spectrum of $[Fe_4S_4(SCH_2CH_2OH)_4]^{2-}$ (see Figure III-46). Thiosulfate was present in this reaction for the purpose of allowing comparison with later experiments where rhodanese was added instead of sulfide. In the absence of sulfide there was no detectable reaction on the time scale in Figure III-46.

Figure III-47 illustrates the UV-visible spectral time course when 2.4 μM rhodanese is substituted for 11 mM Na_2S in the same reaction performed in Figure III-46. Sulfide is generated slowly by the enzymatic catalysis of reaction 5. The progression of the spectra is quite similar to the previously described case using sulfide. Surprisingly, the reaction rate for the rhodanese system is 4-5 times faster than for the sulfide system.

The cluster assembly reactions using the rhodanese/$S_2O_3^{2-}$ system to generate sulfide have also been examined by ^1H NMR (see Figure III-48). The reactions were buffered to pH ~9 with borate instead of Tris-sulfate to remove the Tris signal from the ^1H NMR experiment. The experiments were performed using 15/1 $HOCH_2CH_2SH$/Fe. The 2-mercaptoethanol served two purposes; (i) as the terminal thiolate ligand and (ii) as the thiol reductant for the rhodanese-catalyzed conversion of thiosulfate to sulfide and sulfite. Because of the higher RSH/Fe ratio, the distribution of the iron-thiolate precursors was shifted towards the mononuclear species. When rhodanese is added to the reaction mixture the $[Fe_4(SR)_{10}]^{2-}$ resonance (a^{2-}) disappears. The $[Fe(SR)_4]^{2-}$ resonance (m^{2-}) decreases in intensity until there is just a weak signal at the end of the reaction. At 30 minutes, new resonances are seen at ~32 ppm (broad) and 29 ppm (sharp). Like the reactions using sulfur, the broad resonance at 32 ppm disappears after ~60 minutes. The resonance at 29 ppm grows slightly in intensity and is still present at the end of the reaction. After 2 h the UV-visible spectrum (Figure III-49) of this

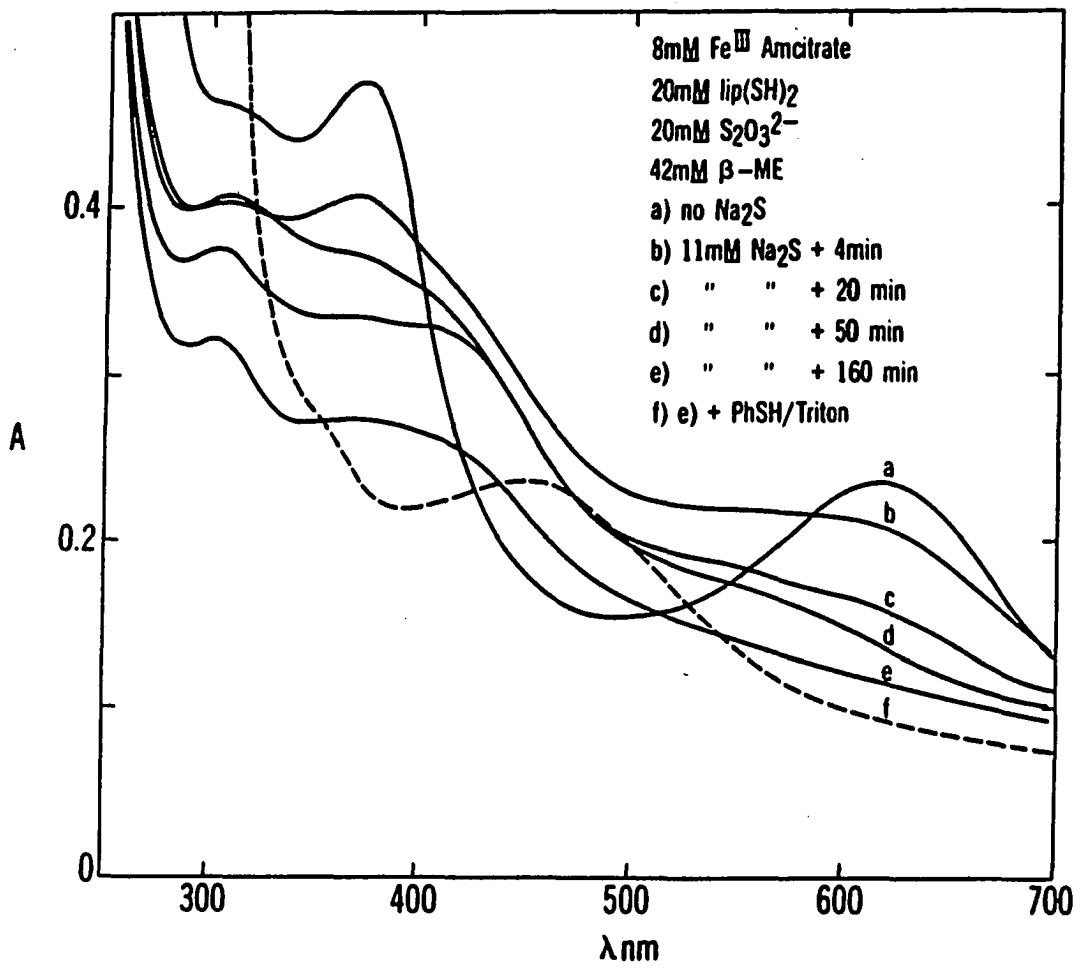

Figure III-46. UV-visible absorption time course for the formation of $[Fe_4S_4(SCH_2CH_2OH)_4]^{2-}$ from the Fe(III)/dihydrolipoate complex in the presence of sodium sulfide. The reaction was performed in 0.2 M Tris-sulfate pH 9.1

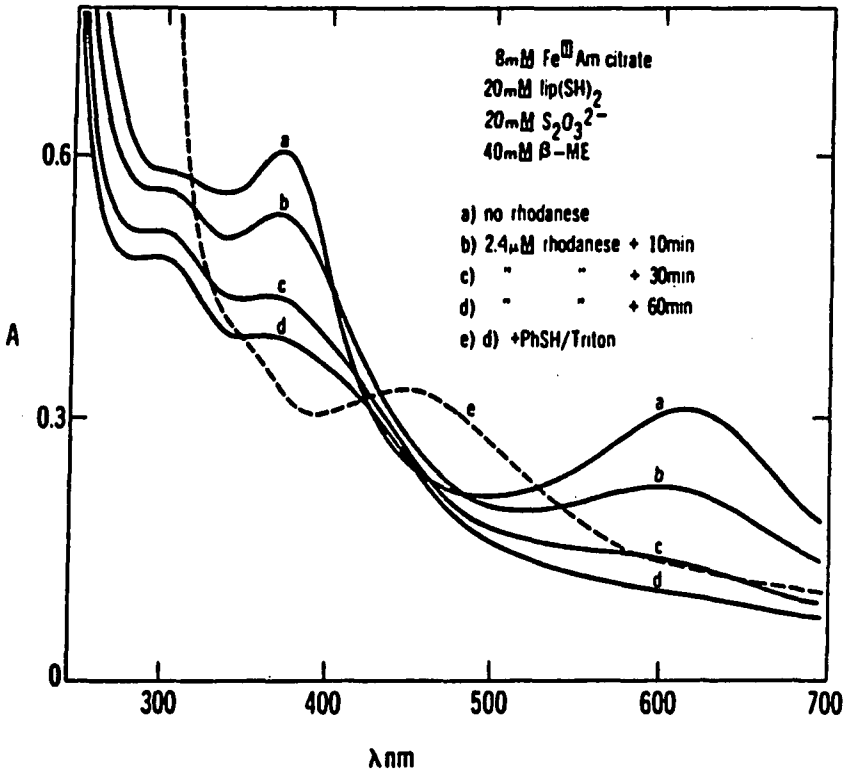

Figure III-47. UV-visible absorption time course for the rhodanese-mediated synthesis of $[Fe_4S_4(SCH_2CH_2OH)_4]^{2-}$ starting from the Fe(III)/dihydrolipoate complex. The reaction was performed in 0.2 M Tris-sulfate pH 9.1

Figure III-48. 300 MHz ^{1}H NMR time course for the rhodanese-mediated synthesis of $[Fe_4S_4(SCH_2CH_2OH)_4]^{2-}$. Reagent concentrations, in order of addition, were 50 mM sodium borate, 22 mM thiosulfate, 8.4 mM iron (II) ammonium sulfate and 120 mM 2-mercaptoethanol. The reaction was initiated by the addition of 25 μL of rhodanese (final concentration 2.4 μM). Spectra were recorded for aliquots withdrawn from the reaction mixture: (A) prior to addition of rhodanese and (B) 60, (C) 90 and (D) 120 minutes after rhodanese addition. The probe temperature was set to 5 °C to improve the quality of the spectra. The final pH (uncorrected) of the reaction was 8.9

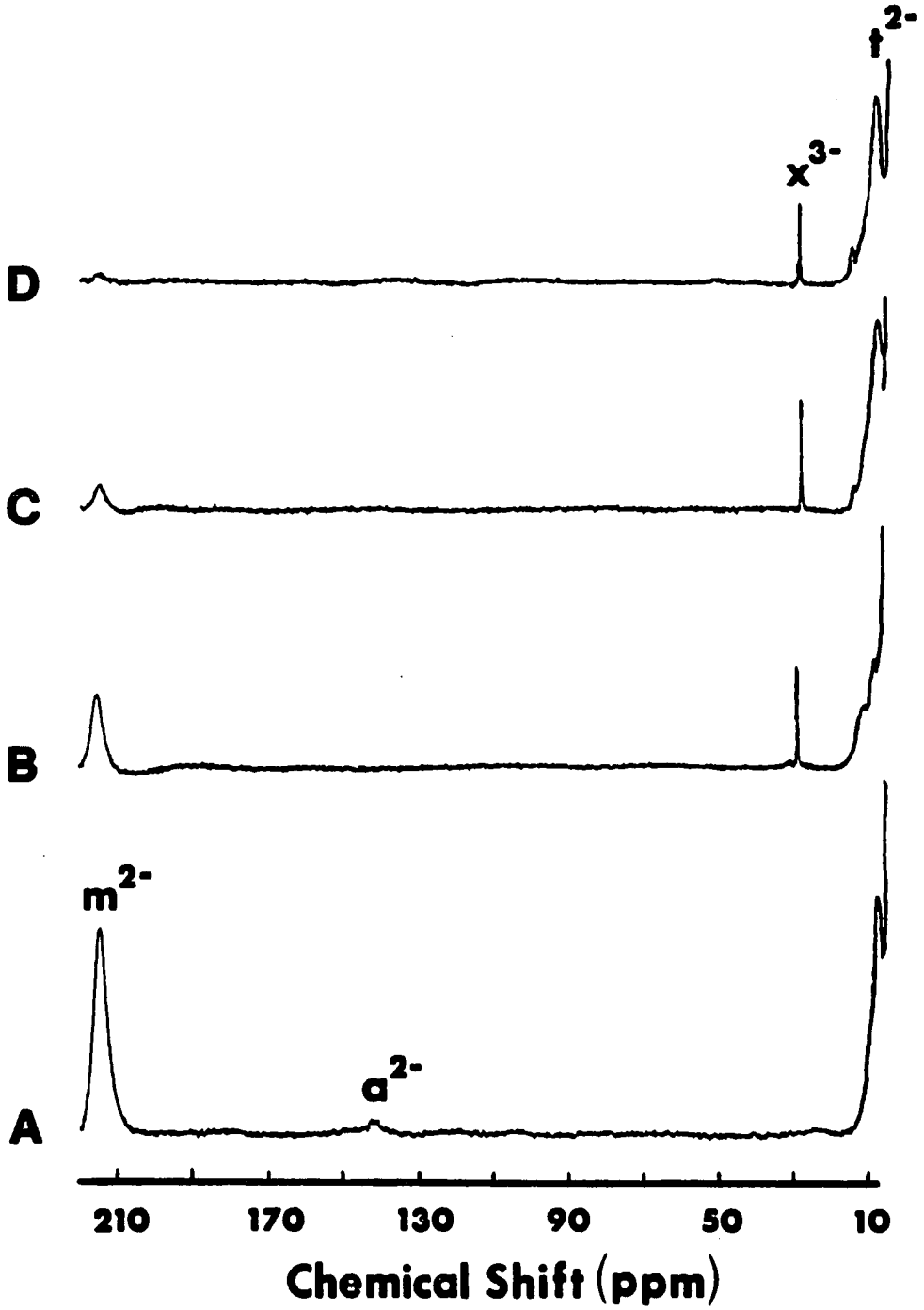
t2-
x3-
D
C
B
m2-
a2-
A
210
170
130
90
50
10
Chemical Shift (ppm)

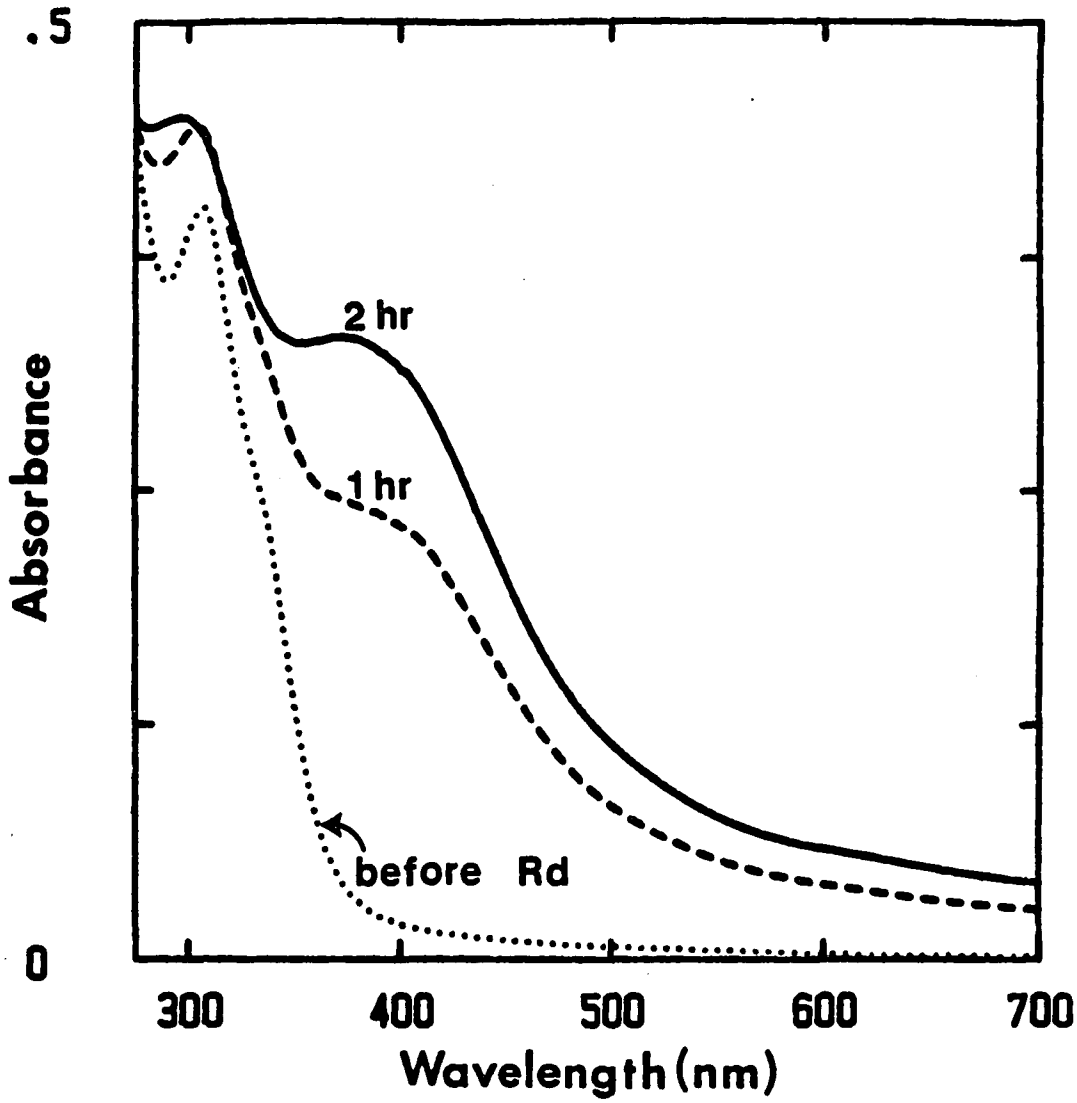

Figure III-49. UV-visible absorption time course for the reaction described in Figure III-48. Cell pathlength = 0.01 cm. No dilution

reaction indicates a 101% spectrophotometric yield of $[Fe_4S_4(SCH_2CH_2OH)_4]^{2-}$ with A_{296}/A_{374} = 1.36. The ^1H NMR spectrum shows resonances at 9 (strong), 14 (weak) and 29 ppm. Presumably, the [4Fe4S] cluster resonance is shifted from 11.8 to 9 ppm due to the lower probe temperature and exchange with thiol. The thiol exchange is observed because of the 15/1 RSH/Fe ratio used in this experiment. The pattern of the reaction from the iron-thiolate precursors to intermediates to the product is similar to that observed when a $[Fe(SR)_4]^{2-}/[Fe_4(SR)_{10}]^{2-}$ mixture is reacted with sulfur. The reaction runs faster with rhodanese/thiosulfate apparently because the dissolution of solid sulfur is no longer the rate limiting step.

IV. DISCUSSION

Iron-Thiolate Complexes

The combination of 4/1 2-mercaptoethanol/Fe(II) in water under argon yields a colorless solution. Addition of one equivalent of base for every equivalent of thiol results in the formation of a pale yellow-colored solution. The UV-visible spectrum (see Figure III-3) of the solution shows that the pale yellow color comes from the tail of absorption bands at 310 and 340 nm. The UV-visible spectrum of the species in aqueous solution is almost identical to that obtained for $Ba[Fe(SCH_2CH_2OH)_4]$ dissolved in Me_2SO (Figure III-1). This simple experiment demonstrates that iron binds to alkylthiols only when the thiol has been deprotonated.

The same experiment was performed with the tripeptide glutathione (gamma-glutamylcysteinylglycine). When one equivalent of base was added for every equivalent of glutathione, the solution remained colorless. The pale yellow color did form when a second equivalent of base was added. The first equivalent of base was required to deprotonate a carboxylate group in the glutathione tripeptide. Once again, the UV-visible spectrum implied that the complex could be formulated as $[Fe(SR)_4]^{2-}$ (neglecting the charges on R). The result also shows that Fe(II) prefers a coordination sphere of tetrahedral thiolate sulfur over coordination with carboxylate oxygen or amino nitrogen ligands found in glutathione. This result is significant because rubredoxins and ferredoxins contain more carboxylate groups than thiol groups. That is, if the cysteine thiolate groups in the apoprotein have been deprotonated, iron will preferentially bind to the thiolate groups over carboxylate groups in the absence of any conformational or steric effects. The unfolded structure of the apoprotein may sterically hinder the formation of a discrete, recognizable species, such as $[Fe(SR)_4]^{2-}$. However, during the

course of this research there has never been any result which would suggest the formation of a multileptic iron complex, e.g., $Fe(SR)_3X$ or $Fe(SR)_2X_2$. Perhaps, the thermodynamic driving force for the formation of the $Fe(SR)_4$ type site in rubredoxin is one of the driving forces responsible for the correct folding of the protein polypeptide.

Dithiols, such as dithiothreitol and dihydrolipoate, also react with Fe(II) in basic solution to give yellow solutions. The UV-visible spectra of these solutions are not as well-defined as the spectra obtained for the monothiols. Instead of a clearly resolved peak at 310 nm and a discernible shoulder at 340 nm, the spectra of these two complexes have only ill-defined shoulders on rising absorbance into the UV. Further support for the formulation of these species as mononuclear complexes comes from their ^1H NMR spectra. Resonances assigned to methylene hydrogens α to the coordinated sulfur appear at 150-250 ppm downfield in the spectra of these complexes. The chemical shift values for such α hydrogens in multinuclear iron-thiolate complexes are found well upfield of 200 ppm (13).

Among the aqueous iron-thiolate complexes prepared in this study, only $[Fe(SCH_2CH_2OH)_4]^{2-}$ has been successfully isolated as a crystalline solid. One of the problems in obtaining these complexes as solids is their high oxygen sensitivity in solution. However, the major problem encountered in the present study was the inability to remove the water-soluble iron complex from solution as a tractable solid. The problem is even more complicated in the cases of glutathione and dihydrolipoate where the extra carboxylate group on the ligand gives the complexes a higher formal charge. The $[Fe(SCH_2CH_2OH)_4]^{2-}$ complex was isolated from an aqueous reaction mixture composed of 2/10/1 $Ba(OH)_2/HOCH_2CH_2SH/Fe(SO_4)$. The barium ion removed the sulfate ion as insoluble barium sulfate. The iron-thiolate anion remained in solution as the barium salt which proved to be readily isolable as a pure, crystalline solid.

The X-ray crystal structure of the barium salt of $[Fe(SCH_2CH_2OH)_4]^{2-}$ has been refined to R= 9.7%. At this level of refinement the positions of the Fe and S atoms are well defined. Moving out from the S atom to the O atom of the thiolate ligand the thermal ellipsoids become progressively larger making further refinement impossible. Therefore, the current discussion will be limited to only the $Fe-S_4$ unit of the crystalline complex. Additional details concerning the X-ray crystal structure are presented in Appendix C. The Fe-S bond lengths in $Ba[Fe(SCH_2CH_2OH)_4]$ are all 2.30(2) Å within experimental error. The iron-sulfur bond lengths for $[Fe(SCH_2CH_2OH)_4]^{2-}$ are ~0.05 Å shorter than the iron-sulfur bonds in the other structurally characterized $[Fe(SR)_4]^{2-}$ complexes (see Table I-1). The iron-sulfur bond lengths for $[Fe(SCH_2CH_2OH)_4]^{2-}$ are within experimental error of the values of the iron-sulfur bond lengths found in the oxidized rubredoxins (see Table I-4). Distortion of the $Fe-S_4$ site in $[Fe(SCH_2CH_2OH)_4]^{2-}$ from perfect T_d symmetry occurs in the bond angles. There are two wide angles of 111.9 (6)° and four narrow angles of 108.3 (6)°. This tetragonal distortion lowers the symmetry of the $Fe-S_4$ unit from T_d to rigorous S_4.

Other $[Fe(SR)_4]^{2-}$ complexes for which crystal structures are available do not have rigorous S_4 symmetry within the $Fe-S_4$ unit (11,12). For these previously reported structures the Fe-S bond lengths within each anion are essentially equal. The S-Fe-S bond angles vary relatively widely in each of three $Fe-S_4$ units (see Table I-1 for distances and angles). For example, in $[Fe(SPh)_4]^{2-}$ the S-Fe-S bond angles range from 97.89(9)° to 119.00(10)°, a difference of 21.11°. The difference between the largest and the smallest bond angles in $[Fe(SCH_2CH_2OH)_4]^{2-}$ is only 3.6°. Each S-Fe-S bond angle in $[Fe(SPh)_4]^{2-}$ differs from the remaining angles by at least 1.2°. This inequivalence among the S-Fe-S bond angles indicates that there are not only axial, but, also rhombic distortions in the $Fe-S_4$ unit of $[Fe(SPh)_4]^{2-}$. Similar rhombic distortions occur in the

structures of $[Fe(S_2C_4O_2)_2]^{2-}$ and $[Fe(S_2\text{-o-xyl})_2]^{2-}$. In contrast, the structure of $[Fe(SCH_2CH_2OH)_4]^{2-}$ shows four angles that are equal to each other within experimental error and the remaining two angles are also equal to each other within experimental error. Because of these equalities, the symmetry of the Fe-S_4 unit is rigorously S_4. Thus, $[Fe(SCH_2CH_2OH)_4]^{2-}$ appears to have the highest Fe-S_4 site symmetry of all known $[Fe(SR)_4]^{2-}$ complexes, at least in the crystalline state.

The ^1H NMR spectrum of $Ba[Fe(SCH_2CH_2OH)_4]$ dissolved in Me_2SO was presented in Figure III-2. The resonance at 211 ppm downfield is assigned to the $FeSC\underline{H}_2CH_2OH$ hydrogens. Rapid rotation around the S-C bond renders the methylene hydrogens equivalent. For spectra where the complex was generated in solution, a similar resonance is observed at 212 ppm in Me_2SO and 201 ppm in D_2O. The spectrum of the solid dissolved in Me_2SO contains resonances at 6.7 and 12 ppm, which are not observed when the anion is generated in D_2O. The former resonance is assigned to the $FeSCH_2C\underline{H}_2OH$ hydrogens on the basis of its chemical shift and area under the resonance. The latter resonance, at 12 ppm, is assigned to hydroxyl hydrogen. The ordering of the methylene and hydroxyl resonances is consistent with the pattern observed in $[Fe_4S_4(SCH_2CH_2OH)_4]^{2-}$ (84). In D_2O solution, the resonance of $[Fe(SCH_2CH_2OH)_4]^{2-}$ near 6 ppm is buried underneath the residual HDO solvent signal and the resonance for the hydroxyl hydrogen is lost due to deuterium exchange with solvent. The similarities between the ^1H NMR and the UV-visible spectra of $Ba[Fe(SCH_2CH_2OH)_4]$ dissolved in solution and the spectra of the complex generated in situ from its components plus base confirm that the same complex is being observed in both cases.

The ^1H NMR spectrum of the glutathione complex has a resonance at 213 ppm which is assigned to the β-CH_2 cysteinyl hydrogens. The appearance of only a single

resonance implies that all eight β-CH_2 hydrogens experience on the average the same interaction with the unpaired electrons on the iron. The glutathione tripeptide is a very bulky monodentate thiolate ligand. The presence of four of these ligands on a single iron atom might be expected to create steric restrictions to bond rotation in the ligand. However, the single resonance in the ^1H NMR spectrum suggests that there is sufficient rotational freedom for each methylene pair that the electron-nuclear dipolar effects are effectively averaged. The ^1H NMR spectrum of this complex also contains a broad resonance centered at ~8 ppm. This resonance is tentatively assigned to the α-CH hydrogens of the coordinated cysteinyl residues in the glutathione ligand. The coordinated cysteinyl residues in glutathione are expected to provide a good model for the chemical environment of the cysteinyl hydrogens in rubredoxin. However, the magnetic environment of the cysteinyl hydrogens in the glutathione complex is not expected to be directly comparable to that in rubredoxin. The cysteinyl hydrogens in rubredoxin are effectively locked in position because of the rigid nature of the protein backbone. Thus, individual rubredoxin cysteinyl hydrogens are not expected to have identical magnetic environments and should therefore experience nonidentical dipolar interactions.

Chelating dithiol ligands, where the hydrogens are locked in place, are expected to provide better models for such magnetic dipolar effects. The ^1H NMR spectrum of the dithiothreitol complex (Figure III-4) has two resonances of approximately equal areas at 196 and 221 ppm. Closer examination reveals some asymmetry in the shapes of the resonances. The asymmetry implies that there are two (or more) roughly equivalent sets of hydrogens which give rise to components of each of the observed resonances. Inspection of Framework Molecular Models of the chelated dithiothreitol complex, formulated as $[Fe(SCH_2(CHOH)_2CH_2S)_2]^{2-}$, suggests that the formation of the 7-

membered S,S' chelate ring would lead to splitting of the formerly equivalent methylene hydrogens into two separate populations. The methylene hydrogens can be loosely envisioned as being split into "axial" and "equatorial" hydrogens (Figure IV-1). According to this model, the "axial" hydrogens are situated closer to the iron than are the "equatorial" hydrogens. Evidence in favor of this assignment comes from a nuclear Overhauser effect (N.O.E.) experiment. Irradiation of the 221 ppm resonance causes a decrease in the intensity of the 196 ppm resonance (Figure III-7). Because the N.O.E. falls off as r^{-6} (95-98), this result suggests that, while the hydrogens are in different magnetic environments, they are close to each other. This N.O.E. result is inconsistent with assignment of each resonance to an individual methylene group. Each individual methylene hydrogen pair is separated from the others by at least three chemical bonds. It is very difficult (if not impossible) to envision a stable Fe-SR structure in which the individual methylene groups are found close enough to allow an intergroup N.O.E. Therefore, according to the model of Figure IV-1, the two major resonances of Figure III-4 are assigned to "axial" and "equatorial" hydrogens on the two chelating dithiothreitol ligands. The "axial" and "equatorial" pairs are each related by a S_4 symmetry element and should give rise to two resonances, as is observed. The inequivalence that produces the asymmetric shapes of the resonances suggests that the S_4 symmetry is closely approached, but not strictly observed. The signals for the $SCH_2C\underline{H}OHC\underline{H}OHCH_2S$ hydrogens in the complex are presumably buried under the HDO signal, and the hydroxyl hydrogen signal is lost because of deuterium exchange.

The corresponding bidentate S,S' chelate with dihydrolipoate, formulated as $[Fe(dihydrolipoate)_2]^{4-}$ has a pair of methylene hydrogens and a single methyne hydrogen α to the coordinated sulfur atoms (see Figure IV-1). This structure immediately suggests the possibility of two separate downfield resonances due to the α

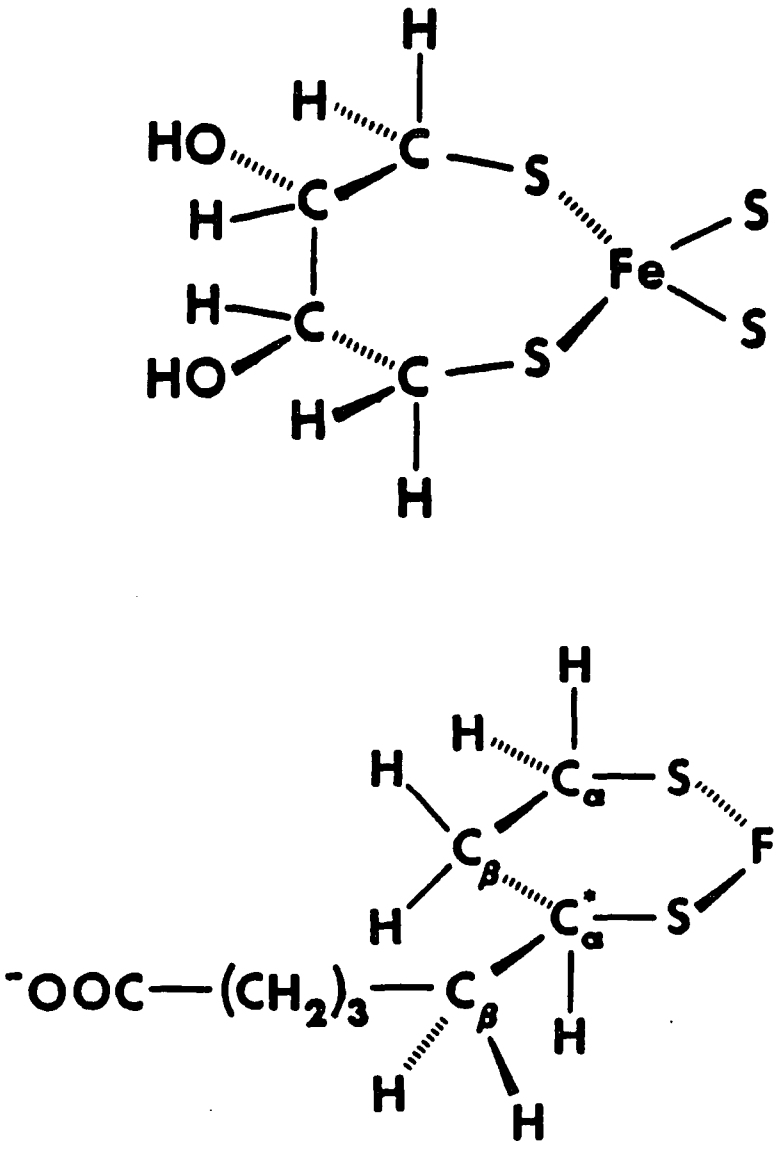

Figure IV-1. Schematic diagrams depicting the arrangement of hydrogen atoms arising from bidentate coordina-tion of alkyldithiols to iron. Upper Figure: Iron with bidentate coordination by dithiothreitol. Note how the methylene hydrogens are fixed in psuedo "axial" and "equatorial" configurations. Lower Figure: Iron with bidentate coordination by dihydrolipoate. The chiral carbon atom in dihydroliopate is marked with an asterisk

hydrogens. The observed inequivalence of the hydrogens on individual methylene groups in the dithiothreitol complex suggests that splitting of the methylene hydrogens of coordinated dihydrolipoate is also possible. These arguments imply that three separate resonances are possible for the hydrogens α to the coordinated sulfur atoms in $[Fe(dihydrolipoate)_2]^{4-}$. In the spectrum of the complex (Figure III-4) four resonances are found from 185 to 271 ppm downfield. Because of technical problems (e.g., low solubility, broad linewidths, baseline roll) it is difficult to analyze the spectrum in terms of peak areas and linewidths. Because of the chiral α-methyne carbon center, diastereomers are also possible, when using D,L-dihydrolipoate. Perhaps the chiral methyne hydrogens (but not the α-methylene hydrogens) are sufficiently inequivalent in the two diastereomers to be resolved in the NMR spectra. Such resolution would give rise to a total of four resonances, as is observed. In the absence of more detailed information it is not possible to further assign the resonances to specific hydrogens. The apparent pair of resonances at ~15 ppm in the ^1H NMR spectrum of the dihydrolipoate complex is actually a trio of resonances that become resolved only when the temperature is varied. These resonances shift upfield with increasing temperature (Figure III-8). The chemical shift positions and temperature dependencies of these resonances are consistent with their assignment to hydrogens β to the coordinated sulfur atoms.

The mononuclear species generated in aqueous solution or organic solvents using dithiothreitol, glutathione, and dihydrolipoate have not proven amenable to crystallization. However, the similarities between the UV-visible and ^1H NMR spectra of these complexes to the corresponding spectra of $[Fe(SCH_2CH_2OH)_4]^{2-}$ strongly suggest that the mononuclear formulations of these complexes are valid.

The appearance of low field (so called g=12) EPR signals from frozen solutions of

$[Fe(SCH_2CH_2OH)_4]^{2-}$ (Figure III-9) was initially surprising. High spin Fe(II) does not have a Kramers' doublet ground state and, therefore, the complex was expected to be EPR silent. At about the time of this discovery, Hagen (77) published a report containing EPR spectra of S=2 heme iron systems which resembled those of $[Fe(SCH_2CH_2OH)_4]^{2-}$. Reports of low field S=2 type EPR signals have previously appeared in the physics literature. In 1956, Tinkham had reported such an EPR resonance for Fe(II) doped into ZnF_2 (90).

Normally, S=2 systems are expected to be EPR silent due to the absence of Kramers' doublet ground state. In these cases Hagen has assigned the EPR resonance to an unusual $\Delta m_S = \pm 4$ transition (77). The $\Delta m_S = \pm 4$ transition between the |-2> and |+2> levels is indicated by the vertical arrow in the energy level diagram for a S=2 system with D>0 and the rhombic zero-field splitting parameter not equal to zero (Figure IV-2). A theoretical treatment of this transition using second order perturbation theory was presented by Abragam and Bleaney in 1970 (91). The energy splitting between the |-2> and |+2> energy levels is approximated by $3E^2/D$ for E/D approaching zero (see Appendix B). Huynh and Kent (92) report that the exact equation for the zero-field splitting of the |±2> doublet is

$$\Delta = 2|D|\{[1+3(E/D)^2]^{\frac{1}{2}}-1\} \qquad (1)$$

For a X-band EPR spectrometer the energy quantum is 0.32 cm^{-1}. Therefore, this transition will not appear unless the value of Δ is less than 0.3 cm^{-1}.

In Abragam and Bleaney's (91) theoretical treatment of the S=2 spin system there are off-diagonal terms present in the energy matrix which allow mixing of the |+2> and |-2> spin states in the presence of a weak magnetic field. Therefore, because the degeneracy has not been completely removed, the transition between the |-2> and |+2> states is $\Delta m_S = 0$ not $\Delta m_S = \pm 4$ as it appears to be in Figure IV-2. The quantum

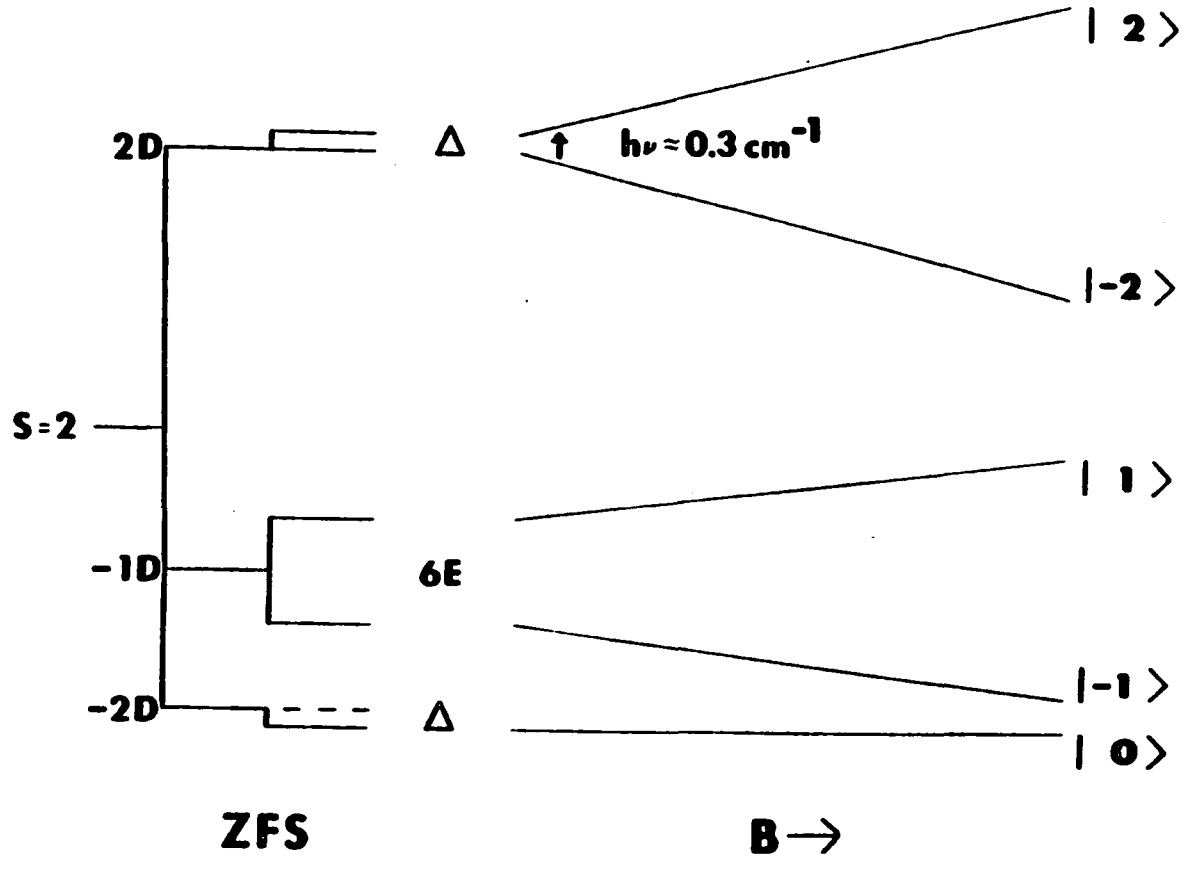

Figure IV-2. Schematic energy level diagram, along the principal molecular axes, of a magnetic quintet (S=2) state. The rhombic zero-field splittings in the diagram are drawn to scale for D = 2.0 cm^{-1} and E = 0.25 cm^{-1}. The vertical arrow represents the forbidden "$\Delta m_S = \pm 4$" transition

mechanical selection rule for a "conventional" EPR spectrometer is $\Delta m_S = \pm 1$. This rule applies to the case of microwave irradiation applied perpendicular to the external magnetic field, which is the standard design for an EPR cavity. Hagen (77) pointed out, that when microwave irradiation is applied parallel to the external magnetic field, the correct selection rule is $\Delta m_S = 0$. According to De Groot and Van Der Waals (93) the EPR signal intensity ratio for perpendicular relative to parallel microwave radiation, i.e., the ratio of $\Delta m_S = \pm 1$ to $\Delta m = 0$ intensity, is equal to $(1/2)\tan^2\theta$. θ is the angle between the principal molecular axis and the magnetic field. In a frozen solution sample molecules are oriented over the entire range of θ. Therefore, S=2 EPR signals deriving from $\Delta m_S = 0$ transitions can be observed in a normal cavity, i.e., with perpendicular microwave irradiation, but, their intensities may be diminished compared to those of $\Delta m_S = \pm 1$ transitions.

In order for a S=2 system to display this type of EPR signal two additional requirements must be met. First, for a X-band EPR spectrometer the resonance condition is created when the energy difference between the two m_S states is 0.32 cm^{-1}. Since the applied magnetic field for an EPR experiment produces Zeeman splitting of the energy levels, the zero field splitting must then be less than 0.3 cm^{-1}. The zero field splitting energy, Δ, is calculated from the values of the zero-field splitting parameters, D and E, according to equation 1 (vide supra). While the equation shows that an increase in either parameter will produce an increase in the zero-field splitting, in practice, the value of Δ is especially sensitive to changes in E. When E is equal to zero, the zero-field splitting of the $|\pm 2\rangle$ doublet is also zero. As E increases, the zero-field splitting energy increases. Since E is the zero-field splitting parameter for rhombic distortion of the ligand field, equation 1 indicates that systems with significant rhombic distortion will not exhibit a S=2 EPR signal.

The second condition required for observation of the S=2 EPR signal is associated with the axial zero-field splitting parameter D. The sign of D determines whether or not the |±2> doublet is the ground state or the highest excited state. When D is negative, this doublet is the ground state. For the case of positive D, the magnitude of D determines how far the |±2> doublet lies above the ground state (see Figure IV-2). The EPR signal intensity decreases rapidly with increasing temperature due to electronic spin relaxation. Therefore, if the excited state doublet is to be observed, it must lie sufficiently close to the ground state so that it can be populated at lower temperatures where the electronic relaxation is slower. The EPR temperature dependences observed for $[Fe(SCH_2CH_2OH)_4]^{2-}$ and $[Fe(SCH_2(CHOH)_2CH_2S)_2]^{2-}$ are consistent with the EPR signal arising from a ground state doublet. This result suggests two possibilities for the source of the EPR signal. Either the sign of D is negative with the |±2 doublet as the ground state or D is positive with the separation between the |0> and |-1> states being $< 0.3\ cm^{-1}$.

Since Hagen's initial study of the S=2 EPR signal in cytochrome c oxidase, the S=2 EPR signal has been observed from iron sites in a number of other biological systems. Hagen and co-workers (94) have reported that the reduced [3Fe4S] cluster in the 7Fe ferredoxin from Thermus thermophilus gives a S=2 EPR signal. The S=2 EPR signal is not observed for the reduced [3Fe4S] cluster in Azotobacter vinelandii ferredoxin I. MCD spectroscopy (95) indicates a significant rhombic distortion in the [3Fe4S] cluster of A. vinelandii Fd I that does not exist in the T. thermophilus Fd. D. gigas hydrogenase that has been reduced with hydrogen and allowed to reoxidize has a low field S=2 type EPR signal (96). The Fe(II),Fe(II) oxidation level of the binuclear iron cluster in hemerythrin also displays a S=2 EPR signal under certain conditions (97). Unfortunately, detailed structural data are unavailable for these proteins at the

oxidation levels that give rise to the S=2 EPR signals.

The $[Fe(SCH_2CH_2OH)_4]^{2-}$ complex provides a case where the structure of the iron site which gives rise to the S=2 EPR signal has been determined. As previously discussed, $[Fe(SCH_2CH_2OH)_4]^{2-}$ has the most symmetric structure in the solid state of any of structuraly characterized $[Fe(SR)_4]^{2-}$. The modest axial distortion and the lack of any rhombic distortion to the tetrahedral structure suggest (but do not guarantee) that the ligand field should also be highly symmetric. Small values of D and E, i.e., small axial and rhombic distortions in orbital angular momentum of the state(s) containing the unpaired spin, is a requirement for the observation of a S=2 type EPR signal. The published structures of other $[Fe(SR)_4]^{2-}$ complexes contain noticeable rhombic distortions. The zero-field splitting of the |+2> and |-2> spin states for each of these complexes can be calculated from the published values of D and E (see Table I-2). In each case the zero-field splitting is greater than 0.3 cm^{-1} and no S=2 type EPR signals have been reported for these complexes. In fact, $[Fe(SCH_2CH_2OH)_4]^{2-}$ appears to be the first example of a mononuclear pseudotetrahedral complex giving rise to a S=2 EPR signal.

In addition to that from $[Fe(SCH_2CH_2OH)_4]^{2-}$, S=2 EPR signals were also observed for the mononuclear complexes when the monodentate glutathione and bidentate dithiothreitol ligands were employed (Figure III-9). However, no such signal was observed when the bidentate dihydrolipoate ligand was used. The dihydrolipoate complex is expected to have lower symmetry than the dithiothreitol complex. The ^1H NMR spectrum of the dihydrolipoate complex exhibits the largest number and chemical shift range of "β-CH_2" hydrogen resonances (Figure III-4) which is consistent with lower structural and/or magnetic symmetry. These factors suggest that the absence of the S=2 EPR signal in the Fe(II)/dihydrolipoate mononuclear complex is the result of

rhombic distortions which increase the zero-field splitting of the $|\pm 2\rangle$ doublet beyond 0.3 cm^{-1}.

By comparison to the spectra of other $Fe(SR)_4^{2-}$ complexes (Table I-2), the low temperature, zero-field Mössbauer spectrum δ_{Fe} = 0.73 mm/s and ΔE_q = -3.48 mm/s further confirms the description of $[Fe(SCH_2CH_2OH)_4]^{2-}$ as a high spin Fe(II) complex with tetrahedral sulfur coordination. The complete analysis of the magnetic Mössbauer spectra have not yet been finished. But, the preliminary analyses have already provided some useful information. The magnitude of ΔE_q is essentially independent of temperature. Therefore, the first orbital excited state must lie $\geq$ 900 cm^{-1} above the ground state. The preliminary analyses of the two magnetically distinct species indicates that the major component comprises ~ 80% of the sample, while the minor component accounts for the remaining 20%. The major component has positive D and negative ΔE_q and appears to be similar to the Mössbauer spectrum of rubredoxin. The minor component resembles desulforedoxin in having negative D and positive ΔE_q (Table I-5). See Appendix B for further details.

The $[Fe(SR)_4]^{1-/2-}$ reduction potentials in synthetic complexes and proteins, span a range of 700 mV from ~ -0.75 V to -0.03 V (vs. N.H.E.). Recently, a new protein isolated D. gigas, called rubrerythrin (98), has been demonstrated to have a rubredoxin type site with a reduction potential of ~ 0.25 V (vs. N.H.E.). This observation, if borne out by further studies, means that the range of reduction potentials of the $Fe(SR)_4$ unit is ~1 V. The factors responsible for this wide range of reduction potentials have not been elucidated. Kassner and Yang (99) suggested that the local dielectric constantis an important factor. Adman (8) has discussed a possible relationship between hydrogen bonding and reduction potential. Hill and co-workers (83) have measured the change in redox potential for the $[Fe_4S_4(SR)_4]^{2-/3-}$ (R= CH_2CH_2OH, Ac-(RS)-Cys-NHMe) couple

in Me_2SO as a function of the percentage of solvent water. The reduction potential (vs. S.C.E.) shifted from -1.17 V in 100% Me_2SO to -0.75 V in 100% water. They cited both dielectric constant and hydrogen bonding as possible factors responsible for the ~400 mV positive shift in reduction potential with the increasing percentage of water.

In this work, the potential of the $[Fe(SCH_2CH_2OH)_4]^{1-/2-}$couple has been examined as a function of the percentage of water in three different organic solvents (Tables III-4, III-5 and III-6). The results in Me_2SO were presented in Figures III-13 and III-14. Me_2SO (ϵ=49) has a dielectric constant lower than that of water (ϵ=78). Figure III-15 shows that the reduction potential shifts to more positive potential by ~450 mV as the solvent ischanged from 100% Me_2SO to 100% water. The curve is not linear (Figure III-15), which implies that there is no simple correlation between percent water and reduction potential. This result is analogous to the result obtained for the tetranuclear cluster by Hill and co-workers (83).

The solvents, formamide (ϵ=110) and N-methylacetamide (ϵ=181), were chosen to test the effect of a solvent with a dielectric constant greater than water. If the reduction potential is largely determined by the dielectric constant, a solvent with a dielectric constant much higher than water should raise the reduction potential of $[Fe(SCH_2CH_2OH)_4]^{2-}$ above that in water. This question is relevant to the difference in reduction potential between rubredoxin and rubrerythrin, discussed above. As shown in Table III-3, the reduction potential for $[Fe(SCH_2CH_2OH)_4]^{1-}$ is highest when water is the solvent. Even though the dielectric constants of formamide and N-methylacetamide are both greater than water, the reduction potential in these solvents is significantly lower than that in water. Addition of water to these solvents produces a positive shift in the reduction potential, analogous to the behavior observed in Me_2SO. Clearly, even a solvent with a high dielectric constant such as N-methylacetamide does not shift the

reduction potential enough to account for the observed range of the reduction potentials in proteins. Water appears to be unique in its ability to produce dramatic positive shifts in the reduction potential of the $[Fe(SCH_2CH_2OH)_4]^{2-}$ analog of the reduced iron site in rubredoxin.

Kassner and Yang (99) have calculated that a dielectric constant change equivalent to changing the solvent from DMF (ϵ=36.7) to water (ϵ=78) should produce a positive shift of ~400 mV in the potential of the $Fe(SR)_4$ site. The observed shift in reduction potential of ~450 mV for the $[Fe(SCH_2CH_2OH)_4]^{1-/2-}$ couple, moving from 100% Me_2SO to 100% H_2O, is consistent with their calculation. However, solvents with dielectric constants greater than water gave less positive values of the reduction potential than those obtained in water. Therefore, other factors, besides dielectric constant, must play a significant role in modulating the reduction potential.

Another means by which the reduction potential of a metal site could be modified by the protein include surface charge and hydrogen bonding. Proteins can group either positively or negatively charged amino acids together to create an environment, which may stabilize one oxidation state relative to another. Rubredoxin has a high negative charge at pH 7 which would be expected to lower the reduction potential. However, the reduction potential of the rubredoxin site is greater, not less, than that of $[Fe(SCH_2CH_2OH)_4]^{2-}$. Therefore, surface charge does not appear to be a reason for the difference between the reduction potentials of rubredoxins and their synthetic analogs. However, surface charge may be an important factor in explaining the difference in reduction potential between rubredoxin and rubrerythrin. Rubrerythrin has a net positive charge at pH 7 (98) and a much higher reduction potential of the rubredoxin-type site.

Hydrogen bonding has been suggested to play a role in modulating the reduction

potentials of iron-sulfur clusters (8,83). The higher reduction potentials for the $Fe-S_4$ site in rubredoxins and the synthetic analogs in aqueous media relative to the synthetic analogs in aprotic solvents is consistent with the idea that hydrogen bonding withdraws electron density from the $Fe-S_4$ site.

Attempts to synthesize the Fe(III) mononuclear iron-thiolate complexes by oxidation of the Fe(II) complexes have met with limited success. It was found in this work that 5/1 RSH/Fe(III) (R=alkyl) leads to the formation of mainly $[Fe(SR)_4]^{2-}$. Mixing of 4/1 $HOCH_2CH_2SH$/Fe(III) in Me_2SO produces significant amounts of $[Fe_4(SR)_{10}]^{2-}$ in which all of the iron is formally reduced to Fe(II). The loss of some of the thiol to disulfide is reflected in the lower RS/Fe stoichiometry of the product. The spectra presented in Figures III-16, III-17 and III-18 show that only a small amount of the oxidized species is present. Attempts to isolate solid products from reactions using 2-mercaptoethanol, dithiothreitol and glutathione have not yielded tractable solids. Mixing Fe(III) salts with dihydrolipoate leads to the formation of a green species. Preliminary characterization of the green species by solution stoichiometry, UV-visible, EPR and Mössbauer spectroscopies suggests that it is a binuclear Fe(III) species which can be formulated as $[Fe_2(\text{dihydrolipoate})_3]^{3-}$. Peptide ligands, which presumably mimic the rubredoxin polypeptide, initially form reddish complexes with Fe(III) (30-33). However, in all cases the color slowly fades, indicating reduction of the iron. So far, there are only two known synthetic analogs of the oxidized $Fe-S_4$ site in rubredoxin, $[Fe(S_2\text{-o-xyl})]^{1-}$ and $[Fe(SC_{10}H_{13})_4]^{1-}$ (11,22,26).

The inability to synthesize $[Fe(SCH_2CH_2OH)_4]^{1-}$ is inconsistent with the measured reduction potential for the $[Fe(SCH_2CH_2OH)_4]^{1-/2-}$ couple. The negative values for the reduction potential (see Table III-3) suggest that the oxidized species should be stable in solution. In an electrochemical study of mononuclear toluene 3,4-dithiol complexes

with several transition metals (Mn, Fe, Co, Ni, Cu, Zn) Sawyer and co-workers (100) found that the one-electron oxidation was best described as a ligand-centered rather than a metal-centered redox process. Therefore, they described the product of the one-electron oxidation of $[Fe(TDT)_2]^{2-}$ as a Fe(II) species with a thiolate radical. Their electrochemical results were supported by solution magnetic susceptibility measurements which indicated that the oxidized complex is S = 3/2. If the oxidation product was an Fe(III) species, a S = 5/2 system would be expected for iron with a tetrahedral thiolate sulfur coordination. The observed S = 3/2 system is consistent with an antiferromagnetically coupling between a Fe(II) S = 2 and a thiolate radical S = 1/2.

Further support for the description of the oxidized $Fe(SR)_4$ unit as an Fe(II) species comes from theoretical calculations. Bair and Goddard (29) calculated the wavefunctions and charge distribution for the ground and excited states of $[Fe(SH)_4]^{1-}$ and $[Fe(SH)_4]^{2-}$. Their calculations suggest that the ground state of $[Fe(SH)_4]^{1-}$ is best described as a combination of 20% $Fe^{3+}L_4^{4-}$ and 80% $Fe^{2+}L_4^{3-}$. The one-electron oxidation effectively produces a delocalized system where a one-electron hole is equally shared by the five atoms of the $Fe-S_4$ unit.

According to these results, the thermodynamic stability of $[Fe(SCH_2CH_2OH)_4]^{1-}$ suggested by the reduction potential is misleading because it carries with it the implicit assumption of a stable Fe(III) state. Apparently, a formal Fe(III) state is not an especially stable state at ambient temperature for Fe(III) tetrahedrally coordinated by thiolate sulfur. The loss of an electron from the thiolate ligand to the metal could easily create a situation where the tendency for the ligand to dissociate would be increased. Obviously, the chances of isolating a discrete species would be significantly lower under these conditions.

The equilibrium between the $[Fe(SR)_4]^{2-}$ and $[Fe_4(SR)_{10}]^{2-}$ in aqueous solution

depends on the concentration of free thiolate. The ratio of thiol to thiolate depends on pH. The concentration of thiolate also depends on the amount of thiolate used to form complexes with the iron. The following equilibria may exist simultaneously in an aqueous mixture of iron and thiol.

$$RSH \rightleftharpoons RS^- + H^+ \qquad (6)$$

$$4Fe^{2+} + 10RS^- \rightleftharpoons [Fe_4(SR)_{10}]^{2-} \qquad (7)$$

$$Fe^{2+} + 4RS^- \rightleftharpoons [Fe(SR)_4]^{2-} \qquad (8)$$

$$[Fe_4(SR)_{10}]^{2-} + 6RS^- \rightleftharpoons 4[Fe(SR)_4]^{2-} \qquad (2)$$

The most practical way of controlling the amount of $[Fe(SR)_4]^{2-}$ versus $[Fe_4(SR)_{10}]^{2-}$ in an aqueous mixture of 5/1 RSH/Fe(II) is to add the appropriate amount of a strong base.

At physiological pH, the position of the $[Fe(SR)_4]^{2-}/[Fe_4(SR)_{10}]^{2-}$ equilibrium depends on the pK_a of the thiol. Benzenethiol has a pK_a of 6.4 (101). At pH 7-7.5 the thiol is mostly deprotonated and the $[Fe(SR)_4]^{2-}$ complex should be the dominant species. When the thiol is 2-mercaptoethanol (pK_a 9.6) the thiol group remains protonated at pH 7. Even at pH 8, the relatively high concentration of protonated thiol favors the formation of $[Fe_4(SR)_{10}]^{2-}$. The pK_a for the thiol group in cysteine is 8.3-8.6 (102). The relatively high pK_a for the cysteinyl thiol group might imply that a $[Fe_4(SR)_{10}]^{2-}$ type complex will form when iron is added to the apoprotein at pH 7. The formation of a $[Fe_4(SR)_{10}]^{2-}$ type, or even a $[Fe_2(SR)_6]^{2-}$ type complex of iron and most apoproteins is probably forbidden due to the insufficient number of closely spaced cysteine thiolates. In the vast majority of rubredoxins, ferredoxins and other iron-sulfur proteins where the amino acid composition and sequence are known, the protein usually contains only the four cysteines required for a single active site. On this basis, the $[Fe(SR)_4]^{2-}$ type site represents a plausible structure for an iron-apoprotein

complex.

Aporubredoxin can be reconstituted by addition of a two fold excess of iron (43). The reconstitution is performed under argon in the presence of a large excess (~60 fold) of 2-mercaptoethanol. The presence of 0.5 M Tris base raises the pH to ~ 8.

Several attempts were made to prepare and characterize an iron-apoprotein complex using both spinach and C. pasteurianum apoferredoxins. Such complexes could be intermediates that form during the reconstitution of the [2Fe2S] and 2[4Fe4S] centers, respectively, in these ferredoxins. The nature of the iron-apoprotein complex that forms may explain how the apoprotein directs the synthesis of the correct iron-sulfur cluster. Addition of Fe(II) salts to solutions of either apoferredoxin, at pH 7-9 in phosphate or Tris buffers, did not give the pale yellow color expected for a $[Fe(SR)_4]^{2-}$ type site. UV-visible spectra of these solutions did not contain any peaks in the 300-350 region. The Fe-$(SR)_4$ site in reduced rubredoxin has well-defined peaks at 310 and 333 nm. Furthermore, The ^1H NMR spectra of reactions in D_2O (pH ~7-9 using carbonate and borate buffers) contained only two paramagnetically shifted peaks at 35 and 75 ppm. No signals were observed in the 200-250 ppm region characteristic of the $[Fe(SR)_4]^{2-}$ site. The pair of resonances at 35 and 75 ppm were observed several times when Fe(II) was added to spinach apoferredoxin. This observation suggests that the binding of Fe(II) to the spinach apoprotein occurs at a specific site, or least one type of site. Magnetic coupling of the iron atoms could explain why there are no resonances farther downfield. The 75 ppm resonance is similar to a 70 ppm resonance reported for the methylene hydrogens of $[Fe_2(SEt)_6]^{2-}$ (13). However, the presence of a site analogous to $[Fe_2(SR)_6]^{2-}$ in this protein is highly unlikely. Spinach ferredoxin has only five cysteine residues in the entire protein. C. pasteurianum ferredoxin has a total of eight cysteines, but, also contains two clusters, and effectively, contains only four

cysteines per cluster. However, a binuclear iron site with each iron having terminal thiolate ligands and bridged to the other iron by hydroxyl or carboxylate groups is a plausible possibility. These results are only preliminary and do not rule out a $[Fe(SR)_4]^{2-}$ type intermediate during the reconstitution of these ferredoxins.

Good and Vasak (103) have studied the binding of Fe(II) to metallothionein. Mammalian metallothioneins typically contain 61 amino acid residues, 20 of which are cysteines (104). Titration of metallothionein with Fe(II) indicates that the protein is capable of binding up to 7 iron atoms. The UV-visible spectra of partially saturated (3-4 mol Fe/mol protein) show a clearly resolved peak at 310 nm with a shoulder at 340 nm. The spectrum is very similar to that of $[Fe(SCH_2CH_2OH)_4]^{2-}$ in water (see Figure III-3). At this point the cysteine/Fe(II) ratio is greater than five. When the protein is saturated with iron (i.e. 7/1 Fe(II)/protein) the UV-visible is best described as a broad band with a shoulder at 310 nm. A spectrum similar to that of a solution of $[Fe_4(SCH_2CH_2OH)_{10}]^{2-}$ is obtained (see Figure III-44). The cysteine/Fe(II) ratio is now less than 3. Thus, it appears that metallothionein is capable of forming different iron-thiolate clusters depending on the cysteine/Fe(II) ratio. It should be noted that these experiments were performed at pH 8.3 under anaerobic conditions.

Sugiura and co-workers (59) claimed to have prepared a mononuclear Fe(III)-apoprotein complex of the [2Fe2S] protein adrenodoxin. The complex is unstable with a half-life of 22 min at room temperature. Since this report, there have been no published reports of further work in this direction. The amino acid sequence of adrenodoxin has two Cys-X-Y-Cys segments similar to the Cys6-X-Y-Cys9 and Cys39-X-Y-Cys42 sequences found in the rubredoxins (2). Spinach ferredoxin has a different arrangement of cysteines in the amino acid sequence (2). The differences in placement of the cysteines in the amino acid sequences of the two proteins may explain why a

"rubredoxin-like" complex can be formed with the adrenodoxin apoprotein, but not with the spinach ferredoxin apoprotein.

Iron-Thiolate Proteins

The discovery of new resonances in the ^1H NMR spectra of rubredoxins was predicted from the ^1H NMR spectra of the synthetic analogs discussed above. The spectra of these synthetic analogs, $[Fe(SR)_4]^{2-}$, contain resonances in the region 200 ppm downfield of DSS. These results prompted the examination of the 200-250 ppm downfield region of the rubredoxin ^1H NMR spectra, which apparently had not been previously explored. From the results of these ^1H NMR experiments, it is now possible to assign several resonances to hydrogens in close proximity to the iron atom in rubredoxin.

Figure IV-3 presents a computer generated space-filling picture of the D. gigas rubredoxin iron site. From the outer surface of the protein the picture shows cysteine residues Cys 9 and Cys 42 bound to the iron atom. The sulfur atoms (in yellow) from Cys 6 and Cys 39, residues which are buried in the protein, are also shown bonded to the iron atom. The isopropyl side chains of valines 8 and 41 are also found close to the iron atom, even though they are not directly bonded to the iron. The picture illustrates the pseudo C_2 symmetry of the iron site.

The newly discovered resonances in the 200 ppm downfield region of the rubredoxin spectra were assigned to the β-CH_2 cysteinyl hydrogens. The following evidence supports this assignment. First, the chemical shift values of these resonances are similar to the chemical shift values obtained for a series of synthetic analogs. Second, the chemical shifts of these resonances show a Curie law temperature dependence as does the magnetic susceptibility of rubredoxin (40). Third, the

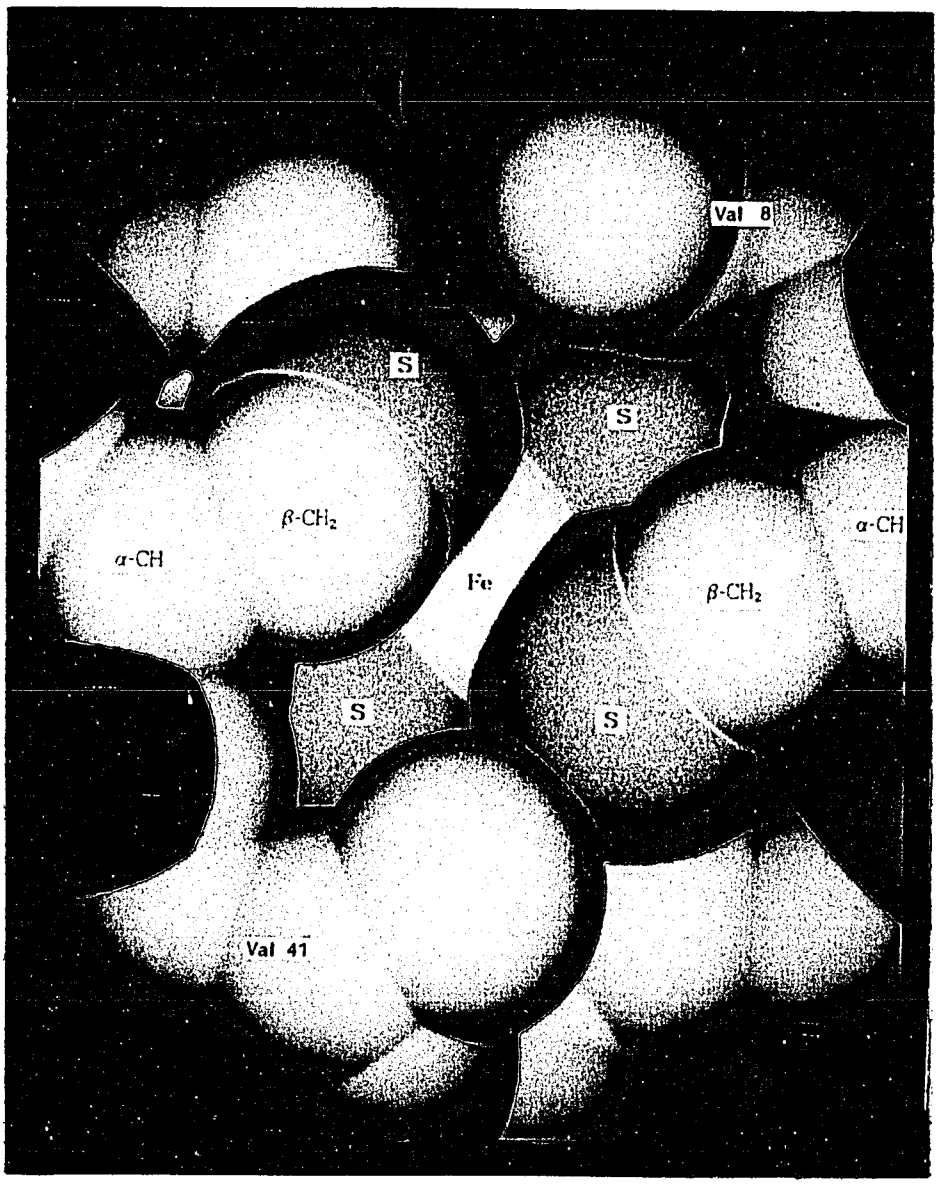

Figure IV-3. Color photograph of a space-filling model of the iron site in D. vulgaris rubredoxin. The picture taken from the display monitor of an Evans and Sutherland computer graphics system. The model was created from the 1.4 Å resolution X-ray diffraction coordinates (38). The color coding is as follows: white, carbon and iron; blue, nitrogen; red, oxygen; yellow, sulfur

temperature dependencies of the rubredoxin and synthetic analog chemical shifts parallel each other. Fourth, the relative areas of the four resonances between 150 and 260 ppm to the four resonances between 11 and 17 ppm are ~2:1. Fifth, the T_1 values for these hydrogens are estimated to be less than 100 μs (vide infra), consistent with the assignment of these resonances to hydrogens very close to the Fe atom.

Similar criteria were used to assign the α-CH cysteinyl hydrogens to the four resonances between 11 and 17 ppm in the D. gigas rubredoxin spectra (Figure III-25). The attenuation of the chemical shifts of this group of resonances with distance from the metal without sign reversal is exactly the expected behavior for dominant contact interactions, assuming σ-spin transfer. The chemical shift values of these resonances are similar to the methylene hydrogens β to the coordinated sulfur atoms in the dihydrolipoate synthetic analog. The relative area of the α-CH resonances to the resonances assigned to β-CH_2 cysteinyl hydrogens is roughly 1:2. The measured T_1's for these resonances range from 0.64 to 1.0 ms (Table III-8). These slower T_1's are consistent with these hydrogens being farther from the iron atom than are the β-CH_2 hydrogens, but still close enough to strongly interact with the unpaired electron spin on the iron. Finally, the temperature dependencies of the chemical shifts of these resonances matches the temperature dependence of the magnetic susceptibility of the iron in reduced rubredoxin (40).

Since the unpaired electron spin gives rise to the paramagnetic shift, the magnitude of the paramagnetic shift is expected to vary as the magnetic susceptibility changes with temperature according to the Curie law (105). For each paramagnetically shifted resonance in the rubredoxin spectra, i.e., those outside of 0-10 ppm range, the chemical shift moved towards the diamagnetic region as the temperature was increased, as linear a function of T^{-1}. Theoretically, the paramagnetic chemical shift should

extrapolate back to the diamagnetic chemical shift value of the resonance (i.e. the y-intercept of a plot of chemical shift vs. T^{-1}). However, the y-intercept values from chemical shift vs. T^{-1} plots for resonances in the synthetic analogues and rubredoxins vary widely and are often outside of the 0-10 ppm range. Similar behavior has been observed for some resonances in high spin ferrous porphyrin complexes (106). The properties of paramagnetically shifted ^1H NMR resonances are not completely understood at the theoretical level, which adds further importance to comparisons between empirical results obtained from synthetic analog and protein systems.

The measurement of nuclear spin-lattice relaxation times, T_1's, has provided additional information for the assignments of resonances in the ^1H NMR spectra of reduced rubredoxin. The analysis is based on the direct proportionality between the T_1 and the Fe--H distance raised to the sixth power (73,74,107). Because the proportionality constant is not known in general, detailed analysis requires the correct assignment of a resonance to a hydrogen at a known distance from the iron and the measurement of its T_1 value. Measurement of the T_1 value for the unassigned resonance then provides an estimate of the distance from the iron of the hydrogen(s) of the unknown resonance according to $T_{1a}/T_{1b} = (d_a/d_b)^6$ (73,74,107). In this analysis the α-CH cysteinyl hydrogen resonances, which appear between 11 and 17 ppm downfield, were used as the standards for interpretations of the rubredoxin spectra. T_1 values were measured using D. gigas rubredoxin. Distances between the iron atom and idealized amino acid hydrogen atom positions have been obtained from computer analyses of the X-ray crystal structures of D. vulgaris and C. pasteurianum rubredoxins. Hydrogen atoms were inserted into the X-ray crystal structure using idealized geometries for the atoms to which the hydrogens were bonded. The complete structure was then energy-minimized to reduce or eliminate strains such as overlapping Van der Waal's radii. The iron-

hydrogen distances are tabulated in Table IV-1. The computer analyses were performed using AMBER by Mr. David Stewart of the Biochemistry Department at the University of Georgia. The AMBER software was developed by Singh and co-workers at the University of California at San Francisco (108). This information when combined with other data, such as relative areas of NMR resonances, can be used to assign resonances to specific hydrogen atoms. This procedure was used to assign two upfield resonances in the spectrum of reduced D. gigas rubredoxin and to "pair up" resonances in the α-CH and β-CH_2 groups.

Using the ratio for the β-CH_2 to the α-CH cysteinyl hydrogen distances and the relationship between T_1 and distance given above, the T_1 for the β-CH_2 hydrogens was estimated to be ~60 μs. This estimate of T_1 is consistent with the large chemical shifts (150-250 ppm) and linewidths (> 1,000 Hz) of the resonances assigned to these hydrogens (Figure III-22, III-24).

The α-CH resonances of D. gigas rubredoxin have T_1 values ranging from 0.64 to 1.0 ms (see Table III-8). These T_1's can be grouped into two sets of faster and slower relaxation times. The resonances at 16.1 and 14.4 ppm have relaxation times of 0.70 and 0.64 ms, respectively, while the peaks at 12.4 and 11.3 ppm both have a relaxation time of ~1 ms. This suggests that two of the α-CH hydrogens should be found closer to the iron atom than the other two α-CH hydrogens. Indeed, examination of the Fe--H distances (see Table IV-1) in rubredoxin reveals that the predicted pattern is found among the iron to α-CH hydrogen distances. The α-CH hydrogens of cysteines 6 and 39 are found at ~ 4.9 Å from the iron. The α-CH hydrogens of cysteines 9 and 42 are found farther from the iron at ~ 5.3 A. If a distance of 4.9 Å is associated with the 0.64 ms relaxation time, then a distance of 5.3 Å from the iron is predicted for hydrogens with a relaxation time of ~ 1 ms using the sixth power relationship between

Table IV-1. Distances from the iron atom to selected hydrogens in oxidized rubredoxins from D. vulgaris and C. pasteurianum[a]

Hydrogen Atom		D. vulgaris	C. pasteurianum
Cys 6	HA[b]	4.849	4.853
Cys 9	HA	5.413	5.258
Cys 39	HA	4.945	4.896
Cys 42	HA	5.346	5.367
Cys 6	HB1	3.102	3.100
	HB2	3.063	2.869
Cys 9	HB1	4.803	4.568
	HB2	3.807	3.456
Cys 39	HB1	3.234	3.100
	HB2	3.035	3.081

[a]The iron-hydrogen distances were obtained using the AMBER software package (116). The hydrogens were first added to the protein coordinates using an idealized geometry. The entire coordinate set was then energy-minimized to relieve steric strain. The computations were performed by Mr. Dave Stewart of the Dept. of Biochemistry, University of Georgia.

[b]The letter following the H designates the carbon to which the hydrogen is bonded using the standard biochemical convention where: A, alpha; B, beta, G, gamma; D, delta.

Table IV-1 (Continued)

Hydrogen Atom		D. vulgaris	C. pasteurianum
Cys 42	HB1	4.691	4.637
	HB2	3.635	3.560
Val 8	HB	3.634	3.906
Val 8	HG1	6.282	6.188
	HG2	5.380	5.335
	HG3	4.882	4.597
Val 8	HG4	5.683	6.121
	HG5	5.823	6.187
	HG6	6.668	6.959
Val 41	HB	6.655	***[c]
Val 41	HG1	5.264	***
	HG2	6.459	***
	HG3	6.835	***
Val 41	HG4	5.582	***
	HG5	5.780	***
	HG6	4.109	***
Leu 41	HB1	***	4.067
	HB2	***	5.614

[c]The amino acid at this position has been substituted in this species of rubredoxin.

Table IV-1 (Continued)

Hydrogen Atom	D. vulgaris	C. pasteurianum
Leu 41 HG	***	5.533
Leu 41 HD1	***	6.803
HD2	***	7.183
HD3	***	5.589
Leu 41 HD4	***	7.158
HD5	***	7.918
HD6	***	7.903
Ala 44 HB1	3.278	***
HB2	4.851	***
HB3	4.199	***
Val 44 HB	***	6.348
Val 44 HG1	***	5.065
HG2	***	5.669
HG3	***	6.674
Val 44 HG4	***	4.876
HG5	***	4.576
HG6	***	3.406

T_1 and distance. It is important to note that the distance geometry of the α-CH hydrogens is also consistent with the C_2 symmetry of the rubredoxin iron site. The C_2 rotation operation exchanges the "close" pair of α-CH hydrogens with each other and, likewise, the "distant" pair of hydrogens with each other.

The β-CH_2 cysteinyl hydrogens can also be grouped into pairs on the basis of iron-hydrogen distance. In this case, the eight hydrogens are found in pairs approximately 3.0, 3.1, 3.7 and 4.7 Å from the iron atom. This pairing is a possible explanation for the appearance of only four instead of eight β-CH_2 resonances. The β-CH_2 resonances can be further grouped by linewidth with the broader resonances (at 195 and 150 ppm) assigned to the pairs of hydrogens at 3.0 and 3.1 Å, while the narrower resonances (at 236 and 227 ppm) are assigned to the pairs of hydrogens at 3.7 and 4.7 Å. Such a pairing scheme would require that a pair of methylene hydrogens on the same carbon have chemical shifts which differ by 10-40 ppm. Precedent for this is found in the N.O.E. result obtained for $[Fe(dithiothreitol)_2]^{2-}$, where the "axial" and "equatorial" methylene hydrogens have resonances that differ in chemical shift by 25 ppm.

Both D. gigas and D. vulgaris rubredoxins have upfield ^1H NMR resonances at -3.4 and -10 ppm at 55 °C. The T_1 value for the -3.4 ppm resonance is 1.7 ms. Very fast relaxation and a weak, broad signal prevented an accurate measurement of the T_1 value of the -10 ppm resonance. The resonance does not appear in a spectrum where the tau delay (i.e., the delay between the 180° and 90° pulses) was 0.1 ms, but grows in with positive intensity as the delay time is increased. From this approximate "null" point, the T_1 for the -10 ppm resonance is crudely estimated to be <0.2 ms. The relative areas of the upfield resonances have been compared to the combined area of the four α-CH cysteinyl hydrogen resonances. Based on this comparison, the resonance at -10 ppm

is comprised of ~2 hydrogen atoms, while the resonance at -3.4 ppm represents approximately sixteen hydrogen atoms. Using 0.2 ms for the T_1 value of the -10 ppm resonance, the hydrogen atom(s) for this resonance are < 4 Å from the iron atom. In the D. vulgaris rubredoxin there is a H_β methyne hydrogen on Val-8 that is 3.67 Å from the iron. The local C_2 symmetry of the rubredoxin iron site relates Val-8 with Val-41 (see Figure IV-3). In the D. vulgaris rubredoxin crystal structure the H_β methyne hydrogen of Val-41 is 6.70 Å away from the iron. These distances are likely to be very similar to those of Valines 8 and 41 in D. gigas rubredoxin. Complete rotation about the C_α-C_β bond is restricted, so it is unlikely that the H_β hydrogen of Val-41 is ever found within 4 Å of the iron. The -10 ppm resonance is tentatively assigned to the H_β methyne hydrogen of valine 8.

The valine methyl hydrogens have been assigned using the same procedure. The -3.4 ppm resonance was assigned on the basis of its T_1 and the area of the peak. The area of the -3.4 ppm resonance indicates roughly sixteen hydrogens. From the T_1 value of 1.7 ms, the hydrogen atoms for this resonance are estimated to be an average of ~5.8 Å from the iron atom. The methyl hydrogens in valines 8 and 41 range from 3.98 to 6.58 Å away from the iron. Assuming rapid rotation of the hydrogens in each methyl group, the average methyl hydrogen to iron distance is 5.6 Å. This value compares well with the distance of ~5.8 Å estimated from the T_1 value. Together the four methyl groups represent twelve hydrogens. The discrepancy between the 16 hydrogens estimated from area and the twelve valine hydrogens may be due to integration errors for these broad resonances or the presence of a fifth methyl group. There is a fifth methyl group from Ala-44, in both D. gigas and D. vulgaris rubredoxin, with an average distance of the methyl hydrogens to the iron atom of 4.38 Å. Although the methyl group of alanine is not strictly chemically equivalent to the valine methyl group, the

magnetic environment of the valine and alanine methyl groups may be essentially equivalent due to their close proximity to the iron atom. Methyl hydrogens from aliphatic amino acid side chains in heme proteins have been shown to be paramagnetically shifted upfield of -1 ppm (73,74,109). The linewidth of the -3.4 ppm resonance could mask the resolution of two (or more) resonances whose diamagnetic chemical shifts differ by only a few tenths of a ppm.

The -3.5 and -10 ppm peaks in the ^1H NMR spectrum of reduced D. gigas rubredoxin have been assigned to hydrogens on aliphatic amino acid residues near the iron atom (Val 8, Val 41, Ala 44). The amino acid residues at positions 8, 41, and 44 are identical in both of the Desulfovibrio rubredoxins. In C. pasteurianum rubredoxin the valine at position 41 has been replaced by leucine, and the alanine at position 44 has been replaced by a valine. In both cases, the substitution into the C. pasteurianum rubredoxin introduces a bulkier aliphatic group. These two amino acid substitutions are most likely the explanation for the different pattern of upfield resonances found in C. pasteurianum rubredoxin.

Nuclear Overhauser effect experiments were attempted to gain additional information for resonance assignments. For example, if the β-CH_2 methylene hydrogens in the same cysteine are inequivalent, then irradiation of one β-CH_2 resonance should perturb the intensity of a second resonance. Likewise, the α-CH resonances can be related to β-CH_2 resonances. However, no N.O.E. effects were observed between or among α-CH or β-CH_2 resonances. Irradiation of the α-CH resonances did produce N.O.E.s to resonances in the aromatic region of the spectrum (Figure III-27). The resonances in this region have not been assigned. There are three possible reasons for the failure to observe N.O.E.s among the cysteinyl hydrogen resonances. The first reason involves the difficulty in saturating the resonance or, in other words, the

inability to produce the steady-state N.O.E. condition required for the maximum N.O.E. intensity. The second reason is that even if weak, transient N.O.E.s were produced, the change in the intensity of these relatively broad resonances would be imperceptible. For Fourier transform NMR spectra the setting of the receiver gain must be based on the intensity of the largest signal, which under the best conditions is the largest protein resonance in the diamagnetic region. The β-CH_2 resonances in rubredoxin are ~1/256 of the intensity of the largest diamagnetic protein resonance. The detection of intensity changes of 10% or less in these resonances requires extremely long data collection times. The last possible reason is that the paramagnetism of the iron interfered with the nuclear Overhauser effect. The nuclear Overhauser effect occurs when the irradiated hydrogen(s) relax and dissipate energy, via a dipolar mechanism, to nearby hydrogens. This process is referred to as cross-relaxation between nuclei. However, if the dominant relaxation mechanism is the electron-nuclear dipolar interaction between the hydrogen and unpaired electrons on the iron, the cross-relaxation effect created in the N.O.E. experiment may be insignificant in comparison. The very short T_1 values for the cysteinyl hydrogen resonances in rubredoxin suggest that electron-nuclear dipolar relaxation, instead of nuclear-nuclear dipolar relaxation, is the major relaxation mechanism for the cysteinyl hydrogen nuclei.

The observation of S=2 type EPR signals in Fe(II) synthetic analogues of rubredoxin and desulforedoxin raised the possibility that similar signals could be observed for the reduced proteins. However, examinations of the EPR spectra of both proteins did not reveal any evidence for S=2 type EPR signals. This result is consistent with the magnitudes of the zero-field splittings of these sites. The relationship between the zero-field splitting parameters and the appearance of a S=2 type EPR signal was reviewed earlier in this chapter. The values of the zero-field splitting parameters, D

and E, have been measured by Mössbauer spectroscopy for reduced rubredoxin and reduced desulforedoxin (see Table I-5). From the published values of the zero-field splitting parameters (42,43) the zero-field splitting energy, Δ, of the $|\pm 2\rangle$ doublet can be calculated (using Equation 1) for both proteins. For reduced rubredoxin, Δ is 1.70 cm^{-1}. For reduced desulforedoxin, Δ, is 0.63 cm^{-1}. Thus, for both proteins, $\Delta > 0.3$ is cm^{-1}, i.e., Δ too large for observation of a transition within the $|\pm 2\rangle$ doublet.

Reactions of Iron-Thiolate Complexes with Sulfur

The successful assembly of $[Fe_4S_4(SCH_2CH_2OH)_4]^{2-}$ by addition of S° to aqueous mixtures of $HOCH_2CH_2SH/FeCl_2$ extends the range of conditions for high yield synthesis of $[Fe_4S_4(SR)_4]^{2-}$ (R=alkyl) to completely aqueous solvent. This result demonstrates the thermodynamic stability of the [4Fe4S] core in an aqueous environment in the presence of excess thiol and the absence of oxygen. This spontaneous assembly in aqueous solution raises the possibility that clusters containing the [4Fe4S] core occur in vivo with natural thiols outside of proteins.

Having demonstrated that the $[Fe_4S_4(SCH_2CH_2OH)_4]^{2-}$ cluster could be formed in totally aqueous media, the next goal was to determine by what pathway the cluster is formed. The ^1H NMR spectra of borate-bufferred reaction mixtures prior to the addition of sulfur indicated that both $[Fe(SR)_4]^{2-}$ and $[Fe_4(SR)_{10}]^{2-}$ were present at the beginning of the reaction. Addition of sulfur caused the iron-thiolate resonances to decrease in intensity. When the mixture of the iron-thiolate precursors was prepared using LiOH instead of buffer the same general trends were observed on addition of sulfur to the iron-thiolate mixture. In addition, the $[Fe_4(SR)_{10}]^{2-}$ complex always disappeared faster, and there was never any trace of this species remaining at the end of the reaction. The results suggest that the favored pathway in water for the

production of the [4Fe4S] cluster is via $[Fe_4(SR)_{10}]^{2-}$ rather than $[Fe(SR)_4]^{2-}$ when R=CH_2CH_2OH at least in the pH range 8-9.

Sulfur was also added to solutions of $[Fe(SCH_2CH_2OH)_4]^{2-}$ and to solutions of $[Fe_4(SCH_2CH_2OH)_{10}]^{2-}$. Solutions containing only $[Fe(SCH_2CH_2OH)_4]^{2-}$ or only $[Fe_4(SCH_2CH_2OH)_{10}]^{2-}$ could be prepared by using the appropriate amount of LiOH in a solution of 5/1 2-mercaptoethanol/Fe(II). ^1H NMR time courses showed a clean reaction of $[Fe_4(SCH_2CH_2OH)_{10}]^{2-}$ with sulfur producing mostly the $[Fe_4S_4(SCH_2CH_2OH)_4]^{2-}$ cluster in 50% yield. The 29 ppm species, tentatively assigned to $[Fe_3S_4(SCH_2C\underline{H}_2OH)_4]^{3-}$, was also present. There was no sign of a 32 ppm resonance, tentatively assigned to $[Fe_2S_2(SC\underline{H}_2CH_2OH)_4]^{2-}$, during the reaction. These assignments are based on the corresponding resonances of $[Fe_2S_2(SC\underline{H}_2CH_3)_4]^{2-}$ and $[Fe_3S_4(SCH_2C\underline{H}_3)_4]^{3-}$ (19). The final pH of these reactions was typically ~7.5. Reaction of $[Fe(SCH_2CH_2OH)_4]^{2-}$ with sulfur produced the 32 ppm resonance, which quickly disappeared, and the 29 ppm resonance which did not disappear. The major product of the reaction was the $[Fe_6S_9(SCH_2CH_2OH)_2]^{4-}$ cluster. The final pH of the reactions of $[Fe(SCH_2CH_2OH)_4]^{2-}$ with sulfur was typically >10. At 5/1 $HOCH_2CH_2SH$/Fe(II), the reaction of $[Fe_4(SCH_2CH_2OH)_{10}]^{2-}$ with sulfur occurs at close to physiological pH and produces the biologically relevant [4Fe4S] cluster. In contrast, the reaction of sulfur with $[Fe(SCH_2CH_2OH)_4]^{2-}$ occurs at a pH much higher than physiological pH and does not produce significant yields of a known biologically relevant product.

These studies of the assembly of the [4Fe4S] cluster in totally aqueous media do not explain the formation of the [2Fe2S] core in the plant ferredoxins. Previous reports have described the tendency of the [2Fe2S] core to dimerize in the presence of water (15,34). Indeed, most of the attempts to prepare $[Fe_2S_2(SCH_2CH_2OH)_4]^{2-}$ in water produced the tetranuclear cluster. The remaining attempts produced solutions or solids

which lacked any sign of discrete product. Stevens and Kurtz (34) and Kurtz and Stevens (60) found that the non-ionic detergent Triton X-100 sequestered $[Fe_2S_2(SPh)_4]^{2-}$ in hydrophobic micelles away from water, thereby, facilitating its isolation as an analytically pure solid. In the present study, inclusion of 5% Triton X-100 in a 5/1/1 $HOCH_2CH_2SH/FeCl_2/S$ reaction mixture containing 26 mM Pr_4NBr actually led to an increased weight yield of $[Fe_4S_4(SCH_2CH_2OH)_4]^{2-}$ but no $[Fe_2S_2(SCH_2CH_2OH)_4]^{2-}$. The broad resonance at ~32 ppm that appears in some of the ^1H NMR time courses suggests that $[Fe_2S_2(SCH_2CH_2OH)_4]^{2-}$ is formed under certain conditions, albeit only briefly and in small amounts. Because of the increased hydrophilicity of $[Fe_2S_2(SCH_2CH_2OH)_4]^{2-}$ over $[Fe_2S_2(SPh)_4]^{2-}$, the inability to trap the former cluster using hydrophobic cations and detergents is not surprising. The question remains as to how the [2Fe2S] apoproteins select for the [2Fe2S] core, instead of the [4Fe4S] core.

In general the synthetic results for the assembly of iron-sulfur clusters in totally aqueous media with $R=SCH_2CH_2OH$ can be explained by adding two conditions to the scheme in Figure I-7. The first condition is that the rate of equilibration between the iron-thiolate precursors is slow relative to the reaction of the iron-thiolate complexes with sulfur. The second condition is that the $[Fe_4(SR)_{10}]^{2-}$ complex reacts faster with sulfur than does the $[Fe(SR)_4]^{2-}$ complex. Thus, the preferred pathway for the assembly of $[Fe_4S_4(SR)_4]^{2-}$ (R=alkyl) in 100% aqueous media appears to be via $[Fe_4(SR)_{10}]^{2-}$. Some assembly of $[Fe_4S_4(SR)_4]^{2-}$ may also occur via $[Fe_2S_2(SR)_4]^{2-}$ in water but there is little direct evidence to support this claim. These results contrast to those of the previous study with R=Ph (34), which suggested that the preferred reaction pathway is via $[Fe(SR)_4]^{2-}$ and $[Fe_2S_2(SR)_4]^{2-}$. The relatively rapid exchange of the terminal thiolates of $[Fe_4(SCH_2CH_2OH)_{10}]^{2-}$ with solvent (Figure III-19) could explain its more

rapid reactivity with S°.

The ^1H NMR time courses for the reactions of $[Fe(SCH_2(CHOH)_2CH_2S)_2]^{2-}$ with sulfur show that these reactions proceed until an equilibrium position is reached. The spectra of the equilibrium mixture suggest the presence of three species. The initial pair of resonances at 200 ppm are still present, indicating that some of the starting mononuclear species remains. The multiplet at ~12 ppm suggests the formation of mixture of species with the [4Fe4S] core. The multiplet at 70 ppm may represent an iron-thiolate dimer, by analogy with the resonances for the methylene protons in $[Fe_2(SCH_2CH_3)_6]^{2-}$ at 69 ppm (13). If correct, this interpretation implies that $[Fe(SCH_2(CHOH)_2CH_2S)_2]^{2-}$ does not react directly with sulfur. This result would then be similar to the 2-mercaptoethanol case, where the reaction of sulfur with $[Fe_4(SCH_2CH_2OH)_{10}]^{2-}$, instead of $[Fe(SCH_2CH_2OH)_4]^{2-}$, is the major pathway to the [4Fe4S] cluster.

The rhodanese/$S_2O_3^{2-}$ system potentially provided a more physiologically relevant source of sulfide for the assembly of iron-sulfur clusters. When the initial iron complex was Fe(III)/dihydrolipoate, the rate of cluster assembly could be estimated using the decrease in absorbance at 620 nm. The conditions for the reaction of the Fe(III)/dihydrolipoate with the rhodanese/$S_2O_3^{2-}$ system were adjusted to match the conditions of experiments where the same reagents were used to reconstitute the 2[4Fe4S] clusters in apoferredoxin from C. pasteurianum. Thus, it was possible to directly compare the rate of cluster assembly in an apoprotein with the rate of synthetic cluster in aqueous solution. The rate of assembly of the synthetic cluster in aqueous was 1-2 orders of magnitude slower than the rate at which the cluster was assembled in apoprotein (110). The mechanism by which the apoprotein achieves the 10-100 fold increase in the rate of cluster assembly remains unknown.

The ^1H NMR and UV-visible spectral time courses for the synthesis of $[Fe_4S_4(SCH_2CH_2OH)_4]^{2-}$ using the rhodanese/$S_2O_3^{2-}$ system are consistent with those obtained when sulfide is generated from elemental sulfur. The relatively high concentration of $[Fe(SCH_2CH_2OH)_4]^{2-}$ relative to $[Fe_4(SCH_2CH_2OH)_{10}]^{2-}$ at pH 9 in this experiment is due to the 15/1 2-mercaptoethanol/Fe ratio. As discussed above, the reaction of $[Fe(SCH_2CH_2OH)_4]^{2-}$ with elemental sulfur at pH > 10 leads to the [6Fe9S] cluster, whereas, at lower pH's, $Fe_4S_4(SCH_2CH_2OH)_4^{2-}$ is the major product via $[Fe_4(SCH_2CH_2OH)_{10}]^{2-}$. In the rhodanese/$S_2O_3^{2-}$ system the reaction pH remains at approximately 9 throughout the reaction and $[Fe_4S_4(SCH_2CH_2OH)_4]^{2-}$ is the major product, as expected. This result suggests that the rhodanese/$S_2O_3^{2-}$ system serves only to generate sulfide gradually and does not significantly alter the assembly pathways of FeS clusters.

REFERENCES

1. Malkin, R. in Iron-Sulfur Proteins Vol. II, Lovenberg, W., Ed.; Academic Press: New York, 1973; p. 1-23.

2. Yasunobu, K. T.; Tanaka, M. in Iron-Sulfur Proteins Vol. II, Lovenberg, W., Ed.; Academic Press: New York, 1973; p. 29-130.

3. Orme-Johnson, W. H. Ann. Rev. Biophys. Chem. 1985, 14, 419-459.

4. Legall, J.; Moura, J. J. G.; Peck, H. D., Jr.; Xavier, A. V. in Iron-Sulfur Proteins, Spiro, T.G., Ed.; Wiley-Interscience: New York, 1982; p. 177-248.

5. Salerno, J. C.; Ohnisi, T. in Iron-Sulfur Proteins, Spiro, T. G., Ed.; Wiley-Interscience: New York, 1982; p. 285-327.

6. Emptage, M. H.; Kent, T. A.; Kennedy, M. C.; Bienhert, H.; Munck, E. Proc. Natl. Acad. Sci. U.S.A. 1983, 80, 4674-4678.

7. Stout, C. D. in Iron-Sulfur Proteins, Spiro, T. G., Ed.; Wiley-Interscience: New York, 1982; p. 97-146.

8. Adman, E. T. Biochim. Biophys. Acta 1979, 549, 107-144.

9. Adman, E.; Watenpaugh, K. D.; Jensen, L. H. Proc. Natl. Acad. Sci. U.S.A. 1975, 72, 4854-4858.

10. Nakamoto, M.; Tanaka, K.; Tanaka, T. J. Chem Soc. Chem. Commun. 1986, 1669-1670.

11. Lane, R. W.; Ibers, J. A.; Frankel, R. B.; Papaefthymiou, G. C.; Holm, R. H. J. Am. Chem. Soc. 1977, 99, 84-98.

12. Coucouvanis, D.; Swenson, A.; Baenziger, N. C.; Murphy, C.; Holah, D. G.; Sfarnas, N.; Simpolous, A.; Kostikas, A. J. Am. Chem. Soc. 1981, 103, 3350-3362.

13. Hagen, K. S.; Holm, R. H. Inorg. Chem. 1984, 23, 418-427.

14. Blower, P. J.; Dilworth, J. R. Coord. Chem. Rev. 1987, 76, 121-186.

15. Cambray, J.; Lane, R. W.; Wedd, A. G.; Johnson, R. W.; Holm, R. H. Inorg. Chem. 1977, 16, 2565-2571.

16. Coucouvanis, D.; Swenson, D.; Stremple, P.; Baenziger, N. C. J. Am. Chem. Soc. 1979, 101, 3392-3394.

17. Hagen, K. S.; Reynolds, J. G.; Holm, R. H. J. Am. Chem. Soc. 1981, 103, 4054-4063.

18. Hagen, K. S.; Holm, R. H. J. Am. Chem. Soc. 1982, 104, 5496-5497.

19. Hagen, K. S.; Watson, A. D.; Holm, R. H. J. Am. Chem. Soc. 1983, 105, 3905-3913.

20. Herriot, J. R.; Sieker, L.; Jensen, L. H.; Lovenberg, W. J. Mol. Biol. 1970, 50, 391-406.

21. Anglin, J. R.; Davison, A. Inorg. Chem. 1975, 14, 234-237.

22. Lane, R. W.; Ibers, J. A.; Frankel, R. B.; Holm, R. H. Proc. Natl. Acad. Sci. U.S.A. 1975, 72, 2868-2872.

23. Lovenberg, W.; Sobel, B. E. Proc. Natl. Acad. Sci. U.S.A. 1965, 54, 193-199.

24. Holah, D. G.; Coucouvanis, D. J. Am. Chem. Soc. 1975, 97, 6917-6919.

25. Kostikas, A.; Petroulas, V.; Simpoulos, A.; Coucouvanis, D.; Holah, D. G. Chemical Physics Letters 1976, 38, 582-584.

26. Millar, M.; Lee, J. F.; Koch, S. A.; Fikar, R. Inorg. Chem. 1982, 21, 4105-4106.

27. Collins, R. L. J. Chem. Phys. 1965, 42, 1072-1080.

28. Eaton, W. A.; Lovenberg, W. in Iron-Sulfur Proteins Vol. II, Lovenberg, W., Ed.; Academic Press: New York, 1973; p. 131-162.

29. Bair, R. A.; Goddard, W. A. J. Am. Chem. Soc. 1978, 100, 5667-5676.

30. Ali, A.; Farenholz, F.; Garing, J. C.; Weinstein, B. Int. J. Pept. Protein. Res. 1973, 5, 91-98.

31. Christou, G.; Ridge, B.; Rydon, H. N. J. Chem. Soc. Chem. Commun. 1977, 908-909.

32. Ueyama, N.; Nakata, M.; Nakamura, A. Bull. Chem. Soc. Jpn. 1981, 54, 1727-1730.

33. Nakata, M.; Ueyama, N.; Fuji, M.; Nakamura, A.; Wada, K.; Matsubara, H. Biochim. Biophys. Acta 1984, 788, 306-312.

34. Stevens, W. C.; Kurtz, D. M., Jr. Inorg. Chem. 1985, 24, 3444-3449.

35. Buchanan, B. B.; Lovenberg, W.; Rabinowitz, J. C. Proc. Natl. Acad. Sci. U.S.A. 1963, 49, 345.

36. Peterson, J. A.; Basu, D.; Coon, M. J. J. Biol. Chem. 1966, 241, 5162-5164.

37. Watenpaugh, K. D.; Sieker, L. C.; Jensen, L. C. J. Mol. Biol. 1979, 131, 509-522.

38. Adman, E. T.; Sieker, L. C.; Jensen, L. H.; Bruschi, M.; Legall, J. J. Mol. Biol. 1977, 112, 113-120.

39. Frey, M.; Sieker, L.; Payan, F.; Haser, R.; Bruschi, M.; Pepe, G.; LeGall, J. J. Mol. Biol. 1987, 197, 525-541.

40. Phillips, W. D.; Poe, M.; Weiher, J. F.; McDonald, C. C.; Lovenberg, W. Nature 1970, 227, 574-577.

41. Rao, K. K.; Evans, M. C. W.; Cammack, R.; Hall, D. O.; Thompson, C. L.; Jackson, P. J.; Jackson, C. E. Biochem. J. 1972, 129, 1063-1070.

42. Schultz, C. E. Ph.D. Dissertation, University of Illinois, 1979.

43. Moura, I.; Huynh, B. H.; Hausinger, R. P.; LeGall, J.; Xavier, A. V.; Munck, E. J. Biol. Chem. 1980, 255, 2493-2498.

44. Bennett, D. E.; Johnson, M. K. Biochim. Biophys. Acta 1987, 911, 71-80.

45. Schultz, C.; Debrunner, P. G. J. Phys. (Paris) Colloque 1976, 37, Suppl. 12, 153-158.

46. Gibson, J. F. in EPR and NMR of Paramagnetic Species in Biological and Related Systems, Bertini, I.; Drago, R. S., Eds.; D. Riedel Publishing Company: Boston, 1980, p. 225-253.

47. (a) Long, T.V.; Loehr, T.M. J. Am. Chem. Soc. 1970, 92, 6384.

(b) Long, T. V.; Loehr, T. M.; Allikens, J. R.; Lovenberg, W. J. Am. Chem. Soc. 1971, 93, 1809.

48. Yachandra, V. K.; Hare, J.; Moura, I.; Spiro, T. G. J. Am. Chem. Soc. 1983, 105, 6455-6461.

49. Czernuszewicz, R. S.; LeGall, J.; Moura, I.; Spiro, T. G. Inorg. Chem. 1986, 25, 696-700.

50. Krishnamoorthi, R.; Markely, J. L.; Cusanovich, M. A.; Przysiecki, C. T. Biochemistry 1986, 25, 50-54.

51. Moura, I.; Bruschi, M.; LeGall, J.; Moura, J. J. G.; Xavier, A. V. Biochem. Biophys. Res. Commun. 1977, 75, 1037-1044.

52. Bruschi, M.; Moura, I.; LeGall, J.; Xavier, A. V.; Sieker, L.C. Biochem. Biophys. Res. Commun. 1979, 90, 596-605.

53. Bruschi, M.; LeGall, J. in Iron and Copper Proteins, Yasunou, K. T.; Mower, H. F.; Hayaishi, O., Eds.; Plenum Publishing Corporation: New York, 1976; p. 57-67.

54. Moura, I.; Xavier, A. V.; Cammack, R.; Bruschi, M.; LeGall, J. Biochem. Biophys.

Res. Commun. 1978, 533, 156-162.

55. Sugiura, Y.; Ishizu, K.; Kimura, T.; Tanaka, H. Bioinorg. Chem. 1975, 4, 291-302.

56. Herskovitz, T.; Averill, B. A.; Holm, R.H.; Ibers, J. A.; Phillips, W. D.; Weiher, J. F. Proc. Natl. Acad. Sci. U.S.A. 1972, 69, 2437-2441.

57. Averill, B. A.; Herskovitz, T.; Holm R. H.; Ibers, J.A. J. Am. Chem. Soc. 1973, 95, 3523-3534.

58. Mayerle, J. J.; Frankel, R. B.; Holm, R. H.; Ibers, J. A.; Phillips, W. D.; Weiher, J. F. Proc. Natl. Acad. Sci. U.S.A. 1973, 70, 2429-2433.

59. Sugiura, Y.; Ishizu, K.; Kimura, T. Biochem. Biophys. Res. Commun. 1974, 60, 334-340.

60. Kurtz, D. M., Jr.; Stevens, W. C. J. Am. Chem. Soc. 1984, 106, 1523-1524.

61. Stevens, W.C. Ph.D. Dissertation, Iowa State University, 1986.

62. Shriver, D. F. The Manipulation of Air-Sensitive Compounds; McGraw-Hill: New York, 1969.

63. Eibeck, R. E. Inorg. Synth. 1963, 7, 128-131.

64. Ellman, G. L. Arch. Biochem. Biophys. 1959, 82, 70-77.

65. Bruschi, M.; LeGall, J. Biochim. Biophys. Acta 1972, 263, 279-282.

66. Petering, D. H.; Palmer, G. Arch. Biochem. Biophys. 1970, 141, 456-464.

67. Meyer, J.; Moulis, J.; Lutz, M. Biochim. Biophys. Acta 1986, 871, 243-249.

68. Blumenthal, K. M.; Heinriksson, R. J. J. Biol. Chem. 1966, 241, 5168-5176.

69. Tagawa, K.; Arnon, D.I. Biochim. Biophys. Acta 1968, 193, 602-613.

70. Sobel, B. E.; Lovenberg, W. Biochemistry 1966, 5, 6-13.

71. Vold, R. L.; Waugh, J. S.; Klien, M. P.; Phelps, D. E. J. Chem. Phys. 1968, 48, 3831-3832.

72. Freeman, R.; Kempsell, S. P.; Levitt, M. H. J. Magn. Reson. 1980, 38, 453-479.

73. La Mar, G. N.; Emerson, D. S.; Lecomte, J. T. J.; Pande, U.; Smith, K. M.; Craig, G. W.; Lehres, L. A. J. Am. Chem. Soc. 1986, 108, 5568-5573.

74. Ramaprasad, S.; Johnson, R. D.; La Mar, G. N. J. Am. Chem. Soc. 1984, 106, 5330-5335.

75. Zimmerman, R.; Huynh, B. H.; Münck, E.; Lipscomb, J. D. J. Chem. Phys. 1978, 69, 5463-5467.

76. Personal communication from Prof. Elizabeth Holt, Department of Chemistry, Oklahoma State University.

77. Hagen, W.R. Biochim. Biophys. Acta 1982, 708, 82-98.

78. Reiff, W. M.; Grey, I. E.; Fan, A.; Eliezer, Z.; Steinfink, J. J. Solid State Chem. 1975, 38, 582.

79. Bard, A. J.; Faulkner, L. R. Electrochemical Methods John Wiley and Sons, Inc.: New York, 1980, p. 213-248.

80. Personal communication from Prof. Steven Koch to Prof. D.M. Kurtz, Jr., Department of Chemistry, University of Georgia.

81. Phillips, W. D.; Poe, M. in Iron-Sulfur Proteins Vol. II, Lovenberg, W., Ed.; Academic Press: New York, 1973, p. 255-285.

82. Werth, M. T.; Kurtz, D. M., Jr.; Moura, I.; LeGall, J. J. Am. Chem. Soc. 1987, 109, 273-275.

83. Hill, C. L.; Renaud, J.; Holm, R. H.; Mortenson, L. E. J. Am. Chem. Soc. 1977, 99, 2549-2557.

84. Christou, G.; Garner, C. D. J. Chem. Soc. Dalton Trans. 1979, 1093-1094.

85. Finazzi-Agro, A.; Cannella, C.; Graziani, M. T.; Cavallini, D. FEBS Lett 1971, 16, 172-179.

86. Tomati, V.; Matarrese, R.; Federici, G. Phytochemistry 1974, 13, 1703-1706.

87. Yachandra, V. K.; Hare, J.; Gewirth, A.; Czernuszewicz, R.S.; Kimura, T.; Holm, R.H.; Spiro, T.G. J. Am. Chem. Soc. 1983, 105, 6462-6468.

88. Pagani, S.; Bonomi, F.; Cerletti, P. Eur. J. Biochem. 1984, 142, 361-366.

89. Bonomi, F.; Pagani, S.; Kurtz, D. M., Jr. Eur. J. Biochem. 1985, 148, 67-73.

90. Tinkham, M. Proc. R. Soc. (London) A 1956, 236, 535-548.

91. Abragam, A.; Bleaney, B. Electron Paramgnetic Resonance of Transition Metal Ions; Clarendon Press: Oxford, 1970; p. 209-216.

92. Huynh, B. H.; Kent, T. A. in Advances in Mössbauer Spectroscopy, Thosar, B. V.; Iyengar, P. K. Eds.; Elsevier Publishing Company: New York, 1983; Chapt. 9, p. 490-560.

93. De Groot, M. S.; Van Der Waals, J. H. Mol. Phys. 1960, 3, 190-200.

94. Hagen, W.R.; Dunham, W. R.; Johnson, M. K.; Fee, J.A. Biochim. Biophys. Acta 1985, 828, 369-374.

95. Johnson, M. K.; Benett, D. E.; Fee, J. A.; Sweeney, W. V. Biochim. Biophys. Acta 1987, 911, 81-94.

96. LeGall, J.; Ljungdahl, P. O.; Moura, I.; Peck, H. D., Jr.; Xavier, A. V.; Moura, J. J. G.; Teixera, M.; Huynh, B. H.; DerVartanian, D. V. Biochem. Biophys. Res. Commun. 1982, 106, 610-616.

97. Reem, R. C.; Solomon, E. I. J. Am. Chem. Soc. 1987, 109, 1216-1226.

98. LeGall, J.; Prickril, B. C.; Moura, I.; Xavier, A. V.; Moura, J. J. G.; Huynh, B.H.; Biochemistry 1988, in press.

99. Kassner, R. J.; Yang, W. J. Am. Chem. Soc. 1977, 99, 4351-4355.

100. Sawyer, D. T.; Srivasta, G. S.; Bodini, M. E.; Schaefer, W. P.; Wing, R. M. J. Am. Chem. Soc. 1986, 108, 936-942.

101. (a) Jencks, W. P.; Salveson, K. J. J. Am. Chem. Soc. 1971, 93, 4433-4436.

(b) Moss, R. A.; Dix, F. M. J. Org. Chem. 1981, 46, 3029-3035.

(c) Daneny, J. P.; Parameswaran, K. N. J. Chem. Eng. Data 1968, 13, 386-389.

102. Metzler, D. M. Biochemistry; Academic Press: New York, 1977; p. 59.

103. Good, M.; Vasak, M. Biochemistry 1986, 25, 8353-8356.

104. Kojima, Y.; Berger, C.; Vallee, B. L.; Kagi, J. H. R. Proc. Natl. Acad. Sci. U.S.A 1976, 73, 3413-3417.

105. LaMar, G. N. in Biological Applications of Magnetic Resonance, Shulman, R. G., Ed.; Academic Press: New York, 1979, p. 305-343.

106. Goff, H.; La Mar, G. N. J. Am. Chem. Soc. 977, 99, 6599-6606.

107. Wagner, G.; Wuthrich, K. J. Magn. Reson. 1979, 33, 675-680.

108. Singh, U.C.; Weiner, P. K.; Caldwell, J. W.; Kollman, P. A. AMBER (U.C.S.F. Version 3.0) Department of Pharmaceutical Chemistry, University of California at San Francisco (1986).

109. Moore, G. R.; Williams, R. J. P. Eur. J. Biochem. 1980, 103, 503-512.

110. Bonomi, F.; Werth, M. T.; Kurtz, D. M., Jr. Inorg. Chem. 1985, 24, 4331-4335.

ACKNOWLEDGEMENTS

I would to like thank my major professor, Dr. Donald M. Kurtz, Jr. for his advice and guidance during the course of my doctoral study.

I would not have been able to obtain some of the most interesting results presented in this dissertation without the help of the following people. Prof. Franco Bonomi, from the University of Milan, who worked with me in the lab on some of the reactions of iron-thiolates, in particular, the work with the "rhodanese system". Dr. Isabel Moura and Prof. Jean LeGall (and their coworkers), at the University of Georgia, provided me with samples of rubredoxin from Desulfovibrio for the ^1H NMR experiments. Prof. B. H. "Vincent" Huynh, at Emory University, collected the Mössbauer spectra of $[Fe(SCH_2CH_2OH)_4]^{2-}$ and directed my analysis of the spectra. I am especially grateful for the contributions that each of these people have made to my research.

I would like to thank the NMR experts; Drs. Dave Scott and Bob Domenick at Iowa State University and Prof. Herman van Halbeek at the University of Georgia for answering my many questions. Prof. James Anderson and Dr. Larry Fosdick helped me get started on the electrochemistry experiments. I would also like to thank Prof. Mike Johnson for his advice and interest in the S=2 EPR work.

Finally, I would like to thank Nita for her support during the completion of this dissertation.

APPENDIX A

Nuclear magnetic resonance (NMR) spectroscopy can be used to monitor chemical reaction rates. As a kinetic method, NMR has been particularly useful for the study of chemical exchange processes in systems at equilibrium. One example of such a system is the electron self-exchange process which occurs when a single chemical species is found in solution as a mixture of two different oxidation levels.

NMR provides several different approaches to monitoring chemical exchange. Each approach has advantages and limitations that combine with the properties of the system (chemical shift, relaxation time) to determine the time scale of the experiment. The first approach, which is the most common, involves analysis of chemical shift and lineshape changes. Another approach is to perform a saturation transfer experiment. In a saturation transfer experiment energy is pumped into a specific resonance in the first species until the resonance is saturated (i.e., reduced to zero intensity). Then after a variable delay, during which the saturation is transferred, the intensity of the corresponding resonance in the second species is measured. Forsen and Hoffman have developed a variation of the saturation transfer experiment. In their experiment, the intensity of the resonance in the first species is inverted instead of saturated. Proper analysis of the results of the experiment yields both the exchange rate and the nuclear spin-lattice relaxation rate. Both of these approaches require some knowledge of assignments for a given nucleus in the spectra of both species under going chemical exchange. A condition which is relatively easy to satisfy in small molecules, but may be impossible to achieve for a metalloprotein. The Forsen-Hoffman formalism has been further refined so that it can be applied when only single resonance from one of the exchanging species has been characterized. The original experiment will be discussed as

a prelude to the description of the experiment where only one resonance is required.

The following scheme describes the behavior a single nucleus in species A and X experiencing both chemical exchange and nuclear relaxation.

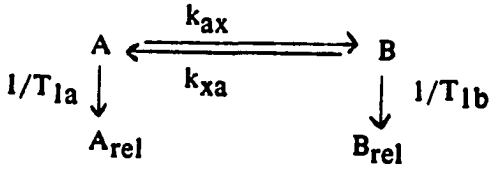

The assumption is made that $k_{ax} = k_{xa}$. The equations for the intensity of the resonance in species A and X as a function of time are as follows:

$$d[A]/dt = -(k_{ax} + 1/T_{1a})[A] + k_{xa}[X] \qquad (A\text{-}1)$$

$$d[X]/dt = -(k_{xa} + 1/T_{1x})[X] + k_{ax}[A] \qquad (A\text{-}2)$$

Equations A-1 and A-2 are integrated. The integrated equations are added to and subtracted from each other to give the following equations

$$[A] + [X] = A_0\exp[-(1/T_{1a})*t] \qquad (A\text{-}3)$$

$$[A] - [X] = A_0\exp[-(1/T_{1a} + k_{ax} + k_{xa})*t] \qquad (A\text{-}4)$$

The intensity data for the resonance in species A and X as a function of time (actually a delay time, tau) are fitted to equations A-3 and A-4. The value of T_{1a} is obtained from the fit to equation A-3. The fit to equation A-4 gives the value of the term $(1/T_{1a} + k_{ax} + k_{xa})$. Since the value of T_{1a} has been obtained from equation A-3 and the assumption has been made that $k_{ax} = k_{xa}$, the value of k_{ax} can be calculated. This formalism requires the ability to measure intensity data for a specific nucleus in both of the forms which are undergoing chemical exchange.

The experiment is performed by selectively inverting the intensity of resonance A. Spectra are collected for a series of delay times after the selective inversion pulse. The intensity of resonance A recovers essentially as a single exponential process. The recovery of the intensity of resonance B is a more complicated process. The intensity

data are analyzed by the previously described equations. The results of the analyses includes both the exchange rate constant, k_{ax}, and the spin-lattice relaxation time for resonance A, T_{1a}.

It should be noted that this experiment requires a selective inversion pulse, instead of the non-selective inversion pulse used in a conventional spin-lattice relaxation experiment. There is a specific rationale for choosing the selective pulse. Self-exchange rate constants are often measured by labeling one of the species (e.g., a radioisotope is often used as the label) and then following the approach to equilibrium for the labeled population. In this particular experiment, the inverted population of nuclei are the "labeled" molecules. The exchange rate information is effectively obtained from the intensity data after correction for the relaxation of the single labeled resonance. Using a non-selective pulse would be the equivalent of labeling all the resonances in both species. Therefore, the use of a non-selective pulse would create an unnecessarily complicated, and probably unsolvable, problem.

Prof. Dabney Dixon (Georgia State University) has presented a version of the experiment to measure the chemical exchange rate using a resonance from only one of the species involved in the exchange process. This version of the experiment measures the rate constant for the exchange process as a perturbation on the spin-lattice relaxation process. The equation for the spin-lattice relaxation process is

$$M_Z = M_0^*[1-2\exp(-t/T_1)] \qquad \text{(A-5)}$$

The revised equation which includes a term to describe the perturbation caused by the chemical exchange process is

$$M_Z = M_0^*[1-2\exp(-t/T_1)-\exp(-Rt)] \qquad \text{(A-6)}$$

For the rubredoxin self-exchange rate experiment, R is defined by the following expression

$$R = k_{11}*[\text{total protein}]*[\text{ox/red}] \qquad (A\text{-}7)$$

In this formalism the need to measure intensity data from two resonances and solve two independent equations is eliminated by performing an additional experiment. There are basically two unknowns in equation A-6, T_1 and k_{11}. The value of T_1 can be obtained independently from a separate selective spin-lattice relaxation experiment in the absence of the second species. The problem is then reduced to the simple case of one equation and one unknown.

There are two interesting consequences of that arise from the particular manner in which the experiment is performed. First, the experiment requires that the same nucleus be found in distinctly different magnetic environments in both species. The Forsen-Hoffman formalism was originally applied to situations such as nuclei which exchange between the cis and trans configurations around double bond. Therefore, the experiment can only be performed using resonances of nuclei in the molecule where the exchange process creates a perturbation in the magnetic field of the nucleus. For example, in a metalloprotein a change in oxidation state of the metal only changes the magnetic environment of nuclei close to the metal site. Secondly, the time scale for the self-exchange rate measurement is set by the spin-lattice relaxation time of the resonance chosen for the experiment. In practice, the ratio of R to T_1 is bounded by the following limits $0.1 \leq R/T_1 \leq 40$. If R and T_1 are substantially different the perturbation of the basic spin-lattice relaxation behavior by the self-exchange process is undetectable

A preliminary experiment has been conducted in which the relaxation behavior of the -3.4 ppm resonance of reduced rubredoxin was used to measure the self-exchange rate constant. In the case of D. gigas rubredoxin, it was impossible to invert the intensity of the -3.5 ppm resonance (i.e., give a selective 180° pulse). It was possible

to saturate the resonance, which is the equivalent of a 90° pulse. Therefore, the T_1 was measured using a selective 90°-t-90° pulse sequence. It should be noted that the equation which descibes the relaxation process is

$$M_Z = M_0*[1-\exp(-t/T_1)] \qquad \text{(A-8)}$$

for this pulse sequence. The selective T_1 experiment was performed on a fully reduced sample of rubredoxin. The T_1 value obtained from the experiment was 1.7 msec. When the same experiment was performed on a mixture of oxidized and reduced rubredoxin, the results indicated a slight perturbation of the basic spin-lattice relaxation behavior. Unfortunately, the perturbation was small and acceptable fits to the data could be obtained using either one or two exponentials. Using a simulation program instead of a curve fitting program may be a better approach to analyzing the data. The simulation program would more effectively treat the exponential with the T_1 term as a known quantity. Because the total protein concentration was lower (to slow the self-exchange rate) and the sample was not completely reduced, the intensity data from this experiment were much noisier than the data from the selective T_1 experiment. The increased noise contributed substantially to the problem of analyzing the data. With the appropriate adjustments in protein concentration, ratio of reduced and oxidized, data aquisition time, sample temperature, etc. it may be possible to obtain the electron self-exchange rate constant from this type of experiment.

Recently, the self-exchange rate constant for azurin was measured by a different ^1H NMR relaxation method (1). Briefly, the method requires a resonance where the effect of the self-exchange process is slow with respect to the relaxation rate of the nucleus. The slow exchange regime is defined by

$$k*[\text{total protein}] << T_{1,p}^{-1} \qquad \text{(A-9)}$$

where $T_{1,p}^{-1}$ is the additional contribution to the relaxation process from the more

paramagnetic species. When the slow exchange condition is met, then the self-exchange rate can be measured. The experiment is performed by measuring T_1 (non-selective) and/or T_2 of a fully reduced sample to which small aliquots of the oxidized species have been added (< 5% of the total protein concentration). The data are analyzed using the following equation

$$T_1^{-1} = T_{1,r}^{-1} + k[\text{oxidized}] \qquad \text{(A-10)}$$

where T_1^{-1} is the measured relaxation rate and $T_{1,r}^{-1}$ is the relaxation rate of the reduced species. The self-exchange rate constant is obtained from the slope of the plot of T_1^{-1} versus the concentration of the oxidized protein.

This approach may possibly be applied to one of the α-CH resonances in the 11-17 ppm region of the reduced rubredoxin spectrum, if the slow exchange limit applies to these resonances. The advantages to this approach include: the ability to use an almost totally reduced sample, ability to use the 180°-t-90° pulse sequence (i.e., a greater intensity change) and possibly the ability to use higher total protein concentrations.

REFERENCE

1. Groeneveld, C. M.; Canters G. W. J. Biol. Chem. 1988, 263, 167-173

APPENDIX B

The ^{57}Fe Mössbauer experiment provides oxidation and spin state information for each distinct population of iron atoms in the sample. This information comes from the analysis of the quadrupole doublet in the form of the isomer shift and quadrupole splitting values. The isomer shift is a measure of the splitting between the ground and excited nuclear spin states. The energy scale for the isomer shift is defined by the isomer shift of ^{57}Fe metal, which is assigned a value of zero mm/s. The interaction of the nuclear excited state quadrupole moment with an electric field gradient splits the excited state into two separate energy levels. Therefore, the Mössbauer spectrum of a single iron component is composed of two lines, i.e., a doublet pattern (Figure B-1). The isomer shift is the energy at the center of the doublet. The quadrupole splitting is the energy separation of the two lines of the doublet. The interpretation of the isomer shift and quadrupole splitting in terms of iron oxidation and spin states for iron-thiolate proteins has been described by Huynh and Kent (1).

The application of an external magnetic field produces Zeeman splitting of the nuclear spin state energy levels. The nuclear spin state doublets are no longer degenerate and there are now six discrete nuclear spin state energy levels (Figure B-2). The selection rule for nuclear spin state transitions is $\Delta m_I = \pm 1$. Application of the selection rule to the nuclear spin state levels gives six allowed transitions for a sample in a magnetic field. The basic two line Mössbauer spectrum becomes a six line spectrum in an applied magnetic field (Figure B-2).

Electron-nuclear hyperfine interactions couple the electrons (predominantly the d electrons) to the nucleus. This hyperfine coupling makes it possible to obtain information about the electronic and magnetic properties of the iron by a nuclear

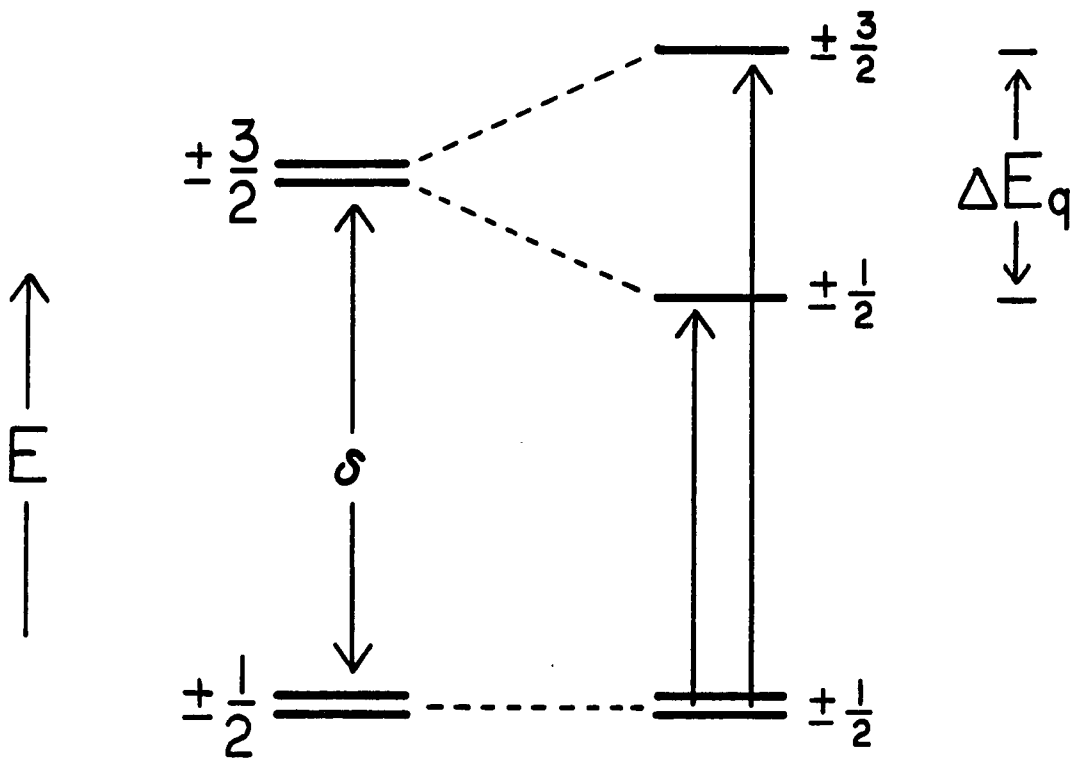

Figure B-1. Schematic energy level diagram depicting the observed transitions in the Mössbauer experiment

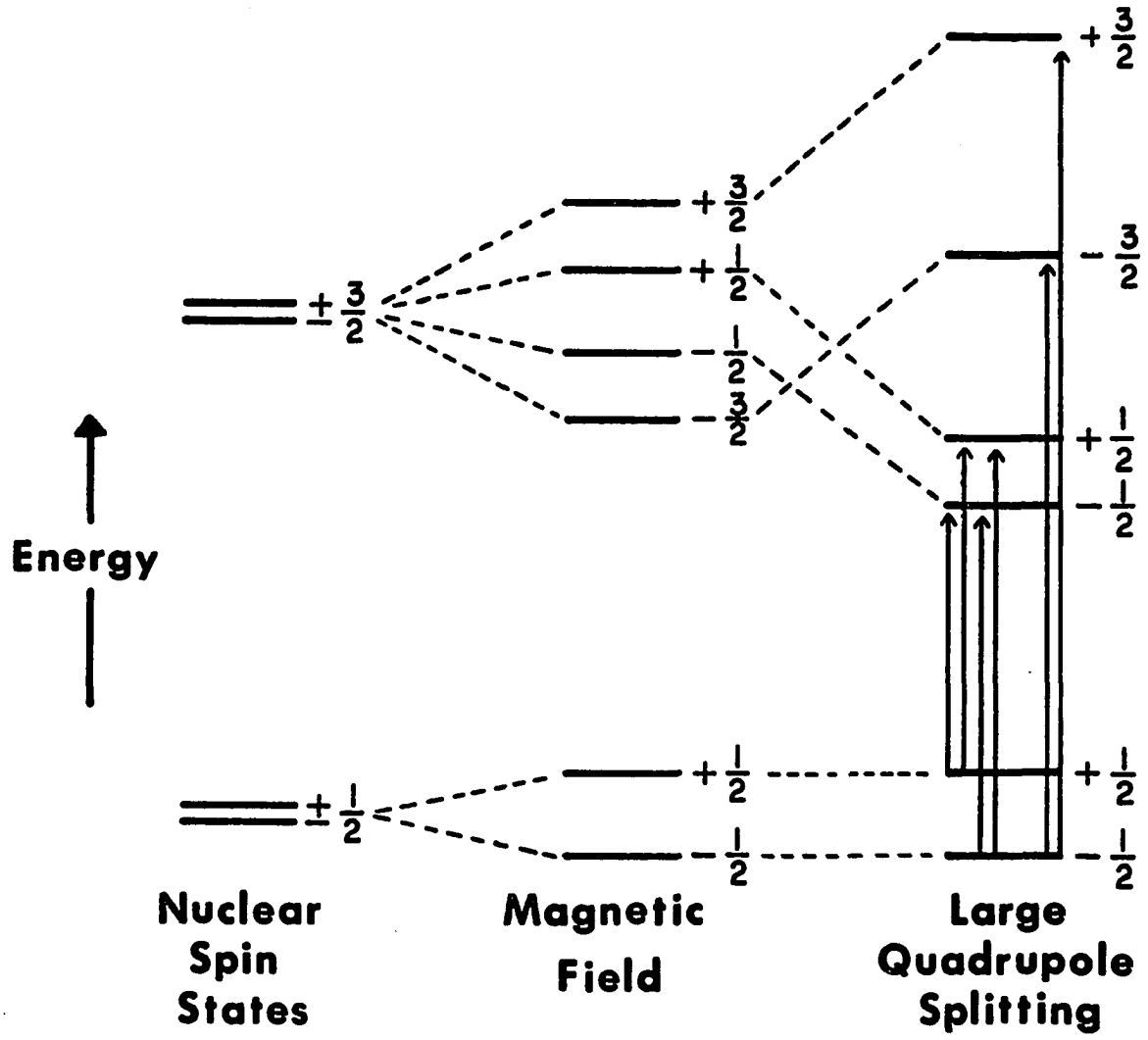

Figure B-2. Schematic energy level diagram depicting the Mössbauer transitions observed for a compound with a large quadrupole splitting in the presence of a strong applied magnetic field

spectroscopic method, i.e., Mössbauer spectroscopy. The chemical and structural enviroment around the iron nucleus is reflected in the distribution of the d electrons. Thus, Mössbauer spectroscopy provides additional information about the physical and chemical properties of the iron site. By recording a series of Mössbauer spectra over a range of temperatures and applied magnetic fields the nature of the electron-nuclear hyperfine interaction can be characterized in detail. The analysis of these spectra provides a wealth of information including: sign of the quadrupole splitting value, asymmetry parameter, electric field gradient components, electron-nuclear hyperfine coupling constants, axial and rhombic zero-field splitting parameters. Discussion of the interactions between the electronic and nuclear spin states is beyond the scope of this Appendix. There are several reviews of Mössbauer spectroscopy of metalloproteins (1,2).

Magnetic Mössbauer experiments were performed on a frozen solution of $[Fe(SCH_2CH_2OH)_4]^{2-}$ in water. Details concerning the sample preparation are given in Figure III-11 and the experimental section. The crystalline solid, $Ba[Fe(SCH_2CH_2OH)_4]$, is not suitable for use in Mössbauer experiments because it contains barium. High atomic number elements, such as barium, scatter the gamma-rays causing a significant decrease in signal intensity. The purpose of this study was to obtain the values of the axial and rhombic zero-field splitting parameters, D and E, for the $[Fe(SCH_2CH_2OH)_4]^{2-}$ complex. The values of these parameters were needed for the interpretation of the S=2 type EPR signal observed for this complex in solution.

Two series of spectra were collected. The first series of spectra were obtained at 4.2 K at magnetic fields of 0, 5, 10, 20, 40 and 70 kG. At this temperature the electronic relaxation is slow relative to the nuclear relaxation. This series of spectra provides insight into the properties of the internal magnetic field. The second series of spectra were obtained in a 70 kG applied magnetic field at temperatures of 4.2, 50, 90,

130 and ~170 K.

The analyses of the magnetic Mössbauer spectra provided the values of the zero-field splitting parameters, D and E. Furthermore, the results also included: the sign of the quadrupole splitting value; the temperature dependence of the quadrupole splitting; the asymmetry value; the values of the electron-nuclear hyperfine coupling constants, A_x, A_y, and A_z. From these results it was possible to calculate the magnitude of the zero-field splitting of the $|\pm 2\rangle$ doublet and values of the electric field gradient components, V_{xx}, V_{yy}, and V_{zz}.

The process of analyzing the spectra is based on the knowledge that the appearance of the Mössbauer spectrum at a given combination of temperature and applied field is dominated by a few specific parameters. By trial and error, the initial value of a parameter is estimated from a spectrum obtained under the appropriate conditions. After the initial estimate of a parameter has been made, the new value is tested in other spectra to ensure that it is valid over the entire range of experimental conditions. Thus, the rigorous determination of D and E, for example, requires the collection and analysis of several spectra.

The low temperature, zero-field spectrum provided the value of the isomer shift (0.73 mm/s) and the magnitude of the quadrupole splitting (3.48 mm/s). These values are consistent with high spin Fe(II) with tetrahedral coordination by sulfur. The spectrum also contains an extremely weak doublet with an isomer shift of ~0.35 mm/s and ΔE_q= ~0.25 mm/s. This second doublet reflects <5% contamination by a high spin, fast relaxing Fe(III) species which is probably polymeric, e.g., iron oxides.

The relatively large value of the quadrupole splitting dramatically affected the appearance of the magnetic Mössbauer spectra recorded at 4 K. When the quadrupole splitting is small, the most intense lines of the magnetic Mössbauer spectrum are the

highest and lowest energy lines. For large quadrupole splitting, the two most intense lines are found at high energy. At high applied magnetic fields, a group of four lines are observed at lower energy and pair of lines are found at higher energy (compare spectrum c in Figure B-3 with the transitions shown in Figure B-2). At low applied magnetic fields, the four lines at lower energy overlap forming a barely resolved doublet. The two higher energy lines begin to overlap, but still remain clearly resolved (see spectrum a in Figure B-3).

The parameters that dominate the appearance of the magnetic Mössbauer spectra of $[Fe(SCH_2CH_2OH)_4]^{2-}$ under various experimental conditions will now be discussed. This discussion will be a very general overview of how to simulate the spectrum of a single high spin Fe(II) site. A rigorous treatment of the analysis of magnetic Mössbauer spectra for other types of iron sites is far beyond the scope of this report (see in particular reference 3 and the references therein).

As previously described, the low temperature, zero-field spectrum (Figure III-11) provides the value of the isomer shift and the magnitude of the quadrupole splitting. The sign of the quadrupole splitting is obtained from the high temperature, strong field (~130 K, 70 kG) spectrum (Figure B-4). In this spectrum a doublet and a triplet are observed. The arrangement of the doublet and the triplet provides the sign of the quadrupole splitting. The high temperature, strong field spectrum is also useful in checking the value of D which is initially estimated from spectra taken at 4.2 K.

The splitting (and intensity) of the high energy doublet in the weak field spectra is sensitive to changes in the values of both D and E/D. These two parameters determine the magnitude of Δ (1), the zero field splitting of the $|\pm 2\rangle$ spin doublet, according to the following equation

$$\Delta = 2|D|([1 + 3(E/D)^2]^{\frac{1}{2}} - 1)$$

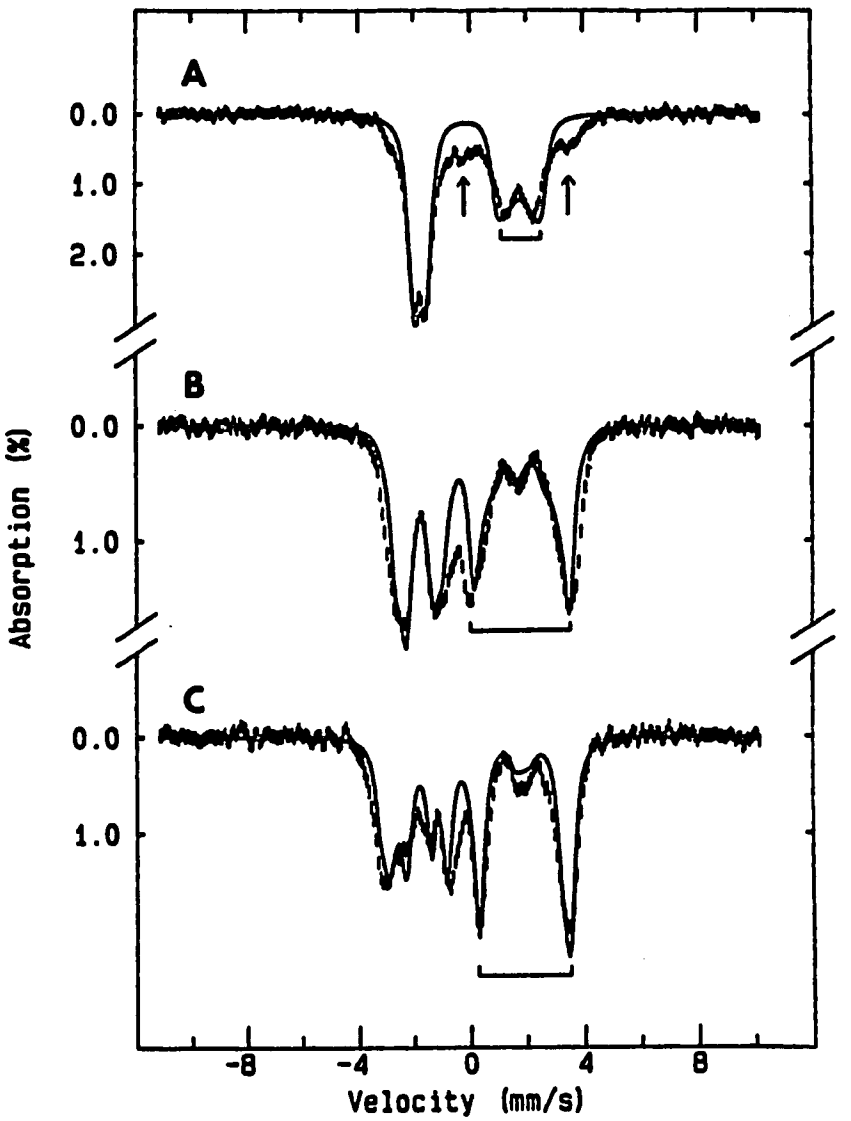

Figure B-3. Magnetic Mössbauer spectra of $[Fe(SCH_2CH_2OH)_4]^{2-}$ recorded at 4.2 K in the presence of applied magnetic fields of 5 (A), 20 (B), and 70 (C) kG. The solid line is a simulation for the major species using the parameters in Table B-1. The simulated spectrum is scaled to 80% of the total area of the experimental spectrum. The splitting of the high energy doublet at each field strength is denoted by the brackets. The arrows denote the "wings" of the 5 kG spectrum which represent the minor species

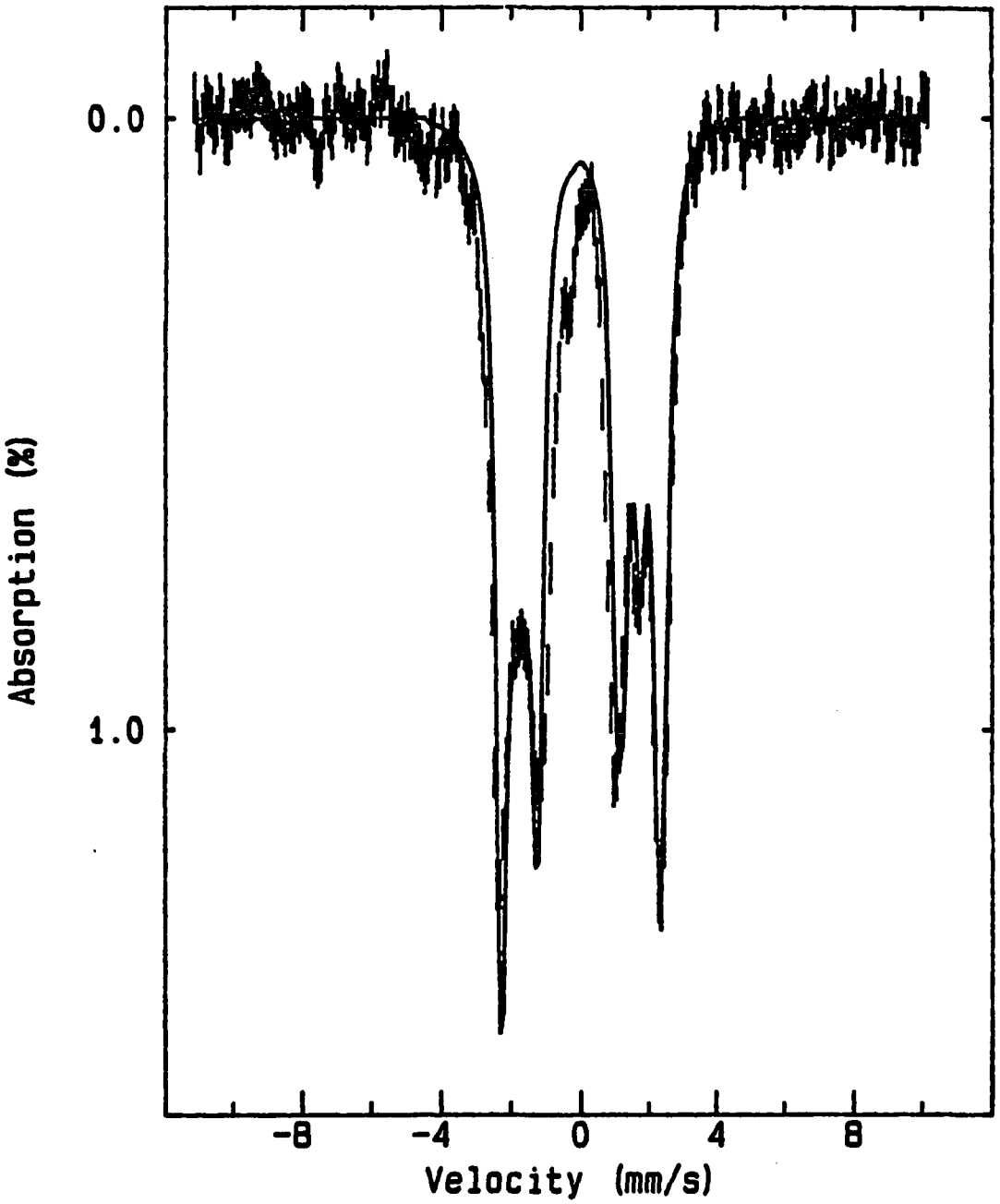

Figure B-4. Magnetic Mössbauer spectrum of $[Fe(SCH_2CH_2OH)_4]^{2-}$ recorded at 130 K in a 70 kG applied magnetic field. The solid line is a simulation for the major species using the parameters in Table B-1. The simulated spectrum is scaled to 80% of the total area of the experimental spectrum

As E/D becomes small, the $[1 + 3(E/D)^2]^{\frac{1}{2}}$ term may be approximated by $[1 + 3/2(E/D)^2]$. Using this approximation the above equation simplifies to $\Delta = 3E^2/D$ in the high symmetry regime, i.e. as E/D approaches zero. The magnitude of the zero field splitting of the $|\pm 2\rangle$ doublet and the sign and magnitude of D are of value in understanding the novel S=2 EPR signals observed for three of the $[Fe(SR)_4]^{2-}$ complexes.

The electron-nuclear hyperfine coupling constants, A_x, A_y and A_z, are estimated from the series of spectra collected at 4 K over a range of magnetic field strengths. The hyperfine coupling constants determine the magnitudes of various splittings between lines in the spectra. In the case of $[Fe(SCH_2CH_2OH)_4]^{2-}$, the A_y parameter controls the splitting of the high energy doublet in the weak field (5 and 10 kG) spectra. The outermost lines of the 70 kG spectrum are dramatically affected by changes in the value of A_x. The spectra at both low and high field are somewhat insensitive to changes in the value of A_z, making the precise determination of this parameter difficult.

At this point it is possible to present an example of the need to evaluate all of the parameters which affect the spectra. The splitting of the high energy doublet, in the weak field spectra (4 K, 5 and 10 kG) is determined both by Δ (through D and E/D) and A_y. Likewise, the magnitude of Δ affects the splitting of the outermost lines in the high field (4 K, 40 and 70 kG) spectra. The splitting of these lines is also dependent on the value of A_x as previously described. Thus, the parameters A_x, A_y and the zero-field splitting parameters, D and E/D, are related. Therefore, even though the weak field (4 K, 5 and 10 kG) spectra are not especially sensitive to changes in A_x, a proper value of A_x is required in the simulations to obtain accurate values of D and E/D.

Using the values of the asymmetry parameter and the quadrupole splitting, the values of the electric field gradient (EFG) components can be calculated. The electric field gradient components V_{xx}, V_{yy} and V_{zz} are found by solving the following series

of equations

$$E_q = V_{zz}(1 + \eta^2/3)^{\frac{1}{2}}$$

$$V_{xx} - V_{yy} = \eta V_{zz}$$

$$V_{xx} + V_{yy} = -V_{zz}$$

A particularly important result from this analysis is the sign of V_{zz}. The sign of this term defines the ground state orbital of the metal center in tetrahedral symmetry (4).

In attempting to simulate the 5 kG spectrum, it was found that the "wings" of the high energy doublet could not be fit. The energy level diagram for the case of large ΔE_q (Figure B-2) shows that the high energy pair of lines should be isolated from the the remaining four lines. The presence of additional intensity around the high energy doublet cannot, therefore, be explained by overlap with one or more of the other four lines. This means that the "wings" on the high energy doublet must be due to another species; either an impurity or a second magnetically distinct species. The zero-field Mössbauer spectrum indicates that > 95% of the sample is high spin Fe(II) in a tetrahedral sulfur coordination sphere. This suggests the presence of a second magnetic species in the sample.

The analysis of the spectra was performed by first attempting to analyze the properties of the major component. Once, a reasonable set of parameters was obtained for the major component, its contribution to the total spectrum was simulated by assuming that it was responsible for the intensity of the high energy doublet in the low temperature, weak field spectra. Using this assumption, it was found that the majority species accounted for ~80% of the total spectrum. Simulations, using the parameters for the majority species, were performed for each set of the conditions under which spectral data had been recorded. From each of the raw spectra a 80% contribution from the major species was subtracted. This generated a subset of spectra which reflected

the characteristics of the minor component. The minor component was then simulated by the procedure already described for the major species.

Table B-1 contains the final values for the major component. The zero-field splitting of the $|\pm 2\rangle$ doublet in the major species is 0.933 cm^{-1}. The large positive value of D indicates the the $|\pm 2\rangle$ is an excited state in the major species. The temperature dependence of the S=2 EPR signal suggests that the EPR signal arises from a ground state. Clearly, the major species is not responsible for the novel S=2 EPR signal.

A preliminary parameter set for the the minor component is also included in Table B-1 to point out the similarities between the minor component and desulforedoxin. While the tentative values of D and E/D indicate that Δ for the minor species is larger than 0.3 cm^{-1}, the final values may actually show that Δ in the minor species is less than 0.3 cm^{-1}.

REFERENCES

1. Huynh, B. H.; Kent, T. A. in Advances in Mössbauer Spectroscopy, Thosar, B. V.; Iyengar, P. K. Eds.; Elsevier Publishing Company: New York, 1983; Chapt. 9, p. 490-560.

2. Munck, E. in Methods in Enzymology Vol. 54, Fleischer, S.; Packer, L., Eds.; Academic Press: New York, 1978; p. 346-379.

3. Zimmerman, R.; Huynh, B. H.; Munck, E.; Lipscomb, J. D. J. Chem. Phys. 1978, 69, 5463-5467.

4. Collins, R. L. J. Chem. Phys. 1965, 42, 1072-1080.

Table B-1. Preliminary results of the magnetic Mössbauer study of $[Fe(SCH_2CH_2OH)_4]^{2-}$

Parameter	Major species[a]	Minor species[b]
δ, mm/s[c]	0.73	0.73
ΔE_q, mm/s	-3.48	3.48
D, cm^{-1}	-8 (1)	-7
E/D	0.20 (0.02)	0.22
Δ, cm^{-1}	0.9	0.9
sign of V_{zz}	(-)	(+)
assymetry	0.75 (0.1)	~0
A_x, kG	-150 (25)	-250
A_y, kG	-85 (5)	-250
A_z, kG	-250 (50)	-70

[a]Values for the major species have been determined to a high degree of confidence. The number in parentheses is the estimated uncertainity.

[b]Values for the minor species are very tentative and presented here to provide a qualitative basis for comparison.

[c]Spectrum was recorded at 4.2 K. The isomer shift is reported relative to iron metal at 300 K.

APPENDIX C

The structure of the new compound, $Ba[Fe(SCH_2CH_2OH)_4]$, has been studied by single crystal X-ray diffraction. The diffraction study was performed by Prof. Elizabeth Holt at Oklahoma State University. The R value for the final refinement was 9.7%. The crystal data are presented in Table 1. Further refinement of the data proved to be impossible due to disorder in the hydroxyethyl side chains. The disorder in the hydroxyethyl groups is clearly evident in the bond distances derived for these atoms from the positions of the final refinement and in the magnitudes of the anisotropic thermal parameters for these atoms. Fortunately, the data were of sufficient quality to clearly establish the coordinates of the Ba, Fe and S atoms. Tables 2-6 contain the atomic coordinates in the space group P4, selected bond distances and angles, anisotropic thermal parameters, and the F_{obs} and F_{calc} values.

The compound was synthesized by the procedure described in the experimental section. The supernatant (25-30 mL) which contained the compound was transferred to a 250 mL flask. Following addition of ~150 mL of acetone, the mixture was stirred until the solution was homogeneous. After 24 h, a dark oily aqueous phase was found at the bottom of the flask. Above the aqueous phase, there was a dark yellow-orange acetone layer. At this time, clear crystals were found along the upper edge of the solution and along the walls of the flask.

The crystals were harvested after four days. The acetone/water mother liquor was removed via canula. The crystals were then washed with 4/1 acetone/water (3x5 mL), which removed color due to residual traces of the mother liquor. The crystals were then washed with methanol (5x6 mL). The methanol wash led to the crystals taking on a slight reddish-orange tint. The crystals were dried in vacuo for six hours. Using an

Table C-1. Crystal data for $Ba[Fe(SC_2H_5O)_4]$

Formula	$BaFeS_4C_8H_{20}O_4$
Mol. Wt.	501.7 g/mol
a	6.900(4) Å
b	6.900(4) Å
c	8.995(5) Å
α	90.00
β	90.00
γ	90.00
F(000)	246
μMoK_α	36.02 cm^{-1}
λMoK_α	0.71069 Å
D_{calc}	1.945 g/cm^3
Z	1
Meas. refl.	305
Obs. refl.	299
R	9.7
Space group	P4

Table C-2. Atomic Coordinates for $Ba[Fe(SC_2H_5O)_4]$

Atom	X	Y	Z
Ba	0.0000	0.0000	0.5000
Fe	0.5000	0.5000	0.5000
S1	0.699(3)	0.310(2)	0.357(2)
O1	0.225(6)	0.094(6)	0.262(6)
C1	0.630(10)	0.240(10)	0.243(10)
C2	0.990(14)	0.723(8)	0.863(10)

Table C-3. Bond Distances (Å) and for $Ba[Fe(SC_2H_5O)_4]$

Atoms	Distance
Ba1-O1	2.72(5)
Fe1-S1	2.30(2)
S1-C1	1.23(10)
C1-C2	1.96(12)
C2-O1	1.38(10)

Table C-4. Bond Angles for $Ba[Fe(SC_2H_5O)_4]$

Atoms	Angle (°)
S1-Fe1-S1'	111.9(6)
S1-Fe1-S1"	108.3(6)
Fe1-S1-C1	116.9(4.0)
S1-C1-C2	126.1(6.0)
C1-C2-O1	96.6(6.0)

' = 1-x, 1-y, z

" = y, 1-x, 1-z

Table C-5. Anisotropic Thermal Parameters for $Ba[Fe(SC_2H_5O)_4]$

Atom	U11	U22	U33	U12	U13	U23
Ba	14(1)	14	28(2)	0	0	0
Fe	19(3)	19	39(6)	0	0	0
S	127(15)	94(12)	42(10)	102(12)	-4(10)	2(9)
C1	130(6)	124(58)	181(79)	61(51)	11(56)	83(55)
C2	195(86)	35(29)	144(63)	-82(44)	54(65)	-16(36)
O1	59(24)	94(31)	98(35)	17(22)	-13(24)	-19(27)

Table C-6. Fobs and Fcalc for $Ba[Fe(SC_2H_5O)_4]$

0,1,L				0,3,L				0,5,L			
0	252	244	36	0	546	494	73	0	46*	68	27
1	136	241	27	1	352	330	52	1	97	134	33
2	212	239	36	2	218	186	42	2	182	197	45
3	337	378	49	3	42	47	24	3	294	241	58
4	309	327	49	4	55	51	27	4	255	237	55
5	243	232	49	5	124	151	36	5	133	154	39
6	97	108	33	6	267	241	55	6	97	91	36
7	37*	79	27	7	215	233	52	7	94	69	39
8	133	111	43	8	173	173	49				
9	146	126	45								
0,2,L				0,4,L				0,6,L			
0	221	198	39	0	597	597	82	0	303	349	61
1	497	502	64	1	500	500	76	1	379	375	67
2	806	817	82	2	476	447	67	2	400	366	70
3	785	788	85	3	446	435	67	3	273	294	58
4	621	635	82	4	373	369	64	4	212	257	52
5	467	469	67	5	349	363	64	5	239	260	58
6	276	300	55	6	324	322	64				
7	188	200	49	7	236	270	55				
8	206	198	52	8	218	232	55				
9	224	233	58								

Table C-6. (Continued)

	0,7,L		
0	100	154	39
1	124	137	42
2	152	144	45
3	112	127	42
	1,1,L		
0	679	746	67
1	925	813	79
2	715	713	76
3	551	567	70
4	467	553	64
5	540	538	70
6	443	425	67
7	349	325	64
8	333	283	64
9	258	232	58

	1,2,L		
0	233	242	39
1	418	399	61
2	291	392	45
3	103	145	30
4	133	139	33
5	127	156	36
6	221	228	49
7	236	203	52
8	149	157	42
	1,3,L		
0	500	394	70
1	518	531	73
2	585	695	79
3	549	575	70
4	440	368	67
5	343	377	61
6	306	373	61
7	249	282	58
8	218	224	55

	1,4,L		
0	176	154	39
1	194	146	42
2	212	265	45
3	255	245	52
4	218	181	49
5	246	212	52
6	121	168	39
7	46*	102	30
8	106	109	39
	1,5,L		
0	424	459	67
1	467	456	70
2	409	367	67
3	303	333	58
4	312	361	61
5	297	299	61
6	258	260	58
7	233	244	58

Table C-6. (Continued)

	1,6,L				2,1,L				2,3,L			
0	124	149	39	0	324	314	45	0	31*	69	24	
1	167	168	45	1	588	648	70	1	224	175	45	
2	191	168	49	2	424	315	55	2	321	337	55	
3	130	135	42	3	139	83	36	3	355	366	58	
4	106	139	39	4	146	148	36	4	294	274	55	
5	100	125	39	5	136	165	39	5	188	181	45	
	1,7,L			6	224	203	49	6	109	125	39	
0	276	300	61	7	224	212	52	7	31*	55	30	
1	252	269	58	8	146	166	42	8	82	73	36	
2	282	287	61	9	106	127	39		2,4,L			
3	285	291	64		2,2,L			0	467	549	67	
				0	585	615	73	1	400	471	64	
				1	864	734	91	2	312	418	58	
				2	758	583	88	3	379	421	64	
				3	376	379	58	4	309	355	61	
				4	370	388	61	5	267	322	58	
				5	376	375	61	6	252	291	58	
				6	370	405	64	7	239	266	55	
				7	382	374	67					
				8	279	266	61					

Table C-6. (Continued)

	2,5,L				3,1,L				3,3,L		
0	230	250	52	0	628	664	79	0	646	632	88
1	230	243	52	1	609	547	79	1	600	536	76
2	139	145	42	2	631	474	82	2	515	429	73
3	49	65	30	3	628	539	85	3	434	360	67
4	136	127	42	4	540	539	73	4	315	299	58
5	127	128	42	5	424	405	67	5	349	330	64
6	103	144	39	6	355	288	64	6	337	337	64
	2,6,L			7	285	263	61	7	306	306	64
0	264	296	58	8	230	243	55		3,4,L		
1	264	317	58		3,2,L			0	288	290	55
2	291	316	61	0	39	20	24	1	212	217	49
3	349	322	67	1	258	196	49	2	161	167	42
4	352	333	70	2	333	242	55	3	179	147	45
5	252	272	61	3	364	318	61	4	91	83	36
	2,7,L			4	343	334	61	5	142	164	42
0	161	149	45	5	230	225	52	6	170	168	49
1	106	110	39	6	115	103	39	7	149	158	45
2	97	130	39	7	12*	49	27				
				8	91	85	36				

Table C-6. (Continued)

	3,5,L				4,1,L				4,3,L		
0	218	256	52	0	194	191	42	0	333	314	61
1	276	330	58	1	221	217	45	1	243	239	52
2	340	364	64	2	243	191	49	2	179	153	45
3	388	381	70	3	282	241	55	3	179	119	45
4	415	400	73	4	258	258	52	4	106	87	36
5	300	308	64	5	273	214	58	5	158	141	45
6	179	203	52	6	133	123	42	6	206	175	52
	3,6,L			7	76	80	33	7	176	162	49
0	103	151	36	8	139	104	45		4,4,L		
2	103	122	39		4,2,L			0	179	234	45
3	136	129	42	0	658	585	88	1	330	305	61
4	112	148	42	1	540	511	73	2	512	441	79
				2	409	400	64	3	509	444	79
				3	461	359	70	4	394	367	70
				4	437	381	70	5	327	321	67
				5	364	337	67	6	233	236	58
				6	315	288	64		4,5,L		
				7	261	263	61	0	91	113	36
								2	188	161	49
								3	127	130	42
								4	115	146	42

Table C-6. (Continued)

	4,6,L				5,3,L				6,1,L			
0	340	371	67	0	282	237	58	0	155	146	45	
1	318	354	67	1	330	281	64	1	182	183	49	
2	249	266	58	2	418	393	70	2	209	176	52	
	5,1,L			3	427	443	73	3	130	121	42	
0	479	452	73	4	418	391	73	4	109	116	39	
1	512	470	76	5	337	303	67	5	136	128	42	
2	455	403	70	6	239	216	58		6,2,L			
3	337	309	61		5,4,L			0	306	256	61	
4	340	296	64	0	112	124	39	1	312	289	64	
5	340	303	64	1	158	142	45	2	337	342	67	
6	291	293	61	2	188	176	49	3	388	363	70	
7	285	257	64	3	146	149	45	4	379	340	70	
	5,2,L			4	115	109	42	5	285	272	64	
0	279	258	55		5,5,L				6,3,L			
1	297	254	58	0	352	385	70	0	139	145	42	
2	155	140	42	1	340	381	67	1	158	149	45	
3	67	76	33	2	315	298	67	2	149	146	45	
4	146	117	42	3	264	178	61	3	173	131	49	
5	152	129	45					4	161	114	49	
6	118	150	42									

Table C-6. (Continued)

	6,4,L		
0	385	391	73
1	358	359	70
2	276	278	61
	7,1,L		
0	276	260	62
1	267	263	61
2	288	295	64
3	324	299	67
	7,2,L		
0	197	138	55
1	139	131	45
2	112	132	42

argon-filled glove bag, the crystals were transferred to ampules which were then flame sealed. The crystals were mailed to Dr. Holt at O.S.U. for X-ray analysis.

The iron-sulfur bonds are all 2.30(2) A long. There are two S-Fe-S angles of 111.9(6)°, the remaining four S-Fe-S angles are 108.3(6)°. The axially distorted FeS_4 unit has S_4 symmetry. The distortions found in the S-Fe-S bond angles define a compression of the tetrahedral structure along the S_4 axis. The oxidized rubredoxin analog, $[Fe(SC_{10}H_{13})_4]^{1-}$, also has S_4 symmetry. At least in crystalline form, these two compounds have the highest symmetry of the FeS_4 site analogs (see Table I-1 for comparison).